NIRS-M-243

Proceedings of

NIRS-ETOILE

2nd Joint Symposium 2011 on Carbon Ion Radiotherapy

Nov.25-27, 2011

Centre ETOILE, Lyon-France

Organized by

NIRS
National Institute of Radiological Sciences, Japan

and

GSC ETOILE
Groupement de Coopération Sanitaire ETOILE

Chair organizers

T. Kamada, NIRS & J. Balosso, ETOLIE

NIRS-ETOILE Joint Symposium on Carbon Ion Radiotherapy

11th Heavy Ion Charged Particle Therapy Symposium

November 25-27, 2011

Venue : The Institute for Cognitive Science

67, boulevard Pinel 69675 BRON CEDEX, France

Organized by

National Institute of Radiological Sciences, Japan

and

Centre ETOILE, France

Preface

Carbon ion therapy, as an efficient and cost effective treatment of the most radioresistant cancers, is still making radiation oncologists dreaming. Although a number of projects are presently developing around the World, some difficulties are appearing on the road. The routine implementation of this treatment process is not yet straightforward. The main economical determinant is the time necessary to treat a patient, making once again technology to be placed at the first place. However in front of the technical realities should be put the financial one. A global appraisal of the feasibility and the medical service is necessary to evaluate the exact price to pay for hadrontherapy on the present base.

The seventeen years experience of NIRS under public management and the ability of Japan to develop a real industrial expertise in the field of hadrontherapy remains up to now the unique global success in the domain. Technical improvement came progressively and step by step the new facilities are using more sophisticated technology as active beam scanning. Active beam scanning, which is the "standard" in Europe, delivers a more precise treatment but needs more time to treat a patient; this aspect is a critical point and must be taken into account for economical balance of the treatment centers.

In France the national project ETOILE is going forward at a slow pace pulling-along heavy commitments to medical demonstration and nationwide organization. In 2010 a private-public procedure has been terminated without success, premonitory of the present difficulties of similar procedures in Germany. Nevertheless, the project is again on tracks with a classical call for bids ongoing with proposals waited for spring 2012 and a national scientific organization, *France HADRON*, applying for funding at the end of 2011.

This second NIRS-ETOILE joint symposium will extend upon 3 days. The first full day will mainly review the clinical experience of NIRS in Japan and HIT in Germany. The second morning will be devoted to ion beam technology and the last morning to ion beam biology. Each day's introduction speeches will provide information on the course of the different projects ongoing in Japan and Europe.

In the present time of economical difficulties, challenging projects as hadrontherapy centers will suffer a lot. It is therefore of utmost importance to make largely available the clinical and scientific results of hadrontherapy to consolidate decision making. A major goal of this symposium is also to intensify Japanese-French collaboration, and to set the course for further joint initiatives in the future development of ion-beam therapy.

We wish you an interesting and fruitful meeting in Lyon.

Jacques Balosso, Lyon

Tadashi Kamada, Chiba

2nd NIRS-ETOILE Joint Symposium on Carbon Ion Therapy

Friday, November 25, 2011

Introduction

	Opening remarks	**presented by**
08:30	Welcome Address and the Medical Hope for Hadrontherapy in France	Officials (to define)
	Opening Remarks by NIRS group	H. Tsujii
	Greetings from the Japanese Consulate in Lyon	S. Noguchi
	The Landscape of Hadrontherapy in Japan and Europe (I) (Chair : J.L. Habrand, H.Tsujii)	
09:00	Current Status of Carbon Ion Radiotherapy in Japan	H. Tsujii
09:20	Present Status of Hadrontherapy in France: ***France HADRON***	L.L. Habrand
09:40	**General discussion**	

Clinical sessions

	Experiences at NIRS (Chair: P. Pommier, H. Tsuji)	
09:50	An Introduction to NIRS	T. Murakami
10:00	Overview of the Carbon Ion Therapy at HIMAC	T. Kamada
10:30	Discussion	
10:40	**Coffee break**	
11:00	Carbon Ion Radiotherapy for Skull Base and Paracervical Tumors	M. Koto
11:15	Carbon Ion Radiotherapy for Malignant Head and Neck Tumors	A. Hasegawa
11:30	Discussion	
11:35	Carbon Ion Radiotherapy in a Hypofraction Regimen for Stage I Non-Small Cell Lung Cancer	N.Yamamoto
11:50	Carbon Ion Radiotherapy for Bone and Soft Tissue Sarcomas	R. Imai
12:05	Discussion	
12:10	Carbon Ion Radiotherapy for Liver Cancer	H. Imada
12:25	Carbon Ion Radiotherapy for Patients with Locally Recurrent Rectal Cancer	M. Shinoto
12:40	Pancreas Cancer	M. Shinoto
12:55	Discussion	
13:00	**Lunch on site**	
13:55	Carbon Ion Radiotherapy for Pancreatic Cancer	H. Tsuji
14:10	**General Discussion**	
	European Clinical Experiences (Chair: M.H. Baron, J. Mizoe)	
14:20	Overview of the Carbon Ion Therapy and Research at HIT	TBD
14:50	Clinical Trials Ongoing and Coming at HIT	S. Combs
15:05	**General Discussion**	
15:20	**Coffee break**	
	Round table about cooperation and data exchanges (Chair: J. Balosso, T. Kamada)	
15:50	The Need of Clinical Outcome Data for Patient Selection Model	B. Ribba
16:10	The Need of Medical Imaging Data for Tumor Motion Simulation	J. Saadé
16:25	**Discussion as a round table for 30 min**	
16:55	**End of the open sessions**	
about 17:30	**Off session discussion about ETOILE-NIRS cooperation**	

Saturday, November 26, 2011

The Landscape of Hadrontherapy in Japan and Europe (II) (Chair: J. Bourhis, T. Kanai from Gunma)(To be confirmed)

08:30	Status of HIMAC	K. Noda
08:45	New particle Therapy Facility in NIRS, Present and Future Plan	T. Shirai
09:00	Current Trends in the Promotion of Carbon-ion Radiotherapy in Japan	A. Kitagawa
09:15	European Organization and Programs for Carbon Ion Therapy	R. Orrechia or M. Dosanjh
09:45	Standards in Particle Therapy	M.F. Moyers
10:05	General Discussion	
10:20	**Coffee break**	

Scientific session

Ion Beam Technology (Chair: J. Collot, K. Noda)

10:35	NIRS Scanning System: Present Status and Future Prospects	T. Furukawa
10:50	Discussion	
10:55	TPS for NIRS Scanning: Present Status and Future Prospects	T. Inaniwa
11:10	Discussion	
11:25	Multi-dimensional Image Guided Particle Therapy	S. Mori
11:30	Discussion	
11:35	Modeling the Clinical and Biol. Effect of Therapeutic Carbon Ion Beam	N. Matsufuji
11:50	Discussion	
11:55	GSI-HIT Scanning System: Present Status and Future Prospects	**Someone from HIT or GSI (To be confirmed)**
12:10	Discussion	
12:15	Imaging System for QI: Present Status and Future Prospects	E. Testa
12:30	General Discussion	
12:45	**End of the symposium**	

Off session specific working party

14:00 17:00	**Workshop for the opening of the HIT-ETOILE trial "PHRC-ETOILE"**	P. Pommier

Sunday, November 27, 2011

The Landscape of Hadrontherapy in Japan and Europe (III) : New Facilities (Chair: R. Mayer, S. Kudo)

09:00	Carbon Ion Therapy at Gunma University	T. Kanai
09:10	CNAO the Italian Particle Therapy Facility	P. Fossati
09:20	The Current Status of Saga-HIMAT	S. Kudo
09:30	MedAustron in Wiener-Neustadt	R. Mayer
09:40	The Belgian Hadron Therapy Center Project: rationale and current status (BHTC in Belgium)	W. De Neve
09:50	Rhön Klinikum AG - University of Marburg	
10:00	NRoCK	
10:10	General Discussion	
10:25	**Coffee break**	

Scientific session

Ion Beam Biology (Chair: C. Rodriguez-Lafrasse, Y. Furusawa)

10:45	Biological specificity of Carbon Ion Beam: Present Status and Future Prospects	C. Rodriguez-Lafrasse
11:15	Discussion	
11:25	RBE of Therapeutic Hadron Beams at Clinical Facilities and the Inter-comparison	Y. Furusawa
11:45	Discussion	
11:55	RBE Modelization: Present Status and Future Prospects	D. Dabli
12:15	General Discussion	

Closing remarks

12:30	Closing remarks	H. Tsujii
	Closing remarks	J. Balosso

13:00 **End of the symposium**

On Thursday 24th evening, before the symposium, in the offices of GCS-ETOILE (60 Avenue Rockefeller, F-69008 Lyon)

17:00	**Workshops for WP2 of ULICE**	WP coordinator(s)
	Other Workshops are possible in the same location on demand	

INDEX

INDEX

Current Status of Carbon Ion Radiotherapy in Japan

Hirohiko Tsujii

National Institute of Radiological Sciences, Chiba, Japan.
Corresponding Author: Hirohiko Tsujii, e-mail address : tsujii@nirs.go.jp

As compared to photon beams, carbon ion beams offer improved dose distributions in cancer radiotherapy, thus enabling dose concentration within a target volume while minimizing the dose in the surrounding normal tissues. Furthermore, carbon ions being heavier than protons provide a higher biological effectiveness, which increases with depth, reaching the maximum at the end of the beam's range. This is an ideal property from the standpoint of cancer radiotherapy. At the National Institute of Radiological Sciences (NIRS), the pioneer clinical study on carbon ion radiotherapy (C-ion RT) was started in 1994 using carbon ions generated by Heavy Ion Medical Accelerator in Chiba (HIMAC). So far, more than 6,000 patients have been treated, where the benefit of C-ion RT over other modalities has been demonstrated for various tumor sites in terms of high local control and survival rates, as well as significant reduction in overall treatment time with acceptable toxicities in most cases. Efficacy of C-ion RT has been also demonstratred in other facilities in the world.

1. Carbon ion therapy facilities

Following the HIMAC, C-ion RT was also started at other facilities in the world: German Ion Research Center (GSI) in Darmstadt, Germany in 1997, Hyogo Ion Beam Medical Center (HIBMC) in Hypgo, Japan in 2001, Institute of Modern Physics (IMP) in Lanzhou, China in 2006, Heavy Ion Therapy facility (HIT) in Heidelberg, Germany in 2009, and Gunma University Heavy Ion Medical Center (GHMC) in Gunma, Japan in 2010. In these five facilities the clinical efficacy of carbon ions has been prospectively investigated in a variety of tumors with successful results. In the Foundation CNAO, Italy, the accelerator complex is completed for proton/carbon treatment. Clinical study on proton therapy started in October 2011 and C-ion RT is due to start in about one year.

As of October 2011, 8 facilities are in operation for ion beam therapy in Japan: 5 for proton therapy, 2 for carbon therapy and one for proton/carbon therapy. Additionally, there are 5 facilities under construction or in preparation: 3 for proton therapy and 2 for C-ion RT. From now on in five years, the number of facilities should become at least 13 in total (Fig 1). It is of note that the technical and clinical achievements of NIRS have led to promotion and dissemination of C-ion RT. The HIBMC was established as the 2nd facility for C-ion RT in Japan and as the first facility in the world employing proton/carbon beams. To date, more than 3,200 patients have been treated. Based on the design study conducted by NIRS, Gunma University constructed a compact facility, 45m x 65m and 20m high, and treated the first patient in March 2010. At present, there are two more facilities to start C-ion RT: one is Saga-HIMAT under construction and the other is Kanagawa Cancer Center in preparation.

As for C-ion RT in the courtiers other than Japan, the first patient was treated in Darmstadt, Germany using GSI's heavy-ion synchrotron, SIS. This accelerator had been jointly used for physics research and clinical

application. The clinical application of SIS was unfortunately terminated in 2008, until then they treated a total of 440 patients with carbon ions. Based on fundamental research on radiobiological effects of ions and development of techniques for treatment planning at GSI, a new facility named Ion Therapy Facility (HIT) was built in Heidelberg. The HIT is the first dedicated proton/carbon therapy facility in Europe. Similar to GSI, an accelerator that was primarily built for physics research has been used for C-ion RT at IMP in China. As compared to standard radiotherapy, they prescribed much higher total dose in smaller fractions for superficial tumors, by which they successfully obtained a high local control with relatively low degree of radiation-induced skin reactions.

Under the license agreement between the GSI and Siemens AG, two facilities modeled on HIT are under construction in Marburg and Kiel in Germany, and one facility in Shanghai, China. At present, however, there is uncertainty whether those institutions will be really built as planned.

Fig 1. Ion Beam Facilities in Japan

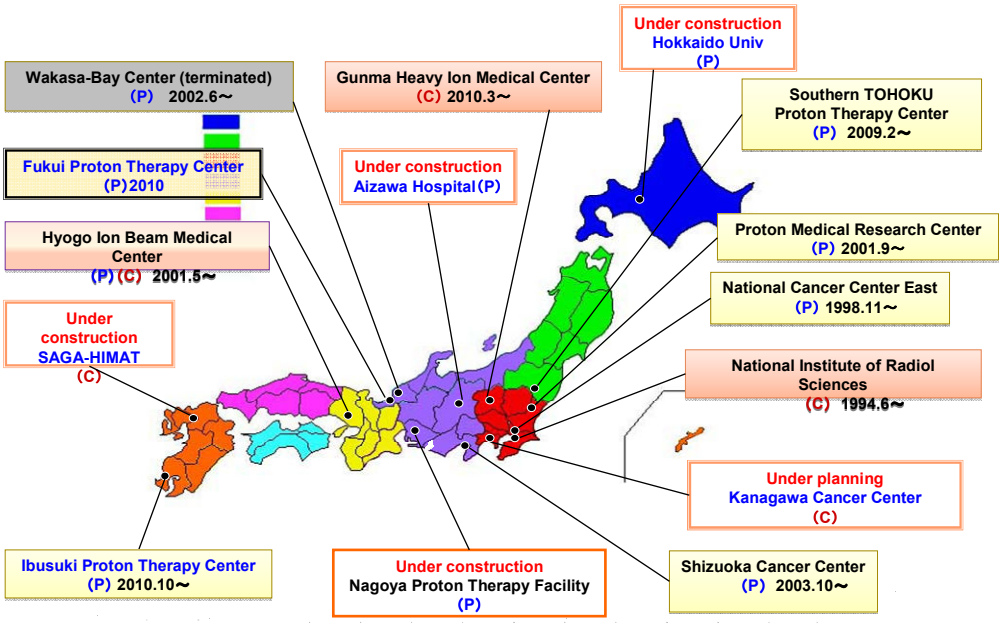

2. Clinical results of carbon ion therapy

In C-ion RT at NIRS, non-squamous cell types of cancer, such as adenocarcinomas and adenoid cystic carcinoma, arising from the head and neck and many other sites have been intensively treated, resulting in improved local control and survival with acceptable toxicities. Bone and soft tissue sarcomas, such as osteosarcoma, chordoma, chondrosarcoma, liposarcoma and malignant fibrous histiocytoma, arising from the pelvis, vertebra/para-vertebral region, and retro-peritoneal region are often found difficult to treat with surgical resection and they are usually photon-resistant, being seldom treated with photon radiotherapy. These types of tumors are good candidates for C-ion RT having advantageous biological effectiveness. Recurrent pelvic tumor of rectal cancer has been also treated with the results being comparable to or even better than surgery. For certain cancers such as malignant melanoma and pancreatic cancer, C-ion RT combined with chemotherapy has

significantly prevented or delayed development of distant metastasis with improved survival and local control.

By taking advantage of unique properties of carbon ions, it has been possible to complete the treatment in a short time and small fractions. For example, stage 1 lung cancer and liver cancer have been treated with only one and two fractions, respectively. Even for prostate cancer and bone and soft-tissue tumors requiring a relatively long course of treatment, only 16 fractions have been sufficient, less than half the number of fractions required in the standard RT. This means that the carbon therapy facility can be operated more efficiently, offering treatment for a larger number of patients than is possible with other modalities over the same period of time.

In contrast to NIRS, GSI/Heidelbeg has been focusing on C-ion RT for head and neck, skull base, and intracranial malignancies. They have also shown excellent results.

3. Development of compact facility and beam scanning method

For successful performance of C-ion RT, fundamental therapeutic techniques have been developed at NIRS. In this context, design and R&D work had been carried out from 2004 to 2006, by which a compact carbon-ion accelerator was successfully developed. Based on this work, a downsized facility, about one-third of the HIMAC in size and construction cost, was constructed at Gunma University (Fig 2), in which the first patient was successfully treated in March 2010. The magnets in the beam transport lines were all made of laminated steel in order to permit a change in the beam line within 1 min. The beam-delivery system employs a spiral beam-wobbling method to form a uniform lateral dose distribution.

In the end of 2010, a new building having 3 treatment rooms was completed next to the HIMAC building. The beam line for carrying out treatment with fast pencil-beam scanning was extended from the HIMAC to the new building, and the first patient was successfully treated with scanning method in May 2011. We intend to develop a respiratory-synchronized irradiation technique for beam scanning method, which will be followed by development of a rotating gantry.

Fig 2. Design and R&D for Compact Facility

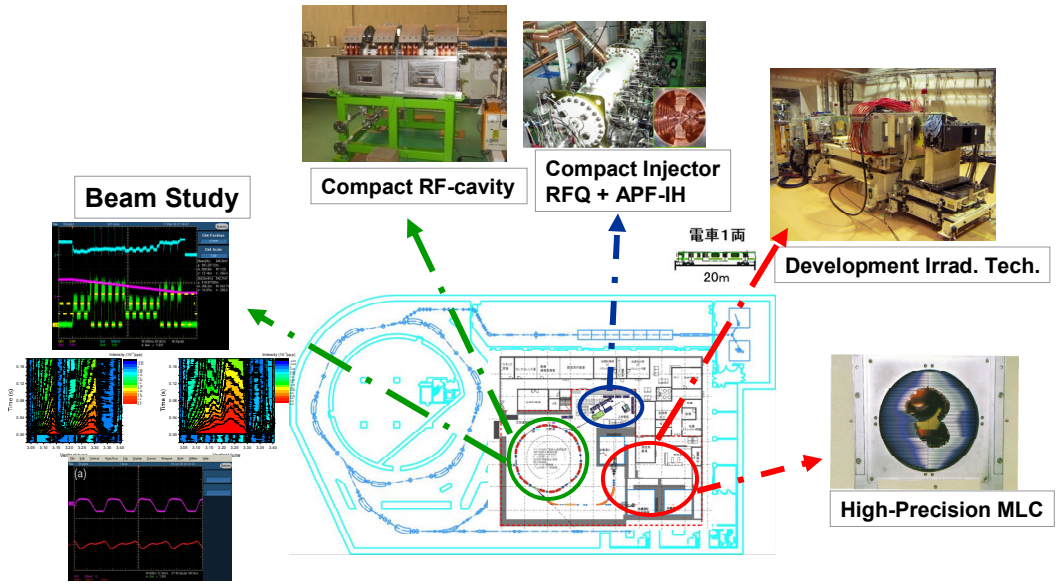

Present Status of Hadrontherapy in France: *France HADRON*

Jean Louis Habrand* and Jacques Balosso[§]

** Université Paris-Sud, Department of Radiation-Oncology at Institute Gustave Roussy, Villejuif, France and Centre François Baclesse, Caen, France,*
§ Joseph Fourier University, Department of Radiation-Oncology, CHU de Grenoble, France and GCS-ETOILE, Lyon, France
e-mail address : habrand@igr.fr & jacques.balosso@centre-etoile.org

Hadrontherapy, the proton and carbon particle therapy, is an advanced form of cancer treatment that takes advantage of the dynamism of oncology in France. It allows the curative treatment of otherwise difficult to cure cancerous tumors that represent 5-10% of the tumors to be irradiated. Even more than conventional radiotherapy, particle therapy is based on particle physics and accelerator technology, areas in which France has global expertise (CERN, CEA, CNRS/IN2P3, GANIL, ESRF, SOLEIL, etc)

Although the protontherapy (hadrontherapy by proton) is already performed in two French centers since 20 years (ICPO in Orsay and Médicyc in Nice) and carbontherapy is developing in Europe and Japan for over a decade, many questions in medicine, biology, physics and technology should be examined further to optimize the treatment process, opening as many opportunities for industrial valorization.

The ***France HADRON*** project filed October 13, 2011 as part of the call for projects of "National Infrastructures for Biology and Health" is based on a multidisciplinary scientific program, organized in four work packages, unifying all French teams, integrated and supported by a national governance coordinated by Jacques BALOSSO (PU-PH, Lyon-Grenoble) and co-coordinated by Jean Louis HABRAND (PU-PH, Caen-IGR). The Work Packages are formed around four main objectives:

- WP1 - How to identify and assess the medical value of hadrontherapy (clinical research)
- WP2 - How to improve treatment plans (modeling and computer simulation)
- WP3 - How to better understand the effect of treatment (radiation biology)
- WP4 - How to improve the quality of treatment (instrumentation).

France HADRON includes actors who are ETOILE in Lyon and ARCHADE in Caen as carbon sites and, as proton sites, the Antoine Lacassagne Centre in Nice, the Institute Curie / ICPO in Paris and the Institute Claudius Regaud in Toulouse but also the CNRS and the IRSN (Radiation protection and nuclear safety institute).

The project received the formal support of INSERM, of the INCa (National Cancer Institute), the CEA, the European consortiia ENGLIGHT (CERN) and ULICE, the academic societies in radiotherapy and more than 16 private and public industrials have formalized their interest in the project for economic developments and the service it will create (high energy particles beam access). Among them are AREVA, EADS-Thales, CNES, IRSN, EDF, GDF-SUEZ, IBA and ten smaller companies.

The project is part of the national strategy for research: particle therapy and its developments in research are explicitly mentioned in the document Strategic Directions for the multi-agency Thematic Institute for Health Technologies issued in March 2010:

"In radiotherapy, the technical platforms are becoming more and more complex in the recent years with the emergence of new technologies .... The development of new methods of irradiation using hadrons (proton or carbon) or the development of compact source of monochromatic X-ray should be the basis for future treatment of radioresistant tumors. The main technological challenges to be resolved include (...):

- The development of efficient and reliable system of quality control of the delivered dose in radiotherapy for personalized treatments based on innovative software components (calculation processing, real-time image guiding, fusion of multimodality patients data), material (accelerators, online dosimetry, imaging, robotics) and methodological (metrological validation, systems integration).
- The achievement of physical and biological data necessary for the development and validation programs for radiotherapy treatment planning (radiobiology and genotyping).
- The development of devices for controlling the beam quality in radiotherapy by relative and absolute dosimetry equipment. "

Each center (node), with its dual structure, care center and research center, is the type of clinical research infrastructure that the Alliance for Life Sciences and Health wishes to develop in France. Finally, the health

project is in line with the recommendations and measures of the Plan cancer 1 and 2 including the centralization at the regional scale of the highly advanced radiation equipment.

This project of national distributed infrastructure aims to develop science, health technology and industry of this sector. Indeed hadrontherapy proton and carbon, with an ultimate potential of a care center for 10 million people in developed countries, represents a very high value market for industrial in the decades to come. Its socio-economic impact is assessed annually as for the care of an amount of 20 to 40 M€ paid each year in the national economy rather than abroad, the creation of twenty jobs related to developments and innovations in medicine and the development of the industrial sector of particle accelerators, instrumentation and new medical equipment.

The governance of France HADRON will be based on a strategic direction, an operational management and a scientific committee. It will have specific financial support and resources made available by the project partners. It will provide direction and coordination of the scientific work, the allocation of beam time, communication, control and reporting to the National Research Agency which will be the funding institution. It will rely on the nodes for the local management of the valorization which is an objective of prime importance.

Training, thanks to multidisciplinary teams, is also at the heart of the Project. It will be integrated into existing training programs at European level and will train professionals from initial training to continuing education (MD, physicists, dosimetrists, technologists) but also organize research training with many master's courses and doctoral programs in conjunction with universities and doctoral schools. Cross-diffusion of scientific communication and activities will valorize and advertise this training.

As a whole, France HADRON represents a comprehensive answer to the challenge of particle therapy in France. All the 5 nodes are build according to the same pattern. In each case the scientific activity is secondary and supported by another activity - mainly medical care - that will make the scientific part free of most of the expenses related to the building, the maintenance and the basic manpower. This way the Infrastructure will be rather economical and the financial contribution of the “investment for future” will really produce a leverage effect (“effet de levier”). Moreover the proximity with operational medical and technical teams will be the warranty of a proper use of the facilities with their own specificities. This will allow an inside dynamic of the researches, not relying only on external proposals and competition. A last we should have active and complementary centres as well in translational activities as in large scale comparative clinical trials. ***France HADRON*** will ultimately sustain and promote a very competitive level of hadrontherapy in France and in Europe.

An Introduction to NIRS

Takeshi Murakami

Research Center for Charged Particle Therapy, National Institute of Radiological Sciences, Chiba, Japan
Corresponding Author: Takeshi Murakami, e-mail address: muraka_t@nirs.go.jp

Abstract

National Institute of Radiological Sciences (NIRS) was founded in 1957, when radiation the effects on humans and the environment generated international concern because of nuclear tests and accidental radioactive contamination. The Japanese government, which posted a policy of peaceful application of radiation, established an institute, NIRS, for studying the effects of radiation, medical applications, and establishment of safety measures. Since then, NIRS has been actively working in these fields.

History

National Institute of Radiological Sciences (NIRS) was founded in 1957. In those days, a series of nuclear weapons tests, especially above-ground tests, in the Cold War era caused international concern about the effects of radiation on the environment as well as on human beings. In 1954, a Japanese fishing boat, Daigo Fukuryū Maru ("Lucky Dragon No. 5"), came in direct contact with the fallout from a thermonuclear hydrogen bomb near Bikini atoll. This was one of the most significant accidents involving radioactive contaminations. This accident, combined with memories of the tragedies in Hiroshima and Nagasaki, reignited Japanese concerns about radiation.

At that time, the Japanese government was just beginning to develop a policy advocating the peaceful application of radiation, including construction of atomic power plants, and investigating the application of radioactive materials for industry and medicine. Because of this situation, the Japanese government had to quickly establish some measures to ensure the safety of radiation use. Thus, the Japanese government decided to establish a new institute, and founded NIRS in 1957.

The objectives of NIRS were set as follows:

1. To study the effects of radiation on humans and the environment, as well as methods of ensuring their protection, and for diagnosis and treatment for radiation exposure.
2. To study the medical applications of radiation.
3. To provide education and training for human resources.

A few years later, the development of countermeasures for accidental radiation emergencies was established as one of the main fields for the institute objectives.

Organization

One of the characteristics of NIRS is its heterogeneity, i.e. its broad spectrum of the research fields and researchers. Although NIRS is a science institute, it has a working hospital for roentgenology. Thus, there is sizable medical staff, including medical doctors, radiological technologists, and nurses. On the other hand, for carbon-ion radiotherapy needs a large accelerator, i.e. HIMAC (Heavy Ion Medical Accelerator in Chiba). Furthermore, several cyclotrons are currently being used in order to produce radioisotopes for diagnostic and

research purposes. Thus, there are physicists and engineers involved in the development, operation and maintenance of these large facilities. Needless to say, numerous biologists work at the institute, because studying methods of radiation protection and predicting/evaluating the effects of radiation on humans and the environment are centerpieces of biology.

These researchers belong to several research centers. At present, there are five research centers and the three administrative sections. They are the following:

- Research Center for Charged Particle Therapy
- Research Center for Radiation Protection
- Research Center for Radiation Emergency Medicine
- Molecular Imaging Center
- Research, Development and Support Center

There are a total of 814 staff members (490 full time workers), including medical staff, scientists, engineers, and administrators, who currently work for NIRS. The part-time workers include post-doctoral fellows, as well as technical and administrative workers.

Research Fields

Although each center concentrates on its own mission, the research activities generally span several centers. For example, there some biologists in the Research Center for Charged Particle Therapy, and the Cyclotron facilities belonging to the Molecular Imaging Center are operated by crews from the Research Center for Charged Particle Therapy.

1. Carbon-ion Radiotherapy

One of the highlights of NIRS achievements is the success of carbon-ion radiotherapy using HIMAC. Since this symposium is focused on carbon-ion therapy, a more detailed discussion can be found in other articles. Here we will list just a few points worth noting. First, NIRS has a long history of studying radiation therapy, using X-rays, protons and neutrons. Such experience contributed to the success of the carbon-ion radiotherapy. Second, we think that the domestic and international promotion of carbon-ion radiotherapy is an important job for NIRS, as is the development of further improvements of heavy-ion radiotherapy. The promotion includes exchanges and/or education of human resources. This point is also detailed in other article. Third, the New Particle Therapy Research Facilities for the fast scanning system just started operating.

New Particle-Therapy Research Facilities.

2. Radiation Protection

Radiation protection and the assessment of the effects of radiation on humans are still an important area of research. Recently not only the radiation from the environment but also the man-made radiation exposure has become more important. People are concerned abut the effects of low dose exposure and the effects on children, which are not clear at present. Recently, the regulations have been increasing in an expanding and complicated

society. Therefore, encouragement and advice about reasonable regulations has become an important job for NIRS.

3. Radiation Emergency Medicine

NIRS has been designated to be a core organization of the National Cooperation System for Radiation Emergency Medicine. A team named the REMAT (Radiation Emergency Medicine Assistant Team) was organized for international cooperation. So far, NIRS has worked on small and large-scale accidents involving radiation contamination, including the Chernobyl accident, the JCO accident in Tokai village, and recently the Fukushima Nuclear Power Plant Accident. The activities of NIRS include:

- Dispatching experts to a site
- Accepting and diagnosing people possibly exposed to radiation, and giving medical treatment, if necessary
- Measuring and/or estimating radiation contamination
- Arranging experts in government offices to provide advice
- Delivering lectures and consulting with the public, etc.

4. Molecular Imaging

Molecular imaging is a new field, in which the molecular behavior and function in the living body is visualized non-invasively. It employs technologies such as positron emission tomography (PET), magnetic resonance imaging (MRI), etc. NIRS is currently operating large and small-size cyclotrons, which are producing some of the necessary radioisotopes for these procedures. An example application of this technology is diagnosing a tumor by 11C-Methionine PET. The activity of this center includes the development of new hardware, such as Open-PET. It may also explore on-site imaging being used in particle radiotherapy.

5. Technical Support, Training, and Education

Various facilities and standard irradiation devices, including X-ray irradiation facilities, a neutron irradiation facility, PIXE, and a micro-beam system, are being operated in NIRS. The maintenance of the animal care system is also important. Various types of training courses are regularly held for outside workers related to radiation, and special seminars and training courses are held on request.

Collaboration with Other Institute, Domestic and International Institute

NIRS collaborates with other institutions and universities, including more than 100 domestic organizations and about 20 foreign organizations. With some of the universities, NIRS provides a cooperation agreement for graduate students. Based on these agreements, a lot of students are able to work at NIRS. Furthermore, about 1000 researchers are registered as collaborators participating in research being performed at NIRS. Cooperation with international organizations is also important. NIRS works with more than 10 international organizations, including IAEA, ICRU, UNSCEAR, etc. NIRS is a collaborating center of IAEA.

Summary

NIRS was founded to study the effects of radiation, its potential medical applications and to establish safety measures, and is actively working in those fields. Collaborations with other institutes are extending to not only domestic but also international organizations. NIRS now welcomes cooperative research with and visits of outside researchers.

Overview of the Carbon Ion Radiotherapy at HIMAC

Tadashi Kamada, MD, PhD

Research Center for Charged Particle Therapy, National Institute of Radiological Sciences, Chiba, Japan
Corresponding Author: Tadashi Kamada, e-mail address:t_kamada@nirs.go.jp

Abstract

In 1994, carbon ion radiotherapy (CIRT) was begun at the research center for charged particle therapy, NIRS (National Institute of Radiological Sciences) using the Heavy Ion Medical Accelerator in Chiba (HIMAC), which was the world's first heavy ion accelerator complex dedicated to medical use. Among several types of ion species, carbon ions were selected for cancer therapy because they were presumed to possess optimal properties in terms of biologically effective dose localization. Since June 1994, almost 50 clinical protocols of CIRT have been conducted in an attempt to determine the optimal dose-fractionation and irradiation method for the treatment of specific diseases. Until August 2011, a total of more than 6000 patients had been registered on to these protocols. These clinical studies revealed that many cancers can be cured safely with a shorter treatment period than conventional radiation. Based on these experiences, we embarked on the research and development of a new generation beam delivery facilities such as a 3D-scanning method with a pencil beam and a compact rotating gantry. A clinical research using the pencil beam scanning was in operation since May 2011.

Introduction

In Japan, the decision for a medical use of heavy ions was made in 1984 at NIRS. HIMAC was the world's first heavy ion accelerator complex intended primarily for clinical use. The accelerator complex took almost a decade to build and was completed by the end of 1993. Almost 6 months later, in June1994, clinical trials using carbon ion beams generated from the HIMAC were initiated. The HIMAC has operated since its opening as a multipurpose facility available for joint cancer treatment and research in biology and physics by both Japanese and foreign investigators.

CIRT at NIRS

The HIMAC has 3 treatment rooms with fixed vertical and/or horizontal beam lines. In order to conform the dose to a target volume, a passive beam delivery method was employed. The beam lines in the treatment room are equipped with a pair of wobbler magnets to modulate the beam width, plus beam scatterers, ridge filters, multileaf collimators, and the ability to administer a compensation bolus. An appropriately sized ridge filter, which corresponds to, and determines the size of the spread-out Bragg peak (SOBP), is chosen to avoid unnecessary dose to normal tissues along the beam path in each port. The patients are positioned in customized cradles and immobilized with a low-temperature thermoplastic. A set of CT images are taken for treatment planning with the immobilization devices in place. Respiratory gating of both the CT acquisition and the therapy is performed when indicated. Three-dimensional treatment planning is performed using our original HIPLAN software, which was developed for CIRT. A margin of 5 mm is usually added to the clinical target volume to create the planning target volume. Dose is calculated for the target volume and any nearby critical structures and

expressed in Gray-Equivalent (GyE = carbon physical dose in Gray x Relative Biological Effectiveness {RBE}). CIRT is given once daily, on 4 days per week (Tuesday to Friday). At every treatment session, the patient's position is verified with a computer-aided online positioning system.

Since June 1994 until spring 2011, almost 50 protocols have been conducted in an attempt to determine the optimal dose-fractionation and irradiation method for the treatment of specific diseases. The HIMAC passive beam delivery system has been showing quite reliable and stable performance for last 17 years, and until August 2011, a total of more than 6000 patients had been registered. (Figure 1)

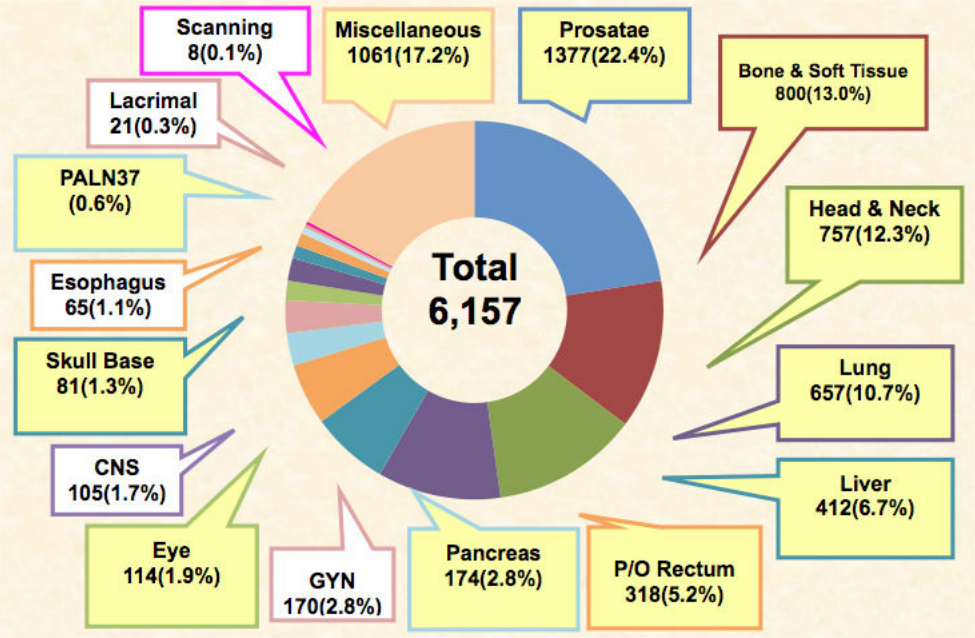

Figure 1. Patient distribution enrolled in carbon ion radiotherapy at NIRS from June 1994 to August 2011.

The categories of disease that can be treated in routine clinical practice include lung cancer, prostate cancer, head and neck cancer, skull base tumors, ocular melanoma, bone and soft-tissue sarcoma, liver cancer, and pelvic recurrences of rectal cancer. The number of patients has increased year by year, and the facility has meanwhile reached a capacity permitting nearly 700 new patients to be treated each year. The clinical trials began with a small dose per fraction. At first, the average number of fractions was almost 18. All these early trials were carried out as dose escalation studies. It was found that a very high dose per fraction could be administered, and the average number of fractions could be reduced from 18 to 12-13 over the last several years, leading to improvements in patient throughput.

The clinical results are summarized as follows. By location, it is effective in the head and neck (including the eye), the base of the skull, lung, liver, prostate, bone and soft tissue, and pelvic recurrence of rectal cancer. By pathological type, carbon ion therapy is effective against adenocarcinoma for which photon beams are relatively ineffective, as well as against sarcomas of the bone and soft tissue. CIRT offers significant advantages over conventional radiotherapy due to its extremely favorable physical and biological dose distribution. These unique features lend themselves to convenient hypofractionated regimens. For lung and liver cancer, in particular, an ultrashort irradiation schedule with only 1 or 2 sessions is available. For prostate, head and neck, base of the skull, pelvic recurrence of rectal cancer, and bone and soft-tissue sarcomas, treatments with 12 fractions over 3 weeks are possible. Toxicities initially associated with dose escalation are no longer encountered. But clinical trials need to be continued not the least to investigate if the therapeutic outcome of up to now intractable tumors

such as cancer of the pancreas, can also be improved. Details of clinical results will be discussed later on in this symposium.

Future Prospect in Carbon Ion Radiotherapy

In so many countries the number of patients with cancer is increasing steadily. The development of therapies to cure cancer with safety and assurance, and with less suffering, is strongly desired by all these countries. Owing to the results of our studies, CIRT has been recognized as a treatment that can achieve this goal, however, it has to be admitted that CIRT is rather costly. The HIMAC with its 42-meter-diameter synchrotron ring was built at costs of roughly 33 billion JPY (about 400 million USD). For the benefits of carbon ions to be available to the public at large, it is of paramount importance to develop a lower-cost and more compact system. In view of this, NIRS embarked on the development of a compact system that has the same performance as the HIMAC at about one third of its cost and size. In March 2010, the new compact facility developed by NIRS was completed at the Gunma University in Maebashi, Japan. They started carbon beam treatment as the third CIRT center in Japan - after NIRS and Hyogo Ion Beam Medical Center.

More than 7,500 patients have been treated with carbon ion beams worldwide since 1994, and nearly 80% were treated at NIRS. At this moment, five carbon ion beam facilities are operating, including the facility at Gunma University. Five more facilities are under construction including the Saga HIMAT in Japan and planning is in progress at ten or more institutions worldwide. There has been a growing interest to use CIRT for cancer treatment in the last decade. NIRS has been pivotal in providing the preclinical and clinical data for this field that have successfully been reproduced at other facilities.

The future development and expansion of CIRT requires further progress. The new NIRS system with 3D scanning and a compact rotating gantry using super-conducting magnet should be instrumental in that respect. Next-generation CIRT equipment will provide more advanced treatment at a drastically reduced cost. To achieve this, cooperation between equipment manufacturers and researches in this field is indispensable, and government support is undoubtedly critical.

Summary

CIRT at NIRS has made significant progress, with a total of more than 6000 patients registered by the end of August 2011. The therapeutic results are internationally acknowledged. A considerable number of CIRT systems are under construction, offering the prospect of achieving more reliable and safer cancer therapy in the near future. Studies conducted over the past 17 years have made it possible to reduce the cost of a CIRT system to about 1/3 that of HIMAC. Next-generation CIRT equipment will provide more advanced treatment at a drastically reduced cost. To achieve this, cooperation between manufacturers, researchers, and government is indispensable. Future CIRT will provide cancer treatment with less suffering for many intractable cancers using more advanced systems and hopefully recent molecular biological techniques.

Carbon Ion Radiotherapy for Skull Base and Paracervical Tumors

Masashi Koto, Azusa Hasegawa, Ryo Takagi, Akira Fujikawa, Takamichi Morikawa, Hirohiko Tsujii, and Tadashi Kamada

Research Center for Charged Particle Therapy, National Institute of Radiological Sciences, Chiba, Japan.

E-mail: koto@nirs.go.jp

Abstract

Purpose: To estimate the toxicity and efficacy of carbon ion radiotherapy for skull base and paracervical tumors in clinical trials.

Patients and Methods: A phase I/II dose escalation study for skull base and paracervical tumors was initiated in April 1997. The patients were treated with 16 fractions for 4 weeks with a total dose of 48.0, 52.8, 57.6, or 60.8Gy equivalents (GyE). In April of 2004, a phase II study was initiated with an irradiation schedule of 60.8GyE in 16 fractions over four weeks. There were 76 patients included in the analysis. Histologically, 44 patients had chordoma, 12 chondrosarcoma, 9 olfactory neuroblastoma, 7 malignant meningioma, 1 giant cell tumor, and 1 had a neuroendocrine carcinoma. The patients were treated with a dose of 48.0 GyE (4 patients), 52.8 GyE (6 patients), 57.6 GyE (9 patients) or 60.8 GyE (57 patients).

Results: The follow-up periods ranged from 3 to 158 months, with a median period of 46 months. At the time of the analysis, there was no evidence of any serious acute (Grade ≥4) or late (Grade ≥3) reactions. The 5-year local control and overall survival rates for all patients were 88% and 82%, respectively. The 5-year local control and overall survival rates for chordoma patients were 88% and 87%, respectively.

Conclusion: A carbon ion dose of 60.8GyE in 16 fractions was effective and safe for the treatment of skull base and paracervical tumors.

Introduction

The limiting factor for photon radiotherapy conventionally applied to skull base and paracervical tumors is the adjacent normal tissue, leading to poor local control by photon radiotherapy. On the other hand, proton radiotherapy with its superior physical-spatial distribution has provided a major improvement in local control with regard to the possibility of dose escalation. It has been pointed out, however, that in certain patient groups, it is difficult to achieve local control with proton radiotherapy, even at elevated doses. It has thus been recognized that 1) chordoma patients have a worse prognosis than chondrosarcoma patients, 2) among the chordoma patients, the prognosis for paracervical chordoma patients is worse than for patients with skull base chordomas, and it is worse for females than for males. Therefore, the high LET of carbon ion radiotherapy has promising potential for treatment of these intractable skull base and paracervical tumors.

Patients and Methods

1. Protocol

A phase I/II clinical trial using a schedule of 16 fractions over 4 weeks was initiated in April 1997. Chordoma, chondrosarcoma, meningioma, and other tumors arising from the skull base or paracervical spine located superior to the C2 vertebra were targeted. Only patients with residual tumors after surgery or with inoperable tumors were permitted to enroll in the carbon ion radiotherapy study. The eligibility criteria for enrollment in this clinical trial were the presence of a histologically proven tumor, patient age ranging from 15 to 80 years, a KPS of 60% or more, neurological function of grade I or II, the absence of anti-cancer chemotherapy within the previous four weeks, asurvival expectancy of six months or more, and no distant metastasis.

2. Treatment planning

A set of 2.5-mm-thick CT images was taken for treatment planning, with the patient placed in a custom-made immobilization device with a dental mouthpiece. The metals in the oral cavity were removed before the treatment planning CT to avoid artifacts on CT images including the tumor. The gross tumor volume (GTV) was delineated on the CT images using CT-MRI fusion. The clinical target volume was defined with an adequate safety margin for the GTV. A margin of 5 mm was usually added to the CTV to create the planning target volume. In case where the tumor was close to critical organs, such as the brain stem or spinal cord, the CTV margin was reduced to spare these organs. Three-dimensional treatment planning was performed with the HIPLAN software program (National Institute of Radiologic Sciences, Chiba, Japan) designed for carbon ion therapy. Carbon ion radiotherapy was given once daily, 4 days a week. The patients were treated with two to five ports. One port was used in each treatment session. At every treatment session, the patient's position was verified with a computer-aided on-line positioning system. The patient was positioned on a treatment couch with the immobilization devices, and digital orthogonal X-ray TV images in that position were taken and transferred to the positioning computer. They were compared with the reference image on the computer screen and the differences were measured. The treatment couch was then moved to the matching position until the largest deviation from the field edge and iso-center position was less than 2 mm.

3. Patients

The carbon ion dose was escalated in successive stages: 48 GyE in 4 patients, 52.8GyE in 6 patients, 57.6GyE in 9 patients and 60.8GyE in 9 patients. The phase I/II clinical trial was concluded in February 2004, and in April 2004, a phase II clinical trial was initiated under the Highly Advanced Medical Technology scheme, with an irradiation schedule of 60.8 GyE in 16 fractions over 4 weeks. Forty-eight patients were enrolled in this trial until February 2011.The 76 patients included in the analysis consisted of 32 males and 44 females. Their ages ranged from 16 to 78 years, with a median of 50 years. Histologically, 44 patients had chordoma, 12 chondrosarcoma, 9 olfactory neuroblastoma, 7 malignant meningioma, 1 giant cell tumor, and 1 had neuroendocrine carcinoma. Sixty-one tumors were located in the skull base region and 15 in the paracervical region.

4. Statistical analysis

Acute toxicity was assessed based on the Radiation Therapy Oncology Group (RTOG) score, and late toxicity was determined based on the RTOG/European Organisation for Research and Treatment of Cancer (EORTC) score. Local control and overall survival rates were calculated according to the Kaplan-Meier method.

Results

1. Toxicity

The follow-up periods ranged from 3 to 158 months, with a median period of 46 months. Acute reactions were of a minor nature, as one of the patients in the 48 GyE group showed a grade 3 skin reaction, and one patient in the 57.6GyE group and 3 patients in the 60.8 GyE group developed a grade 3 mucosal reaction. A late grade 2 brain reaction was detected in one of the patients in the 57.6 GyE group and 2 patients in the 60.8GyE group, but no other adverse reactions were observed. At the time of analysis, there was no evidence of any serious acute (≥ Grade4) or late (≥Grade3) reactions.

2. Local Control and Survival

The effect on the tumor was primarily stable disease within six months after carbon ion radiotherapy, and there were no significant changes in tumor size in most cases during the follow-up periods. Local control was defined as showing no evidence of tumor regrowth by MRI, CT, physical examination, or biopsy. The 5-year local control and overall survival rates for all patients were 88% and 82%, respectively (Fig. 1). The 5-year local control rate according to histological types was 88% for the 44 chordomas, 86% for the 12 chondrosarcomas, 100% for the 9 olfactory neuroblastomas, and 80% for the malignant meningiomas. The five-year overall survival rate was 87% for patients with chordomas, 63% for chondrosarcomas, 56% for olfactory neuroblastomas, and 69% for malignant meningiomas. The 5-year local control and overall survival rates for the patients treated with a dose of 60.8 GyE were 91% and 77%, respectively.

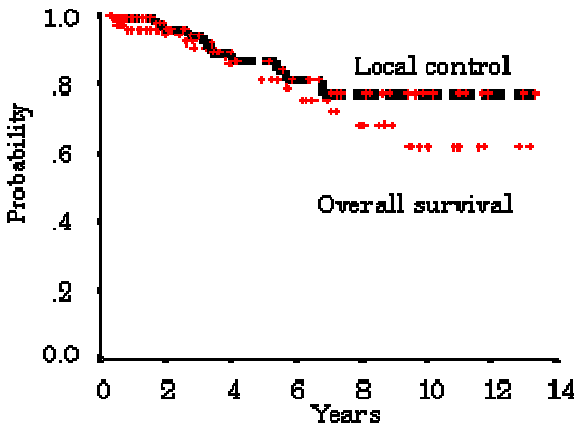

Fig. 1. The local control and overall survival of skull and paracervical cancer patients treated with carbon ion radiotherapy (n=76).

3. Chordomas

Of the 76 patients, 44 patients (58 %) had chordomas. The 5-year local control and overall survival rates of these patients were 88% and 87%, respectively. Of the 44 patients, 6 patients developed in-field recurrence. The local recurrence (in-field) patterns for chordomas were analyzed (Table 1). All of the recurrent sites were located on the edge of the tumors. There were no patients with in-field recurrence from the center of the tumor. Of the 6 who developed in-field recurrence, 4 of the sites were very close to an organ at risk, such as the brain stem or spinal cord.

Table 1. Local recurrence patterns of chordomas

	Age	Gender	Tumor location	Dose (GyE)	Recurrent site
1	47	F	P	48.0	Marginal (spinal cord)
2	64	F	P	57.6	Marginal (pharynx)
3	63	M	P	60.8	Marginal (pharynx)
4	67	F	P	60.8	Marginal (spinal cord)
5	47	F	S	52.8	Marginal (brain stem)
6	30	M	S	60.8	Marginal (brain stem)

* P: paracervical, S: skull base

Discussion

A carbon ion dose of 60.8GyE shows excellent local control. Additionally, we did not observe any severe toxicity to critical organs, such as the brain stem, spinal cord or optic nerves at any of the doses used. Beginning in April 2004, a phase II trial using carbon ion radiotherapy was initiated under the Highly Advanced Medical Technology scheme with an irradiation schedule of 60.8 GyE in 16 fractions over 4 weeks.

High LET charged particles such as carbon ions have excellent dose localizing properties, and this can cause severe damage to the tumor while minimizing the effect on normal tissues. When the tumor was located close to critical organs, delineation of the clinical target volume was done in an effort to prevent damage to these organs. In particular, when both optic nerves were involved in the high dose area, treatments were planned to spare the contralateral optic nerve and chiasm based on our previous dose criteria [1]. For tumors close to the brain stem or spinal cord, we recommended surgical resection to create a space between the tumor and these organs before carbon ion radiotherapy was administered. This allowed for better prevention of severe toxicity to the brain stem and spinal cord, and may have improved the local control rate, because most local recurrences arise from the marginal site adjacent to the critical organs. Tumors such as chordomas can only be judged on the results of the long-term prognosis. Consequently, it will take more time to reach a definitive conclusion about the efficacy of the carbon ion radiotherapy in our series of patients. However, it is already clear that, compared with photon or other charged particle radiotherapy, carbon ion radiotherapy will provide higher local control rates with lower toxicity to the surrounding normal tissues (Table 2) [2-14].

Table 2. The clinical characteristics of the reported cases of skull base chordoma

			Median	Median f/u	Local control rate (%)		
	Authors	N	dose	(y)	3-y	5-y	10-y
Photon	Catton et al . [4]	24	50	5.2		23	15
	Romero et al. [5]	18	50	3.1		17	
	Forsyth et al. [6]	39	50	8.3		39	31
	Magrini et al. [7]	12	58	6		25	25
Proton (+/- photon)	Munzenrider et al. (MGH) [8]	169	66-83	3.4		73	54
	Noel et al (CPO) [9]	100	67	2.6	86 (2y)	54 (4y)	
	Igaki et al. (Tsukuba) [10]	13	72	5.8	67	46	
	Ares et al. (PSI) [11]	42	73.5	3.2 (mean)		81	
Helium	Castro et al. (LB) [12]	53	65	4.3		63	
Carbon	Shults-Ertner et al. (GSI) [13]	96	60	2.6 (mean)	81	70	
	NIRS [14]	39	60.8	4.7		82	82

Conclusions

In this phase I/II clinical study for skull base and paracervical tumors, a dose escalation study was performed up to the fourth-stage dose level. Finally, a dose fractionation regimen of 60.8GyE in 16 fractions over 4 weeks was recommended. Our data from a phase I/II study have demonstrated that a carbon ion dose 60.8GyE was effective and safe for the treatment of skull base and paracervical tumors.

References

［1］ Hasegawa A, Mizoe J, Mizota A, Tsujii H. Outcomes of visual acuity in carbon ion radiotherapy: analysis of dose–volume histograms and prognostic factors. *Int J Radiat Oncol Biol Phys*, 2006; 64: 396-401.

［2］ Tsujii H, Mizoe J, Kamada T, *et al*. Overview of clinical experiences on carbon ion radiotherapy at NIRS. *Radiother Oncol* 2004;73:41–49.

［3］ Tsujii H, Mizoe J, Kamada T, *et al*. Clinical results of carbon ion radiotherapy at NIRS. *Radiat Res* 2007;48:A1–13.

［4］ Catton C, O'Sullivan B, Bell R, *et al*: Chordoma: Long-term follow-up after radical photon irradiation. *Radiother Oncol.* 1996; 41: 67-72.

［5］ Romero J, Cardenes H, la Torre A, *et al*: Chordoma: Results of radiation therapy in eighteen patients. *Radiother Oncol.* 1993; 29: 27-32.

［6］ Forsyth PA, Cascino TL, Shaw EG, *et al*: Intracranial chordomas: A clinicopathological and prognostic study of 51 cases. *J Neurosurg.* 1993; 78: 741-747.

［7］ Magrini SM, Papi MG, Marletta F, *et al*: Chordoma- natural history, treatment and prognosis. The Florence Radiotherapy Department experience (1956-1990) and a

critical review of the literature. *Acta Oncol.* 1992; 31: 847-851.

［8］ Munzenrider JE, Liebsch NJ: Proton therapy for tumors of the skull base. *Strahlenther Onkol.* 1999; 175: 57-63.

［9］ Noël G, Habrand JL, Jauffret E, *et al*: Radiation therapy for chordoma and chondrosarcoma of the skull base and the cervical spine. Prognostic factors and patterns of failure. *Strahlenther Onkol.* 2003; 179: 241-248.

［10］ Igaki H, Tokuuye K, Okumura T, *et al*: Clinical results of proton beam therapy for skull base chordoma. *Int J Radiat Oncol Biol Phys.* 2004; 60: 1120-1126.

［11］ Ares C, Hug EB, Lomax AJ, *et al*: Effectiveness and safety of spot scanning proton radiation therapy for chordomas and chondrosarcomas of the skull base: first long-term report. *Int J Radiat Oncol Biol Phys.* 2009; 75: 1111-1118.

［12］ Castro JR, Linstadt DE, Bahary JP, *et al*: Experience in charged particle irradiation of tumors of the skull base: 1977-1992. *Int J Radiat Oncol Biol Phys.* 1994; 29: 647-655.

［13］ Schulz-Ertner D, Karger CP, Feuerhake A, *et al*: Effectiveness of carbon ion radiotherapy in the treatment of skull-base chordomas. *Int J Radiat Oncol Biol Phys.* 2007; 68: 449-457.

［14］ Mizoe J, Hasegawa A, Takagi R, , *et al*: Carbon ion radiotherapy for skull base chordoma. *Skull Base,* 2009; 19: 219-224.

Carbon Ion Radiotherapy for Malignant Head-and-Neck Tumors

Azusa Hasegawa, Masashi Koto, Ryo Takagi, Akira Fujikawa, Takamichi Morikawa,
Tadashi Kamada, and Hirohiko Tsujii

Research Center for Charged Particle Therapy, National Institute of Radiological Sciences, Chiba, Japan.
E-mail: azusa@nirs.go.jp,

Abstract

To evaluate the efficacy of carbon ion radiotherapy for malignant head-and-neck tumors.

Between April 1997 and February 2011, 407 cases with locally advanced, histologically proven, and primary or recurrent malignant tumors of the head-and-neck were treated with carbon ions. Treatment dose was 64.0 GyE in 16 fractions over 4 weeks (or 57.6 GyE when a wide area of skin was included in the target volume).

There were no acute reactions worse than grade 3 and no late toxicities worse than grade 2. The five-year local control and overall survival rates were 73% and 53%, respectively. But the five-year local control rate was 24% for bone and soft tissue sarcomas, and the five-year overall survival rate was 35% for malignant melanomas.

Carbon ion radiotherapy for malignant head-and-neck tumors can be described as presenting no clinical problems. Although local control of carbon ion radiotherapy was promising for malignant head-and-neck tumor excluding sarcoma, the survival rate was not commensurate with the favorable local control rate of malignant melanoma. On the basis of the results of the analysis, this part of the study was divided into two additional protocols, one for bone and soft tissue sarcomas and another for mucosal malignant melanomas.

1. Phase II Clinical Trial for Malignant Head-and-Neck Tumors (Protocol 9602)

Introduction

A clinical trial of carbon ion radiotherapy for malignant head-and-neck tumors was conducted under the "Phase I/II Clinical Trial (Protocol 9301) on Heavy Particle Radiotherapy for Malignant Head-and-Neck Tumors", that was initiated in June 1994 by way of a dose escalation study using18 fractions over 6 weeks. This trial was followed by another dose escalation study that commenced in April 1996 under the title of "the Phase I/II Clinical Trial (Protocol 9504) on Heavy Particle Radiotherapy for Malignant Head-and-Neck Tumors" using 16 fractions over 4 weeks. Based on the outcome of these two studies [1], the "Phase II Clinical Trial on Heavy Particle Radiotherapy for Malignant Head-and-Neck Tumors (Protocol 9602)" was initiated using 64.0GyE in16 fractions over 4 weeks (or 57.6 GyE in16 fractions over 4 weeks when a wide area of skin was included in the target volume) in April 1997 (Fig. 1).

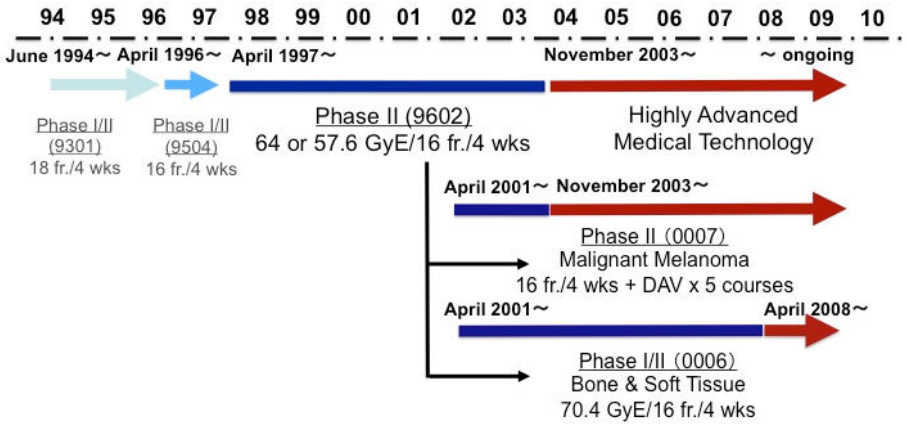

Figure 1. Carbon Ion Radiotherapy for Malignant Head-and-Neck Tumors

Patients and Methods

The eligibility criteria for enrollment in this phase II study were the presence of histologically proven malignancy, a measurable tumor in the head-and-neck region including N0M0 in principle, with no co-existent malignant active tumor, no distant metastasis to other parts, an age range from 15 to 80 years and a prospective prognosis of at least 6 months or longer. The candidates were also required to have a Karnofsky performance status index (KPS) of 60% or more and to give their written informed consent for inclusion in this clinical study. A further requirement was the absence of prior radiotherapy for the carbon-ion treated area, the absence of intractable inflammatory lesion and an interval of at least four weeks from completion of the last chemotherapy.

The phase II study commenced in April 1997, and by February 2011 a total of 409 patients with 412 lesions was registered (three patients had secondary lesions after the initial treatment). Five of the 409 patients were excluded from the analysis because of 1) carbon ion radiotherapy had to be cancelled for two patients with malignant melanoma due to a deterioration of their symptoms, 2) one patient with lacrimal gland tumor was diagnosed as a metastasis from the thyroid gland before carbon ion radiotherapy, 3) the ameloblastoma patient was diagnosed as a benign tumor after histological re-examination and 4) the histological confirmation was done by cytology only. The data for 407 lesions of 404 patients treated until February 2011 are recorded as follows: Patient age range was from 16 to 80, with a median of 58 years, with 192 males and 212 females. Histologically, the tumors were classified as follows: 151 with adenoid cystic carcinoma, 102 with malignant melanoma, 50 with adenocarcinoma, 25 with squamous cell carcinoma, 15 with mucoepidermoid carcinoma, 13 with papillary adenocarcinoma, 7 with acinic cell carcinoma, 7 with undifferentiated carcinoma, 6 with osteosarcoma and 31 with other histological types. There were six cases of T1, 34 of T2, 63 of T3, 174 of T4, 92 of post operative, 27 of post chemotherapy, 9 of post operative and post chemotherapy and one of post carbon ion radiotherapy. Carbon ion radiotherapy was administered using 16 fractions over 4 weeks. The 407 lesions were irradiated with a dose of 57.6GyE in 265 cases and with 64.0GyE in 142 cases.

Results

Acute reactions were of a minor nature, as 16 patients (4%) showed a grade 3 skin reaction, 68 patients (17%) showed a grade 3 mucosal reaction. Late toxic reactions comprised of a grade 2 skin reaction in 8

patients (2%) and mucosal reactions in 14 patients (4%), with no evidence of radiation-induced toxicities worse than these. This therapy can therefore be described as presenting no clinical problems.

The local tumor reactions within six months consisted of CR for 51 patients, PR for 190 patients, NC for 162 patients, and PD for 5 patients. The response rate was 59%. The five-year LC and OS rates were 73% and 53%, respectively. The five-year LC rate according to histological type was 77% for the 50 adenocarcinomas, 74% for the 151 adenoid cystic carcinomas, 79% for the 102 malignant melanomas, 77% for the 25 squamous cell carcinomas and 24% for the 14 bone and soft tissue sarcomas. The five-year OS rate was 62% for adenocarcinomas, 72% for adenoid cystic carcinomas, 35% for malignant melanomas.

Discussion

The overall LC rate was 73% at 5 years. The therapeutic effectiveness was particularly outstanding for adenoid cystic carcinoma, a tumor type that is intractable to photon radiotherapy. Treatment results of surgery with or without radiotherapy ranged from 56% to 93% for the five-year LC rate and from 57 to 77% for the five-year survival rate [2-5] (Table 1). In the present study, the five-year LC rate was 74%, in spite of including 78 cases (52%) of T4 and 40 cases (26%) that had recurrent tumors after surgery and/or chemotherapy.

Table1. Clinical characteristics of reported cases of adenoid cystic carcinoma

Institutions	N		5-year local control rate (%)	5-year survival rate (%)
Florida [2]	101	Radiotherapy alone	56	57
		Radiotherapy + Surgery	91	77
MGH [3]	23	Proton +/- Surgery	93	77
Washington [4]	151	Neutron	57	77
Heidelberg [5]	29	Neutron +/- Surgery	75	59
NIRS	151	Carbon	74	72

Although the local control of carbon ion radiotherapy was promising for malignant head-and-neck tumor excluding sarcoma, the survival rate was not commensurate with the favorable local control rate of the malignant melanoma. Based on the results of preliminary analysis of this protocol (Protocol 9602), two protocol were derived with effect from April 2001 into 1) the “Phase I/II Clinical Trial of Carbon Ion Radiotherapy for Bone and Soft Tissue Sarcomas in Head-and-Neck (Protocol 0006)” designed as a dose escalation study for bone and soft tissue tumors, and 2) the “Phase II Clinical Trial of Carbon Ion Radiotherapy Combined with Chemotherapy for Mucosal Malignant Melanoma in Head and Neck (Protocol 0007)” for the treatment of malignant melanoma with concomitant chemotherapy.

2. Phase I/II and II Clinical Trials for Bone and Soft Tissue Sarcomas in Adult Head-and-Neck (Protocol 0006)

Introduction

Phase I/II protocol was commenced in April 2001 for the purpose of a dose escalation study against bone and soft tissue sarcomas in the head-and-neck, since the preliminary analysis of the phase II clinical trial for malignant head-and-neck tumors (Protocol 9602) suggested that the local control and survival of bone and soft tissue sarcomas in the head-and-neck was clearly worse than other malignant tumors. We adopted 70.4 GyE in 16 fractions over 4 weeks as an initial prescribed dose in the present study. According to following toxicities, we might be able to proceed to the next irradiation dose; however, in the present study, because the local control rate had been approximately 100% with the initial dose for the period of the present study and because it was definitive that more than 70.4 GyE would make many unacceptable adverse effects from the results of carbon ion dose escalation study for sarcomas in the trunk in our institution, Kamada et al. described that 4 of 17 patients had grade3 late toxicities in the trunk with more than 70.4 GyE [6], we determined that 70.4 GyE is a recommend irradiation-dose for unresectable bone and soft tissue sarcomas in adult head-and-neck. This phase I/II study was completed on February 2008. From April 2008, phase II clinical study was started with same dose fractionation.

Patients and Methods

The 41 patients included in the analysis between April 2001 and February 2011 consisted of 20 males and 21 females. Two of the 41 patients were excluded from this analysis because of 1) one female patient had past history of whole body irradiation for her acute lymphocytic leukemia, 2) another female patient with MFH was diagnosed as a benign tumor after histological re-examination. The age range of the 39 patients was from 17 to 78, with a median of 48 years. They consisted of 12 patients with osteosarcoma, 5 with MFH, 3 with chondrosarcoma, 3 with hemangiopericytoma, 3 with spindle cell sarcoma, 2 with myxofibrosarcoma, 2 with leimyosarcoma, 2 with small round cell sarcoma, and 7 with other histological types.

Results

In preliminary analysis of the 39 patients who had follow-up period for more than six months, almost of all patients presented less than grade 2 acute reactions; however, five patients presented a grade 3 mucosal reaction. All late skin and mucosal reactions were grade 1 or less. The local tumor reactions within six months consisted of CR for 3 patients, PR for 11 patients, SD for 25 patients, and PD for no patients. The response rate was 36%. The five-year LC and OS rates were 73% and 48%, respectively (Fig. 2).

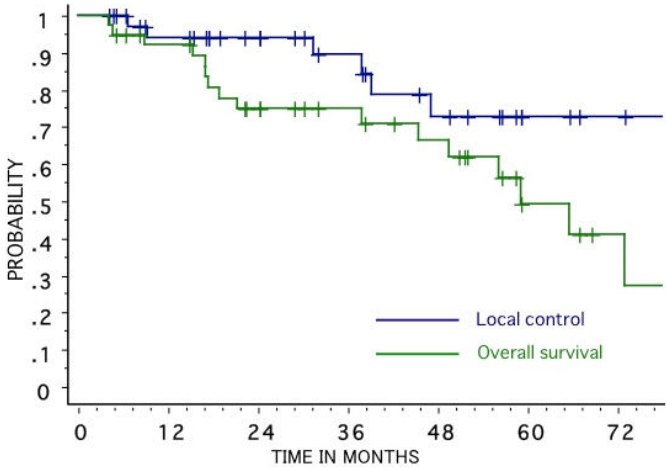

Figure 2. Local Control and Overall Survival of Bone and Soft Tissue Sarcomas

Discussion

Bone and soft tissue sarcomas in the head-and-neck are rare mesenchymal malignant neoplasms accounting for less than 10% of all bone and soft tissue sarcomas and approximately 1% of all head-and-neck neoplasms. Willers et al. said that wide resection margins are anatomically difficult to achieve, and the delivery of high radiation dose can be limited by the vicinity of critical normal tissue structures (spinal cord, brain stem, optic chiasm, eyes). Accordingly, the local control rates for head-and-neck sarcomas are lower compared to the extremities [7]. The five-year LC rate of combined surgery and radiotherapy is 60-70%. The LC of surgery alone is around 54% and that of radiotherapy alone is 43- 50% [8]. However, in unresectable sarcomas, the LC and survival prognosis were miserable. Conventional radiotherapy with a total dose less than 65 Gy showed no local control [9-11].

Results of carbon ion radiotherapy in our previous study (9602) for bone and soft tissue sarcomas in the head and neck, in which study patients were treated using 64.0 or 57.6 GyE in 16 fractions, showed 24% of the five-year LC rate. On the other hand, the five-year LC rate of this study (0006) was 73%. This result showed improved tendency compared with surgery with or without radiotherapy.

3. Phase II Clinical Trial for Mucosal Malignant Melanoma in Head-and-Neck Combined with Chemotherapy (Protocol 0007)

Introduction

Although the phase II clinical study for malignant head-and-neck tumors (Protocol 9602) had achieved a satisfactory local control rate for mucosal malignant melanomas, the survival rate was not commensurate with the favorable local control rate of malignant melanomas. In view of this result, this protocol was started in April 2001 for the purpose of prophylactic therapy against distant metastasis, the major cause of death in malignant melanoma of the head-and-neck region.

Patients and Methods

Carbon ion dose was 57.6 GyE in 16 fractions over 4 weeks. Concomitant chemotherapy (DAV: Day 1: DTIC 120mg/m2 + ACU 70mg/m2 + VCR 0.7mg/m2; Days 2~5: DTIC 120mg/m2, 4 weeks' interval, a total of 5 courses) was administered at two courses before, and three courses after carbon ion radiotherapy. The results for the seven patients treated until February 2002 show that at the time of completion of the two courses of DAV chemotherapy prior to carbon ion radiotherapy, there were PR for 2 patients, NC for 2 patients and PD for 3 patients, necessitating the early commencement of carbon ion radiotherapy. From April 2002, carbon ion radiotherapy and DAV chemotherapy were carried out concurrently.

The 103 patients included in the analysis between April 2001 and February 2011 consisted of 47 males and 56 females. Their age ranged from 26 to 79 years, a median of 62 years. Their KPS ranged from 70% to 100%, with a median of 90%. As for the tumor site studied, there were 82 nasal cavity and paranasal sinus, 13 oral cavity, 5 pharynx and 3 orbit.

Results

The acute reactions of 103 patients who have a follow-up time more than 6 months were consisted of one patient with a grade 3 skin reaction and 21 patients (20%) with a grade 3 mucosal reaction while the other toxicities that were observed were grade 2 or less. All late reactions in both the skin and mucosa were grade 1 or less.

The local tumor reactions within six months consisted of CR for 22 patients, PR for 47 patients, SD for 35 patients, and PD for no patients. The effective rate was 66%. The five-year LC and OS rates of all patients were 79% and 55%. In 96 concomitant patients, the five-year LC and OS rates were 81% and 58%, respectively.

Discussion

The reported local failure of systemic therapy including surgery, radiotherapy and chemotherapy is very high (45-54%) [12,13]. The five-year LC rate of carbon ion radiotherapy showed 79% in this protocol. These results will show an effectiveness of carbon ion radiotherapy for the local control of mucosal malignant melanoma in the head-and-neck. The review articles [14-20] reported the five-year survival rates of 17-35% (Table 2), which is attributed mainly to distant metastasis. The five-year OS rate of carbon ion radiotherapy showed 37% in 9602 and 55% in 0007 protocol. There will be some tendency of improving result in concomitant and adjuvant chemotherapy (Protocol 0007) (Fig. 3).

Table2. Clinical characteristics of reported cases of mucosal malignant melanoma

	Authors	N	5-year OS (%)
Radiotherapy	Gilligan [14]	28	18
(+/- Surgery)	Shibuya [15]	28	25
Surgery	Chang [16]	163	32
(+/- RT, +/- Chemo)	Shah [17]	74	22
	Patel [18]	59	35
	Lund [19]	58	28
	Chaudhry [20]	41	17
Carbon ion alone	NIRS	102	37
Carbon ion + Chemo	NIRS	89	58

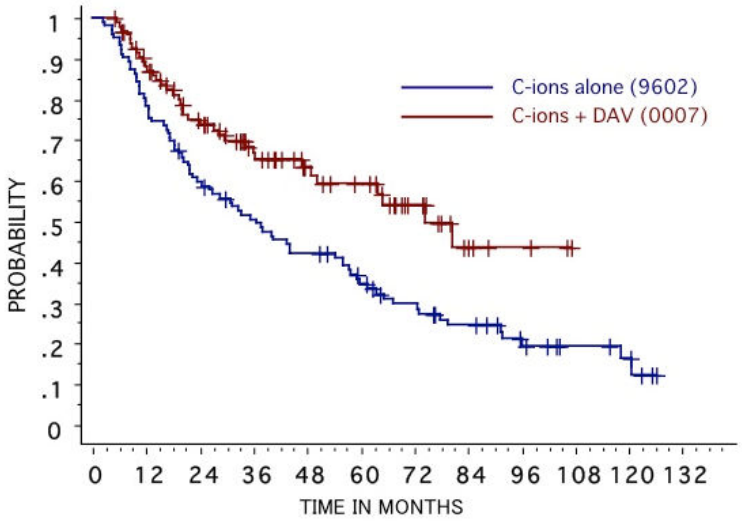

Figure 3. Overall Survival of Mucosal Malignant Melanomas

Conclusion

Malignant head-and-neck tumors are therapeutically very diverse because of the many important organs present in this region and the great variety of tissue types. Carbon ion radiotherapy also requires considerable versatility in terms of the use of a specific radiation dose suited for the particular histological type and the application of concurrent chemotherapy. At present, efforts are being made to increase the patient numbers in order to produce results that can provide cogent clinical evidence.

References

［1］ Mizoe J, Tsujii H, Kamada T, *et al*: Dose escalation study of carbon ion radiotherapy for locally advanced head-and-neck cancer. *Int J Radiat Oncol Biol Phys*. 2004; 60: 358-364.

［2］ Mendenhall WM, Morris CG, Amdur RJ, *et al*: Radiotherapy alone or combined with surgery for adenoid cystic carcinoma of the head and neck. *Head Neck*. 2004; 26(2): 154-162.

［3］ Pommier P, Liebsch NJ, Deschler DG, *et al*: Proton beam radiation therapy for skull base adenoid cystic carcinoma. *Arch Otolaryngol Head Neck Surg*. 2006; 132(11): 1242-1249.

［4］ Douglas JG, Laramore GE, Austin-Seymour M, *et al*: Treatment of locally advanced adenoid cystic carcinoma of the head and neck with neutron radiotherapy. *Int J Radiat Oncol Biol Phys.* 2000; 46(3): 551-557.

［5］ Huber PE, Debus J, Latz D, *et al*: Radiotherapy for advanced adenoid cystic carcinoma: neutrons, photons or mixed beam? *Radiother Oncol.* 2001; 59(2): 161-167.

［6］ Kamada T, Tsujii H, Tsuji H, *et al*: Efficacy and safety of carbon ion radiotherapy in bone and soft tissue sarcomas. *J Clin Oncol.* 2002; 20: 4466-71.

［7］ Willers H, Hug EB, Spiro IJ, *et al*: Adult soft tissue sarcomas of the head and neck treated by radiation and surgery or radiation alone: patterns of failure and prognostic factors. *Int J Radiat Oncol Biol Phys.* 1995; 33: 585-593.

［8］ Mendenhall WM, Mendenhall CM, Werning JW, *et al*: Adult head and neck soft tissue sarcomas. *Head Neck.* 2005: 27: 916-922.

［9］ Le QT, Fu KK, Kroll S, *et al*: Prognostic factors in adult soft-tissue sarcomas of the head and neck. *Int J Radiat Oncol Biol Phys.* 1997; 37: 975-984.

［10］ Barker JL Jr, Paulino AC, Feeney S, *et al*: Locoregional treatment for adult soft tissue sarcomas of the head and neck: an institutional review. *Cancer J.* 2003; 9: 49-57.

［11］ Chen SA, Morris CG, Amdur RJ, *et al*: Adult head and neck soft tissue sarcomas. *Am J Clin Oncol.* 2005; 28: 259-263.

［12］ Mendenhall WM, Amdur RJ, Hinerman RW, *et al*: Head and neck mucosal melanoma. *Am J Clin Oncol.* 2005; 28: 626-630.

［13］ Lengyel E, Gilde K, Remenár E, *et al*: Malignant Mucosal Melanoma of the Head and Neck -a Review-. *Pathology Oncology Research.* 2003; 9: 7-12.

［14］ Gilligan D, Slevin NJ: Radical radiotherapy for 28 cases of mucosal melanoma in the nasal cavity and sinuses. *Br J Radiol*. 1991; 64:1147-1150.

［15］ Shibuya H, Takeda M, Matsumoto S, *et al:* The efficacy of radiation therapy for malignant melanoma in the mucosa of the upper jaw: an analytic study. *Int J Radiat Oncol Biol Phys.* 1992; 25: 35-39.

［16］ Chang AE, Karnell LH, Menck HR: The National Cancer Data Base Report on cutaneous and noncutaneous melanoma. *Cancer.* 1998; 83: 1664-1678.

［17］ Shah JP, Huvos AG, Strog EW: Mucosal melanomas of the head and neck. *Am J Surg.* 1977; 134: 531-535.

［18］ Patel SG, Prasad ML, Escrig M, *et al*: Primary mucosal malignant melanoma of the head and neck. *Head*

Neck. 2002; 24: 247-257.

［19］ Lund VJ, Howard DJ, Harding L, *et al*: Management options and survival in malignant melanoma of the sinonasal mucosa. *Laryngoscope*. 1999; 109: 208-211.

［20］ Chaundhry AP, Hampel A, Gorlin RJ: Primary melanoma of the oral cavity. *Cancer.* 1958; 11: 923-928.

Carbon Ion Radiotherapy in a Hypofraction Regimen for Stage I Non-Small Cell Lung Cancer

Naoyoshi Yamamoto, Masayuki Baba, Mio Nakajima, Kyosan Yoshikawa, Naruhiro Matsufuji, Shinichi Minohara, Hiroshi Tsuji, Tadashi Kamada, and Hirohiko Tsujii

Hospital, Research Center for Charged Particle Therapy, National Institute of Radiological Sciences, Chiba, Japan
e-mail address: nao_y@nirs.go.jp

Abstract

From 1994 to 1999, we conducted a phase I/II clinical trial for patients with stage I non-small cell lung cancer (NSCLC) by using carbon ion beams alone, demonstrating optimal doses of 90.0GyE in 18 fractions over 6 weeks (Protocol #9303) and 72.0GyE in 9 fractions over 3 weeks (Protocol #9701), which achieved a more than 95% local control rate with minimal pulmonary damage. In the present study, the total dose was fixed at 72.0GyE in 9 fractions over 3 weeks (Protocol #9802), and at 52.8GyE for stage IA and 60.0GyE for stage 1B in 4 fractions in 1 week (Protocol #0001). Following this schedule, we conducted a phase II clinical trial for stage I NSCLC from 1999 to 2003. We also conducted a phase I/II single fractionation clinical trial (Protocol #0201) as a dose escalation study. The total dose was initially 28.0GyE in 2003, and it was increased to 50.0GyE in 2011. This article describes the intermediate steps. Most targets were irradiated from four oblique directions. A respiratory-gated irradiation system was used for all sessions. Local control and survival were assessed by the Kaplan-Meier method. For statistical testing, the Log-rank test was used.

The local control rate for all patients (#9802 and #0001) was 91.5%, and those for T1 and T2 tumors were 96.3% and 84.7%, respectively. While there was a significant difference (p=0.0156) in the tumor control rates between T1 and T2 tumors, there was no significant difference (P=0.1516) between squamous cell carcinomas and non-squamous cell carcinomas. The 5-year cause-specific survival rate was 67.0% (IA: 84.4, IB: 43.7), and the overall survival was 45.3% (IA: 53.9, 1B: 34.2). No adverse effects greater than grade 2 occurred in the lungs.

In a single fractionation trial, the 5-year local control rate for 131 patients was 80.5%, and the control rates for T1 and T2 tumors were 82.8% and 78.4%, respectively. No adverse effects greater than grade 2 occurred in the lungs.

Carbon beam radiotherapy, an excellent new modality in terms of high QOL and ADL, was proven to be a valid alternative to surgery for stage I NSCLC, especially for elderly and inoperable patients.

Introduction

In 1998, lung cancer became the leading cause of cancer-related death in Japan, as it had been in Western countries. Surgery plays a pivotal role in the curative treatment for non-small cell lung cancer (NSCLC), but it is not necessarily the best treatment for elderly persons and/or patients with cardiovascular and pulmonary complications. Conventional radiotherapy as an alternative, however, leads to a five-year survival rate in merely 10-30% of the patients due to poor control of the primary tumor. Dose escalation is essential to improve the efficacy of radiotherapy, but this involves an increasing risk of pulmonary toxicity. Carbon ion radiotherapy (CIRT) is a promising modality because of its excellent dose localization and high biological effect on the tumor. Our clinical trials led us to conclude that irradiation with heavy particle beams, notably carbon ion beams, offers a significant potential for improving tumor control without increasing the risk of toxicity.

Between 1994 and 1999, a phase I/II study of the treatment of stage I NSCLC by CIRT was first conducted using a dose escalation method to determine the optimal dose. An additional purpose was to develop correct, reliable and safe irradiation techniques for CIRT for the treatment of NSCLC. As reported in our phase I/II study [1], the following results (Table 1) were obtained: 1) The local control rate was dose-dependent, reaching more than 90% at 90.0GyE with a regimen of 18 fractions over 6 weeks, and at 72.0GyE given in 9 fractions over 3 weeks. Both doses were determined to be optimal. It was found that setting the provisional target by allowing for the differences in the CT values can prevent marginal recurrence [2]. 2) Damage to the lungs in this study was minimal, with grade 3 radiation pneumonitis occurring in 2.7% of the cases. Respiratory-gated and 4-portal oblique irradiation directions, excluding opposed ports, proved successful for reducing the incidence of radiation pneumonitis. 3) The patient survival was strongly influenced by the local control and tumor size of the primary lesion. The early detection of nodal and intralobar metastasis, followed by irradiation with carbon beams, can help ensure a better survival rate. Local failure, distant metastasis and malignant pleurisy were responsible for decreases in survival.

Adverse reactions in the lungs
1) minimum damage to lungs (grade 3 radiation pneumonitis in 2.7% of patients)
2) influenced by dose, respiratory movement, and port direction and number
Local control
1) dose-dependent, but less dependent on tumor size and histological type
2) more than 90% by the optimal dose, and demonstrated by the pathological CR
Survival
1) influenced by the local control status and tumor size
2) less decreased by nodal and intralobar metastasis, but more by local failure, malignant pleurisy and distant metastasis

Table1. The results of the phase I/II study of carbon beam radiotherapy for stage I non-small cell lung cancer

In the present study, a phase II clinical trial and a phase I/II dose escalation clinical trial were performed. In the phase II clinical trial, the total dose was fixed at 72.0GyE in 9 fractions over 3 weeks [3], and at 52.8GyE for stage IA NSCLC and 60.0GyE for stage IB NSCLC in 4 fractions administered during one week [4]. Using this optimal schedule, the phase II clinical trial was initiated in April in 1999 and closed in December in 2003, after accruing a total of 127 patients.

The phase I/II dose escalation clinical trial was initiated in April 2003. The initial total dose was 28.0GyE administered in a single fraction using respiratory-gated and 4-portal oblique irradiation directions, with the total irradiation dose being escalated in increments of 2.0GyE each, up to 50.0GyE. This clinical trial is still in progress. This article describes the intermediate steps of the phase I/II clinical trial and the preliminary results of the phase II clinical trial in terms of the local control and survival after CIRT.

Materials and Methods

[The phase II clinical trial]

One hundred and twenty-nine patients with 131 primary lesions were treated with CIRT. Fifty-one primary tumors of 50 patients were treated by carbon ion beam irradiation alone using a fixed total dose of 72GyE in 9 fractions over 3 weeks (#9802 protocol [3]). The remaining 79 patients had 80 stage I tumors (#0001 protocol [4]). For the analysis of survival, 127 patients were evaluated, as 2 patients had been treated twice, one in the first protocol #9802, and one in the second protocol #0001. The patients with IA and IB stage tumors were treated with fixed doses of 52.8GyE and 60.0GyE in 4 fractions in one week, respectively. Their mean age was 74.5 years, and the gender breakdown was 92 males and 37 females. The tumors included 72 T1 and 59 T2

tumors, with a mean tumor diameter of 31.5 mm, By type (determined by biopsy), there were 85 adenocarcinomas, 43 squamous cell carcinomas, 2 large cell carcinomas and 1 adenosquamous cell carcinoma. Medical inoperability was diagnosed for 76% of the lesions.

[The phase I/II clinical trial (single fractionation)]

One hundred and thirty-one patients were treated in this clinical trial between April 2003 and August 2010. As mentioned above, the intermediate steps of this still ongoing phase I/II clinical trial included a total dose of 36.0GyE or more, and the follow-up time was 6 months or more after CIRT. The local control rate was as high as 80%. The 131 primary tumors of the 131 patients were treated by carbon ion beam irradiation alone using a total dose of 36.0GyE (n=18), 38.0GyE (n=14), 40.0GyE (n=20), 42.0GyE (n=15), 44.0GyE (n=44) or 46.0GyE (n=20) per single fractionation. The mean patient age was 73.6 years, and the gender breakdown was 43 females and 88 males. The tumors were 78 T1 and 53 T2 tumors with a mean diameter of 29.0 mm . By type (cancer type was determined by biopsy), there were 90 adenocarcinomas, 40 squamous cell carcinomas, and one large cell carcinoma. Medical inoperability diagnosed in 57.3% of cases (Table 2).

Age (mean)		46-87 (73.6)
Gender	Female	43
	Male	88
PS	0	99
	1	31
	2	1
Tumor size (mean)		10-62 (29.0)*
Stage	IA	78
	IB	53
Histology	Adenoca.	90
	Sq cell ca.	40
	Large cell ca.	1
Reason for inoperability		
	Refusal	56 (42.7)**
	Medically inoperable	75 (57.3)**
Total dose (GyE)		
	36.0	18
	38.0	14
	40.0	20
	42.0	15
	44.0	44
	46.0	20

*mm, **percent Aug. 31, 2010

Table2. The treatments and characteristics of the 131 patients with stage I NSCLC

[Carbon ion beam irradiation]

The same system for carbon ion beam irradiation was used in both the phase II and phase I/II clinical trials. The targets were usually irradiated from four oblique directions without prophylactic elective nodal irradiation (ENI). A greater than 10-mm margin was set outside the gross target volume (GTV) to determine the clinical target volume (CTV). The planning target volume (PTV) was established by adding an internal margin (IM) to the CTV. The IM was determined by extending the target margin in the head and tail direction by a width of 5 mm, leading to a successful prevention of marginal recurrence possibly resulting from respiratory movement [2]. Fig. 1 shows the dose distribution maps for a representative case. A respiratory-gated irradiation system was used in all irradiation sessions. Fig. 2 shows the CIRT room. We used vertical or horizontal beams in 2 oblique positions, including a total of 4 irradiation directions.

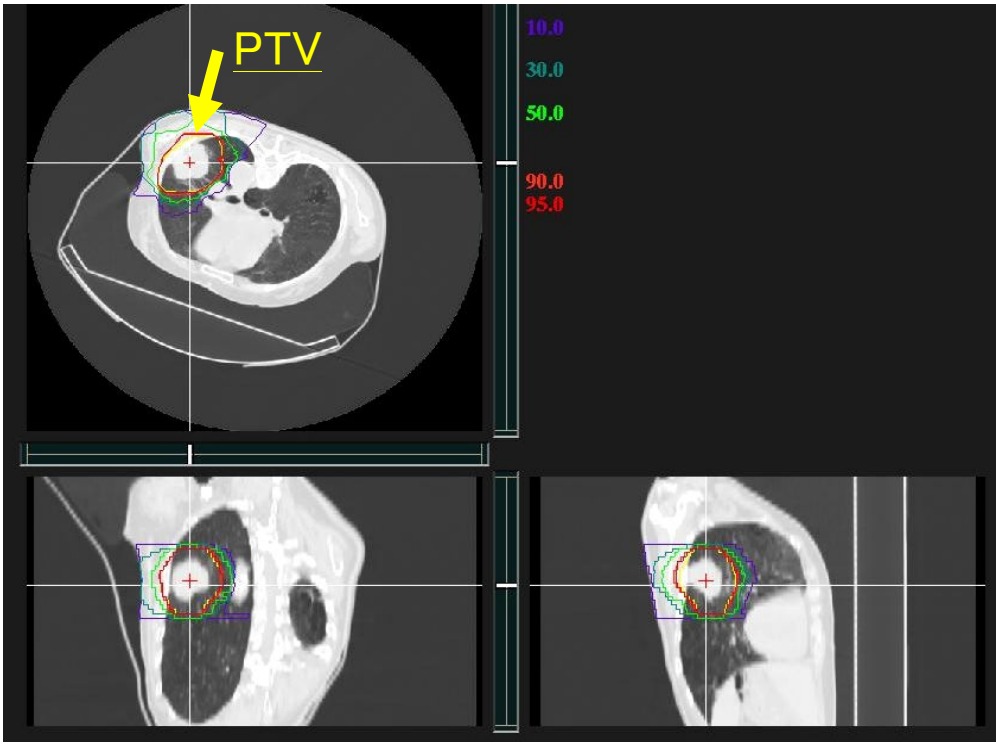

Fig. 1. Dose distribution maps for a 71-year-old female

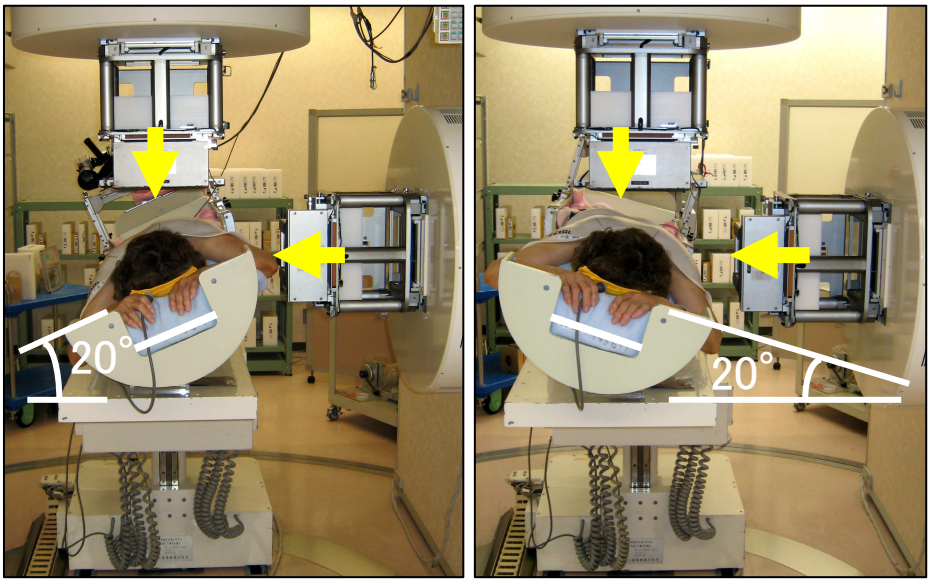

Fig.2. The CIRT treatment room

[Statistical analysis]

The local control and survival rates were assessed by the Kaplan-Meier method. For statistical analyses, the Log-rank test was used.

Results

[The phase II clinical trial (#9802, #0001)]

All patients were followed up until death, with a median follow-up time of 50.8 months, ranging from 2.5 months to 70.0 months. The local control rate for all 131 primary lesions was 91.5% (Fig. 3), while those for T1 (n=72) and T2 (n=59) tumors were 96.3% and 84.7%, and for the squamous cell type (Sq) (n=43) and non-squamous cell type (Non-Sq) (n=88) were 87.1% and 93.8%, respectively. While there was a significant difference (p=0.0156) in the tumor control rate between T1 and T2 tumors, there was no significant difference (P=0.1516) between the results for squamous and non-squamous cancers within the T1 group, nor between theT1 and T2 groups. However, with respect to squamous cell cancer, the local control was 100% for T1 (n=17) and 78.0% for T2 (n=26) tumors, which was nearly significant (p=0.0518). The local control rate for non-squamous tumors was 95.3% for T1 (n=55) and 91.0% for T2 tumors (n=33), which was not significantly different (p=0.3364).

The 5-year cause-specific survival rate of the 127 patients was 67% (Fig. 3), breaking down into 84.8% for stage IA and 43.7% for stage IB tumors (Fig. 4A). The 5-year overall survival rate was 45.3% (Fig. 3), breaking down into 53.9% for stage IA and 34.2% for stage IB tumors (Fig. 4B).

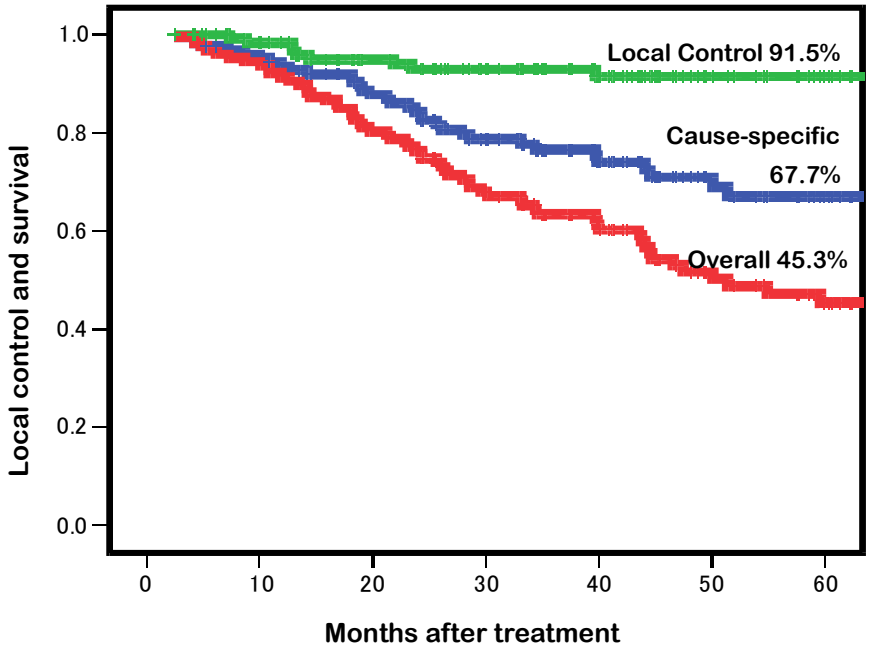

Fig. 3. The local control (n=131) and survival (n=127) rates after CIRT

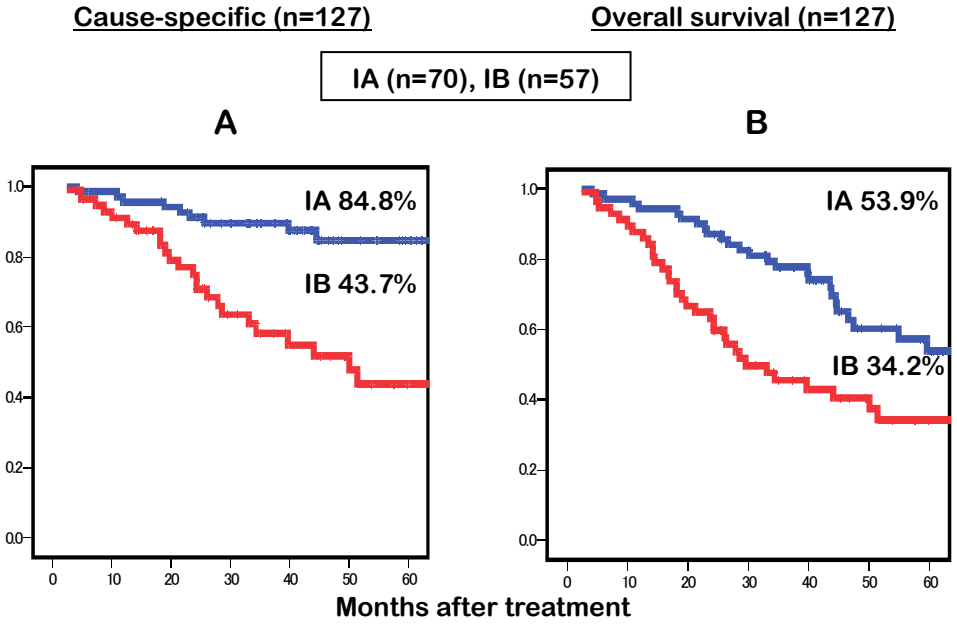

Fig. 4. The survival rates of patients by stage (IA vs IB)

The toxicities to the skin and lungs caused by CIRT were assessed according to the RTOG (early) and RTOG/EOTRC (late) as shown in Tables 3 and 4. Early skin reactions were assessed for 131 lesions and late skin reactions for 128 lesions. Of the early reaction lesions, 125 were grade 1 and 6 were grade 2. Among the late reaction , 126 were grade 1, 1 was grade 2, and 1 was grade 3. Lung reactions were clinically assessed in 129 patients. One hundred twenty-seven had grade 0 and 2 had grade 2 early reactions. Late effects were followed up in 126 patients: 7 patients had grade 0, 116 patients had grade 1, and 3 patients had grade 2 reactions. No adverse events higher than a single grade 2 reaction were observed.

Skin		Early reaction (RTOG)						Late reaction (RTOG)					
		Lesion	Grade					Lesion	Grade				
		No.	0	1	2	3	≧4	No.	0	1	2	3	≧4
	#9802	51	0	50	1	0	0	51	0	49	1	1	0
	#0001	80	0	75	5	0	0	77*	0	77	0	0	0
	Total	131	0	125	6	0	0	128	0	126	1	1	0

* 3 cases were not observed due to early death

Table 3. Adverse skin reactions following CIRT

Fifty-three of the 127 patients (41.7%) developed a recurrence, all occurring between 1 and 54 months (median, 10.5 months) after the commencement of therapy. No occurrence was observed in the other 74 patients (58.3%). The 9 primary recurrences (7.1%) and 11 regional metastases (8.7%) consisting of 7 regional nodes (5.5%), one intrabronchial (0.8%), and 3 intralobar metastases (PM1) (2.4%) occurred in the loco-regional site. In one patient, the primary recurrence was seen at the margin, while in another it occurred in-field.

Skin		Early reaction (RTOG)						Late reaction (RTOG)					
		Lesion	Grade					Lesion	Grade				
		No.	0	1	2	3	≧4	No.	0	1	2	3	≧4
	#9802	50	49	0	1	0	0	50	0	48	2	0	0
	#0001	79	78	0	1	0	0	76*	7	68	1	0	0
	Total	129	127	0	2	0	0	126	0	116	3	0	0

* 3 cases were not observed due to early death

Table4 . Adverse lungs reactions following CIRT

Based on the sub-stage classification, the incidence of loco-regional recurrence, pleural dissemination, and distant metastasis for stage IB (63%) was much higher than that for IA (24%). The total incidence of first recurrence for stage IB (63%) also tended to be higher than that for stage IA (24%). Verification by the $\chi 2$ test showed no significant difference ($\chi 2=1.63$).

The causes of death in the patients were as follows: 62 out of the 127 patients (48.8%) died, half of disease progression. Among the patients with recurrence, 5 of the 9 with primary recurrence (55%) died from disease progression. Ten of the 11 patients with regional metastases were re-treated, 9 with CIRT and 1 with photons. Seven of these patients, although they had no further recurrence, died due to intercurrent disease, and 1 with node metastasis but no re-treatment died of disease progression. Eight of the 11 patients with regional metastases (72%) died, and 9 of the 10 patients (90%) with malignant pleurisy and 17 of the 23 patients (74%) with distant metastases died of disease progression. Five of them died due to primary recurrence, and 26 due to metastasis and dissemination. For the remaining 31 patients, intercurrent diseases were the cause of death [3, 4].

[The phase I/II clinical trial (single fractionation)]

All patients were followed up until death, with a median follow-up time of 35.2 months, ranging from 1.6 months to 68.4 months. The 5-year overall local control rate for the 131 primary lesions was 80.5%, and those for the T1 (n=78) and T2 (n=53) tumors were 82.8% and 78.4%, respectively (Fig. 5). The overall survival rate was 52.6% and the cause-specific survival rate was 71.5%.

The toxicities of CIRT to the skin and lungs were assessed according to NCI-CTC (early) and RTOG/EOTRC (late) as shown in Tables 5 and 6. Early skin reactions were assessed for 131 lesions and late skin reactions for 128 lesions. Of the early reaction lesions, 126 were grade 1 and 3 were grade 2. Among the late reaction lesions, 123 were grade 1 and one was grade 2. Lung reactions were clinically assessed in the 131 patients. Forty-seven had grade 0, 83 had grade 1 and one had grade 2 among early reactions. Late reactions were followed up in 126 patients, with 114 showing grade 1 and one showing a grade 2 reaction.

The clinical course of a representative 71-year-old female is shown in Figs. 6 and 7. Tumor shrinkage and slight lung fibrosis were apparent, and a grade 1 skin reaction was observed.

Discussion

In the present study, the local control, cause-specific, and overall survival rates for the 127 patients in the phase II clinical trial were 91.5%, 67.0%, and 45.3%, respectively. Also, the overall local control, local control in T1 tumors, and local control in T2 tumors were 80.5%, 82.8%, and 78.4%, respectively, by single fractionation. The toxicities to the skin, lungs and bone were minimal.

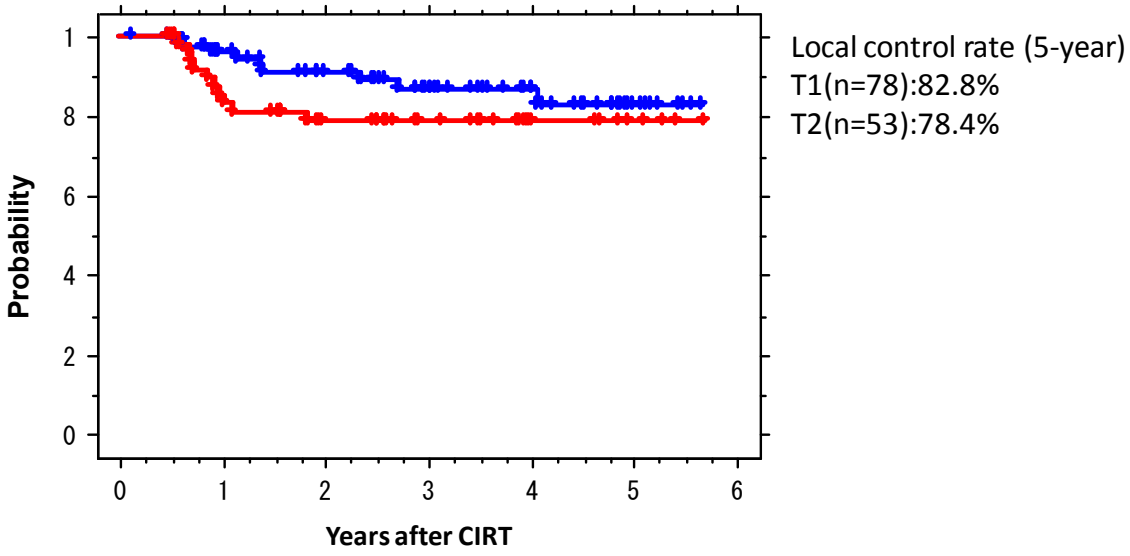

Fig.5. The tumor control rates after CIRT using single fractionation

Skin	Total dose (GyE)	Early reaction (NCI-CTC)						Late reaction (RTOG/EORTC)					
		No. of Case	Grade					No. of Case	Grade				
			0	1	2	3	≧4		0	1	2	3	≧4
	36.0	18	0	18	0	0	0	17*	0	17	0	0	0
	38.0	14	0	14	0	0	0	13*	0	13	0	0	0
	40.0	20	1	18	1	0	0	20	2	17	1	0	0
	42.0	15	0	15	0	0	0	14	1	14	0	0	0
	44.0	44	1	41	2	0	0	43*	1	42	0	0	0
	46.0	20	0	20	0	0	0	20	0	20	0	0	0
	Total	131	2	126	3	0	0	128	4	123	1	0	0

*One case was not observed in each group

Table5. The incidence of adverse skin reaction after CIRT using single fractionation

Lung	Total dose (GyE)	Early reaction (NCI-CTC)						Late reaction (RTOG/EORTC)					
		No. of Case	Grade					No. of Case	Grade				
			0	1	2	3	4=<		0	1	2	3	4=<
	36.0	18	12	6	0	0	0	17*	2	15	0	0	0
	38.0	14	9	5	0	0	0	13*	2	11	0	0	0
	40.0	20	10	10	0	0	0	19*	4	15	0	0	0
	42.0	15	10	5	0	0	0	14*	1	14	0	0	0
	44.0	44	6	37	1	0	0	44	2	40	1	0	0
	46.0	20	0	20	0	0	0	19*	0	19	0	0	0
	Total	131	47	83	1	0	0	126	11	114	1	0	0

*One case was not observed in each group

Table 6. Adverse lung reactions after CIRT using single fractionation

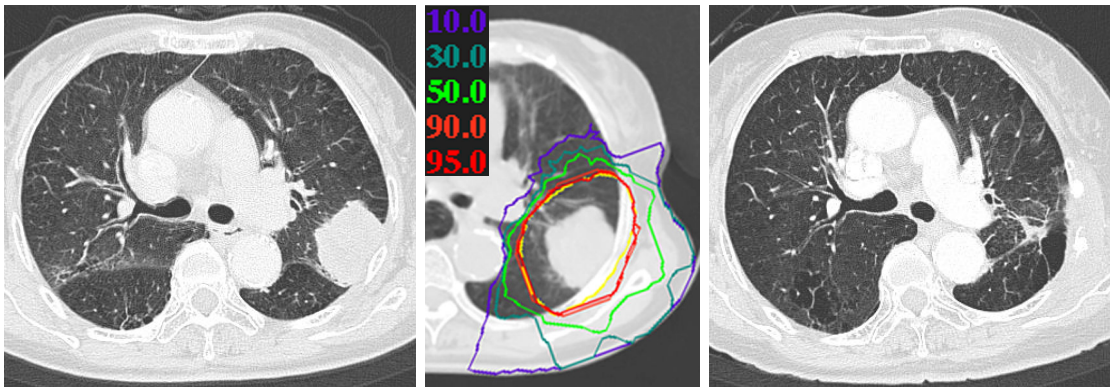

Fig. 6. The clinical course of 71-year-old female (T2N0M0 squamous cell carcinoma) after CIRT (40GyE/ single fractionation). An initial CT scan (A), dose distribution map (B), and a CT scan (C) taken 18 months after CIRT are shown. Apparent tumor shrinkage was observed

Out of the 131 primary cancers in 127 patients, local recurrence developed in 9 patients (6.8%). The average time of recurrence was 17.2 months, ranging from 7 to 39 months. According to our previous study, the observation period required to determine local control of the irradiated lesions was at least 3 years post- therapy [1]. However, the present study suggested the need for a longer observation period. It is evident that prolonged survival guarantees a more reliable observation of the local control results.

To correctly assess the local control rate of patients who could not be observed for such a long duration because of death resulting from metastasis/dissemination or intercurrent disease, a histological approach based on repeated bronchoscopy was used, providing evidence of the absence of viable tumor cells in the collected specimens [3]. Furthermore, definite tumor control was also confirmed by the autopsies of CIRT-treated patients and in cases treated by surgery [5]. Such high and definite tumor control appears to be an outstanding feature of CIRT. Presumably, this is primarily due to the radiobiological nature of the high LET beams, which may account for the higher survival rate of stage I NSCLC patients. On the other hand, the failure of local control for primary tumors directly affected the poor survival of stage I NSCLC patients [1, 3]. Among our cases, 5 of the 9 patients with primary recurrence (55%) died due to disease progression.

Eleven regional recurrences were detected. This incidence was close to that of surgery (7.5% [6], 11% [7]). Eight of the patients (72%) died. Only one patient, who did not undergo retreatment, died due to disease progression. The other 7 retreated patients died due to intercurrent discase. Martini et al. [7] reported that any resection less than lobectomy and no lymph node dissection had adverse effects on recurrence and survival. In contrast, our treatment strategy for regional recurrence is thought to have gained validity compared to the standard surgical procedure for stage I NSCLC.

Nine of the 10 patients (90%) with malignant pleurisy and 17 of the 23 patients (74%) with distant metastasis died of disease progression. The poor prognosis of stage IB cases was the result of the high incidence of pleural

and distant metastasis.

Fig. 7. A skin reaction after CIRT (40.0GyE/1fr) in the 71-year-old female.
A grade 1 reaction was observed.

For the patients with clinical stage I NSCLC, our 5-year overall survival results were somewhat inferior to those of surgery [3, 5]. This difference may be due to the significant age gap between the two groups. The incidence of death due to recurrence in the surgical groups in previous studies was 29% or 36%, whereas that due to intercurrent diseases was 19% or only a few percent [6, 7]. In contrast, our patients showed a higher incidence of death due to intercurrent diseases (60%) than death due to recurrence (40%). A comparison of stage IA with stage IB patients revealed that while there was a large difference between the overall (53.9%) and cause-specific (84.8%) survival in stage IA patients, there was a smaller difference in stage IB between the overall (34.2%) and cause-specific (43.7%) survival in stage IB patients. Such differences in the survival rates in the two stage I subgroups might be explained by the low incidence of recurrence-related death in stage IA patients(24%) and the relatively high incidence in stage IB patients (63%). The high frequency of intercurrrent death might be related to the advanced age of our patients, as they were on average 10 years older than the surgical patients [6, 7]. As we have reported previously, elderly patients 80 years and older can be treated safely by CIRT [8].

Compared with the pulmonary damage reported after stereotactic radiotherapy for stage I NSCLC [9-11], the incidence and severity of damage in our patients seemed to be remarkably low. These less severe and less common adverse effects on the lungs were likely achieved as a result of the small volume irradiated. This advantage results from the excellent dose distribution properties unique to carbon ion beams and the formation of a Bragg peak in contrast to the permeating beam associated with x-rays

Conclusions

One hundred twenty-seven stage I NSCLC patients with 131 primary tumors were treated with CIRT using a total dose of 72GyE in a regimen of 9 fractions over 3 weeks, and with 52.8GyE for stage IA and 60GyE for stage IB in 4 fractions over the course of one week. In addition, 131 stage I NSCLC patients with 131 primary tumors were treated with single-fraction CIRT using total doses ranging from 36.0GyE to 46.0GyE.

This study demonstrated seven major findings. First, the local control rate of the 131 primary lesions was 91.5%. There was a statistically siginificant difference between the local control rates for T1 and T2 tumors, and near significance between the rates for T2 squamous cell carcinoma versus T2 non-squamous cell carcinoma .

Second the 5-year overall and cause-specific survival rates of 127 patients were 45.3% and 67.0%, respectively.

Third the 5-year overall survival rates of the patients with stage IA and stage IB disease were 53.9% and 34.2%, while the 5-year cause-specific survival rates of those with stage IA and stage IB were 84.8% and 43.7%, respectively.

Fourth, there was high incidence of intercurrent death due to the advanced age and related complications in our patients. Fifth, the adverse effects on the skin and lungs were minimal, indicating the safety of the modality. Carbon beam radiotherapy, which is an excellent new modality in terms of a high QOL and ADL, is a valid alternative to surgery for stage I cancer, especially for elderly and inoperable patients. Sixth, in the trial of CIRT using single fractionation with a total dose range from 36.0GyE to 46.0GyE, the local control rate for the 131 primary lesions was 80.5%, and those for the T1 (n=78) and T2 (n=53) tumors were 82.8% and 78.4%, respectively. Finally, CIRT using single fractionation is effective, at least as viewed during an intermediate step, and is a safe treatment modality for stage I NSCLC patients.

References

[1] Miyamoto T, Yamamoto N, Nishimura H, et al. Carbon ion radiotherapy for stage I non-small cell lung cancer. Radiother Oncol 2003;66:127-140.

[2] Koto M, Miyamoto T, Yamamoto N, et al. Local control and recurrence of stage I non-small cell lung cancer after carbon ion radiotherapy. Radiother Oncol 2004;71:147-156.

[3] Miyamoto T, Baba M, Yamamoto N, et al. Curative treatment of stage I non-small cell lung cancer with carbon ion beams using a hypo-fractionated regimen. Int J Radiat Oncol Biol Phys 2007;67:750-8.

[4] Miyamoto T, Baba M, Sugane T, et al. Carbon ion radiotherapy for stage I non-small cell lung cancer using a regimen of four fractions during 1 week. J Thorac Oncol 2007;2:916-26.

[5] Yamamoto N, Miyamoto T, Nishimura H, et al. Preoperative carbon ion radiotherapy for non-small cell lung cancer with chest wall invasion - pathological findings concerning tumor response and radiation induced lung injury in the resected organs. Lung Cancer 2003;42:87-95.

[6] Harpole DH, Herndon JE, Yung WG, et al. Stage I nonsmall cell lung cancer. A multivariate analysis of treatment methods and patterns of recurrence. Cancer 1995;76:787-796.

[7] Martini N, Bains MS, Burt ME, et al. Incidence of local recurrence and second primary tumors in resected stage I lung cancer. J Thorac Cardiovasc Surg 1995;109:120-129.

[8] Sugane T, Baba M, Imai R, et al. Carbon ion radiotherapy for elderly patients 80 years and older with stage I non-small cell lung cancer. Lung Cancer (2008), doi:10.1016/j.lungcan.2008.07.007.

[9] Nagata Y, Takayama K, Matsuo Y, et al. Clinical outcomes of a phase I/II study of 48Gy of stereotactic body radiotherapy in 4 fractions for primary lung cancer using a stereotactic body frame. Int J Radiat Oncol Biol Phys 2005;63:1427-1431.

[10] Onishi H, Shirato H, Nagata Y, et al. Hypofractionated stereotactic radiotherapy (HypoFXSRT) for stage I non-small cell lung cancer: updated results of 257 patients in a Japanese multi-institutional study. J Thorac Oncol 2007;2 (7 Suppl 3):S94-100

[11] Timmerman R, McGarry R, Yiannoutsos C, et al. Excessive toxicity when treating central tumors in a phase II study of stereotactic body radiation therapy for medically inoperable early-stage lung cancer. J Clin Oncol 2006;24:4833-4839

Carbon Ion Radiotherapy for Bone and Soft Tissue Sarcomas

Reiko Imai, Tadashi Kamada, Hiroshi Tsuji, Katsuya Maruyama, Keiji Matsumoto and Hirohiko Tsujii

Research Center for Charged Particle Therapy, National Institute of Radiological Sciences, Chiba, Japan
Corresponding Author: Reiko Imai, e-mail address: r_imai@nirs.go.jp

Abstract

A clinical trial was first initiated in 1996 to evaluate the safety and efficacy of carbon ion radiotherapy for bone and soft tissue sarcomas not suitable for surgery. As of February 2011, a total of 800 patients were enrolled in the clinical trials. Through a dose escalation trial and a subsequent fixed dose trial, it was revealed that carbon ion radiotherapy provided definite local control and offered a survival advantage without unacceptable morbidity for patients with bone and soft tissue cancers that were either difficult or impossible to cure using other modalities.

Introduction

Malignant tumors that originate in the bone and soft tissues (e.g., muscle and adipose tissue) are termed sarcomas, which differ from carcinomas (e.g., lung cancer and stomach cancer). Sarcomas have a much lower incidence than other cancers. In Japan, some 500 and 2000 patients are diagnosed every year with malignant tumors originating from the bone and soft tissue, respectively (1,2). Unlike carcinomas, sarcomas are not lifestyle-related, and they occur at a considerably high rate among young subjects. Sarcomas involve a wide variety of histological types (e.g., osteosarcoma, chondrosarcoma, liposarcoma) and can develop in any part of the body. Depending on the combination of the histological type and the original site of the tumor, the therapeutic approaches vary, and the same treatment can result in different outcomes in different patients depending on these and other factors (3).

Multidisciplinary approaches including surgery, chemotherapy (anti-cancer drugs), and radiotherapy have been most successful for the treatment of bone and soft-tissue tumors in the last 30 years. In particular, the survival rate has been greatly improved for patients with osteosarcomas of the extremity due to progress in chemotherapy (4). In addition, dramatic advances in surgical techniques and prosthetic technology have markedly increased the limb salvage rate. The first-line treatment for bone and soft-tissue tumors is inevitably surgery. However, not all cases are resectable, depending on the tumor site, size, and depth of invasion. The resection of tumors of the extremities is often curative, whereas tumors involving the spine, pelvis, and other axial parts of the body are generally not amenable to surgery, especially advanced cases. Some patients undergoing surgical resection may also run the risk of being deprived of excretory function or suffering a major loss of ambulatory ability (5).

Until recently, unresectable tumors were treated with external radiation therapy and/or brachytherapy combined with chemotherapy. However, chemotherapy was not always effective for the treatment of a wide variety of sarcomas, and conventional radiotherapy achieved good results for only a few types of sarcomas. Therefore, unresectable sarcomas had a very poor prognosis due to the lack of any effective local treatment (6).

Clinical trials of carbon ion radiotherapy for bone and soft tissue sarcomas

Between June 1996 and February 2000, a phase I/II study was carried out to evaluate the efficacy and safety of carbon ion radiotherapy for bone and soft tissue sarcoma (7). This study presented a dose escalation trial using the same fractionation starting from a total dose of 52.8 GyE (3.3GyE per fraction). These patients were not suited for surgical resection. The eligibility criteria for the study are shown in Table 1. Following the trial, a fixed –dose phase II trial has been ongoing since April 2000 using a total dose of 70.4GyE or 73.6GyE. While the phase II trial included patients with radiation–associated sarcoma, patients with intravascular tumor thrombosis were

excluded. A central review of the surgical or biopsy specimens was carried out for all candidates. All patients enrolled in the trials signed an informed consent form approved by the local institutional review board (7-11).

Table 1

Eligibility Criteria
• Histological confirmed bone and soft tissue sarcomas
• Unresectable tumor or the patient declines surgery
• Gross measurable lesion
• Lesion size <15cm in maximum diameter
• KPS 60-100%
• No tumor thrombus
• Signs informed consent form

KPS: Karnofsky Performance Status

Carbon ion radiotherapy for bone and soft tissue sarcomas

The carbon ion beam has higher biological effectiveness and more favorable dose distribution profiles than ordinary radiation beams, like x-ray. The use of the particles provides the target tumor site with a large amount of irradiation possessing a high tumoricidal effect. Three-dimensional treatment planning was performed with the HIPLAN software program (National Institute of Radiological Sciences, Chiba, Japan) specifically designed for planning carbon ion radiotherapy. The standard protocol for the treatment of bone and soft-tissue tumors consists of 16 irradiation sessions delivered over four weeks, once daily four times per week, from Tuesday to Friday Tuesday to Friday. A total dose ranging 52.8 to 73.6 GyE (GyE= carbon physical dose (Gy) x Relative Biological Effectiveness (RBE)) was administered . The fraction dose was modified to be 3.3-4.6GyE. Energies of 350 and 400MeV/n are used mainly for the treatment for axial bone and soft tissue sarcomas, respectively. A margin of 5mm was usually added to the clinical target volume to create the planned target volume. The clinical target volume was covered by at least 90% of the prescribed dose. The patients were usually treated with 3 ports to avoid severe reactions in the normal tissue. One port was used in each session. During the irradiation, the patients lie down in either the supine or prone position with tailor-made immobilization devices on the treatment couch for 20 to 30 minutes in the treatment room. The irradiation with the carbon ion beams lasts for a few minutes.

Results

The phase I/II dose escalation study was carried out on 64 lesions of 57 patients between June 1996 and February 2000 (7). This study produced a favorable tumor control rate of 89% at 1 year, and 63% at 3 years and 5 years, respectively. The overall survival rates were 82% at 1 year, 47% at 3 years, and 37% at 5 years, respectively. The median survival was 31 months. There was a significant difference in the results for the local control rate achieved with a total dose of 57.6GyE or less and that with 64.0GyE or more. As
7 of the 17 patients treated with 73.6GyE were found to have Grade 3 RTOG acute reactions in the skin, the dose escalation was halted at this dose level. These findings made it clear that with a dose fractionation regimen of 16 fractions over 4 weeks, a total dose of 70.4GyE was the maximum applicable dose in patients for whom there was sufficient skin close to the tumor, while a total dose of 73.6GyE was possible in other cases. When we started using at least three portals in order to reduce the dose delivered to the skin, such severe reactions were no longer observed. In view of these findings, the recommended dose for axial bone and soft tissue sarcomas was fixed at 70.4 GyE in 16 fractions over 4 weeks.

In the subsequent fixed-dose phase II study started in April 2000, 500 have been enrolled as of February 2011. The clinical characteristics of this study are summarized in Table 2.

Table 2

The patient characteristics of the phase II study

Characteristics		No (N=495 pts)
Age		
Median		58 (11-87)
Sex		
Male:Female		288:207
Tumor sites		(N=514 lesions)
Pelvis		388
Spine/para-spine		96
Extrimities/others		30
Histology		
Bone		405
	Chordoma	177
	Chondrosarcoma	81
	Osteosarcoma	81
	Ewing/ PNET	28
	Others	38
Soft Tissue		109
	MFH	21
	MPNST	15
	Synovial sarcoma	11
	Leiomyosarcoma	11
	Others	51

The number of patients analyzed for six months or longer after the treatment included 514 lesions of 495 patients. The total a dose of 73.6GyE (4.6GyE /fraction) was applied for 10 patients, 64.0GyE (4.0GyE /fractions) for 32 patients and 67.2GyE (4.2GyE/fractions) for 70 patients. The remaining 376 patients were treated with a dose of 70.4GyE (4.4gyE/fraction). As of August 2011, the 2-year and 5-year local control rates were 85% and 69%, respectively. The two–year and 5-year overall survival rates were 79% and 59%, respectively (Fig 1). The types of radiation-related toxicity are summarized in Table 3. Overall, the toxicity was acceptable, with 2% skin/soft tissue late G3/4 toxicity observed. Late skin toxicities including, grade 3 in 6 patients and 4 in 1 patient were also observed. These late skin reactions suggest that there are other risk factors, in addition to the total dose. These are thought to include the following: 1) subcutaneous tumor invasion, 2) a large tumor volume, 3) sacrococcygeal involvement, 4) previous surgery, 5) additional chemotherapy and 6) irradiation using 2 portals. It was possible to prevent the skin reactions by irradiation using over 3 portals in order to reduce the dose administered to the skin surface (12). The incidence of Grade 3 or higher late akin reactions in the patients receiving a total dose of 70.4GyE with over 3 portals has been within the acceptable level for the past several years.

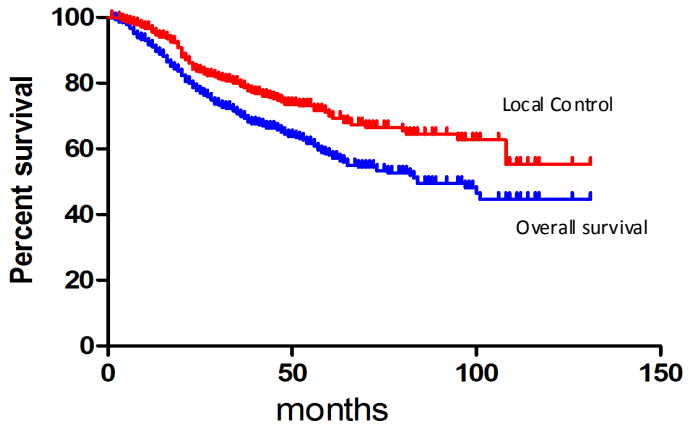

Figure1. Actual local control and overall survival rate in the 495 patients with bone and soft tissue sarcomas enrolled to phase II study. The 5-year local control rates was 69% and the 5-year overall survival rates was 59%.

Table 3

Late radiation morbidities in the phase II study

		Grade					
	No	0	1	2	3	4	5
Skin	506	4	475	20	6	1	0
GI tract	439	437	2	0	0	0	0
Spinal Cord	46	45	0	1	0	0	0

Among the bone and soft-tissue sarcomas treated with carbon ion radiotherapy at our hospital, sacral chordomas accounted for the largest proportion. Sacral chordoma is a rare tumor. Surgery is the first-choice of treatment, but it is not always possible. Since sacral chordomas usually develop gradually, they are often left undetected until they start to cause pain and other symptoms. A lot of patients referred to our hospital presented with a sacral chordoma over 10 cm in diameter. The sacrum houses the sacral nerves, which innervate the excretory functions and ambulation. Depending on the level of the tumor involvement to the sacral bone, excision of these nerves causes permanent gait, excretory and other disabilities, and it impairs the patients' quality of life. Therefore, curative surgery for sacral chordoma (sacrectomy) is one of the most invasive surgeries. Sacral chordomas frequently occur among the elderly population, who are also often contraindicated for surgery because of either comorbid diseases or overall frailty. Ninety-five patients with sacral chordoma received carbon ion radiotherapy between 1996 and 2007(8). The median age of the 95 patients was 66 years. Eighty–four patients had not been treated previously, while the other 11 patients had a locally recurrent tumor following a previous resection. The median tumor diameter was 9 cm. The carbon ion dose ranged from 52.8GyE to 73.6G. The 5-year local control rate was 88%, and the median time to local failure was 35 months (13-60 months). The 5 year overall survival rate was 86%, with a median follow-up of 42 month (13-112 months) (Fig2).

Of the 95 patients, 91% remained ambulatory with or without a supportive device. Two patients experienced severe skin or soft tissue reactions requiring a skin graft. Fifteen patients experienced severe sciatic nerve complications requiring continuing medication, and had impairment of their ordinary life. As of February 2011, 183 chordomas of various types were treated with carbon ion radiotherapy.

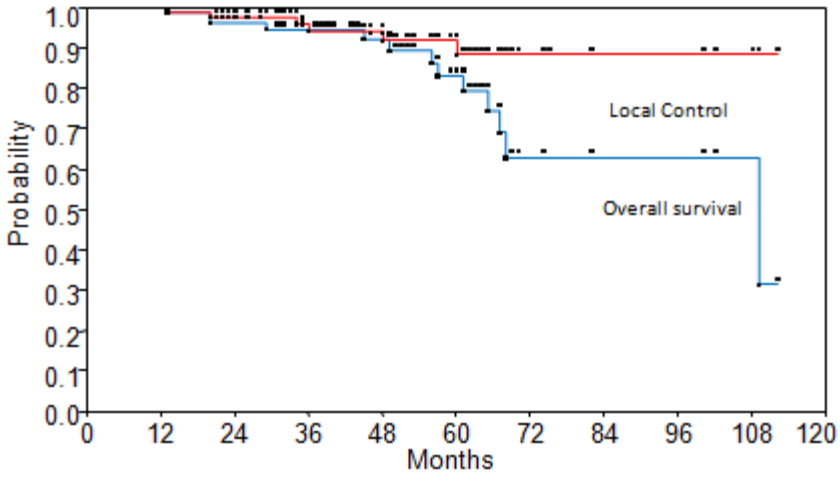

Figure2. Actual local control and overall survival rate in the 95patietns with sacral chordoma. The 5-year local control rate was 88% and the 5 year overall survival rate was 86%.

Osteosaromas of the trunk constituted the next largest group. For the treatment of osteosarcomas of the extremity, which develop with a high incidence among youth, the paradigm based on a combination of surgery and chemotherapy has been well-established, and carbon ion radiotherapy is unlikely to outweigh their advantages. The 5-year local control and 5-year overall survival rates for the 78 patients with unresectable osteosarcoma of the trunk were 61% and 32%, respectively (Fig3). The median diameter of the tumors was 9 cm. As reported in the literature, in the cases of unresectable osteosarcoma, the survival rate was 10% or less. Therefore, carbon ion radiotherapy appears to provide a survival benefit. The tumor size was one of the most important prognostic factors in surgery cases. In patients with unresectable osteosarcoma of the trunk who received carbon ion radiotherapy, the tumor volume was a prognostic factor for the survival and local control rate as well. Thirty-eight patients with a tumor volume of less than 500cc showed a 5-year local control rate of 87%, while forty patients with a volume of more than 500cc had a rate of 21%. The five-year survival rate of the 38 patients with smaller tumors was 46%, while that of the larger tumor group was 19%.

Chondrosarcoma is the second most common primary malignant bone tumor. Surgery has been considered the main form of treatment for chondrosarcoma, and the definitive en bloc resection of the tumor is mandatory to obtain long term disease free survival. However, radical surgical intervention for chondrosarcoma of the trunk has sometimes been associated with substantial morbidities. From 1996 to 2009, 71 patients with chondrosarcoma received carbon ion radiotherapy. The clinical target volumes ranged between 25 and 2900 cm3 (median 488 cm3). At 5 years, the actuarial overall local control rate and overall survival rate were 60% and 60%, respectively (Fig4). Four patients experienced grade 3 and/or 4 skin/soft tissue late reactions in this series.

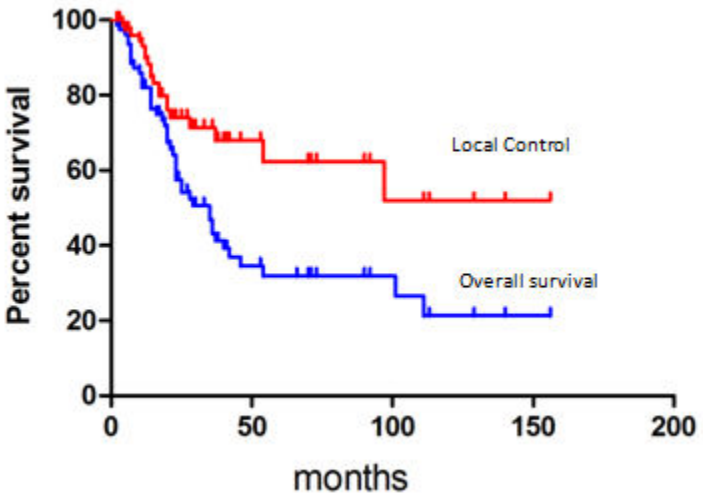

Figure3. Actual local control and overall survival rate in the 78 patients with osteosarcoma of the trunk.The 5-year local control and 5-year overall survival rates were 61% and 32%, respectively.

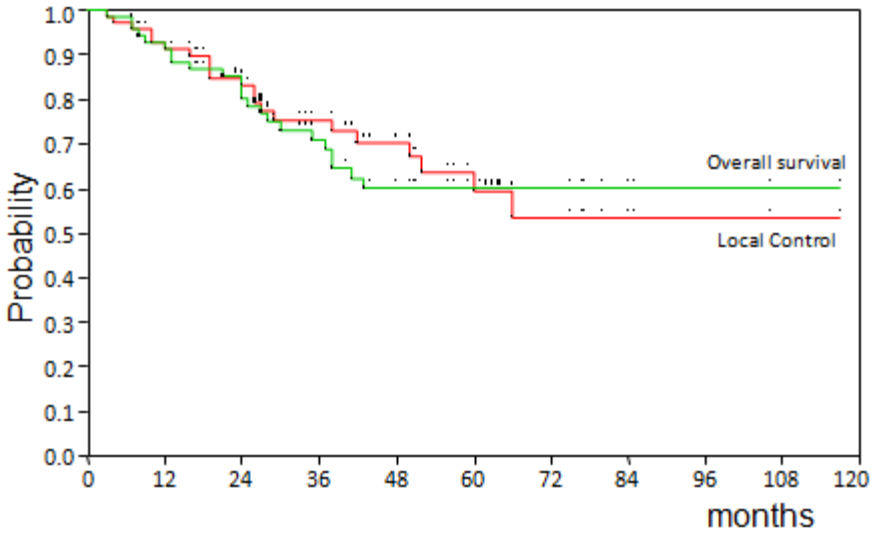

Figure4. Actual local control and overall survival rate in the 71patietns with chondrosarcoma. The 5-year local control rate was 60% and the 5 year overall survival rate was 60%.

Table 4

The result for carbon ion radiotherapy for sacral chordoma

	No of pts	Treatment	5y-LC	5y-OS	10y-OS
MGH(13)	27	Surgery+proton	72%	82%	62%
LBL(14)	14	Surgery+He-ion	55	85	22
Mayo(15)	52	Surgery	56	74	52
NIRS(8)	95	C-ion	88	86	

LC: local control, OS: overall survival

Discussion

In this study, carbon ion radiotherapy was well tolerated and demonstrated substantial activity against sarcomas. These results were obtained in patients with advanced and/or chemo-resistant gross lesions not suited for surgical resection, and were located mainly in the trunk. The results of carbon ion radiotherapy using a total dose of 64GyE to 73.4GyE in 16 fractions over four weeks were satisfactory, considering the candidates were disqualified from surgery. However, it is imperative to continue with long term follow-up to assess the safety and efficacy of carbon ion radiotherapy. With the development of the current research, the possibility of a shorter fractionation regimen should also be explored. The use of a hypofractionated regimen would allow the facility to operate more efficiently and to offer treatment for a larger number of patients. The indications should be expand to not only unresectable cases, but also elderly patients and patients with major functional loss subsequent to surgical resection. While previous experience with carbon ion radiotherapy to the extremities has so far been observed for patients intractable to limb-salvage surgery, widening the scope to limb-retaining therapy should thus be considered.

Conclusion

Carbon ion radiotherapy is an effective local treatment for patients with bone and soft tissue sarcomas for whom surgical resection is not a viable option, and it shows great promise as an alternative to surgery. The morbidity rate of carbon ion radiotherapy has so far been acceptable although the long-term safety of this approach for patients with sarcomas will need to be monitored.

Reference

[1] General rules for clinical and pathological studies on malignant bone tumors, the 3rd edition, The JOA committee of tumors

[2] General rules for clinical and pathological studies on malignant soft tissue tumors, the 3rd edition, The JOA committee of tumors

[3] Jaffe N. Osteosarcoma: review of the past, impact on the future. The American experience .Cancer Treat Res. 2009;152:239-62.

[4] Kawai A, Huvos AG, Meyers PA, et al. Osteosarcoma of the pelvis. Oncologic results of 40 patients. Clin Orthop Relat Res. 1998 ;348:196-207.

[5] Ozaki T, Flege S, Kevric M, et al. Osteosarcoma of the pelvis: experience of the Cooperative Osteosarcoma Study Group. J Clin Oncol. 2003 ;21(2):334-41.

[6] Ritter J, Bielack SS. Osteosarcoma. Ann Oncol. 2010 ;21 Suppl 7:vii320-5.

[7] Kamada T, Tsujii H, Tsuji H, et al. Efficacy and safety of carbon ion radiotherapy in bone and soft tissue sarcomas. J Clin Oncol. 2002 ;20(22):4466-71.

[8] Imai R, Kamada T, Sugahara S, et al. Carbon ion radiotherapy for sacral chordoma.Br J Radiol. *in press*

[9] Imai R, Kamada T, Tsuji H,et al. Effect of carbon ion radiotherapy for sacral chordoma: results of Phase I-II and Phase II clinical trials.Int J Radiat Oncol Biol Phys. 2010;77(5):1470-6.

[10] Imai R, Kamada T, Tsuji H, et al. Carbon ion radiotherapy for unresectable sacral chordomas. Clin Cancer Res. 2004;10(17):5741-6.

[11] Serizawa I, Kagei K, Kamada T, et al. Carbon ion radiotherapy for unresectable retroperitoneal sarcomas. Int J Radiat Oncol Biol Phys. 2009;75(4):1105-10.

[12] Yanagi Kamada T, Tsuji H, Dose-volume histogram and dose-surface histogram analysis for skin reactions to carbon ion radiotherapy for bone and soft tissue sarcoma. Radiother Oncol. 2010;95(1):60-5.

[13] Park L, Delaney TF, Liebsch NJ, et al. Sacral chordomas: Impact of high-dose proton/photon-beam radiation therapy combined with or without surgery for primary versus recurrent tumor. Int J Radiat Oncol Biol Phys. 2006;65(5):1514-21.
[14] Schoenthaler R, Castro JR, Petti PL, et al. Charged particle irradiation of sacral chordoma.Int J Radiat Oncol Biol Phys. 1993 20;26(2):291-8.
[15] Fuchs B, Dickey ID, Yaszemski MJ, et al. Operative management of sacral chordoma.J Bone Joint Surg Am. 2005;87(10):2211-6.

Carbon Ion Radiotherapy for Liver Cancer

Hiroshi Imada, Shigeo Yasuda, Shigeru Yamada, Makoto Shinoto, Kazuhiko Oonishi, Satoshi Endo, Tadashi Kamada, and Hirohiko Tsujii

Hospital, Research Center for Charged Particle Therapy, National Institute of Radiological Sciences, Chiba, Japan
e-mail address: h_imada@nirs.go.jp

Abstract

A trial of carbon ion radiotherapy (C-ion RT) for hepatocellular carcinoma (HCC) was first conducted in April 1995 at the National Institute of Radiological Sciences (NIRS) in Japan. A total of 193 patients with HCC were enrolled in this clinical trial. In the first and second phase I/II clinical trials, dose escalation studies were carried out in incremental steps of 10%, resulting in the confirmation of both the safety and efficacy of short-course regimens of 12, 8, and 4 fractions. Based on the results, a phase II clinical study with fixed fractionation, that is, 52.8 GyE/4 fractions, was performed. A total of 47 patients were treated during this phase II study, which resulted in low toxicity and attained a high local control rate (96%) for 5 years after treatment. The last clinical study was conducted from April 2003 to August 2005, with a more hypofractionated regimen of 2 fractions/2 days, in which 36 patients were safely treated within a dose escalation range from 32.0 GyE to 38.8 GyE. The 2-fraction therapy protocol is continuing under the license of Highly Advanced Medical Technology. There have been no therapy-related deaths and no severe adverse events. We conclude that, because of the low toxicity and high local control rate, C-ion RT is a promising new, radical, and minimally invasive therapeutic option for HCC.

Introduction

Hepatocellular carcinoma (HCC) is one of the most common malignant tumors worldwide and is the third leading cause of death from cancer (1). Various therapeutic options are presently available for patients with HCC. With regard to radiotherapy, the role for patients with HCC was previously limited and unsatisfactory on the basis of the poor hepatic tolerance to irradiation (2, 3). However, technological advances have made it possible to deliver a higher dose of radiation to focal liver tumors more accurately, reducing the degree of toxicity (4, 5). Carbon ion beams possess a Bragg peak and provide excellent dose distribution to the target volume by specified beam modulations (6-8). They have advantageous biological and physical properties that result in a higher cytocidal effect than that of photons and protons (9-10). Since 1995, carbon ion radiotherapy (C-ion RT) has been performed for the treatment of HCC, and clinical trials were initiated at the National Institute of Radiological Sciences (NIRS) in Japan.

Methods and Materials

1. An outline of carbon ion radiotherapy for HCC: Clinical trials to medical treatment (Table 1)

In the first and second phase I/II clinical trials, dose escalation studies were carried out in incremental steps of 10% in order to identify the optimum dose. In the first of these trials, 24 patients were treated with a 15-fraction regimen at a total dose range of 49.5-79.5 GyE. In the second trial, 86 patients were treated with short-course regimens, at total dose ranges of 54.0-69.6 GyE in 12 fractions, 48.0-52.8 GyE in 8 fractions, and 48.0-52.8 GyE in 4 fractions. Based on the results of these studies, a third protocol was established to implement a phase II clinical trial using a fixed total dose of 52.8 GyE spread over 4 fractions of 13.2 GyE each (11). The fourth

protocol, a phase I/II clinical study, was performed using an even more hypofractionated regimen of 2 fractions/2 days at total dose levels ranging from 32.0 GyE to 38.8 GyE (12). The eligibility criteria common to all four of these protocols were as follows: (a) biopsy-proven HCC (histological diagnosis); (b) no tumor thrombosis of the main trunk of the portal vein; (c) no multiple viable lesions outside the planning target volume; (d) no previous treatment to target tumors by other forms of RT; (e) ECOG performance status of 0–2; (f) no other active cancers; and (g) digestive tract not in contact with the clinical target volume. Most of the subjects enrolled under these protocols had been judged not to be amenable to, or as having had recurrence after, other treatments, or as having no prospect of an adequate treatment effect with any of the existing therapies. Two-fraction therapy is currently ongoing according to the guidelines allowing careful step-wise dose escalations at a 5% increase rate under the license of Highly Advanced Medical Technology.

Table 1. An outline of the use of carbon ion radiotherapy for HCC

Carbon Ion Radiotherapy for HCC

April, 1995～February, 2011 Total n=274

Protocol	Category	Fractionation	Period	Number
9401	Phase I/II study	15f/5w	1995.4～1997.3	24
9603	Phase I/II study	12f/3w	1997.4～2001.3	34
		8f/2w		24
		4f/1w		28
0004	Phase II study	4f/1w	2001.3～2003.3	47
0202	Phase I/II study	2f/2days	2003.4～2005.8	36
0202(2)	Highly Advanced Medical Technology	2f/2days	2006.4～	81

2. Carbon ion radiotherapy

2-1. Preparation for treatment

One or two metal markers (0.5 × 3 mm) made of iridium wire were inserted near the tumor under ultrasound imaging guidance as landmarks for target volume localization. The irradiation fields were established with a three-dimensional therapy plan based on 5-mm-thick CT images. CT planning was performed using the HIPLAN, which was originally developed for 3D treatment planning (13). The clinical target volume was defined according to the shape of the tumor plus a 1.0-1.5-cm margin. The median target volume was 159 ml (range: 37-1466 ml). Double right-angled field geometry was used for irradiation in most patients (double right-angled field: 77%, double oblique field: 7%, 3-field: 14%, 4-field: 2%). The supine or prone position was selected according to the location of the tumor. Respiratory gating was employed in the CT scan planning and irradiation stages to ensure more accurate delivery of the radiation (14).

2-2. Verification of patient position and target volume localization

To accurately reproduce the patient position, a low-temperature thermoplastic sheet and a customized cradle were used. Patients were immobilized on a rotating couch to permit either vertical or horizontal beam irradiation from any angle. To assess the accuracy of patient positioning and target volume localization, orthogonal fluoroscopy and radiography were used immediately prior to each treatment session.

3. Follow-up and evaluation criteria

All patients were assessed according to a predetermined schedule. After C-ion RT, patients were evaluated on the basis of physical examinations and blood tests once a month for the first year, once every 3 months for the following year, and once every 3–6 months thereafter. Contrast-enhanced CT or MRI was performed every 3 months for the first 2 years and every 6 months thereafter. Local control was defined as no sign of regrowth or new tumors in the treatment volume. Local recurrence was defined as failure of local control. The overall survival was measured from the starting date of treatment until the date of death from any cause. Acute and late toxicities were assessed using the National Cancer Institute Common Criteria, version 2.0, and the Radiation Therapy Oncology Group/European Organization for Research and Treatment of Cancer late radiation morbidity scoring scheme. In addition, liver toxicity was assessed by the Child-Pugh score, a commonly used marker of hepatic functional reserve in patients with chronic liver disease, on a rating scale from 5 to 15 points, with the score increasing with a deterioration of hepatic function.

Results

A. Protocols 9401, 9603, and 0004 (4-15 fraction regimen C-ion RT for HCC)

The results of the clinical trials up to the 4-fraction regimen for which observations have been continued for 5 years or longer are described below.

1. Toxicities

No therapy-related deaths occurred in the patients treated under any of the three protocols. There was no grade 4 hepatic toxicity. With regard to the Child-Pugh score, the increase in the score associated with C-ion RT remained within 1 point or below in many patients in the early (within 3 months of the start of radiotherapy) and late phases (after 3 months) (Fig. 1). This demonstrated that the changes in liver function remained minor after C-ion RT was initiated. The number of cases reported to have a score increase of 2 points or more in the late phase, which is of particular clinical significance, tended to be smaller with decreasing fraction numbers. No serious adverse effects were noted in the digestive organs.

2. Anti-tumor effects

HCC develops in a successive manner, fostered by the underlying cirrhosis of the liver. Patient survival is therefore determined by the overall results, including the treatment of recurrent lesions and also the treatment of hepatic insufficiency in cases where there is a decline in liver function. As a result, the survival rate does not reflect the efficacy of any particular treatment alone. In comparing the effectiveness of the different therapies for HCC, it is therefore easier to make a judgment on the basis of the local control rate rather than the survival rate. In the present clinical trials, other treatments proved ineffective or led to recurrence in 57% of the patients, and as the phase I/II trials were conducted as dose escalation studies to determine the recommendable dose, there is a possibility that some of the patients may have been treated with a dose that was less than optimal. It is therefore not possible to make a simple comparison of the survival rates achieved in these clinical trials with other treatments.

The local control rates for the analyzed lesions are shown separately according to the protocol and fractionation regimen (Table 2). There were no significant differences in the control rates among the patients treated with the different fractionation schedules.

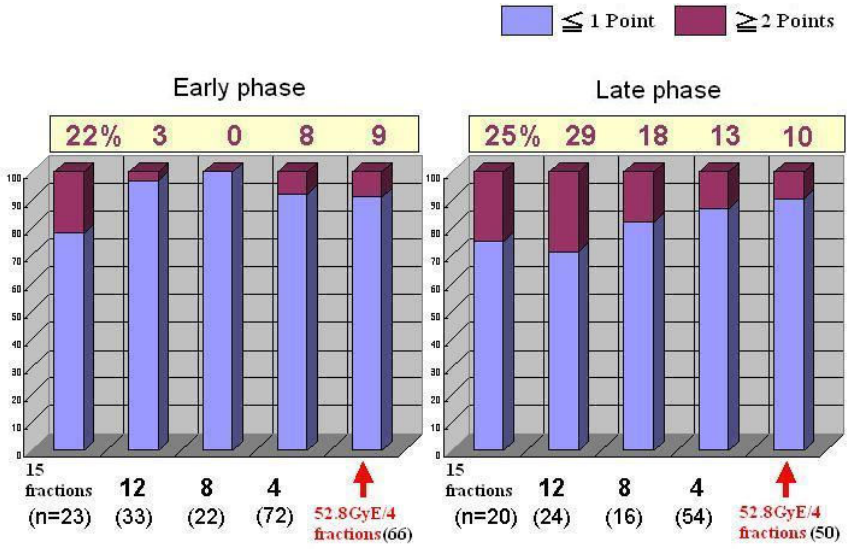

Fig. 1: The changes in the Child-Pugh score before and after C-ion RT

Variations in the Child-Pugh score, an international standard used to assess the degree of hepatic insufficiency before and after irradiation, were studied. The degrees of hepatic insufficiency can be evaluated with the Child-Pugh score on a scale from 5 to 15 points. The score increases as the degree of hepatic insufficiency increases.

The increase in score associated with C-ion RT remained within 1 point or below in many patients in the early (within 3 months of start of radiotherapy) and late phases (after 3 months) after treatment.

Table 2. The results of clinical trials for HCC with C-ion RT

Trial		Phase I/II	Phase I/II			Phase II	52.8GyE/4f
Number of fractions		15	12	8	4	4	4
Total dose (GyE)		49.5-79.5	54.0-69.6	48.0-58.0	48.0-52.8	52.8	52.8
Number of lesions		24	34	24	28	47	69
Maximum tumor diameter (cm)	Median	5.0	3.7	3.1	4.6	3.7	4.0
	Range	2.1-8.5	1.5-7.2	1.2-12.0	2.2-12.0	1.2-7.5	1.2-12.0
Recurrent Tumor	yes	18 (75%)	18 (53%)	16 (67%)	18 (64%)	20 (43%)	35 (51%)
	no	6 (25%)	16 (47%)	8 (33%)	10 (36%)	27 (57%)	34 (49%)
1-year local control (%)		92	97	91	89	96	94
3-year local control (%)		81	86	86	89	96	94
5-year local control (%)		81	86	86	89	96	94

B. Protocol 0202, 0202(2) (2 fractions/2 days)

1. Toxicities

No therapy-related deaths occurred in the hypofractionation trial. There were no cases of grade 4 hepatic toxicity. With regard to the Child-Pugh score, in the late phase (3 months after treatment), an increase of 2 points and more occurred in 5% and 7% in the smaller tumor group (≦5 cm) and the larger tumor group (>5 cm), respectively. There was no significant difference between the two groups (P=0.8424). This demonstrated that the changes in liver function remained minor after C-ion RT was initiated. No serious adverse effects were noted in

the digestive organs.

2. Anti-tumor effects

The local control rates were 94.5% and 90.8% at 1 year, and 94.5% and 73.7% at 3 years in the higher dose group (≧42.8GyE) and the lower dose group (≦40.8GyE), respectively. The patients in the higher dose group showed a better local control rate than those in the lower dose group (P=0.0785). In the higher dose group, the local control rates after both 1 and 3 years were 92.7% in the smaller tumor group (≦5 cm) and 100% in the larger tumor group (>5 cm), respectively.

Discussion

1. Standard therapies for HCC

The standard therapies for HCC are hepatectomy, transcatheter arterial embolization (TAE), percutaneous ethanol injection (PEI), radio-frequency ablation (RFA), and liver transplantation. According to the Survey and Follow-up Study of Primary Liver Cancer in Japan, the relative use of these therapies in the treatment records of all patients for the two-year period from January 1, 2004 through December 31, 2005 were: hepatectomy in 32% of case, TAE in 32%, and percutaneous local therapy involving PEI, percutaneous microwave coagulation therapy (PMCT), and RFA in 31%. Each of these procedures has merits and drawbacks. For example, while hepatectomy provides the best certainty of removing cancer cells, the procedure also results in serious stress on both the liver and the body as a whole. TAE is clinically useful and has a relatively low degree of invasiveness, but is of limited radicality. PEI and RFA, on the other hand, are simple procedures offering a high degree of radicality, but their effect is limited to comparatively small tumors (less than 3 cm in diameter). The use of radiotherapy for HCC has been considered difficult in view of the problems associated with radiation-induced hepatic insufficiency (15, 16). However, progress in the development of irradiation devices in recent years has made it possible to achieve highly localized irradiation. This has spurred advances in radiotherapy research for liver cancer (17-22).

2. Optimal candidates for C-ion RT

We have already reported that C-ion RT used for the treatment of HCC is safe and effective, and that it causes only minor liver damage (10). We investigated the reason why liver function is retained, then, non-irradiated lesion of liver is considered to contribute to the retention of liver function (23). For patients with extensive infiltration and those with multiple lesions, it is difficult to achieve radicality with C-ion RT alone. C-ion RT is therefore indicated for patients with a level of liver function corresponding to Child-Pugh grade A or B. For small lesions 3 cm or less, however, other minimally- invasive, effective, and low-cost therapies, such as PEI and RFA, are available. In contrast, lesions larger than 3 cm are difficult to treat with PEI or RFA alone, making them ideal targets for C-ion RT. Moreover, even for lesions less than 3 cm in diameter that are adjacent to the porta hepatis, minimally-invasive treatment without complications is an important issue. We compared the efficacy and toxicity of C-ion RT of 52.8GyE in 4 fractions for patients with HCC in terms of the tumor location (adjacent to the porta hepatis or not) and found that there were no significant differences in liver toxicity. Excellent local control was obtained independent of the tumor location. Therefore, in certain patients with a higher risk of injury to the bile duct when undergoing RFA, C-ion RT appears to offer a promising therapeutic alternative (24).

Conclusion

C-ion RT is safe and effective, and it seems to have promise as a new, radical, and minimally invasive therapeutic option for HCC. However, further careful follow-up is still needed to confirm its clinical efficacy in practical medicine.

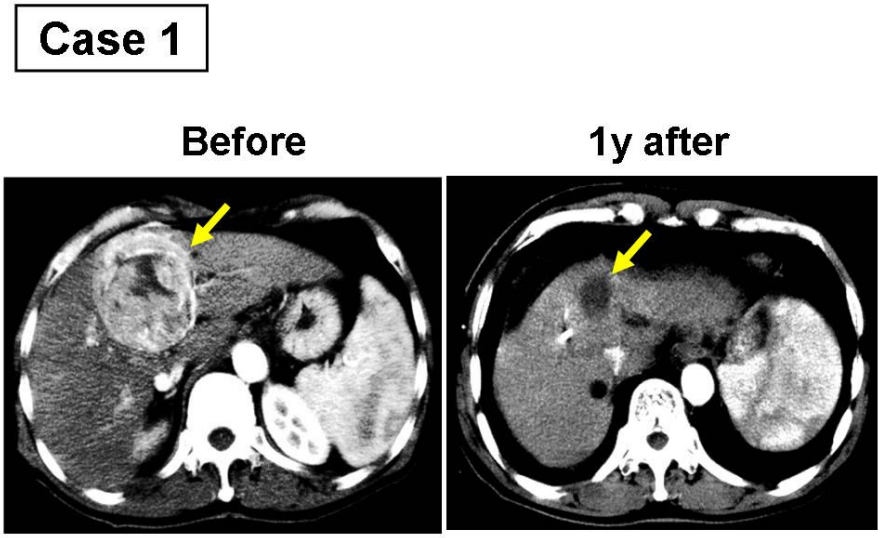

Case 1

A 67-year-old male had a HCC lesion of 7 cm in diameter in segment IV. He survived 5 years after C-ion RT of 72.0 GyE delivered in 15 fractions.

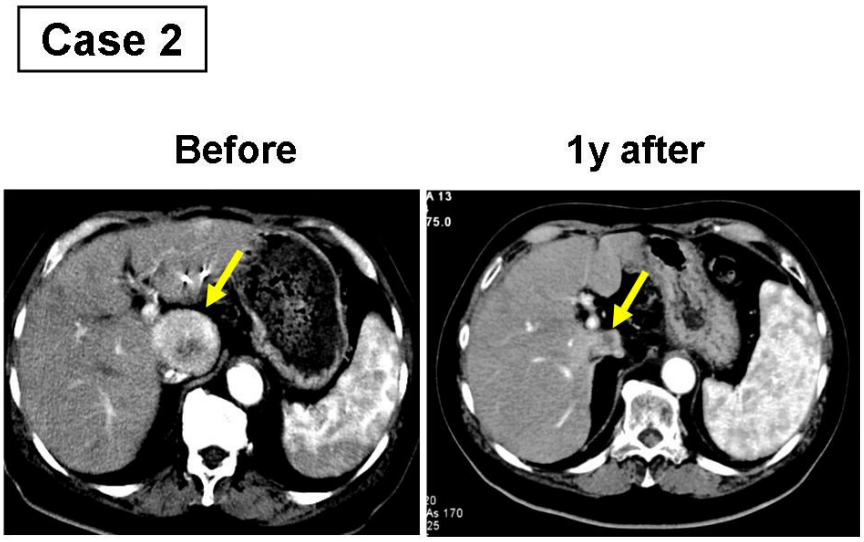

Case 2

A 72-year-old male had a HCC tumor that was 4.6 cm in diameter in segment I. He survived for 7 years after C-ion RT using 52.8 GyE in 4 fractions.

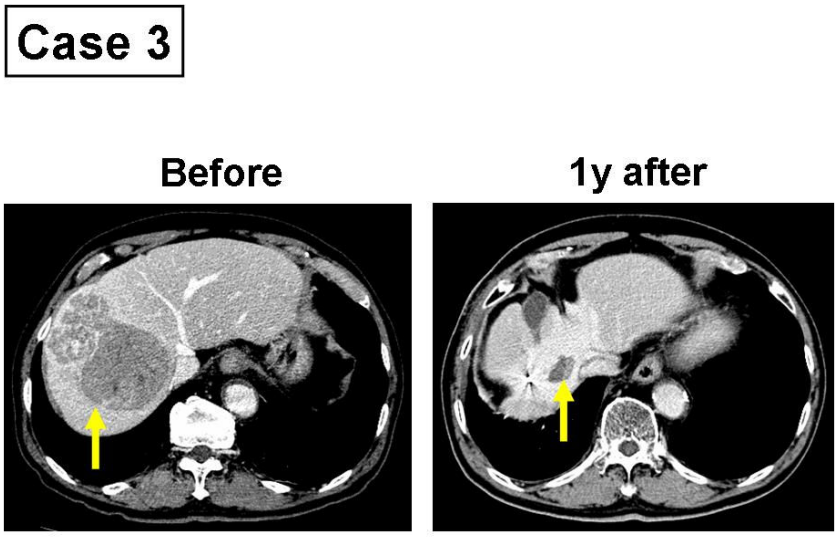

Case 3
A 77-year-old male had a HCC that was 10.5×7.7 cm in the right hepatic lobe. He is still alive 4 years after C-ion RT of 38.8 GyE in 2 fractions.

References

[1] Bosch FX, Ribes J, Borras J. Epidemiology of primary liver cancer. Semin Liver Dis 1999;19:271-285.

[2] Phillips R, Murakami K. Preliminary neoplasms of the liver. Results of radiation therapy. Cancer 1960;13:714-720.

[3] Stillwagon GB, Order SE, Guse C, et al. 194 hepatocellular cancers treated by radiation and chemotherapy combinations: Toxicity and response: a Radiation Therapy Oncology Group study. Int J Radiat Oncol Biol Phys 1989;17:1223-1229.

[4] Robertson JM, Lawrence TS, Dworzanin LM, et al. Treatment of primary hepatobiliary cancers with conformal radiation therapy and regional chemotherapy. J Clin Oncol 1993;11:1286-1293.

[5] Xi M, Liu MZ, Deng XW, et al. Defining internal target volume (ITV) for hepatocellular carcinoma using four-dimensional CT. Radiother Oncol 2007;84:272-278.

[6] Sato K, Yamada H, Ogawa K, et al. Performance of HIMAC. Nucl Phys 1995;A588:229-234.

[7] Kanai T, Furusawa Y, Fukutsu K, Itsukaichi H, Eguchi-Kasai K and Ohara H. Irradiation of mixed beam and design of spread-out Bragg peak for heavy-ion radiotherapy. Radiat Res 1997;147:78-85.

[8] Kanai T, Endo M, Minohara S, et al. Biophysical characteristics of HIMAC clinical irradiation system for heavy-ion radiation therapy. Int J Radiat Oncol Biol Phys 1999;44:201-210.

[9] Tsujii H, Morita S, Miyamoto T, et al. Preliminary results of phase I/II carbon ion therapy. J Brachyther Int 1997;13:1-8.

[10] Kato H, Tsujii H, Miyamoto T, et al. Results of the first prospective study of carbon ion radiotherapy for hepatocellular carcinoma with liver cirrhosis. Int J Radiat Oncol Biol Phys 2004;59:1468-1476.

[11] Kato H, Yamada S, Yasuda S, et al. Phase II study of short-course carbon ion radiotherapy (52.8GyE/4-fraction/1-week) for hepatocellular carcinoma. Hepatology 2005;42(Suppl.1):381A.

[12] Kato H, Yamada S, Yasuda S, et al. Two-fraction carbon ion radiotherapy for HCC: Preliminary results of a

phase I/II clinical trial. J Clin Oncol 2005;23,Suppl.:338s.
[13] Endo M, Koyama-Ito H, Minohara S, et al. HIPLAN-A HEAVY ION TREATMENT PLANNING SYSTEM AT HIMAC. J. Jpn. Soc. Ther. Radiol. Oncol. 1996; 8: 231-238.
[14] Minohara S, Kanai T, Endo M, et al. Respiratory gated irradiation system for heavy-ion radiotherapy. Int J Radiat Oncol Biol Phys 2000;47: 1097-1103.
[15] Ingold DK, Reed GB, Kaplan HS, et al. Radiation hepatitis. Am J Roentgenol 1965;93:200-208.
[16] Phillips R, Murikami K. Primary neoplasms of the liver. Results of radiation therapy. Cancer 1960;13:714-720.
[17] Ohto M, Ebara M, Yoshikawa M, et al. Radiation therapy and percutaneous ethanol injection for the treatment of HCC. In: Okuda K, Ishak KG, editors. Neoplasm of the Liver. Tokyo: Springer-Verlag; 1987. p. 335-341.
[18] Yasuda S, Ito H, Yoshikawa M, et al. Radiotherapy for large HCC combined with transcatheter arterial embolization and percutaneous ethanol injection therapy. Int J Oncol 1999;15:467-473.
[19] Cheng J C-H, Chuang VP, Cheng SH, et al. Local radiotherapy with or without transcatheter arterial chemoembolization for patients with unresectable HCC. Int J Radiat Oncol Biol Phys 2000;47:435-442.
[20] Guo W-J, Yu E-X. Evaluation of combined therapy with chemoembolization and irradiation for large HCC. Br J Radiol 2000;73:1091-1097.
[21] Matsuzaki Y, Osuga T, Saito Y, et al. A New, Effective, and Safe Therapeutic Option Using Proton Irradiation for HCC. GASTROENTEROLOGY 1994;106:1032-1041.
[22] Kawashima M, Furuse J, Nishio T, et al. Phase II Study of Radiotherapy Employing Proton Beam for HCC. J Clin Oncol 2005;23: 1839-1846.
[23] Imada H, Kato H, Yasuda S, et al. Compensatory enlargement of the liver after treatment of hepatocellular carcinoma with carbon ion radiotherapy – Relation to prognosis and liver function. Radiother Oncol 2010;96:236-242.
[24] Imada H, Kato H, Yasuda S, et al. Comparison of efficacy and toxicity of short-course carbon ion radiotherapy for hepatocellular carcinoma depending on their proximity of the porta hepatis. Radiother Oncol 2010;96:231-235.

Carbon Ion Radiotherapy for Patients with Locally Recurrent Rectal Cancer

Shigeru Yamada, Makoto Shinoto, Satoshi Endo, Shigeo Yasuda, Hiroshi Imada, Tadashi Kamada and Hirohiko Tsujii

Research Center Hospital for Charged Particle Therapy, National Institute of Radiological Sciences

1. Characteristics of Locally Recurrent Rectal Cancer

The large intestine starts at the ascending colon, which is connected to the small bowel, and ends at the rectum, which extends from the sacral promontory to the anal canal. In 2008, approximately 43,000 patients died of colorectal cancer in Japan which is the third most common cause of cancer deaths, after lung and stomach cancers. Approximately 100,000 patients were diagnosed with colorectal cancer in 2004, thus making it the second most common type of cancer after stomach cancer. The analysis of the post-operative recurrence rates of colorectal cancer indicates a higher rate for rectal cancer than colon cancer. When compared by the site of recurrence, rectal cancer had a more than three times higher local recurrence rate than colon cancer.

With the recent advances in surgical techniques and procedures, the pelvic recurrence rate of rectal cancer has been decreasing, however the post-operative recurrence rate is still 5% to 20% today. Surgical resection is the first choice for locally recurrent rectal cancer, although total pelvic extenteration or another highly invasive procedure is often required. In many cases, locally recurrent rectal cancers are not completely resectable so generally surgical resections are not selected. The comparison of resection rates by the type of tumors shows that the resection rates were in the range of 40% to 50% for liver metastases and 20% to 40% for lung metastases, whereas the rate was 10% to 40% for locally recurrent colorectal cancers (Table 1)[1,2] Curative resection of these tumors will lead to a survival rate similar to those for other types of recurrences and metastases.

Table 1. Resection and Survival Rates by Site of Recurrence

	Resection rate	5-Year survival rate
Local Recurrence	10-40%	20-40%
Liver metastasis	40-50%	35-55%
Lung metastasis	20-40%	40-50%

Radiation therapy is often indicated for unresectable cases of locally recurrent rectal cancer; most of the past studies on conventional x-ray radiotherapy reported a 12-month median survival and a 10% 3-year overall survival. The use of adjuvant chemotherapy elevated the local control rate up to around 20%, which is far from satisfactory. Heavy charged particle beams have been shown to exert potent anti-tumor effects against radioresistant adenocarcinomas. To improve both the long-term local control and survival of locally recurrent rectal cancer, we have initiated a radiation dose-escalation trial using heavy charged particles.

2. Summary of the Phase I/II and Phase II Studies of Post-Operative Carbon Ion Radiotherapy for Recurrent Rectal Cancer

A phase I/II study of post-operative carbon ion radiotherapy for the treatment of recurrent rectal cancer was started in April 2001. The purpose of the study was to evaluate the tolerance for and effectiveness of heavy charged particle radiotherapy in patients with locally recurrent rectal cancer. In order to determine the appropriate radiation dose, this study adopted a dose-escalation design. This study was continued until February 2004, and enrolled 38 patients for treatment. Subsequent to this study, a phase II study was initiated in April 2004, as part of the government-sponsored Highly Advanced Medical Technology program. In this study, the total radiation dose was fixed at 73.6GyE. This study is ongoing as of the time of writing.

3. Study Treatment

The patient inclusion criteria for this study included (1) post-operative recurrence of a tumor limited to the pelvis (including its surrounding soft tissue) after curative resection of rectal cancer, and (2) at least a 5-mm gap between the recurrent lesion and radiosensitive organs, including the gastrointestinal tract and bladder. Exclusion criteria were (1) a history of radiation therapy on the planned target site of the carbon ion radiotherapy and (2) the presence of multiple primary tumors. Patients were first treated with a total dose of 67.2 gray equivalent (GyE) in 16 fractions over 4 weeks. The total dose was increased by 5% in a stepwise manner to 70.4 and 73.6 GyE, depending on the tumor response and adverse effects. The phase II study employed a total dose of 73.6 GyE, which was the highest total dose attained in the preceding study. A preliminary analysis was conducted on 140 patients (148 lesions) who completed the treatment by the end of February 2010.

4. Treatment Outcomes

(A) Normal-tissue Reactions

No acute grade 3 or higher adverse reactions have been found to date for the gastrointestinal tract and the urinary system. Late adverse events (defined as those occurring no earlier than 3 months after the start of therapy) were observed in 4 patients, who developed a pelvic abscess after tumor necrosis. The tumor was well controlled in all patients.

(B) Tumor response and Survival Rate

The 3- and 5-year local control rates were 88.5% and 88.5% for patients treated with 70.4 GyE, and 95.2%

and 95.2% for those treated with 73.6 GyE. These results showed that radiation doses above 70 GyE achieved excellent outcomes (Figure 1A). The 3- and 5-year survival rates were 36.0% and 24.0% for patients treated with 67.2 GyE, 51.7% and 27.5% for patients treated with 70.4 GyE, and 73.5% and 42.3% for those treated with 73.6 GyE. The survival rates showed an increasing trend with the radiation dose (Figure 1B). A significant proportion of study patients reported rapid pain relief.

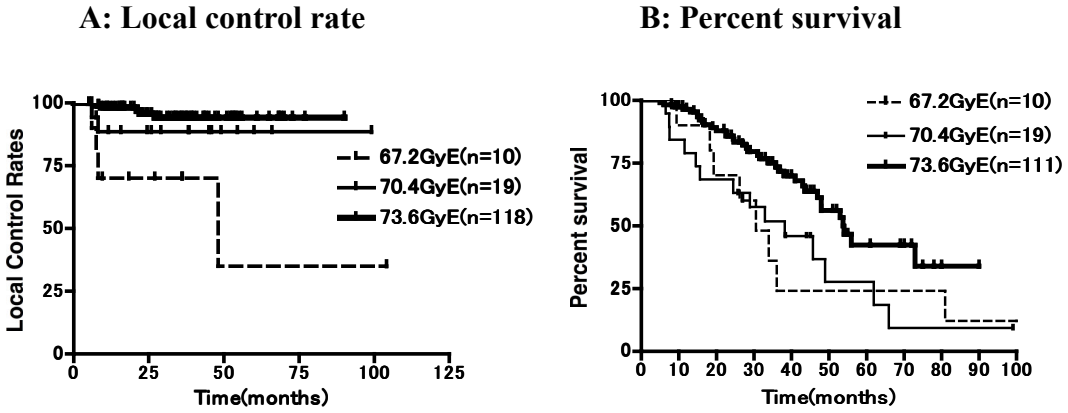

Figure 1. Results of Carbon Ion Radiotherapy for Patients with Locally Recurrent Rectal Cancer

(C) Comparison with Other Studies

The results of the patients treated with 73.6 GyE carbon ion radiotherapy were compared with those of other studies in which patients with locally recurrent rectal cancer were treated with other radiation therapies.[3-6] The results are summarized in Table 2.

Table 2. Results of Radiation Therapy for Patients with Locally Recurrent Rectal Cancer

Author (year)		No. of patients	Radiation dose (Gy)	2-Year survival	5-Year survival	Local control rate
Ciatto S	1982		108	35-50Gy	5%(3y)	3%
O'Connell	1982	17	50	45%	0%	24%(2y)
Wong CS	1991	22	45-50	27%	16%	9%(5y)
Lybeert MLM	1992	76	6-66	61%(1y)	3%	28%(3y)
Knol HP	1995	50	60	27%	8%	-
Murata	1997	18	12-60	44%(1y)	-	46%
NIRS	**2010**	**111**	**73.6**	**86%**	**42%**	**95%(5y)**

Compared with the conventional radiation therapies yielding local control rates below 30% and 5-year survival rates below 10%, the carbon ion radiotherapy produced excellent results. Next, our results were compared with the surgical results reported from other institutions (Table 3).

Table 3. Results of Surgical Therapy for Patients with Locally Recurrent Rectal Cancer[7-9)]

Author (year)	No. of patients	1-Year survival	2-Year survival	5-Year survival
Kato 1994	32	93%	82%	46%
Garcia-Aguilar J1999	42	88%	62%	35%
Wanebo 1999	53	91%	62%	31%
Salo JC 1999	71	88%	75%	31%
Saito N 2003	43	91%	78%	39%
Moriya 2004	48	95%	76%	36%
NIRS 2010	**111**	**97%**	**86%**	**42%**

Our results were comparable to or higher than the published surgical results. In light of the fact that most of our cases involved unresectable tumors, our treatment yielded dramatically improved outcomes. In addition, the carbon ion radiotherapy provided a high quality of life for patients during and after treatment, because patients were spared from undergoing artificial sphincter insertion surgery, and were treated in the out-patient setting.

5. Carbon ion radiotherapy for locally recurrent rectal cancer in patients with prior pelvic irradiation

Among gastrointestinal malignancies, many studies have shown the safety and efficacy of pelvic reirradiation for rectal cancer [10-14]. Reirradiation to the pelvis could potentially play a role in palliation of symptoms or local control. Locally recurrences are located close to critical organs such as the small intestine, colon and bladder and in these patients reirradiation would be expected to be associated with a higher risk of acute and late toxicity at these organs than primary irradition.

The purpose of this study was to asses carbon ion radiation therapy performed as re-irradiation in patients with locally recurrent rectal cancer.

Twenty-three patients were treated with carbon ion RT as re-irradiation for locally recurrent rectal cancer. Nine relapses originated in the presacral region, 8 in the p for pelvic sidewalls and 6 in the perineal region. The total dose ranged of 70.4 gray equivalent (GyE) and was administered in 16 fixed fractions over 4 weeks (4.4 GyE/fraction).

All patients completed the scheduled treatment course. Grade 3 toxicities occurred in 6(26%) patients. The major late toxicities were peripheral neuropathy and infection.

No other severe acute reactions (grade ≥3) were observed at this study.

The one-year and three-year overall survival rates were 83% (95% CI, 68% to 98%) and 65% (95% CI, 43% to 87%), respectively. The one-year and three-year disease-free survival rates were 71% (95% CI, 51% to 91%) and 51% (95% CI, 27% to 75%), respectively.

Carbon ion radiotherapy as re-irradiation appears to be a safe and effective modality in the management of locally recurrent rectal cancer, providing good local control and offering a survival advantage without unacceptable morbidity.

6. Widening the Applicability of Carbon Ion Radiotherapy

Pelvic recurrent tumors are often located in close proximity to the digestive tract. Consequently, a significant proportion of patients were often judged as ineligible for carbon ion radiotherapy, because the digestive tract could not be excluded from the irradiation field. At our hospital, therefore, we adopted a surgical preparatory procedure, to place a spacer between the target tumor and the digestive tract before conducting carbon ion radiotherapy, when the tumor was located close to a sensitive organ. This preparatory procedure has been shown to improve the outcome. We are also currently treating patients with para-aortic lymph node recurrence with 12 fractionated-dose radiation over three weeks, with highly positive outcomes.

7. Conclusion

Carbon ion radiotherapy produced results comparable to the surgical outcomes for patients with locally recurrent rectal cancer. In addition, this minimally invasive therapy ensured a high quality of life for the treated patients.

References

[1] Kobayashi H, Hashiguchi Y, Ueno H：Follow-up for recurrent colorectal cancer. J Ppn Soci Coloproctology 59：851-856, 2006

[2] Sugihara K：Guidelines for treatment of recurrent rectal cancer, P89-149. Nankodo Co. Ltd, Tokyo 2003

[3] Ciatt S: Rdaition therapy of recurrences of carcinoma of the rectum and sigmoid after surgery. Acta Radiol Oncolo 21: 105-109, 1982

[4] O'Connel MJ: A prospective control ed evaluation of combined pelvic radiotherapy and methanol extraction residue of BCG for locally unresectable or recurrent rectal cancer. Int J Radiat Oncol Biol Phys 8: 1115, 1982

[5] Knol HP, Hanssens J, Rutten HJT. Effect of radiation therapy alone or in combination with surgery and/or chemotherapy on tumor and symptom control of recurrent rectal cancer. Strahlenther Onkol 173: 43-49, 1997

[6] Murata T, Fujii I, Yoshino M. Radiation therapy with or without chemotherapy and hyperthermia for recurrent rectal cancer. J Jpn Soc Ther Radiol Oncol 9: 63-71, 1997

[7] Wanebo HJ, Antoniuk P, Koness RJ, et al. Pelvic resection of recurrent rectal cancer. Dis Colon Rectum 42: 1438-1448, 1999

[8] Saito N, Koda K, Takiguchi N. Curative surgery for local pelvic recurrence of rectal cancer Dig Surg

20:192-200, 2002

[9] Moriya Y, Akasu T, Fujita S. Total pelvic exenteration with distal sacrectomy for fixes recurrent rectal cancer in the pelvis. Dis Colon Rectum 47: 2047-2054,2004

[10] Valentini V, Morganti AG, Gambacorta MA,: Preoperative hyperfractionated chemoradiation for locally recurrent rectal cancer in patients previously irradiated to the pelvis: A multicentric phase II study. Int J Radiat Oncol Biol Phys 2006, 64:1129-1139.

[11] Mohiuddin M, Lingareddy V, Rakinic J, Marks G: Reirradiation for rectal cancer and surgical resection after ultra high doses. Int J Radiat Oncol Biol Phys 1993, 27:1159- 1163.

[12] Mohiuddin M, Marks GM, Lingareddy V, Marks J: Curative surgical resection following reirradiation for recurrent rectal cancer. Int J Radiat Oncol Biol Phys 1997, 39:643-649.

[13] Mohiuddin M, Marks G, Marks J: Long-term results of reirradiation for patients with recurrent rectal carcinoma. Cancer 2002, 95:1144-1150.

[14] Lingareddy V, Ahmad NR, Mohiuddin M: Palliative reirradiation for recurrent rectal cancer. Int J Radiat Oncol Biol Phys 1997, 38:785-790.

Carbon Ion Radiotherapy for Pancreatic Cancer

Makoto Shinoto, Shigeru Yamada, Shigeo Yasuda, Hiroshi Imada, Tadashi Kamada, and Hirohiko Tsujii

Hospital of Research Center for Charged Particle Therapy, National Institute of Radiological Sciences

e-mail address: shinoto@nirs.go.jp

<Background>

The number of deaths from pancreatic cancer in Japan exceeds 26,000 per year, and the number is increasing every year[1]. Pancreatic cancer is the fifth leading cause of cancer death and it is considered to be one of the most lethal cancers in Japan. Complete surgical resection is the only curative treatment. However, only a small percentage of patients (10-20%) are candidates for surgical resection because of local progression or metastatic spread at the time of diagnosis[2, 3]. Even if a curative resection is performed, the disease usually recurs and 5-year survival rates are less than 20% [4, 5].

Chemotherapy or chemoradiotherapy is selected as a standard treatment for unresectable pancreatic cancer. However, since pancreatic cancer is often resistant to chemotherapy or radiotherapy, the local control rate is very low. Recently, along with the development of new anticancer agents, the irradiation techniques have greatly progressed following the introduction of highly advanced radiotherapy. However, the outcome from therapy is still not satisfactory, with the median survival being approximately 10 months[6, 7]. We started phase I/II clinical trial for pre-operative carbon ion radiotherapy (CIRT) with 16 fractions in 4 weeks for resectable pancreatic cancer in 2000 (Figure 1).

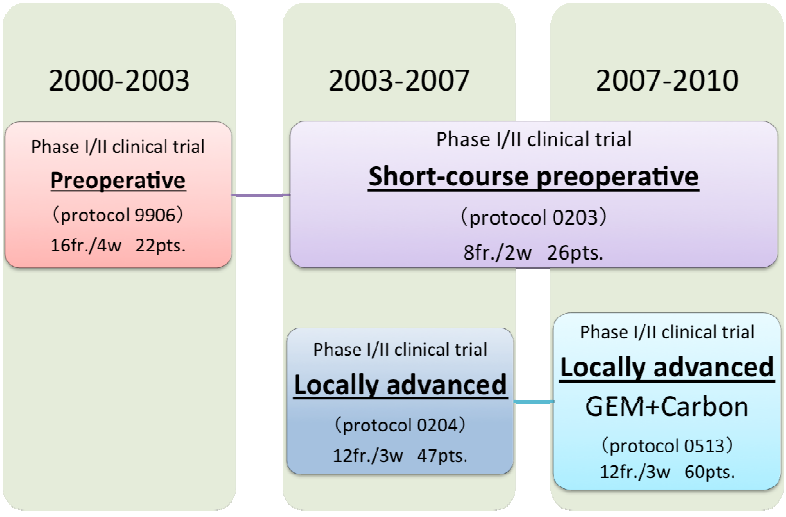

Figure 1. The clinical trial pathway of carbon ion radiotherapy against pancreatic cancer

The purpose of this treatment was to reduce the risk of postoperative local recurrence, which accounts for approximately 50% of total recurrences. We established the tolerance and effectiveness of preoperative CIRT and performed a clinical trial aimed at shortening the fraction size to 8 fractions in 2 weeks beginning in 2003 (Protocol 0203). In addition, we started phase I/II clinical trial for patients with locally advanced pancreatic cancer and showed that the treatment was safe and provided excellent local control rates. Accordingly, we are currently performing a clinical trial of using carbon ion radiotherapy combined with gemcitabine (Protocol 0513).

I. Preoperative carbon ion radiotherapy for patients with resectable pancreatic cancer (Protocol 0203)

<Objective>

The purpose of this study was to evaluate the tolerance and efficacy of CIRT as preoperative irradiation, and to determine the recommended dose needed to reduce the risk of postoperative local recurrence without excess injury to normal tissue.

<Materials and methods>

The eligibility criteria for this study were: that the pancreatic cancer was judged to be radically resectable without involvement of the celiac trunk or superior mesenteric artery. We performed CIRT with 8 fractions in 2 weeks, and resection 2-4 weeks after the irradiation (Figure 2). We started irradiation at a dose of 30GyE/8 fractions, fixed the irradiation fractions and increased the radiation dose by 5% increments.

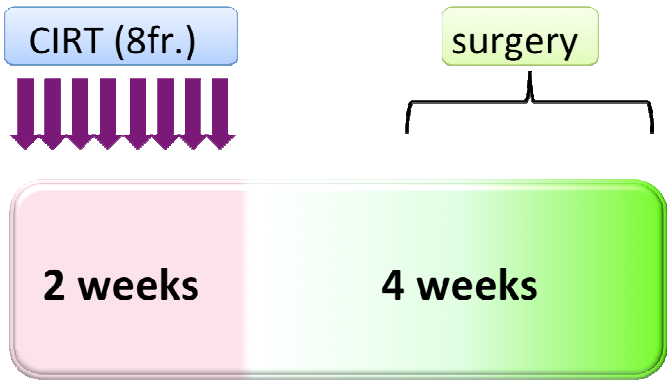

Figure 2. Schedule of preoperative CIRT and surgery (Protocol 0203)

<Results>

Twenty-six patients were registered from April 2003 through February 2010, and dose escalation was performed from 30GyE to 36.8yE (Table 1).

Table 1. Dose schedules of preoperative CIRT

CIRT (GyE)	No. of patients	No. of pts with resection
30.0	6	3
31.6	4	3
33.6	3	3
35.2	6	6
36.8	7	6

We have administered CIRT to all patients as scheduled. The clinical stage according to the UICC was stage IIA in 15 cases and stage IIB in 11 cases. Twenty-one out of 26 patients received curative resection (resection rate 81%), however, the remaining 5 patients did not undergo surgery due to liver metastases or refusal. Although grade 3/4 toxicities were noted in 2 patients (liver abscess-1, PV thrombus-1), both of them were unrelated directly to CIRT. No other serious adverse effects were observed. In the 21 surgical cases, the 5-year local control rates and overall survival rates were 100% and 53%, respectively.

＜Conclusion＞

Preoperative CIRT for patients with resectable pancreatic cancer appears to be acceptable toxicity. And preoperative CIRT reduces the risk of postoperative local recurrence and contributes to improvement of overall survival. This study did not reach the maximum tolerated dose but the dose at 36.8 GyE was estimated to be the recommended dose because of the sufficient local control rate.

II. Gemcitabine combined with carbon-ion radiotherapy for patients with locally advanced pancreatic cancer (Protocol 0513)

<Objective>

The purpose of this trial was to establish the recommended dose of gemcitabine and CIRT, evaluating the tolerance and efficacy of gemcitabine, which is a standard anti-cancer agent for advanced pancreatic cancer, combined with CIRT.

<Materials and methods>

The eligibility criteria for this study were: locally advanced pancreatic cancer which involved the celiac trunk or superior mesenteric artery without distant metastasis. All patients had histologically- or cytologically-proven pancreatic adenocarcinoma or adenosquamous carcionoma. The radiation fractions were fixed at 12 fractions in 3 weeks, and the dose of gemcitabine and radiation were gradually increased. First, the dose was fixed at 43.2GyE/8 fractions and the gemcitabine dose was increased from 400, to 700 to 1000mg/m^2. Subsequently, the gemcitabine dose was fixed at 1000mg/m^2 and the radiation dose was increased by 5% increments (Figure 3). Gemcitabine was administered for 3 consecutive weeks, once a week (Figure 4). The irradiation field was set in the range that included the primary tumor, perineural lesions and prophylactic regional lymph node area.

CIRT*	GEM**
43.2GyE	400mg/m^2 ↓ 700mg/m^2 ↓ 1000mg/m^2
45.6GyE ↓ 48.0GyE ↓ 50.4GyE ↓ 52.8GyE	1000mg/m^2

CIRT*: Carbon Ion Radiotherapy, GEM**: gemcitabine

Figure 3. The dose enhancement trial (Protocol 0513)

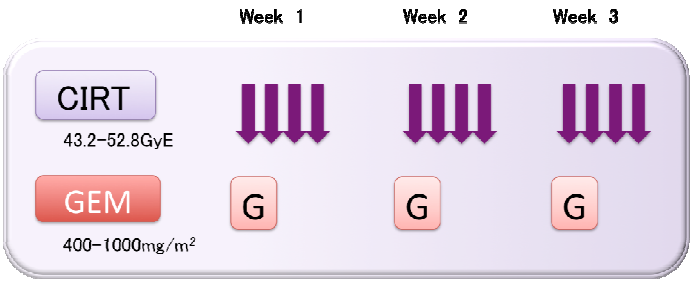

Figure 4. Treatment schedule (Protocol 0513)

<Result>

Sixty patients were registered from April 2007 through February 2011. The median age was 63 (range: 39-74) years. Performance status was 0 in 10 patients (17%), 1 in 48 (80%), and 2 in 2 (3%). The median serum CA19-9 level was 305.3 (range: 0.2-16830). Patients were treated with CIRT over five dose levels and concurrent weekly gemcitabine over three dose levels, an listed in Table 2.

Table 2. Dose schedule of CIRT with concurrent GEM

CIRT (GyE)	GEM (mg/m^2)	Number of patients
43.2	400	7
43.2	700	7
43.2	1000	12
45.6	1000	8
48.0	1000	8
50.4	1000	11
52.8	1000	11

Their clinical stage according to the UICC was stage III in 54 cases and stage IV in six cases. Dose limiting toxicity (DLT) developed as an early adverse event in three of 60 patients, which was a low incidence. One patients treated at the 50.4GyE dose level experienced grade 3 gastric ulcer 10 months after CIRT, but the patient recovered with conservative management. No other serious side effects were found. The combinations with full-dose gemcitabine (1000mg/m2) did not show any increased incidence of adverse effects with dose escalation. The two-year local control rate and two-year overall survival rate were 26% and 32% in all patients. The median survival time was 19.3 months. The Local control and overall survival by CIRT increased along with the dose escalation. In the high dose group, in which patients were irradiated with at least 45.6 GyE, the two-year local control rate and two-year overall survival rate were 47% and 66%.

<Conclusion>

CIRT was well tolerable even when concomitantly administered with the highest dose of gemcitabine ($1000mg/m^2$). Long-term survival or radical cure can be expected by performing further dose escalation or maintenance chemotherapy. This dose escalation trial is now underway.

References

[1] Matsuda T, Marugame T, Kamo KI, Katanoda K, Ajiki W, Sobue T. Cancer Incidence and Incidence Rates in Japan in 2005: Based on Data from 12 Population-based Cancer Registries in the Monitoring of Cancer Incidence in Japan (MCIJ) Project. Jpn J Clin Oncol 2010.

[2] Jemal A, Siegel R, Ward E, et al. Cancer statistics, 2008. CA Cancer J Clin 2008;58:71-96.

[3] Sa Cunha A, Rault A, Laurent C, et al. Surgical resection after radiochemotherapy in patients with

unresectable adenocarcinoma of the pancreas. J Am Coll Surg 2005;201:359-65.

[4] Oettle H, Post S, Neuhaus P, et al. Adjuvant chemotherapy with gemcitabine vs observation in patients undergoing curative-intent resection of pancreatic cancer: a randomized controlled trial. JAMA 2007;297:267-77.

[5] Geer RJ, Brennan MF. Prognostic indicators for survival after resection of pancreatic adenocarcinoma. Am J Surg 1993;165:68-72; discussion -3.

[6] Willett CG, Czito BG, Bendell JC, Ryan DP. Locally advanced pancreatic cancer. J Clin Oncol 2005;23:4538-44.

[7] Koong AC, Christofferson E, Le Q-T, et al. Phase II study to assess the efficacy of conventionally fractionated radiotherapy followed by a stereotactic radiosurgery boost in patients with locally advanced pancreatic cancer. Int J Radiat Oncol Biol Phys 2005;63:320-3.

Carbon Ion Radiotherapy for Prostate Cancer

Hiroshi Tsuji, Nobutaka Mizoguchi, Shingo Toyama, Tadashi Kamada, Hirohiko Tsujii,
and the Working Group for Genitourinary Tumors

Research Center for Charged Particle Therapy, National Institute of Radiological Sciences, Chiba, Japan
e-mail address:h_tsuji@nirs.go.jp

Abstract

Therapeutic outcome of hypofractionated conformal carbon ion radiotherapy towards localized prostate cancer was investigated. We analyzed the biochemical relapse-free rate of 1,084 cases which were observed for 6 months or more after carbon ion radiotherapy at the time of February 2011, also we analyzed survival rate, and the incidence of toxicity. 5-year biochemical relapse-free rate of whole cases was 90.6%. The Gleason score, PSA value and clinical stage were the significant prognostic factor of relapse-free rate. The difference of relapse-free rate by method of fractionation (20 fractions and 16 fractions) was not found. None but one out of 1,005 cases who were followed up at least 1 year developed grade 3 lower urological impairment, and incidences of grade 2 were 5.6% in lower urinary tract and 2.3% in the rectum, respectively. Furthermore, in the 16 fractions, the toxicity incidence was lower than 20 fractions. Accordingly, hypofractionation made it possible to reduce the toxicity incidence without reducing the relapse-free rate.

1.Introduction

As for the prostate cancer, recent irradiation therapy including brachytherapy, proton therapy and intensity modulated radiation therapy play active roles, and improving dose distribution and attendant dose escalation is showed to be connected to the outcome improvement. The National Institute of Radiological Sciences, Chiba, Japan (NIRS) has been challenging the prostate cancer treatment from June 1995 taking the advantage of the quality of carbon ion beam which has distinguished dose convergence and high anticancer efficacy. First, in order to establish an appropriate dose fractionation regimen for C-ion RT, two phase I/II clinical studies have been performed since 1994, using carbon ion beams generated by the Heavy Ion Medical Accelerator in Chiba (HIMAC). A phase II clinical study was then started in April 2000, using the established treatment method of hypofractionated C-ion RT with the recommended dose of 66.0GyE in 20 fractions over 5 weeks that had been proved effective in the phase I/II studies. The safety and efficacy of this treatment strategy of C-ion RT was further confirmed with this phase II study, and approval for its use as a highly advanced medical technology was obtained in November 2003. This article presents the methods and updated outcomes of this established C-ion RT, and also describes its future prospects at NIRS.

2. Materials and methods

We performed carbon ion radiotherapy against 1305 cases of prostate cancer from the start of clinical trial to February 2011. We treated 96 cases in the early dose escalation trials, 175 cases in the phase II clinical trial, thereafter 989 cases were treated in the approved highly advanced medical technology and 45 cases are in ongoing new clinical trial. The annual cases are gradually increasing, especially greatly increased in 2003 when we gained the approval of highly advanced medical technology and in 2007 when we shortened the therapy term from 20

times in 5 weeks to 16 times in 4 weeks (Figure 1).

The eligible patient had no metastases and pathological diagnosis was confirmed as prostate cancer case. As for the carbon ion radiotherapy, first we performed 20 fractions in 5 weeks and after establishing the appropriate dose of radiation and transferred to the highly advanced medical technology, we started 16 fractions in 4 weeks up to today. 562 out of 1305 cases are 20 fractions and 698 are 16 fractions. In a portion of cases, we started clinical trial of 12 fractions in 3 weeks, and have performed therapy for 45 cases.

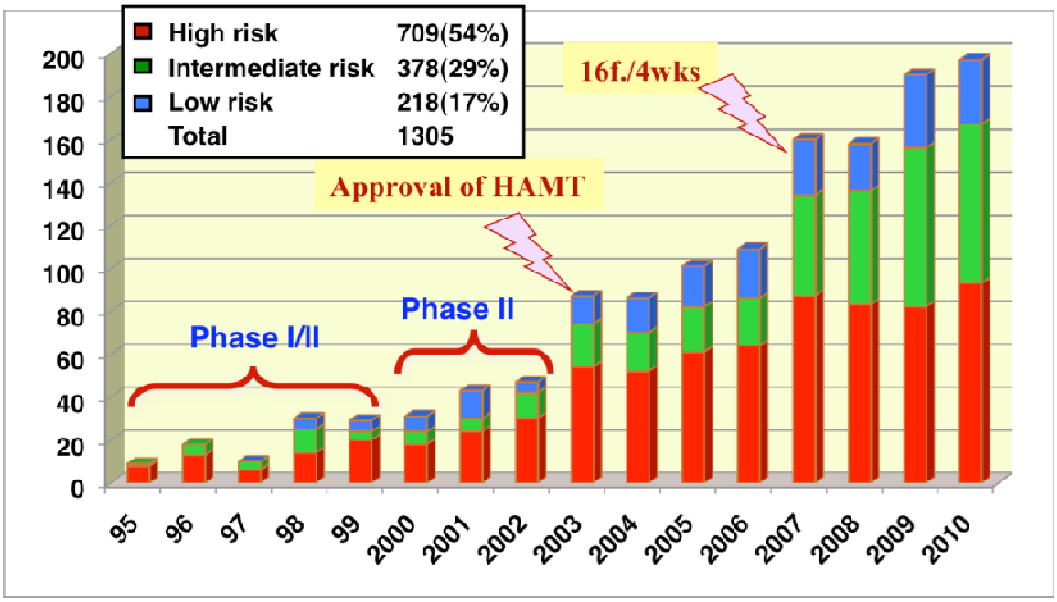

Figure 1. Transition by fiscal year of the number of prostate cancer carbon ion radiotherapy cases. (Risk group total)

In the current approach to therapy, the cases are classified into 3 groups (high risk, intermediate risk and low risk) according to the clinical stage, initial PSA value, and pathological Gleason score. For the high risk and intermediate risk groups, we combine long-term and short-term endocrine therapy, respectively (Figure 2). Among actual treated cases, high risk group account for more than a half of the whole cases (Figure 1).

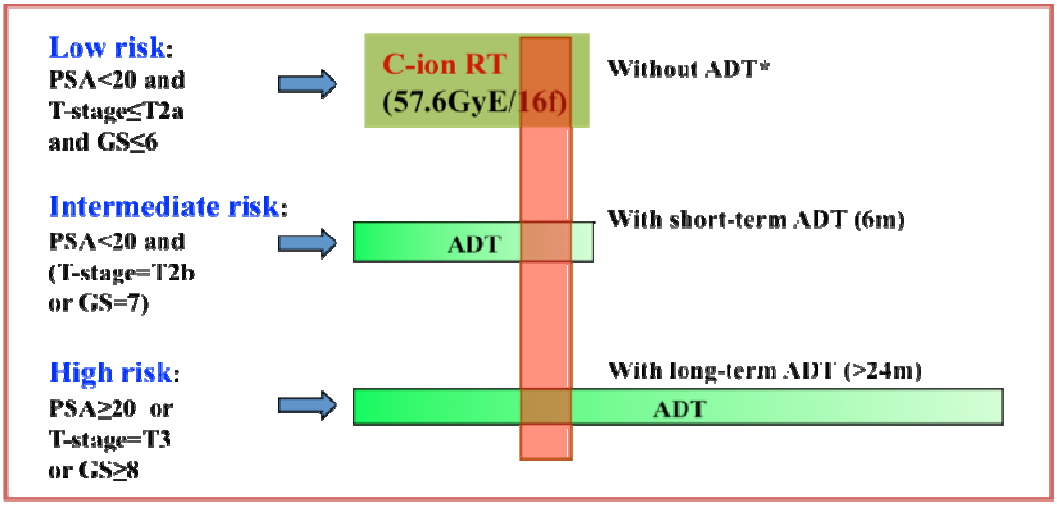

Figure 2. Current treatment strategy for prostate cancer at NIRS.
Patients were divided into three risk groups of high, intermediate, and low according to their T-stage, initial PSA, and Gleason score

For the treatment planning, a set of 2.5-mm-thick CT images was taken, with the patient placed in immobilization devices. Three-dimensional treatment planning was performed using HIPLAN software (National Institute of Radiological Sciences, Chiba, Japan). Clinical target volume (CTV) was defined as consisting of the prostate and the seminal vesicle (SV) demonstrated by CT images, irrespective of T-stage or other risk factors. MRI was also taken in all the patients and used as a reference for defining CTV. However, the whole SV should not always be included in the CTV, in the case of patients with a low risk. Thus, for example, the CTV of the patients staged as T1 or T2a did not cover the SV tips. Further, anterior and lateral safety margins of 10mm and a posterior margin of 5mm were added to the CTV to create the initial planning target volume (PTV-1). In order to reduce the dose to the anterior rectal wall, a rectum-sparing target volume (PTV-2) was used for the latter half of the C-ion RT, where the posterior margin was reduced to the anterior boundary of the rectum. Evaluation of the plan was routinely performed at the case conferences before the actual treatment, using the dose-volume histograms (DVH) for the CTV, PTV-1, PTV-2, and the rectum. Particularly, the DVH of the rectum was evaluated with comparing the reference DVH that was obtained from the analysis using actual DVH data of preceded dose-escalation studies. If the rectal DVH of the new patient was beyond the reference DVH at the high dose area, the treatment planning was revised. Fig. 3 shows the representative dose distribution.

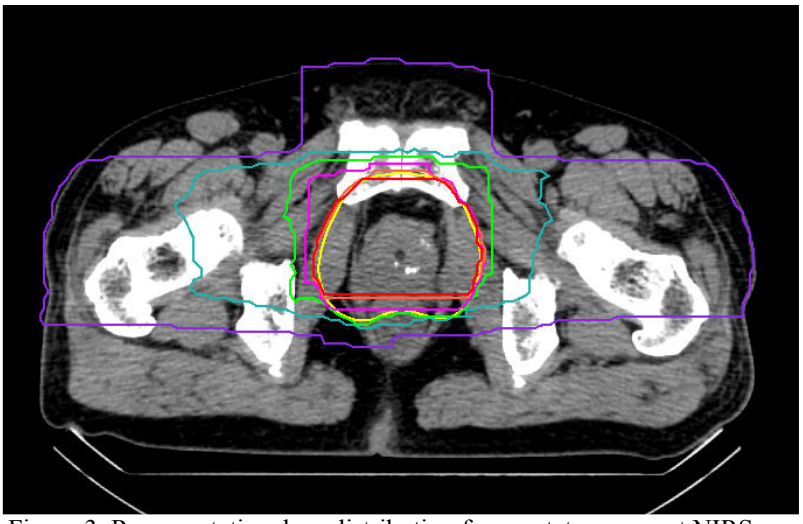

Figure 3. Representative dose distribution for prostate cancer at NIRS

The irradiated dose was fixed at 63.0GyE or 66.0GyE/20fractions as the recommended dose fractionation schedule established in the two previous phase I/II studies. In addition, more hypofractionated schedule of 57.6GyE/16fractionas was applied since September 2007. Furthermore, a new clinical trial of C-ion RT of 12 fractions over 3 weeks is also ongoing,. The analysis objects were treated by 20 fractions or 16 fractions after the phase II clinical trial and observed for 6 months and more.

3. Results

Of the 1305 patients treated until February 2011, 1084 patients who were treated in or after the phase II study were analyzed with regard to patient survival and biochemical relapse free rate judged according to the Phoernix criteria, PSA over nadir+2.0 = biochemical failure. Of those, 1005 cases who were observed 12 months or more were added up regarding an incidence of late radiation toxicity.

3-1） Toxicity

The result of comparison of late toxicity incidence on various radiotherapies and carbon ion radiotherapy is

shown in Table 1, 2. Compared with other various radiotherapies, carbon ion radiotherapy exhibited lower rate toxicity incidence rate, especially, the significant low rate of rectal toxicity. As for the toxicity incidence rate of lower urinary tract system, the carbon ion radiotherapy of 63.0GyE/20 fractions, intensity modulated radiation therapy and proton were approximately the same, however, as for the 57.6GyE/16 fractions, lowering of the incidence rate was gained. As for the toxicity of the rectum, even in 63.0GyE it showed lower rate than X-ray or proton. 57.6GyE showed further lowering of the rate.

Table 1. Late gastrointestinal and genitourinary morbidity after C-ion RT in patients followed up more than 12 months

Dose GyE/f.	No.pts.	Rectum				Bladder/urethra			
		Grade0	G1	G2	G3	Grade0	G1	G2	G3
66.0/20250	195	47	8	0	101	115	34	0	
	(%)	(78.0)	(18.8)	(3.2)	(0)	(40.4)	(46.0)	(13.6)	(0)
63.0/20216	184	27	5	0	110	93	12	1	
	(%)	(85.2)	(12.5)	(2.3)	(0)	(50.9)	(43.1)	(5.6)	(0.5)
57.6/16539	505	31	3	0	305	224	10	0	
	(%)	(93.7)	(5.8)	(0.6)	(0)	(56.6)	(41.6)	(1.9)	(0)
Total	1005	884	105	16	0	516	432	56	1
	(%)	(88.0)	(10.4)	(1.6)	(0)	(51.3)	(43.0)	(5.6)	(0.1)

Table 2. Incidence of Late Radiation Toxicity in various radiotherapy for Prostate

Institutes	Radiotherapy	Dose(Gy/f)	No. of pts.	Morbidity ≥ G2	
				Rectum	GU
Christie H.[1)]	IMRT	60/20	60	9.5%	4.0%
Princess Margaret H.[2)]	IMRT	60/20	92	6.3%	10.0%
Cleveland CF.[3)]	IMRT	70/28	770	4.4%	5.2%
Stanford U.[4)]	SRT	36.25/5	41	15.0%	29.0%
RTOG9406[5)]	3DCRT	68.4-79.2/38-41	275	7-16%	18-29%
	3DCRT	78.0/39	118	25-26%	23-28%
Loma Linda U.[6)]	Proton	75.0/39	901	3.5%	5.4%
NIRS	Carbon	63.0/20	216	2.3%	6.1%
	Carbon	57.6/16	539	0.6%	1.9%

1) JH Coote et al. IJROBP 74, 2009 2) JM Martin et al. IJROBP 69, 2007
3) PA Kupelian et al. IJROBP 68, 2007 4) CR King et al. IJROBP 73, 2009
5) JM Michalski et al. IJROBP 76, 20106) RW Schulte et al. Strahlenther Oncol 176, 2000

3-2) Relapse-free rate and survival rate

The Kaplan-Meier estimates of overall and biochemical relapse free (bNED) survivals for the 1084 patients at five years were 95.4% and 90.6%, respectively (Fig.4). By the date of analysis, 46 patients had died, 11 of metastasis from the prostate, and 35 of other malignancies or intercurrent diseases. So far, no patient belonging to the low-risk and intermediate-risk groups has died of prostate cancer.

A total of seven patients, three presenting with slowly elevated PSA and positive biopsies at 24 months, 38

months, and 48 months after C-ion RT, and four with apparent growth of tumor on the MRI images, were judged as having local recurrence. By the date of analysis, 72 patients met the Phoenix criteria of biochemical failure: more than 2.0 ng/ml rise of PSA from the nadir. Of these 72 patients, 31 patients were diagnosed as having metastasis, 7 were judged as having local recurrence, and the remaining 34 patients had no clinical evidence of recurrent lesions at the date of analysis.

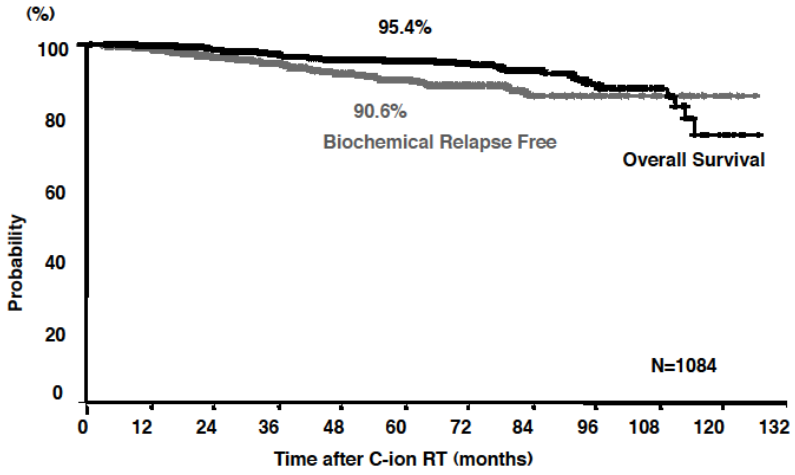

Figure 4. Overall survival and biochemical relapse free rate of patients treated with C-ion RT at NIRS

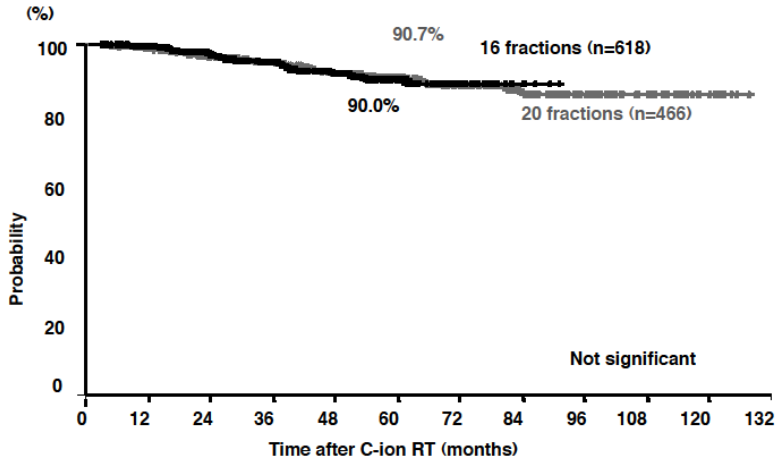

Figure 5. Biochemical relapse free rate by fractionation of C-ion RT

Additional analysis was carried out to evaluate the influence of several prognostic factors on bNED and cause-specific survival rate (CSS; survival rate limited to the prostatic cancer caused death), such as pretreatment serum PSA, GS, clinical stage, and dose fractionation. As a result, initial PSA of more than or equal to 20.0ng/ml was a significant factor for CSS (p=0.0301) and marginally significant for lower bNED (p=0.0678). Clinical stage

of the primary lesion (T-stage) and the centrally reviewed GS also had significant influence on bNED and CSS, that is primary lesion of T3 and GS ≥ 8 was related to poor prognosis (Table 3). However, 5-year bNED of 84.1% in T3 patients and 83.8% in GS ≥ 8 patients were both quite high compared to other radiotherapy series.

Table 3. Biochemical relapse free rate (bNED) and Cause-specific survival rate (CSS) according to risk factors

			5-year rates (%)			
		No.pts.	bNED	p-value	CSS	p-value
All		861	91.0		94.7	
Stage	T1/2	614	94.0	0.0000	100	0.0001
	T3	247	84.1		95.8	
PSA	< 20	595	92.1	0.0678	99.5	0.0301
	20 ≤	266	88.7		97.2	
Gleason score	≤ 6	206	92.3	0.0072	100	0.0110
	7	412	94.3	0.0004	99.2	
	8 ≤	243	83.8		96.6	

Table 4 is a risk grouped comparison of survival rate on large-scale clinical studies of combined therapy of X-ray therapy and endocrine therapy performed in the U.S. and the survival rate on carbon ion radiotherapy. The result shows that the survival rate is higher in the carbon ion radiotherapy in any groups.

Table 4. Comparing Overall Survival Rate of C-ion RT with Results of Meta Analysis of RTOG studies

Studies	Dose (Gy/fr.)	Overall Survival Rate					
		Group 2		Group 3		Group 4	
		No. pts.	5-y OS	No. pts.	5-y OS	No. pts.	5-y OS
RTOG Meta Analysis*							
RT alone	65-70/30-35	443	82%	338	68%	324	52%
RT + Hormone	65-70/30-35	114	76%	138	79%	103	63%
Carbon + Hormone	66-63/20 or 57.6/16	381	99%	321	94%	143	87%

*RTOG: Radiation Therapy Oncology Group; IJROBP 2000; 47(3): 617-627, Mack Toach III et al

4. Discussion

We introduced the treatment results of carbon ion radiotherapy in an established therapeutic approach after the phase II trial.

As for the treatment morbidity, in the lower urinary tract, the incidence was approximately the same in 63.0GyE/20 fractions carbon ion radiotherapy, intensity modulated radiation therapy and proton, which is interesting that it shows that this dose has comparable impact against lower urinary tract tissues. While for the

57.6GyE/16 fractions, the lowering of incidence was realized as a real outcome for shortening the treatment term. As for the rectal toxicity, even 63.0GyE showed lower rate than X-ray or proton, this is thought to be the proof of eminent dose convergence of carbon ion beam. In addition, 57.6GyE gained further lowering. Adding shortening to the high dose convergence, significant reduction of toxicity was obtained.

Regarding the antitumor effect, especially in the high risk groups, high survival rate was gained. It is caused by the carbon ion's excellent curative effect along with the distinguished treatment strategy. There was no difference in relapse-free rate and survival rate between 20 fractions and 16 fractions, while the result showed that the toxicity was less in 16 fractions. Therefore reducing the fractions to 16 made it possible to achieve not only the improvement of efficiency but also the improvement of outcome from therapy.

5. Conclusion

Carbon ion radiotherapy is an ideal therapeutic approach as radiation therapy against prostatic cancer. Furthermore, regarding the point of both toxicity and curative effect, previous outcome strongly illustrated the fact. Shortening the treatment period also contribute to the better outcome, hereafter, further shortening and promotion of streamlining can be expected. Prostatic cancer is a target disease of therapy utilizing the characteristics of carbon ion beam, and prospected to have a great role in popularization of carbon ion radiotherapy.

Reference

[1] Tsuji H, et al.: Hypofractionated radiotherapy with carbon ion beams for prostate cancer. Int J Radiat Oncol Biol Phys. 2005; 63(4): 1153-1160.

[2] Ishikawa H, et al.: Carbon ion radiation therapy for prostate cancer: Results of a prospective phase II study, Radiotherapy and Oncology, 81(1), 57-64, 2006

[3] Ishikawa H, et al.: Risk Factors of Late Rectal Bleeding after Carbon Ion Therapy for Prostate Cancer. Int J Radiat Oncol Biol Phys 2006; 66: 1084-1091

[4] Coote JH, et al.: Hypofractionated intensity-modulated radiotherapy for carcinoma of the prostate: analisys of toxicity. Int J Radiat Oncol Biol Phys 2009; 74: 1121-1127.

[5] Martin JM, et al.: Phase II trial of hypofractionated image-guided intensity-modulated radiotherapy for localized prostate adenocarcinoma. Int J Radiat Oncol Biol Phys 2007; 69: 1084-1089.

[6] Kupelian PA, et al.: Hypofractionated intensity-modulated radiotherapy (70Gy at 2.5Gy per fraction) for localized prostate cancer: Cleveland Clinic Experience. Int J Radiat Oncol Biol Phys 2007; 68: 1431-1437

[7] King CR, et al.:Stereotactic body radiotherapy for localized prostate cancer: Interim results of a prospective phase II clinical trial. Int J Radiat Oncol Biol Phys 2009; 73: 1043-1048.

[8] Michalski JM, et al.: Long-term toxicity following 3D conformal radiation therapy for prostate cancer from the RTOG 9406 phase I/II dose escalation study. Int J Radiat Oncol Biol Phys 2010; 76: 14-22.

[9] Schulte RW, Slater JD, et al.: Value and perspectives of proton radiation therapy for limited stage prostate cancer. Strahlenther Onkol 2000; 176: 3-8

The Need of Clinical Outcome Data for patient Selection Model

The example of a Tumor growth inhibition modeling: Why not using it for hadrontherapy clinical research?

Benjamin Ribba[1]
[1] *INRIA Research Center Grenoble Rhone-Alps, Innovalée, 655 avenue de l'Europe, Montbonnot Saint Martin, 38334 Saint Ismier, France.*
e-mail address: benjamin.ribba@inria.fr

Introduction

The efficacy of anticancer treatments, including ionizing therapy, is often appreciated in early clinical studies by the Response Evaluation Criteria In Solid Tumors (RECIST) or similar criteria (see (1) as an example for the evaluation of treatment efficacy in brain tumors). Based on the change in tumor size after treatment with respect to the size before treatment, these criteria lead to the classification of the response into a short list of categories in which, in general, 'Complete response' is used to indicate the disappearance of all evidences of the disease; 'Partial response' indicates a 50% decrease at least in the sum of diameters of all lesions, 'Progressive disease' indicates a 25% increase at least in the sum of diameters of all lesions; and 'Stable disease' is used for all remaining cases. Using these criteria allow for a simple and quick appreciation of treatment efficacy, however, they only integrate the information on tumor size on two different time points potentially omitting precious information in between.. Major critics have been indeed formulated regarding the crude evaluation provided by RECIST in phase II clinical trials (2).

Analyzing the dynamic of tumor response to treatment can prevent some of the shortcomings of the static evaluation of response rate through RECIST (3). So far, models have been developed to analysis the dynamic of tumor response to several chemotherapy regimen for non-small cell lung cancer (NSCLC) and colorectal cancer; and the US Food and Drug Administration through the 'Critical Path Initiative' has recommended the use of this approach for leveraging existing knowledge from clinical data in oncology.

The modeling of tumor dynamic in response to treatments relies on the concept of 'Tumor growth inhibition (TGI)' model. In this paper, we present the TGI concept and develop few examples already published in literature for preclinical data and for clinical data. We show the predictive potential of the latest to evaluate treatment response in terms of long term clinical outcome based on the analysis of tumor size change in early clinical phases. We finally suggest to apply the same technics to ionizing treatments in particular to tackle the most important challenges related to hadrontherapy clinical research.

Tumor growth inhibition modeling

Most historical achievements of modeling tumor growth and response to treatments

As for many applications of modeling to describe biological systems, the 'Gompertz equation' is at the basis of numerous models of tumor growth and response to treatments (4).

Applied to the growth of tumor cell colony in vitro, the Gompertz model was written as follows in a paper from Laird in 1964:

$$w(t) = w_0 e^{\frac{A}{\alpha}\left(1-e^{-\alpha t}\right)}$$

where w denotes the number of tumor cells or 'tumor size', w_0 the initial number of tumor cells also called 'baseline tumor size', and A and α two positive constants. This model reproduces the growth of tumor cell colony starting at size w_0 and reaching the size $w_0 e^{\frac{A}{\alpha}}$ for longer time. Note that because A and α two positive constants, $\frac{A}{\alpha} > 0$ which leads to $e^{\frac{A}{\alpha}} > 1$ so that the final size is bigger than the initial one.

In 1970, the Gompertz equation was successfully used to describe tumor growth in animal models (5), and application to clinical data was carried out by Sullivan and Salmon in 1972 (6) and in 1976 by Norton and Simon which generalized the use of the Gompertz model for several ranges of solid tumors (7, 8). The results

obtained by Norton and Simon were at the basis of the so-called 'Norton-Simon hypothesis' according to which, increasing chemotherapy dose intensity can lead to optimize treatment effect by reducing tumor regrowth between chemotherapy cycles. The Norton-Simon hypothesis reached validation in clinical trials in 2003 (9).

From those initial attempts, several models have been proposed to analyze the dynamic of tumor growth in response to treatments for animal and human data.

In 2004, based on the Gompertz equation, Simeoni and coworkers proposed the first TGI model that describes tumor time-course in untreated and treated mice with several chemotherapeutic compounds, such as 5FU and Irinotecan and paclitaxel (10). This model is extensively used in preclinical research to analyze the effect of chemotherapeutic compounds.

More recently, TGI models have been also proposed for the analysis of clinical data. A simple model assuming a linear growth of the tumor with an exponential decay of the size caused by the treatment was proposed based on the analysis of more than 2,000 patients from four different clinical trials corresponding to the drugs bevacizumab, docetaxel, erlotininb, and pemetrexed.

The model was written as follows:

$$TS(t) = BASE\ e^{-SR \cdot t} + PR \cdot t$$

where TS denotes the tumor size, $BASE$ the tumor baseline, SR is the exponential tumor shrinkage rate and PR, the linear tumor progression rate (3). The model is shown to correctly predict tumor dynamic in patients.

A second model that deserves to be cited here has been developed for colorectal cancer patients. Based on tumor size data in phase III trial where 301 patients received 5FU and phase II trial where 34 patients received Capecitabine, Claret and co-workers developed proposed a TGI model where tumor size is governed by a growth term (exponential low) and a decay term (exponential decrease) as a function of the drug concentration (11).

A schematic view of the process to build a TGI model relevant to clinical data is shown figure 1.

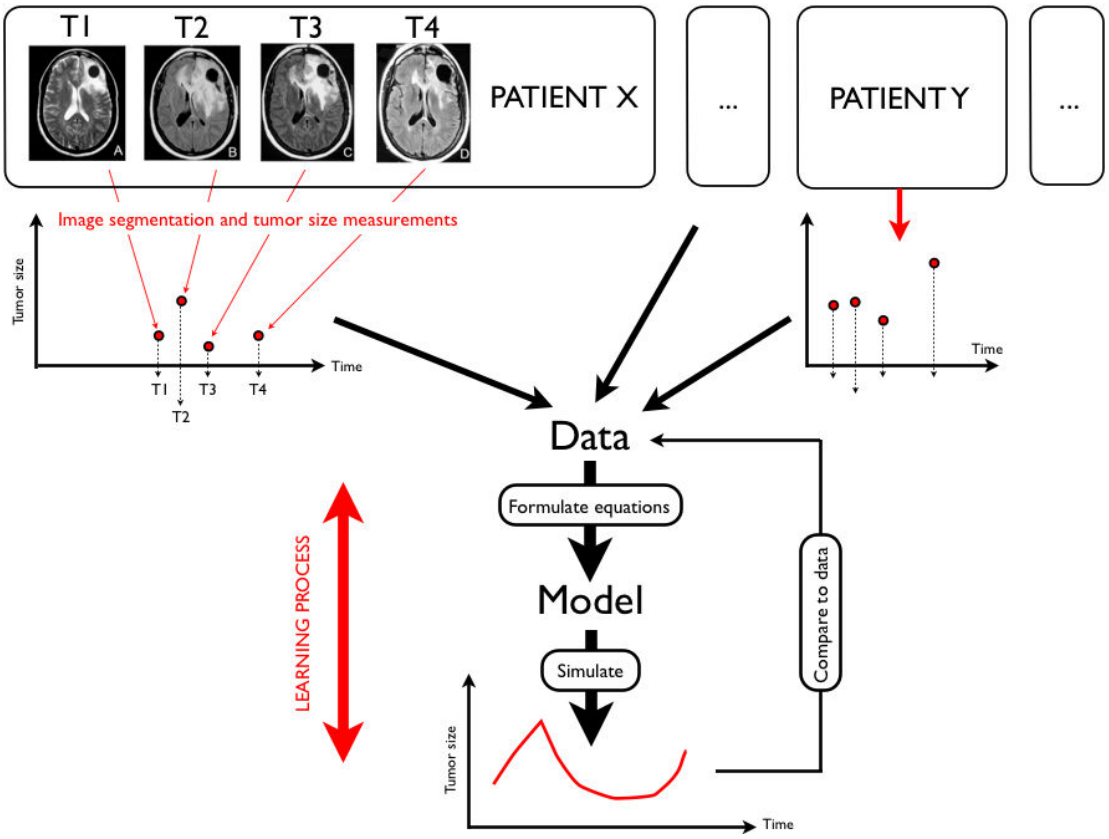

Figure 1: Schematic representation of the concept of TGI modeling to reproduce tumor size dynamic in patients. MRI images are analyzed to reconstruct the observed dynamic of tumor size in patients. Taking into account the data from different individuals, a regression model with time as the variable is developed to fit the observed tumor size observations.

Translational relevance: link to long-term clinical outcomes

The main interest of TGI models lies in their potential to highlight new predictors of long-term clinical outcomes based on early evaluation of tumor size change during treatment. Figure 2 shows schematically the process of coupling a TGI model such as the one presented in the previous paragraph which process has been described in figure 1.

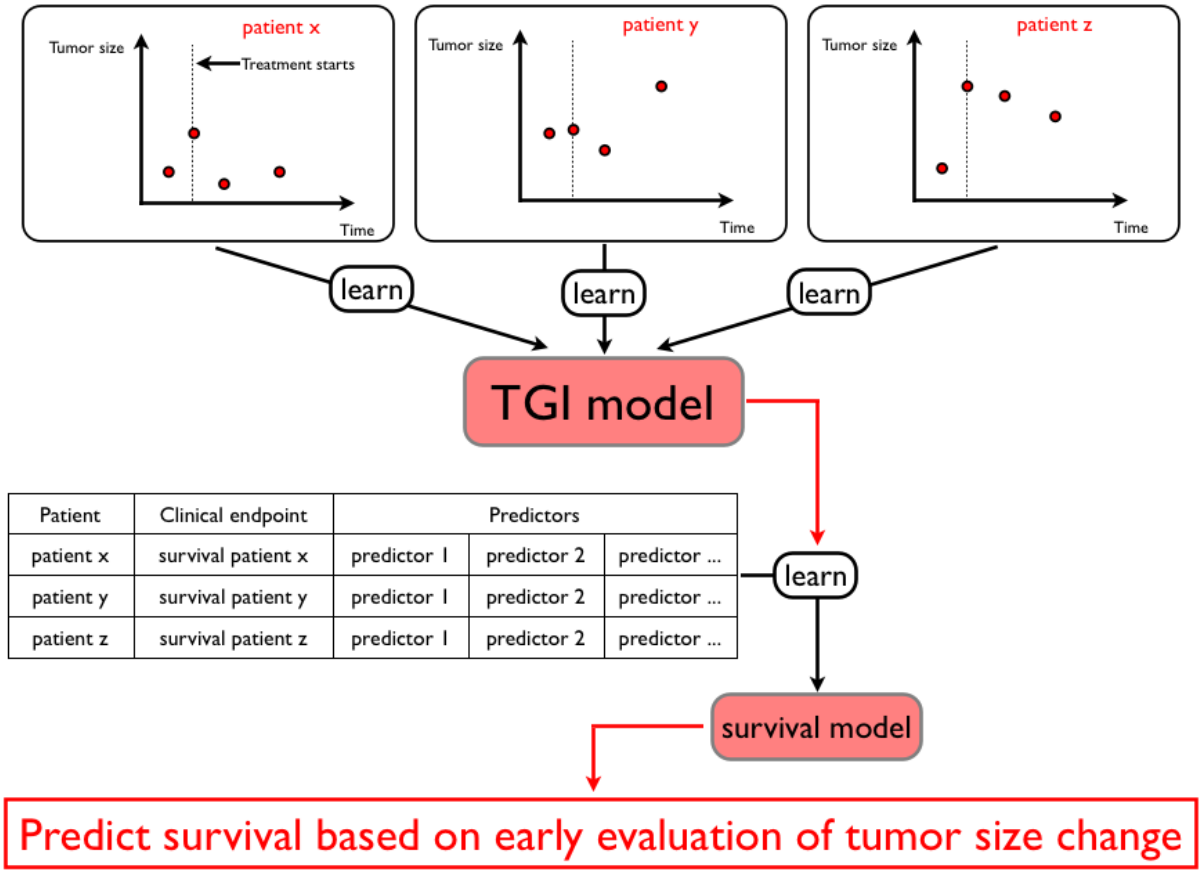

Figure 2: Schematic representation of the concept of TGI modeling extended to the prediction of long-term clinical outcomes. The TGI model, built on the basis of patient's tumor size dynamic observations, is used together with usual patient's covariate (ECOG status, tumor baseline, …) to build a survival model. This model links the early change in tumor size (through TGI) to long-term clinical outcome thus providing a method for early assessing the efficacy of a given treatment.

The two models previously mentioned for the analysis of clinical data (3, 11) have been successfully used to predict long-term survival based on tumor size dynamic as predicted by the TGI models. In the paper from Wang and coworkers, the baseline tumor size and the percentage of change in tumor size 8 weeks after treatment starts as predicted by the model, together with ECOG status of the patients where identified as the best predictors of time to death (3).

In the paper by Claret and coworkers, the baseline tumor size and the percentage of tumor size reduction 7 weeks after treatment starts as predicted by the model were identified as the best predictors of the survival time (11). These two examples show that modeling tumor size dynamic can offer a powerful tool to predict long-term clinical outcomes from early evaluation of tumor size dynamic. This method is promoted by the Food and Drug Administration (FDA), through the 'Critical Path Initiative', for leveraging existing knowledge from clinical data. Figure 3 represents this concept.

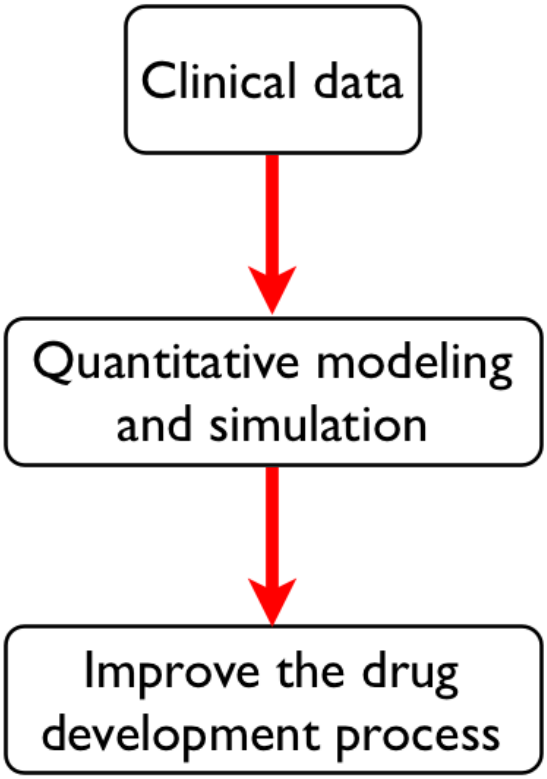

Figure 3: Since 2004, the Food and Drug Administration, through the Critical Path Initiative, promotes the use of quantitative modeling and simulating method for leveraging existing knowledge from clinical data.

Application to ionizing therapy and hadrontherapy

Interestingly, to our knowledge, no TGI models have been yet proposed for the analysis of tumor size dynamic in patients treated with radiation treatments. In general, as this was shown in the case of radiotherapy, TGI models can constitute a tool to assess long-term clinical outcome from early evaluation of tumor dynamic. A model, capable of reproducing the dynamic of tumor size in patients treated with radiotherapy may provide new predictors of survival in addition to the ECOG status or the others criteria classically used such as the gross tumor volume (GTV).

Interestingly, we have presented very simple model but in the future, those models will be certainly extended to take into account the spatial structure of the tumor and treatment delivery and could thus be directly linked to treatment planning platforms. In the case of hadrontherapy, these types of models could be helpful to better identify responders and, together with the other criteria, could constitute a tool to support the choice for hadrontherapy treatment.

Conclusions

Tumor growth inhibition modeling relies on the analysis of the dynamic of tumor size during treatment. Applied to clinical data, this technique has recently shown potential to predict, based on early assessment of tumor size reduction, long-term survival. It constitutes thus a powerful tool for rational decision taking to optimize patient care. It seems interesting to promote the development of these quantitative approaches for hadrontherapy research for which, the cost and infrastructure involved for treating patient, must require the best existing tools to support decision to treat. It is possible that the existing data collected on patients already treated by hadrontherapy would be sufficient to build a relevant tumor growth inhibition model.

References

[1] van den Bent M, Wefel J, Schiff D, Taphoorn M, Jaeckle K, Junck L, et al. Response assessment in neuro-oncology (a report of the RANO group): assessment of outcome in trials of diffuse low-grade gliomas. Lancet Oncol. 2011.

[2] Ratain MJ, Eckhardt SG. Phase II studies of modern drugs directed against new targets: if you are fazed, too, then resist RECIST. J Clin Oncol. 2004;22:4442-5.

[3] Wang Y, Sung C, Dartois C, Ramchandani R, Booth BP, Rock E, et al. Elucidation of relationship between tumor size and survival in non-small-cell lung cancer patients can aid early decision making in clinical drug development. Clinical pharmacology and therapeutics. 2009;86:167-74.

[4] Laird AK. Dynamics of Tumor Growth. Br J Cancer. 1964;13:490-502.

[5] Simpson-Herren L, Lloyd HH. Kinetic parameters and growth curves for experimental tumor systems. Cancer Chemother Rep. 1970;54:143-74.

[6] Sullivan PW, Salmon SE. Kinetics of tumor growth and regression in IgG multiple myeloma. The Journal of clinical investigation. 1972;51:1697-708.

[7] Norton L, Simon R, Brereton HD, Bogden AE. Predicting the course of Gompertzian growth. Nature. 1976;264:542-5.

[8] Norton L. A Gompertzian model of human breast cancer growth. Cancer research. 1988;48:7067-71.

[9] Citron ML, Berry DA, Cirrincione C, Hudis C, Winer EP, Gradishar WJ, et al. Randomized trial of dose-dense versus conventionally scheduled and sequential versus concurrent combination chemotherapy as postoperative adjuvant treatment of node-positive primary breast cancer: first report of Intergroup Trial C9741/Cancer and Leukemia Group B Trial 9741. Journal of clinical oncology : official journal of the American Society of Clinical Oncology. 2003;21:1431-9.

[10] .Simeoni M, Magni P, Cammia C, De Nicolao G, Croci V, Pesenti E, et al. Predictive pharmacokinetic-pharmacodynamic modeling of tumor growth kinetics in xenograft models after administration of anticancer agents. Cancer research. 2004;64:1094-101.

[11] Claret L, Girard P, Hoff PM, Van Cutsem E, Zuideveld KP, Jorga K, et al. Model-based prediction of phase III overall survival in colorectal cancer on the basis of phase II tumor dynamics. Journal of clinical oncology : official journal of the American Society of Clinical Oncology. 2009;27:4103-8.

The need of medical imaging data for tumor motion simulation: Biomechanical Modelling of the Respiratory System and Applications in Hadrontherapy

Jacques Saadé[1], Petre Manescu[1], Hamid Ladjal[1,2], Behzad Shariat[1], Michael Beuve[2], Jozeph Azencot[1], Jean-Michel Moreau[1]

[1]*Université de Lyon, CNRS, Université Lyon 1, LIRIS, UMR5205, F-69622, France*
[2] *Université de Lyon, CNRS, Université Lyon 1, IPNL, UMR5822, F-69622, France*
e-mail addresses : jacques.saade, petru.manescu, behzad.shariat@liris.cnrs.fr

Abstract

Tumour motion is an essential source of error for treatment planning in radiation therapy. This motion is mostly due to patient respiration. To account for tumour motion, we propose a solution that is based on the biomechanical modelling of the respiratory system. To compute deformations and displacements, we use continuous mechanics laws solved with the finite element method. In this paper, we propose a biomechanical study on the diaphragm which is the principal muscle of the respiratory system. This study is achieved by building a finite element mesh using the CT-scan data of a patient. Results are in accordance with the anatomic reality, showing good concordance between the biomechanical simulation of motion and the CT images.

Introduction

Patients internal motions have large implications in different domains such as imaging and treatment (chirurgical operations or radiation therapy). Thereby the respiratory motion reduces the efficiency of radiotherapy benefits. Indeed, thoracic and abdominal tumours can move and deform due to respiration. It is then essential to know their position and deformation to be able to optimize the dose to tumour and healthy tissues. Lung tumours are particularly concerned by this motion (Mori *et al,* 2007; Seppenwoolde *et al.*, 2002). Several management strategies including breath holding (Gagel *et al*, 2007; Wong *et al*, 1999), beam gating (Ozhasoglu and Murphy, 2002) and tracking have been discussed in the literature to account for tumour displacement (Giraud *et al*, 2006). A disadvantage of breath holding and beam gating is that, part of the time, the beam is off. Another disadvantage is that they do not take into account some irregularities in the breathing cycle. Indeed, both methods deduce tumour position from an external breathing parameter (spirometry, abdominal or thoracic height...). Ozhasoglu and Murphy (2002) demonstrated that respiratory compensation strategies that use an external breathing signal to infer tumour position lack the ability to detect and adapt to continuously changing characteristics of respiratory motion during treatment. Other studies (Shirato et al, 2006) show that the respiratory motion has some non-reproducible aspects that need to be taken into account during radiotherapy. This non-reproducibility will be explained later in the anatomy part. Tracking fiducial markers implanted inside the tumour or tracking the tumour using the CyberKnife® robotic radiosurgery system are techniques that take into account the non-reproducibility of the breathing cycle. While the implantation of fiducial markers is an intrusive method that may lead to medical complications such as pneumothorax (Jiang, 2006), the CyberKnife® system has also some inconveniences such like the long treatment time requirement and the irradiation of the patient by the tracking device.

Alternatively we propose a model based solution that takes into account the non-reproducible aspects of breathing motion: a biomechanical modelling of the respiratory system monitored by at least two external parameters (Thoracic motion and spirometry). Ribs and diaphragm displacements can be computed out of thorax outer-surface motion and spirometry measurements. Lungs deformations, and then tumour displacements, can be deduced considering the organ interactions. All deformations and displacements are calculated using continuous mechanics laws, solved with the finite element method.

Another requirement, particularly important in the context of hadrontherapy, is the ability to predict not only tumour motion but also motion, deformation and density changes of any tissue traversed by the beam.

Our group has been active in the biomechanical modelling of the respiratory system (Villard *et al*, 2005, Didier *et al*, 2007, 2009) and the transformation of biomechanical data into 4D-CT data (Villard *et al*, 2006). Previously, we have validated a chest wall model based on rib kinematics that enables the computation of rib displacements out of thorax outer-surface motion (Didier *et al*, 2009). In this paper, we develop a feasibility study of a diaphragm model. First, we summarize previous studies concerning the biomechanical modelling of the respiratory system. Then we expose a model of the respiratory system, using a patient's CT-scan data, and the results on the diaphragm motion estimation.

Anatomy of the respiratory system

Lungs are passive structures that inflate under muscles action. The increase of thoracic volume, due to inspiratory muscles action, induces lung expansion, leading to internal negative pressure and consequently to inspiration. Contact of the lungs with the ribcage and the diaphragm is maintained by the pleura. The pleura is composed of two membranes (figure 1): the first, referred to as parietal, covers the chest wall, the mediastinum and the diaphragm while the second, referred to as visceral, covers the outer surface of the lungs.

The space in between the parietal and visceral pleura, known as the pleural space, is filled with an incompressible fluid which lubricates the pleural space and allows the lungs to easily slide against the chest wall and the diaphragm during their expansion. Lungs mainly expand under the action of the external intercostal muscles (EIM) and the diaphragm. The role of the EIM is relatively important in both quiet and forced respiration. They are inserted between the ribs from the second to the twelfth rib and they are responsible for the rib elevation during inspiration.

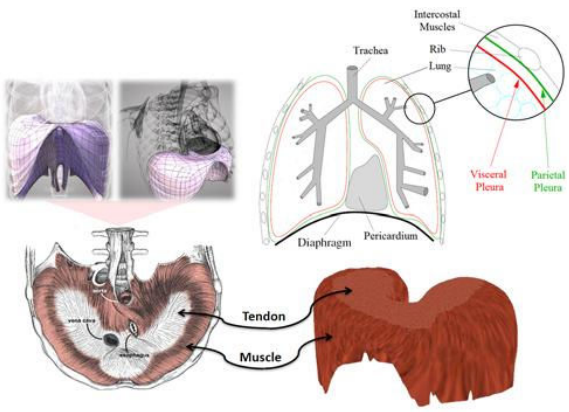

Figure 1: Anatomy of the respiratory system.

The diaphragm is a digastric muscle which separates the thoracic and abdominal cavity. It is composed of two domes (figure 1): the right dome comes up to the fourth intercostal space whereas the left dome remains below the fifth rib. The diaphragm is constituted of a peripheral part (muscular fibre) and a central tendon (figure 1). The peripheral part is linked to the lower thoracic cavity perimeter and has three major insertions: lumbar, sternum and ribs. During inspiration, the muscular contraction fibres bring down the central tendon. This lowering increases the vertical diameter of the thorax. As for the lungs, EIM action induces posto-anterior and transversal inflation while the diaphragm action causes vertical motion. The EIM and the diaphragm may act independently, making respiration a non-reproducible and an unpredictable movement. Thereby, in general, lung motion cannot be simply predicted by a correlation with one single parameter.

Biomechanical modelling of the respiratory system

In the past, several studies were achieved to model the lung environment. A description of these studies can be

found in Baudet *et al.* (2003), Villard *et al.* (2005) and Al-Mayah *et al.* (2007). Thus, we focus on the more recent studies. Villard *et al.* (2005) used a patient's CT scan images to build the geometry of a finite element lung model. They also studied lung motion sensitivity to Poisson's ratio, elastic modulus (Young modulus) and contact conditions at the pleura. It appeared that Poisson's ratio has an effect on the amplitude and the orientation of the displacements while Young modulus should be carefully chosen because a change in its value may either induce a faulty implementation of contact conditions or increase the computing time needs. Brock *et al.* (2005) developed a platform to perform multi-organ deformable image registration using finite element modelling. The model was developed using images from magnetic resonance (MR) scanning. The lungs were included in this model and good agreement was found between the finite element simulation using orthogonal displacement (OD) and the MR data. Didier *et al.* (2007) showed the significant role of the pleura and the necessity to include its effect in the model. The role of the pleura is simulated by applying contact conditions that allow sliding on the lungs surface (contact without friction). The results of this model were compared to those of the OD model and showed an improvement in predicting the position of the lungs while the computing time requirement was higher. Al-Mayah *et al.* (2007) included the role of the pleura and two other nonlinearities to the model (hyperelastic nonlinear materials and nonlinear geometry due to large displacements). They also added the chest wall and the tumour to the model and achieved a good precision on lung and tumour position. An inconvenience of adding the nonlinearities was the increase in the computation time needed to complete the simulation. All the models mentioned above, focused on deformable registration of soft tissues in the thorax and did not invest in the bone tissues of the rib cage. Going from the fact that the bones of the rib cage can relatively be considered as rigid bodies, Didier *et al.* (2007) introduced a rigid transformation that simulates the kinematic behaviour of the rib cage intead of simulating the action of each intercostal muscle. The transformation is based on the Finite Helical Axis (FHA) method. Didier *et al* (2009) developped this method in order to build a model of the chest wall. This model proposed a correlation between ribs motion and thorax-outer surface motion and achieved a good precision on lungs position in the upper thorax. This model is essential to enable monitoring of lung motion out of thorax motion. Thus, to be able to build a complete model of the respiratory system and to include a second parameter to the monitoring process of the lungs, we introduce in this paper a biomechanical study of the diaphragm and results concerning a finite element simulation of its motion.

Diaphragm biomechanical model

In order to build a complete model of the respiratory system, the diaphragm is modelled. This model should be added to the thorax and the lung models. As mentioned in the anatomy part, the diaphragm is composed of a peripheral part (muscular fibre) and a central tendon. During inspiration, muscular fibres contract under the action of a force *F* and the ribs undergo a displacement *Dc*. Both actions cause the lowering of the central tendon (figure 3).

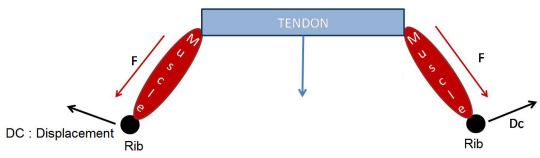

Figure 3: An illustration of the diaphragm motion.

In order to build a patient specific biomechanical model of the diaphragm, a patient specific geometrical model should be generated out of 3D images of the diaphragm. To validate the biomechanical model, there should be at least two geometrical models, one model to which the biomechanical model is applied, and another model that serves as a comparison. We chose to generate a geometrical model at full exhalation and another at full inhalation in order to have a big motion between the two states and thus be able to evaluate the biomechanical model's ability to predict this motion. To build the geometrical model, we have chosen 4D CT scan data covering the whole thorax of a patient. The 4D CT set is issued from a pre-treatment procedure of a

lung cancer patient. From the 4D set, we chose two 3D sets of images that correspond to the maximum and to the minimum of the respiratory cycle. In terms of resolution, the CT images voxel size is 1.17*1.17*3 mm^3 with 512*512*130 voxels respectively in the left-right (X), dorsoventral (Y) and craniocaudal (Z) directions. The diaphragm was segmented manually on the images using the ITK-SNAP software (http://www.itksnap.org). Being a thin membrane that cannot always be identified on the images (figure 4), the diaphragm cannot be segmented automatically. Thus, neither the threshold method proposed above, nor the active contour method proposed by ITK-SNAP can give satisfactory results for diaphragm segmentation. To segment the diaphragm we proceeded by manual delineation while navigating through the images as in Pettiaux *et al.* (1997) and Behr *et al.* (2006). When the diaphragm membrane is not visible (figure 2-a), we identify the diaphragm thanks to the surrounding organs.

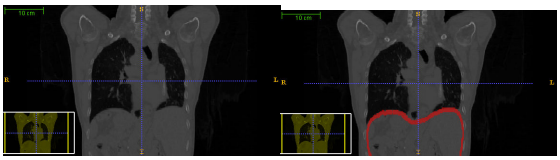

Figure 4: CT coronal slice of the thorax with (a) the original image and (b) the image with the segmented diaphragm (using a red marker).

After segmentation, a 3D surface mesh was created using ITK-SNAP module to save the segmented image as a triangular mesh. This module uses VTK marching cubes algorithm. The resulting mesh consists of a two-layer closed membrane. Each layer consists of a triangular surface mesh. Anatomically speaking, the superior layer is the one in contact with the thoracic organs and the ribs while the inferior layer is the one in contact with the abdominal viscera. Because of the high resolution of the CT images, the marching cubes and marching tetrahedrons algorithms generate a big number of nodes and triangles. In order to reduce time consuming operations, especially in the mechanical simulations explained in later sections, the diaphragm and the ribcage meshes were smoothed and simplified by reducing the number of nodes and triangles using *Remesh* software. These operations were achieved without reducing the details on the mesh surface. The different meshed parts are presented in figure 3 after simplification and smoothing. All parts are then imported to *Abaqus* software platform where their volumes are meshed separately with tetrahedrons. The final diaphragm mesh consists of 15328 nodes and 62296 tetrahedrons.

We apply on this geometrical model the mechanical laws and boundary conditions and material properties as follow.

1. Mechanical behaviour laws

We use continuous mechanics laws to compute the deformations with a non-linear geometric behaviour law that allows large displacements. We considered elastic materials. Calculations were made in the static mode which means that only the initial and final states of deformations are computed after the application of boundary conditions.

2. Boundary conditions

Diaphragm / Ribcage

In order to simulate the diaphragm environment and to solve the partial differential equations of the continuous mechanics laws, boundary conditions of the diaphragm should be adequately defined. These boundary conditions are inferred from the anatomy. All diaphragm insertions (lumbar, sternum and ribs) are taken into account by fixing those regions and not allowing them to move.

Contraction of the muscular fibres

Because the diaphragm mesh is a thin membrane, we chose to apply a tension $\vec{t}$ on the surface of the diaphragm mesh that represents the muscles. Surface tension models generate forces that only depend in amplitude on the surface area of the geometrical model which is obviously correct because a larger or longer muscle generates a bigger force. When applying the tension $\vec{t}$ on the diaphragm muscles mesh, the resulting force is computed as shown in equation (1), with S, α and $\vec{d}$ respectively the mesh surface, the force amplitude and direction.

$$\vec{f} = \int_S \vec{t}\, dS = \int_S \alpha\, \vec{d}\, dS \tag{1}$$

Furthermore, because diaphragm muscle fibres direction is not always vertical (figure 4), the resulting forces direction should be along the curvature of the fibres. This means that we must project the cranial to caudal direction $\overrightarrow{CC}$ to the surface of the diaphragm muscles. Thus, the direction $\vec{d}$ used in our model can be written as shown in equation (2), where $\vec{N}$ is the normal vector to the corresponding triangle of the muscle surface mesh. This direction tends to mimic the reality of the arrangement of diaphragm muscle fibres. In fact, the muscle fibres originate radially from the central tendon.

$$\vec{d} = \overrightarrow{CC} - \overrightarrow{CC} \cdot \vec{N}\ \vec{N} \tag{2}$$

3. Material properties

Table 1 illustrates the biomechanical parameters (Young modulus and Poisson's ratio) of the lungs, ribs, fat tissues, skin and diaphragm. The diaphragm has two different parts (muscle and tendon) and each part has different mechanical properties. All

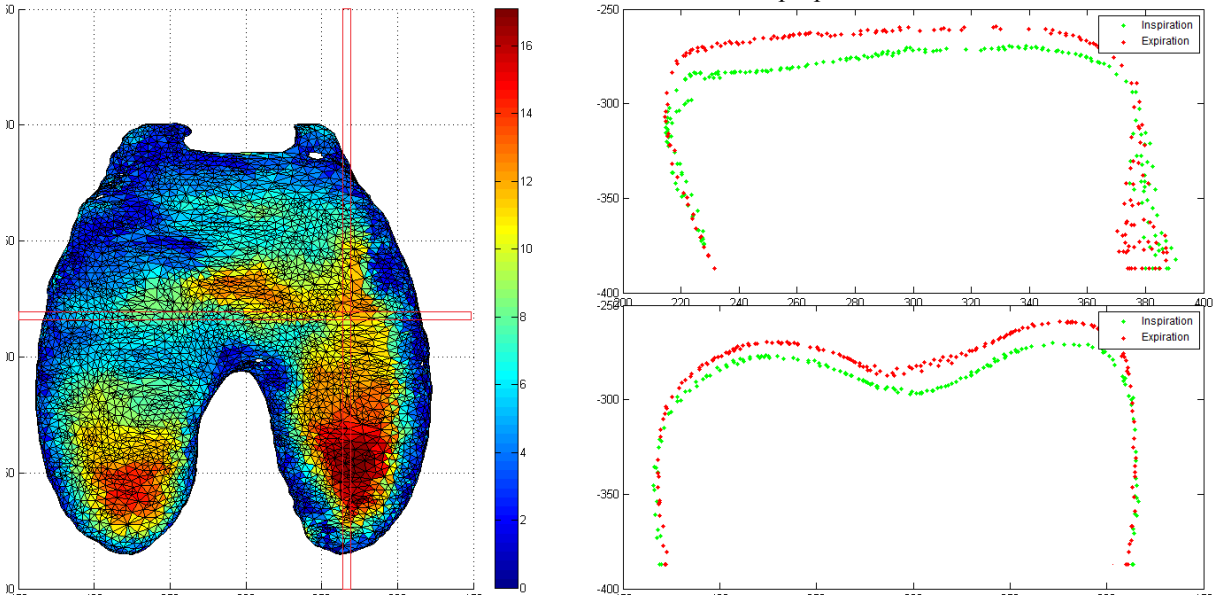

Figure 5: Diaphragm motion between expiration and inspiration with the 3D distance map (left), a sagittal slice (up-right) and a coronal slice (down-right) of expiration (red) and inspiration (green) mesh nodes.

parameters are taken from the bibliography (Handriks, 2001; Promayon and Baconnier, 2008).

Table 1: The biomechanical properties of the diaphragm

	Diaphragm (Muscle)	Diaphragm (Tendon)
Young Modulus (MPa)	5.32	33
Poisson's ratio	0.3	0.3

Results

1. Evaluation of the motion

The diaphragm was segmented on the expiration and inspiration states. Thus, we can measure the geometrical distance between the two segmentations and deduce the three-dimensional diaphragm motion. We measure the

distance only between the upper layers of the diaphragm surface nodes on the expiration and inspiration states. Figure 5 shows a 3D motion map of the diaphragm with sagittal and coronal slices.

2. Evaluation of the motion

The aim of this study is to simulate the diaphragm motion during inspiration. This means that we apply the boundary conditions on the diaphragm mesh segmented on the expiration state, and if the model is precise, the deformed mesh should resemble to the mesh that was segmented on the inspiration state (i.e. the mean distance between the two meshes should be negligible). As to muscle tension, all we need to define is the value of α and the direction $\overrightarrow{CC}$. During inspiration, $\overrightarrow{CC}$ should be cranial to caudal so that the muscle forces are oriented downwards in order to push down the diaphragm central tendon. α represents the amplitude of the tension from expiration to inspiration. As a matter of fact, the amplitude of diaphragm deformation depends on the amplitude α of the tension applied to the muscles. In order to determine α, we use an iterative process. We begin by an arbitrary value of α. We then compare the diaphragm deformed mesh with the diaphragm mesh segmented at inspiration. We keep changing α and repeating the procedure until the mean distance between the two meshes is minimal. Thus, α is fixed to the value (α = 40 000 N/m^3) that corresponds to the minimal distance. Using this value of α, we obtain the results shown in figure 6. This figure presents a distance map measured from each node of the diaphragm at inspiration to the nodes of the simulated inspiration. This distance gives direct evaluation of the precision of our simulation.

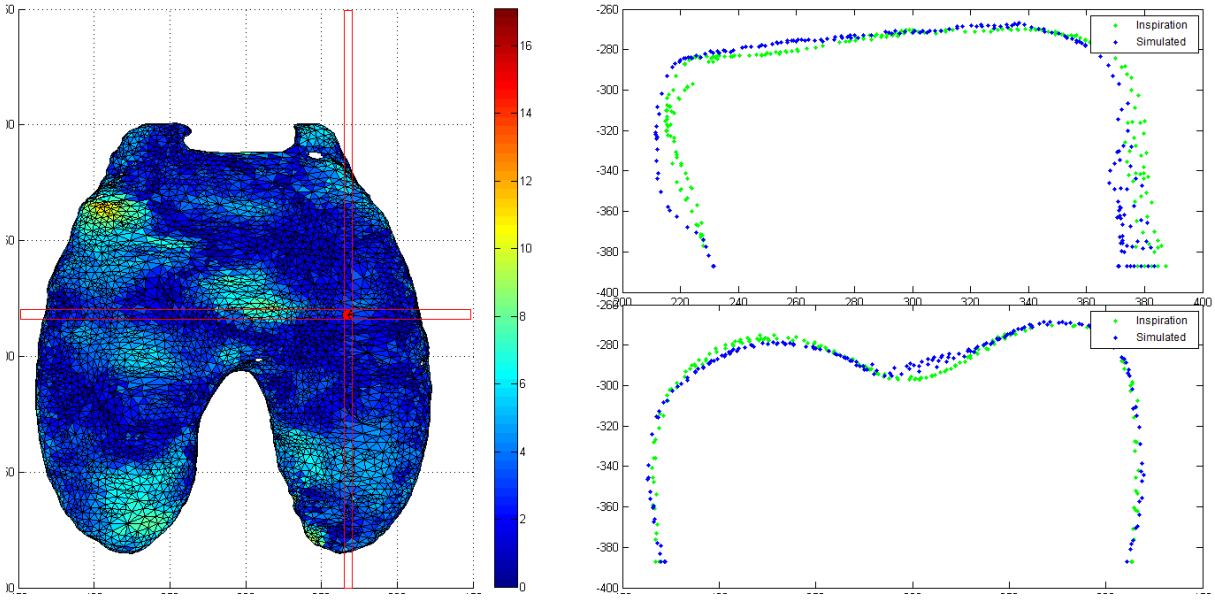

Figure 6: 3D distance map on the diaphragm between inspiration and simulated inspiration (left), a sagittal slice (up-right) and a coronal slice (down-right) of inspiration (blue) and simulated inspiration (blue) mesh nodes

Conclusions

While studying the motion between expiration and inspiration states (figure 5), we notice a larger motion to the posterior side of the diaphragm than to the anterior side. This was also noticed by Cragheiro et al. (2005). More, we notice a slightly larger motion to the right-posterior side than to the left-posterior side. This was also noticed by Whitelaw et al. (1987). The explanation of this may be the fact that the muscles are longer on the posterior side of the diaphragm as explained in the anatomy and maybe even more on the right side than on the left side.

The simulation gives accurate results. All the colors in the distance maps are in light and dark blue except on the left-anterior side where there is a small yellow region (figure 7 and 8). This big error zone is remarked on the simulation of inspiration and expiration. After further investigations and comparisons of our segmented

diaphragms and the CT images, we deduced that this error comes from a segmentation error of the diaphragm at the expiratory state. This is rather encouraging and shows that our biomechanical model is robust enough and cannot be influenced by some local segmentation errors.

The mean errors of 3.68 mm and the corresponding standard deviation can be accepted in the domain of radiation therapy. Therefore, in future work, we should verify diaphragm localisation error and its influence on tumour localisation. To do so, a complete model of the thorax should be created including lungs and tumour.

Other than this study, the only biomechanical model of the diaphragm that shows quantitative evaluation of the errors is the model of Villard et al. (2009). Villard's model applied on two patients showed 4.29 mm and 12 mm mean errors for the first and second patients. In order of comparison, the mean errors of our model are smaller.

The last value to compare is the value of the tension amplitude that we apply on the diaphragm muscles. Indeed diaphragm muscles tension of the inspiration process has been measured in-vivo by Rochester et al. (1984). These measurements concluded that the maximum contractile force of the diaphragm muscle lie between 90 000 N/m^2 and 140 000 N/m^2. The tension used to simulate inspiration in our model has been determine as 40 000 N/m^2. This does not lie in the range specified above. The reason is that in reality, the abdomen and the lungs impose a resistance to the diaphragm muscular tension and the consequent displacement. The abdomen and the lungs are not included in our study and though we cannot evaluate the tension amplitude. The next step in our work is to include a lung and abdomen models.

We have developed a complete model of the respiratory system built from "virtual patient" data. A simple model of the diaphragm, which was missing in our previous studies, has been introduced. We showed preliminary results, which are in accordance with the anatomical reality. The central part of the diaphragm tends to move downwards, while the muscular part motion tends to be lateral oriented downwards due to rib motions. In future works, the model should be applied on a real patient's data to enable quantitative comparisons of the results. The applied nodal forces should be replaced by more appropriated formulations. In particular, the forces could be parallel to muscular fibres in agreement with anatomy and derived from biomechanical considerations. Last, the forces should be correlated to thoracic motion and air flow to the lungs.

Acknowledgments

The authors would like to thank PRRH ETOILE to their financial support, and Centre Léon Bérard for the CT-scan data.

References

[1] Al-Mayah, J. Moseley, and KK. Brock. Contact surface and material nonlinearity modeling of human lungs. Physics in medicine and biology, 53 : 305-317, 2008.

[2] N. Aspert, D. Santa-Cruz, and T. Ebrahimi. Mesh : measuring errors between surfaces using the hausdorff distance. IEEE conference in multimedia and expo (ICME), pages 705-708, 2002.

[3] Behr, M.; Thollon, L.; Arnoux, P.-J.; Serre, T.; Berdah, S. V.; Baque, P. & Brunet, C. (2006), '3D reconstruction of the diaphragm for virtual traumatology', *Surg Radiol Anat* **28**, 235-240.

[4] A.M. Boriek and J.R. Rodarte. Effects of transverse stiffness and central tendon on displacement and shape of a simple diaphragm model. Journal of applied physiology, 82(5) : 1626-1636, 1997.

[5] KK. Brock, MB. Sharpe, LA. Dawson, SM. Kim, and DA. Jaffray. Accuracy of a finite element model-based multi-organ deformable image registration. Medical Physics, 32(6) : 1647-1659, 2005.

[6] Cragheiro, S.; Promayon, E.; Baconnier, P.; Lebas, J.-F. & Coulomb, M. (2005), 'Dynamic echo-planar MR imaging of the diaphragm for a 3D dynamic analysis', *Eur Radiol* **15**, 742-748.

[7] A.L. Didier, P.F. Villard, J.Y. Bayle, M. Beuve, and B. Shariat. Breathing thorax simulation based on pleura behaviour and rib kinematics. Information Visualisation, IEEE Computer Society, pages 35-40, 2007.

[8] A.L. Didier, P.F. Villard, J. Saadé, J.M. Moreau, M. Beuve, and B. Shariat. A chest wall model based on rib kinematics. Information Visualisation, IEEE Computer Society, pages 159-164, 2009.

[9] B. Gagel, C. Demirel, A. Kientopf, M. Pinkawa, M. Piroth, S. Stanzel, C. Breuer, B. Asadpour, T. Jansen, R. Holy, J.E. Wildberger, and M.J. Eble. Active breathing control (abc): determination and reduction of breathing-induced organ motion in the chest. Int. J. Radiation Oncology Biol. Phys., 67(3) : 742-749, 2007.

[10] P. Giraud, E. Yorke, S. Jiang, L. Simon, K. Rosenzweig, and G. Mageras. Reduction of organ motion effects in IMRT and conformal 3d radiation delivery by using gating and tracking techniques. Cancer radiothérapie, 10 : 269-282, 2006.

[11] F. M. Hendriks. Mechanical behaviour of human skin in vivo - a literature review. In Nat.Lab. Unclassified Report 820. Philips Research Laboratories, 2001.

[12] S.B. Jiang. Radiotherapy of mobile tumors. Seminars in Radiology Oncology, 16 : 239-248, 2006.

[13] S. Mori, M. Endo, S. Komatsu, T. Yashiro, S. Kandatsu, and M. Baba. Four-dimensional measurement of lung tumor displacement using 256-multi-slice ctscanner. Lung Cancer, 56 : 59-67, 2007.
[14] C. Ozhasoglu and M.J. Murphy. Issues in respiratory motion compensation during external-beam radiotherapy. Int. J. Radiation Oncology Biol. Phys., 52(5) : 1389-1399, 2002.
[15] Pettiaux, N.; Cassart, M.; Paiva, M. & Estenne, M. (1997), 'Three-dimensional reconstruction of human diaphragm with the use of spiral computed tomography', *J Appl Physiol* **82**, 998-1002.
[16] E. Promayon and P. Baconnier. A 3D discrete model of the diaphragm and human trunk. ESAIM Proceedings, 23 : 66-77, 2008.
[17] Rochester, D.; Arora, N. & Braun, N. (1982), 'Maximum contractile force of human diaphragm muscle, determined in vivo', Trans Am Clin Climatol Assoc 93, 200-208.
[18] Y. Seppenwoolde, H. Shirato, K. Kitamura, S. Shimizu, M. Van Herk, J.V. Lebesque, and K. Miyasaka. Precise and real-time measurement of 3d tumor motion in lung due to breathing and heartbeat, measured during radiotherapy. Int. J. Radiation Oncology Biol. Phys., 53(4) : 822-834, 2002.
[19] H. Shirato, K. Suzuki, GC. Sharp, K. Fujita, R. Onimaru, M. Fujino, N. Kato, Y. Osaka, R. Kinoshita, H. Taguchi, S. Onodera, K. Miyazaka. Speed and amplitude of lung tumor motion precisely detected in four-dimensional setup and in real-time tumor-tracking radiotherapy. Int. J. Radiation Oncology Biol. Phys., 64(4) : 1229-1236, 2006.
[20] P.F. Villard, M. Beuve, and B. Shariat, V. Baudet, and F. Jaillet. Simulation of lung behavior with finite elements : influence of bio-mechanical parameters. Information Visualisation, IEEE Computer Society, pages 65-70, 2005.
[21] P.F. Villard, M. Beuve, and B. Shariat : An Approach to Convert 4D Geometry into a 4D CT Scan. WSCG (Winter School of Computer Graphics), UNION Agency ed. Plzen (Czech Republic). pp. 163-170. ISBN 80-86943-05. 2006.
[22] Villard, P.-F.; Bourne, W. & Bello, F. (2009), Interactive simulation of diaphragm motion through muscle and rib kinematics, *in* Springer London, ed., 'Recent Advances in the 3D Physiological Human', Springer London, , pp. 91-103.
[23] J.W. Wong, M.B. Sharpe, D.A. Ja_ray, V.R. Kini, J.M. Robertson, J.S. Stromberg, and A.A. Martinez. The use of active breathing control (ABC) to reduce margin for breathing motion. Int. J. Radiation Oncology Biol. Phys., 44(4) : 911-919, 1999.

Status of HIMAC

Koji Noda, Takashi Fujita, Shigekazu Fukuda, Takuji Furukawa, Taku Inaniwa, Yoshiyuki Iwata, Nobuyuki Kanematsu, Atsushi Kitagawa, Tadafusa Kumagai, Naruhiro Matsufuji, Shinichi Minohara, Manabu Mizota, Kota Mizushima, Shinichiro Mori, Takeshi Murakami, Masayuki Muramatsu, Shinji Sato, Toshiyuki Shirai, Eiichi Takada, Yuka Takei, Shunsuke Yonai

Research Center for Charged Particle Therapy, National Institute of Radiological Sciences, Chiba, Japan
Corresponding Author: Koji Noda, e-mail address:noda_k@nirs.go.jp

Abstract

The first clinical trial with carbon beams generated from HIMAC was conducted in June 1994. The total number of patients treated was in excess of 6,100 as of August 2011. The impressive advance of carbon-ion therapy using HIMAC has been supported by high-reliability operation and by the development of accelerator technology. The status of HIMAC is described in this report.

1. Introduction

Heavy-ion beams are very suitable for the treatment of deeply seated cancer because of an excellent physical-dose distribution and high-LET characteristics around the Bragg peak. Therefore, NIRS decided to carry out heavy-ion cancer therapy with HIMAC [1]. The first clinical trial of cancer treatment with carbon beam was conducted in June 1994. In the view of the significant growth in the number of protocols, in 2003, the Japanese government approved the carbon-ion radiotherapy (RT) with HIMAC as an advanced medical technology. The total number of patients treated until August 2011 was more than 6,100. The impressive advance of carbon-ion therapy using HIMAC has been supported by high-reliability operation and by the development of accelerator technology. Furthermore, we carried out the R&D work with HIMAC for a standard carbon-ion RT facility and the improvement of the HIMAC accelerator and beam delivery systems for the further development of the HIMAC treatment such as the “New Treatment Facility Project” [2]. This report describes the study for the HIMAC improvements.

2. Progress of the HIMAC technology

The carbon-ion radiotherapy with HIMAC has been progressed, and the treatment number has been increasing year-by-year as shown in Fig. 1. The HIMAC beam-delivery system has employed the beam-wobbling and ridge filter method, which is one of the broad beam methods, in order to deliver its dose safely and reliably. Using this method, at present, around 100 irradiations a day at maximum are carried out under one-shift operation, and around 750 patients a year were treated under 180 days operation. Since the HIMAC treatment was initiated in 1994, we have developed both accelerator and beam-delivery technologies in order to obtain higher irradiation accuracy.

The new treatment research facility has been constructed for the further development of the HIMAC treatment, which is described in the Ref [3]. The new facility is connected with the upper synchrotron at HIMAC. In the treatment hall, placed underground of the facility, three treatment rooms are prepared in order to treat more than the present number of patients with the HIMAC treatment. Two of the treatment rooms are equipped with both horizontal and vertical beam-delivery systems, and the other one is equipped with a rotating gantry. Two treatment-simulation rooms are also equipped for patient positioning as a rehearsal, and for

observing any change in the target size and shape during the entire treatment period with an X-ray CT. Furthermore, there are six rooms devoted to patient preparation before irradiation. A schematic view of the new treatment facility is shown in Fig. 2. One of the treatment room was completed and the treatment has been carried out since May 2011.

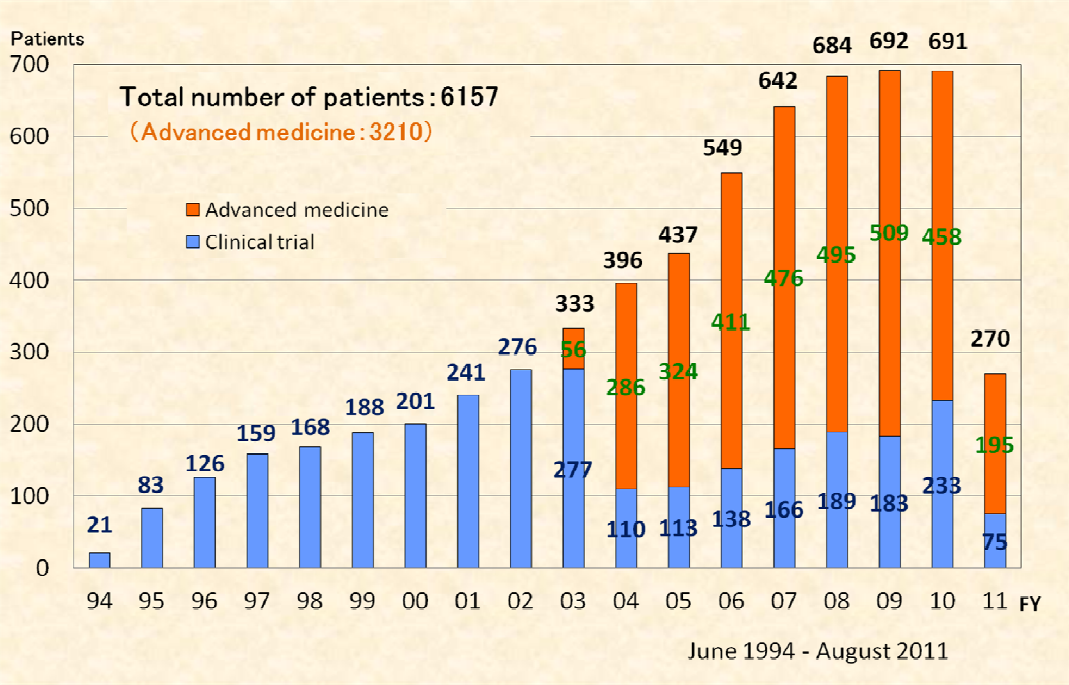

Fig. 1. Treatment number since 1994.

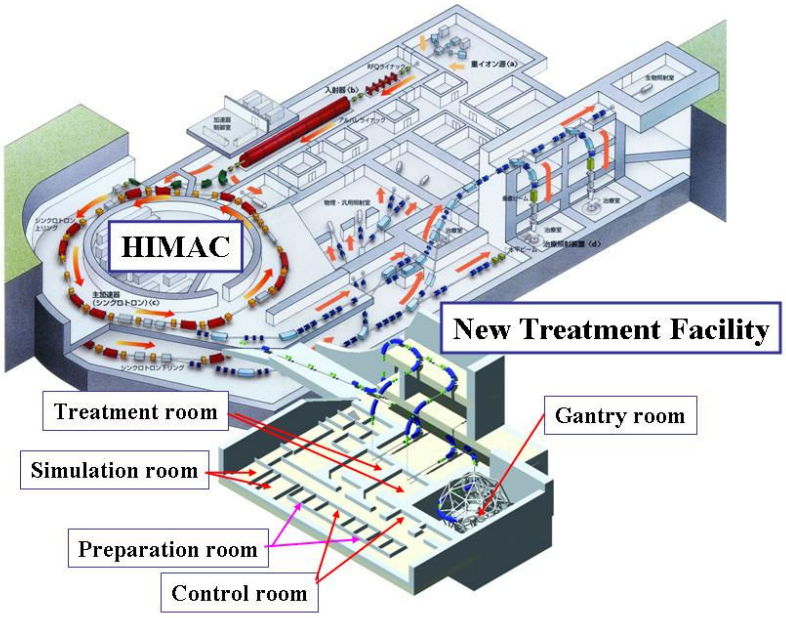

Fig.2. Schematic view of the HIMAC facility with the new treatment research facility.

2.1 Development of the HIMAC beam-delivery system

Respiratory-gated irradiation

Damage to normal tissues around tumor was inevitable in treatment of a tumor moving along with respiration of a patient. A respiration-gated irradiation system, therefore, which can respond quickly to irregular respiration, was developed [4]. In this system, the irradiation-gate signal is generated only when target is at the design

position and the synchrotron can extract a beam. The beam is delivered by the RF-KO extraction method [5], according to the gate signal. This method has been applied to liver, lung and uterus cancers since February 1996.

Layer-stacking irradiation method

In a conventional irradiation method, the fixed SOBP (Spread-Out Bragg Peak) produced by a ridge filter results in undesirable dosage to the normal tissue in front of target, because the width of an actual target varies within the irradiation field. In order to suppress the undesirable dosage, thus, the layer-stacking irradiation method was proposed [6], and the HIMAC irradiation system has been upgraded to put the technique including the treatment planning [7] into practice.

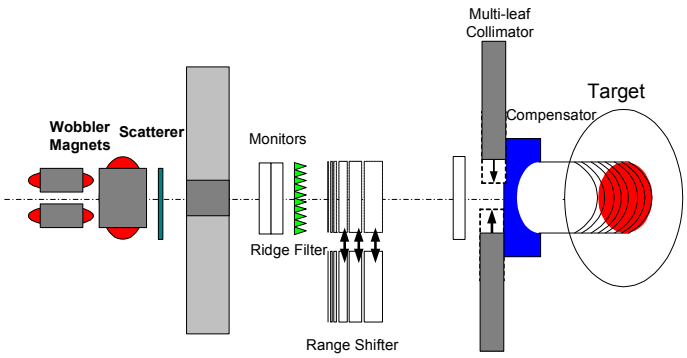

Fig. 3. Schematic drawing of the layer-stacking irradiation method.

3D scanning irradiation method

In order to keep the sophisticated conformations of the dose distributions even in shrinkage of the target size and a change of its shape during the entire treatment, it has been required that treatment planning is carried out just before each fractional irradiation, which we call adaptive cancer therapy. The new treatment research facility should employ a pencil-beam 3D scanning method for a fixed target, a moving target and/or a target near critical organs, toward the target of the implementation of adaptive cancer therapy. For the purpose, we have developed a phase-controlled rescanning (PCR) method [8] with a pencil-beam, especially for treatment of moving target. It was verified by the simulation study that the PCR method can give uniform dose distribution even under irradiation of a moving target. For realizing the PCR method, the following technologies were developed: (1) intensity-modulation technique for a constant irradiation time on each slice having a different cross-section and (2) fast pencil-beam scanning technique for completing several-times rescanning within a tolerable time. After the performance of the PCR was successfully verified [9,10], the fast 3D scanning irradiation port was constructed in the new treatment research facility. In the design of the rotating gantry [11], thus, the PCR method has been employed in order to realize high irradiation accuracy through the multi-field optimization.

2.2 Development of the HIMAC accelerator system

RF-KO slow extraction method

We developed the RF-KO slow extraction method for a respiration-gated irradiation system using the broad-beam irradiation (wobbler) method. This method has a huge spill ripple due to the coherency in its extraction mechanism. However, the huge spill ripple has never disturbed the dose distribution in the wobbler method, because the ripple frequency of around 1 kHz is much different from the wobbling one of around 60 Hz. In the beam-scanning method, on the other hand, the huge spill ripple affects the lateral dose distribution. As a result of study, we proposed the dual FM method and the separated function method [12], which were already verified by the experiment and has been routinely utilized. Further, the intensity modulation of the extracted beam is an essential feature of the PCR method. Thus we have also developed the global-spill (Hz-order) control method [13]. Since this control method can predict the extra-dose occurred when the beam moves between raster points, the scanning speed can be increased by five times compared with the conventional one [14].

Intensity upgrade and extended flat-top operation

For efficient operation of the 3D scanning, the beam intensity extracted from the synchrotron has been increased in order to complete single-fractional irradiation with one operation cycle. In this case, the efficiency of the gated irradiation will be increased, because we can extend the flattop infinitely in principle. As a result, the extended flattop operation will save considerably irradiation time. In order to increase the beam intensity, we have thus carried out a tune survey during beam injection. As a result, it was found that the 3rd-order coupling resonance caused beam loss. This resonance was corrected by four sextupole magnets, and the beam lifetime in the injection-energy level was increased by more than 5 times. In addition, we tried multi-harmonics operation of the RF acceleration system in order to suppress the space-charge effect after bunching. This operation increased the acceleration efficiency by around 40%. Consequently, around 2×10^{10} carbon ions can be accelerated to the final energy. This intensity is sufficiently high to complete single-fractional irradiation for almost all tumors treated with HIMAC when using the 3D-scanning method with beam-utilization efficiency more than 90%. The extended flattop operation was successfully tested at the HIMAC synchrotron, and the stability of the beam-profile was investigated. The horizontal and vertical beam profiles during extraction duration of 100 s were measured by a multi-wire proportional counter. As a result of an analysis of the measurement, it was estimated that both the position and the size duration of 100 s were stabilized within ±0.5 mm at the iso-center.

Variable energy operation

Even in the broad-beam irradiation method, quick energy change is useful for an efficient operation. In the pencil-beam 3D scanning, variable energy operation by accelerator itself has great advantages over the range shifter method: keeping the spot size small and suppressing secondary neutron production. GSI developed the variable energy operation in cycle-by-cycle. In this case, it takes a few second of the operation cycle to change the energy for one slice change in the scanning method. Hitachi also developed the similar variable energy operation of the synchrotron for proton RT. NIRS is under developing the variable energy operation within one operation cycle of the HIMAC synchrotron. In the NIRS method, the energy of the extracted ion can be changed by step-wised energy pattern at the flattop of synchrotron operation. The duration of the flattop can be arbitrarily determined by a clock on/off in the flattop period, as shown in Fig. 4. As the first step, an eleven-step energy operation was developed. This operation has been routinely utilized for the treatment by the fast 3D scanning, although the beam energy is fixed during the one fractional irradiation because a part of transport line consisted of some block-iron magnets. As the second step, the 147-step energy pattern, which can change the energy ranging from 430 to 80 MeV/n, has been developed. The energy change in one step corresponds to a range shift of 2 mm, and it will take less than 100 ms to change a slice [15]. A beam commissioning for the variable energy operation will start after the block-iron magnets in a part of transport line from the synchrotron to the new treatment research facility will be replaced to laminated-iron magnets.

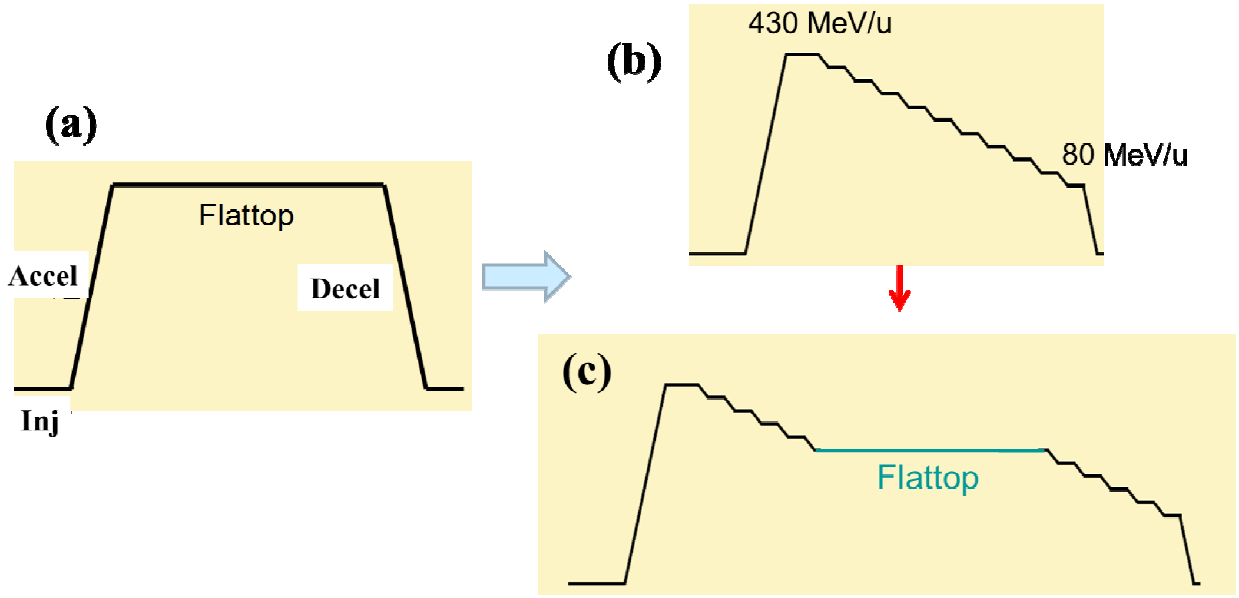

Fig. 4. Schematic diagram of variable energy operation at HIMAC. (a) Conventional operation pattern, (b) Variable energy operation pattern and (c) Extended flattop with arbitrary energy by the clock on/off.

4. Summary

Figure 5 shows the development flow of the heavy-ion cancer radiotherapy facility in Japan. Carbon-ion radiotherapy with HIMAC has treated more than 6, 100 pts since 1994. In these treatments, the new technologies such as the respiratory-gated irradiation and layer stacking irradiation methods, developed by NIRS, has applied to the cancer therapy with HIMAC. On the basis of the clinical study and the related technologies developed by NIRS, the downsized carbon-ion radiotherapy facility was developed and its pilot facility was constructed by Gunma University in cooperation with NIRS. The pilot facility has been initiated since March 2010. The new treatment research project, based on the fast 3D scanning technology, has carried out treatments since May 2011. One has expected the further developments of heavy-ion radiotherapy using a pilot facility in Gunma University and the new treatment research facility in NIRS, and these technologies will play an important role to heavy-ion cancer radiotherapy in the world.

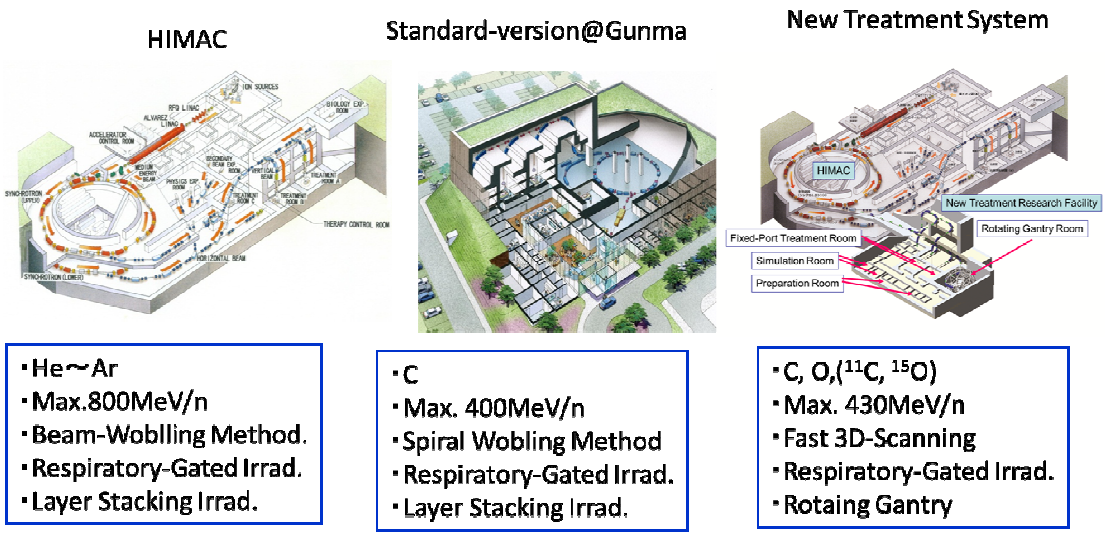

Fig. 5. Development flow on heavy-ion cancer radiotherapy technologies.

References

［1］ Y. Hirao et al., Nucl. Phys. A 538, 541c–550c (1992).

［2］ K. Noda et al., J. Rad. Res., 48 (2007) A43-A54.

［3］ T. Shirai et al., in these proceedings.

［4］ S. Minohara et al., Int. J. Rad. Oncol. Bio. Phys. 2000;47:1097-1103.

［5］ K. Noda et al., Nucl. Instrum. Meth. A 374 (1996) 269.

［6］ T. Kanai et al., Med. Phys. 10, 344 (1983).

［7］ T. Kanai et al., Med. Phys. 33, 2989 (2006).

［8］ T. Furukawa et al., Med. Phys. 34 (3), 1085-1097 (2007).

［9］ T. Furukawa et al., Medical Physics, 37, 4874-4879, (2010).

［10］ T. Furukawa et al., Medical Physics, 37, 5672-5682, (2010).

［11］ T. Furukawa et al., Nucl. Instrum. Meth. B 266 (2008) 2186-2189.

［12］ K. Noda et al., Nucl. Instr. Meth. Res. A492 (2002) 253-263.

［13］ T. Furukawa and K. Noda, Nucl. Instrum. Meth. A 565 (2006) 430.

［14］ T. Inaniwa et al., Med. Phys. 34 (8) 3302-3311 (2007).

［15］ Y. Iwata et al., Nucl. Instrum. Meth. A 624 (2010) 33-38.

New Particle Therapy Facility in NIRS, Present and Future Plan

Toshiyuki Shirai, Takuji Furukawa, Taku Inaniwa, Yoshiyuki Iwata, Nobuyuki Kanematsu, Ken Katagiri, Yosuke Koba, Yoshiki Kubota, Motoki Kumagai, Naruhiro Matsufuji, Yuka Matsuzaki, Shinichi Minohara, Kota Mizushima, Shinichiro Mori, Takeshi Murakami, Shinji Sato, Eiichi Takada, Yuka Takei and Koji Noda

Research Center for Charged Particle Therapy, National Institute of Radiological Sciences, Chiba, Japan
Corresponding Author: Toshiyuki Shirai, e-mail address: t_shirai@nirs.go.jp

Abstract

A new particle therapy facility has been constructed in NIRS. In order to realize the adaptive charged particle therapy, a 3D scanning irradiation system is installed in the new facility. We have also developed a new treatment planning system and a patient handling system. The therapeutic irradiation of carbon beam to the first patient was started on May 17, 2011 and finished on June 10, after a half year commissioning program. The treatments for 8 patients were finished before the summer shutdown and the clinical studies will be continued for a more than a dozen patients until this November. A compact rotating gantry for carbon beam is also an important subject in the new facility. A superconducting rotating gantry has been developed and it will have a similar size and weight to proton gantry.

Introduction

Since 1994, the carbon beam therapy has been continued at Heavy Ion Medical Accelerator in Chiba (HIMAC). The total number of patients is more than 6,000 in 2011. Based on more than ten years of experience, we have developed a new treatment system at New Particle Therapy Research Facility in NIRS. The project was started in 2006 and the progress is shown in Table 1. The new facility is designed to investigate the following subjects,

I. Adaptive charged particle therapy,

II. Compact rotating gantry for carbon beam.

The size and shape of the tumors vary during the treatment period. The adaptive therapy is a method to meets the change of the targets. The 3D scanning method with a pencil beam is employed in the new facility to realize this subject and we have developed following four systems,

1. 3D scanning irradiation system for moving targets [1],
2. Treatment planning system [2],
3. Patient handling system with robotic arms [3],
4. Treatment management system.

The 3D scanning irradiation system adopts a phase-controlled rescanning (PCR) method for the moving target [4]. The fast scanning irradiation system in NIRS can complete the several times rescanning of each slice during a single gated period of the respiration. We have developed the new treatment planning system, which supports the PCR method and implements the equivalent biological model of the carbon beam to that of HIMAC [5]. The patient handling system supports a precise patient positioning

Table 1: Progress of the new facility project.

Year	Events
2006/4	Project was started.
2009/2	New facility construction was started.
2010/3	New facility building was completed.
2010/5	Machine installation was started.
2010/9	1st carbon beam was delivered to Room E.
2010/10	Beam commissioning was started.
2011/5	Irradiation to 1st patient was started.

with a robotic arm bed and a tracking of the organ motion.

The rotating gantry improves the dose conformity and less sensitivity to range uncertainties. It also reduces the patient's load. The challenge of the rotating gantry for carbon beam is a cost and size, including the building. We have developed the rotating gantry with superconducting magnets. We expected that it leads to the reduction of the total size and the weight.

Table 2: Major parameters of irradiation system.

Ion species	Carbon
Irradiation method	Scanning
Max. beam energy	430 MeV/n
Beam intensity	1 x 10^7 ~ 1 x 10^9 pps
Max. irradiation Area	220 mm x 220 mm
Max. SOBP	150 mm

Based on the design study, the budget was approved except the rotating gantry and the construction of the facility was started in 2009. After the completion of the building in May, 2010, the machine installation had been carried out. The first carbon beam was delivered to the room E in September, 2010 from HIMAC synchrotron. It was followed by the beam commissioning of the irradiation system and the treatment planning system.

Figure 1 shows the view of the new facility and the existing HIMAC facility. There are three treatment rooms in the new facility. Two of them are equipped with fixed beam delivery systems in both the horizontal and vertical directions (Room E & F), and the other will be equipped with a rotating gantry (Room G). The heavy ion beam is provided from the HIMAC upper synchrotron through the tunnel. The table 2 shows the major parameters of the irradiation system. The maximum ion energy is designed to be ^{12}C, 430 MeV/n in order to obtain the residual range of 30 cm. Figure 2 shows the horizontal and vertical irradiation ports and the beam line to the room E.

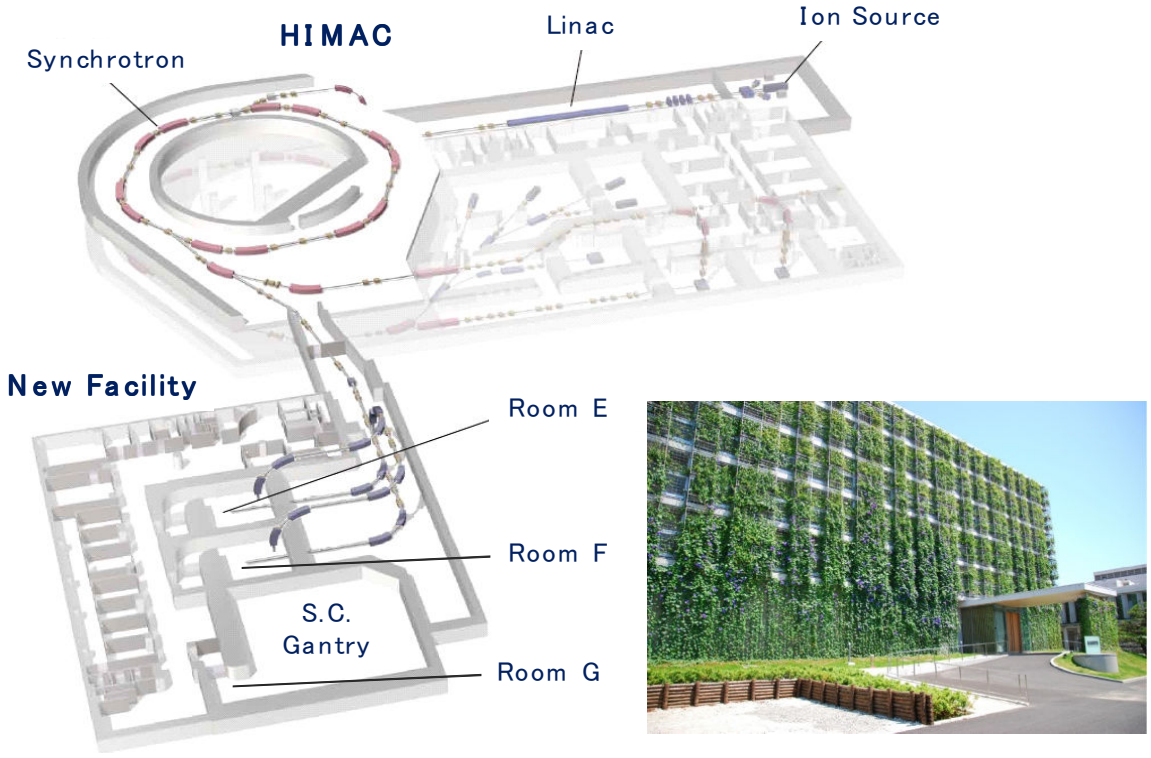

Figure 1: Schematic view of the new facility (New Particle Therapy Research Facilities) and the existing HIMAC facility. The front gate of the new facility is shown in the right figure. There are three treatment rooms (E/F/G) in the new facility. There are horizontal and vertical irradiation ports in room E/F and a gantry port in room G.

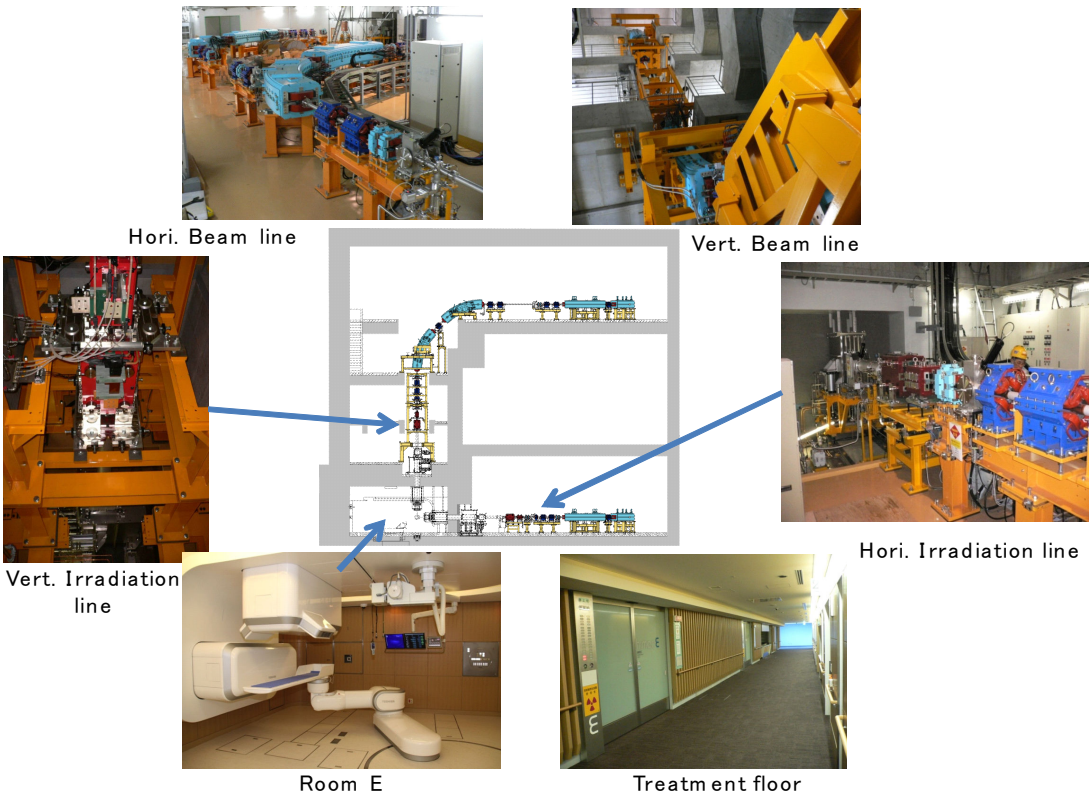

Figure 2: Schematic view and photos of the horizontal and vertical beam lines to the room E in the new facility. The lower photos show the inside of the room E and the treatment floor in the second basement.

Present Status

Although the starting day was delayed due to the Tohoku Earthquake, the therapeutic irradiation to the first patient was started on May 17, 2011 as a clinical study and finished on June 10. The clinical study has been continued until November, 2011 with the summer shutdown of two months. Before the summer shutdown, the number of the patients treated in the new facility is 8 and their targets are in pelvic and head regions. The inside of room E is shown in Fig. 2. The horizontal and vertical irradiation equipments such as range shifters, ridge filters, dose and position monitors are covered by the boxes. Patients are fixed on the treatment table with robotic arms. The irradiation area in the target was confirmed for each patient by the observation of the autoactivation

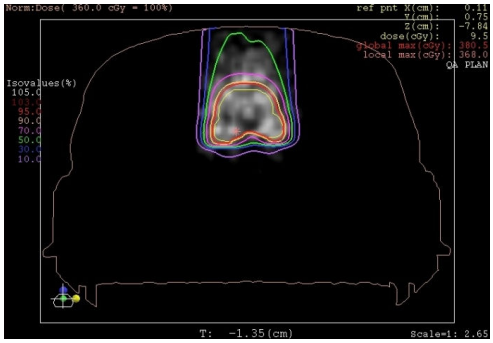

Figure 3: Cross sectional view of the dose distribution in the treatment plan and the PET-CT image of the autoactivation. A green line shows a 50% contour line.

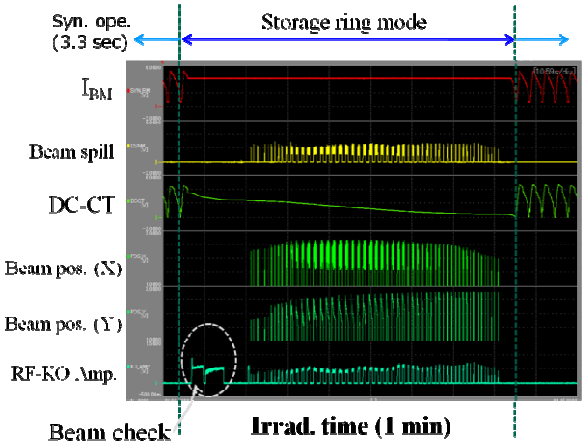

Figure 4: Operation pattern of the 3D scanning system. Beam positions are measured by the beam position monitors near the isocenter.

using the positron emission tomography (PET). Figure 3 shows an example of the fusion image of the treatment plan and the PET-CT image.

Before the summer shutdown, the beam operation period is 52 days (13 weeks) and about 2 hours per day, which includes the beam QA time. The total irradiation number is 124 and the irradiation time is 1–3 min. The average treatment time is 19 min per one patient including the patient positioning. Figure 4 shows the typical operation pattern of the synchrotron and the 3D scanning irradiation system. When the irradiation is started, the beam energy is kept constant (see I_{BM}) until the irradiation is finished or the stored beam in the synchrotron becomes empty. The total slice number and the dose is 55 and 3.6 GyE in this case, respectively. The irradiation time is 80 sec, including the beam position check before the irradiation.

3. Future Plan

In 2012, the therapeutic irradiation will be carried out in room E and F in the new facility. We are preparing the two subjects in parallel. One is the 3D scanning irradiation for the moving target in room E & F and the other is the superconducting rotating gantry in room G.

We have already developed the phase-controlled rescanning (PCR) method for the moving target [4]. It is realized by the very fast scanning system and the intensity control system in the slow beam extraction from synchrotron in order to provide the optimum beam rate. The both technology are already implemented in the present system and the commissioning of the 3D scanning irradiation with PCR method will start in 2012. The clinical study is schedule in 2013.

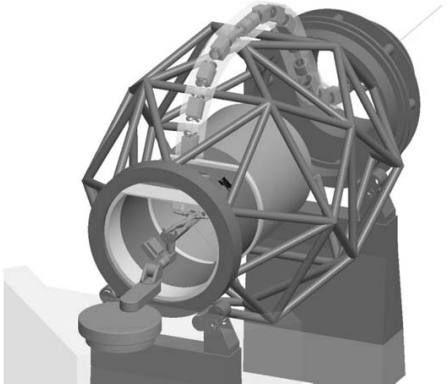

Figure 5: Schematic view of the superconducting rotating gantry for carbon beam. The size and weight of the gantry is almost the same as those of the proton one.

In the previous design of the rotating gantry in NIRS using normal conducting magnets, the weight is about 350 tons. The almost half of the weight is the magnets and the counterweight of the magnets. We have developed the superconducting magnets for the rotating gantry in order to reduce the size and the weight. In the present design, 8 superconducting magnets are used and the maximum magnetic field is about 3 T, when the maximum beam energy is 430 MeV/n [6]. The gantry radius is 5.5 m and the total length is 13 m. The total weight is less than 200 tons. We expect that the size and weight of the carbon gantry become those of the proton gantry (Fig. 5). The 3D scanning system is identical with that of the fixed port. We have already constructed the test magnets and hope to install the superconducting rotating gantry within a few years.

References

［1］ Furukawa T, et al. NIRS Scanning System: Present Status and Future Prospects, in this proceedings.

［2］ Inaniwa T, et al. TPS for NIRS Scanning: Present Status and Future Prospects, in this proceedings.

［3］ Mori S, et al. Multi-dimensional Image Guided Particle Therapy, in this proceedings.

［4］ Furukawa T, et al. Moving target irradiation with fast rescanning and gating in particle therapy, Med. Phys. 2010;37: 4874-4879.

［5］ Matsufuji N, et al. Modeling of Clinical and Biological Effect of Therapeutic Carbon Ion beam, in this proceedings.

［6］ Iwata Y, et al. Design of Superconducting Rotating-gantry for Heavy-ion Therapy, Proc. of IPAC'11. 2011: 3601-3603.

Current Trends in the Promotion of Carbon Ion Radiotherapy in Japan

Atsushi Kitagawa

Research Center for Charged Particle Therapy, National Institute of Radiological Sciences, Chiba, Japan
e-mail address:kitagawa@nirs.go.jp

Abstract

The HIMAC project awakens an interest in carbon ion radiotherapy all over Japan. NIRS has leaded its promotion in Japan under the Japanese government's comprehensive strategy. With a cooperation of existing charged particle radiotherapy facilities in Japan, a scheme of facility's construction has been established commercially, core human resources for treatment has been developed, and guidelines for good medical practice has been set. These approaches realized two new projects in Saga and in Kanagawa.

History and yield of the HIMAC project

The Heavy Ion Medical Accelerator in Chiba (HIMAC) at the National Institute of Radiological Sciences (NIRS) in Chiba, Japan is the first medical dedicated heavy ion accelerator complex and had an aim to develop heavy ion radiotherapy as a safe and secure irradiation technologies. The research project was conducted under the Japanese government's "The 1st and 2nd Comprehensive 10-year Strategy for Cancer Control (1984 - 1993 and 1994 - 2003)". The clinical data have been accumulated under prescribed clinical protocols since 1994. The results have clearly demonstrated the advantages of carbon ions. In 2003, the Japanese Ministry of Health, Labour and Welfare (MHLW) approved carbon ion radiotherapy as an "advanced medicine", which is an intermediate step to be approved as a treatment under the Japanese national health insurance system. In the approval procedure, the effectiveness and the safety have already been verified, and start the discussion on an equitable share and medical economy carefully.

The approval of "advanced medicine" has awakened an interest in carbon ion radiotherapy all over Japan. In order to summarize the status of research and treatment, to provide information necessary for the construction of a facility, to study technical or institutional subjects, and to make a roadmap for research and development, the Japanese Ministry of Education, Culture, Sports, Science and Technology (MEXT) held an unofficial internal workshop for popularization of the charged-particle radiotherapy in 2004. The discussion of the workshop was summarized as an internal report by the workshop committee[1]. The report was distributed to ambitious people like public or private medical institutions, universities, local governments, members of Parliament and so on. Many plans have started and were guided in this report.

Approaches for the promotion in Japan

The Japanese government is promoting development of new downsizing technologies under "The 3rd Comprehensive 10-year Strategy for Cancer Control (2004 - 2013)"[2]. NIRS designed a hospital-specified carbon ion radiotherapy facility and developed prototypes of various components. The feature of the design is an exhaustive optimization for treatment by carbon beams. This realized a cost-effective and sure facility's design. The successful results of developed prototypes also certified manufacturing companies of the minimum business risks. Based on these results, MEXT funded the project of the Gunma University Heavy Ion Medical Center (GHMC) as a demonstration facility in April 2006. The construction was supported on a cooperation framework between Gunma University and NIRS shown in Fig.1. GHMC has been successfully operated since March 2010. The facility was approved as a commercial medical device by MHLW.

MEXT is also promoting a training system, “Program for the Human Resources Development Relating to Charged Particle Radiotherapy”, since 2007[3]. The purpose of the program is to develop core human resources, such as radiation oncologists, medical radiological technologists, and medical physicists. Six existing charged-particle radiotherapy facilities in Japan cooperate to give on-the-job-training to medical staff in a common curriculum. Over 40 persons have been trained until 2011.

Since carbon ion radiotherapy involves various processes and professions in multiple sections using advanced and complicated equipments, the quality control and quality assurance in radiotherapy is very important. Guidelines and standard methods have been developed to satisfy this purpose under the cooperation framework of existing facilities. The guideline for charged particle radiotherapy in Japan was authorized by the Japan Society of Medical Physics (JSMP)[4]. The radiological protection for medical workers and related persons is also important. The exposure was studied under the same framework supported by MHLW[5].

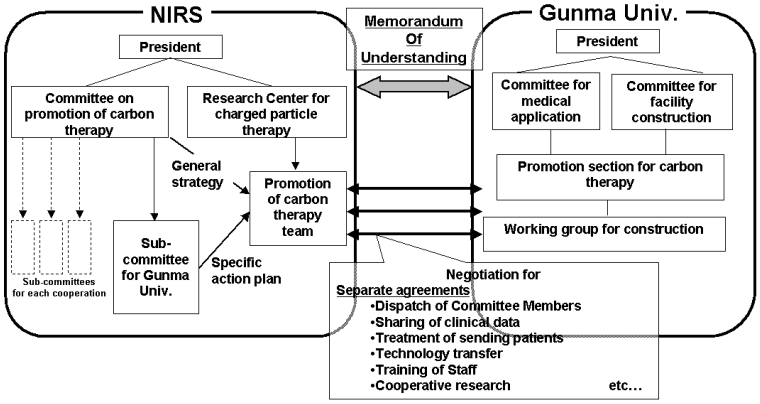

Fig. 1 A cooperation framework between Gunma University and NIRS for the construction of GHMC.

Longer and broader perspective

The construction of the 4th carbon ion radiotherapy facility, named SAGA-HIMAT (Heavy Ion Medical Accelerator in Tosu), will be finished in 2013. The 5th facility at Kanagawa Cancer Center also start off on the work. On the other hand, many kinds of problems have been increasingly recognized, i.e. continuing efforts for cost reduction, development of systematic patient selection, development of specialists in related industrial fields, and so on. It is required to improve a framework of technology and knowledge transfer, to enlarge the human resources development, to achieve worldwide standardization, and to cooperate for new researches and developments. A new roadmap for the next step of promotion is now under consideration by NIRS. It will clarify a goal of 5 years later. A cooperation of related public and private organizations in wide fields will become more important. International activities and collaborations will be also required.

References

［1］ “For popularization of the charged-particle radiotherapy”, edited by the committee of the workshop for popularization of the charged-particle radiotherapy, December 2004 (in Japanese).

［2］ “Summary at the 10th anniversary of the heavy ion radiotherapy”, Monbu-Kagaku Jihou No.1541 (ISSN1346-325X), edited by MEXT, August 2004, pp. 10-49 (in Japanese).

［3］ “Progress to date in carbon ion radiotherapy –Present status and outlook-”, edited by NIRS, Radiological Sciences Vol.50 no.7 (ISSN0441-2540), September 2007, pp. 4-65. (See Section III.3.)

［4］ “Guidelines of Physical and Technological Quality Assurance for Particle Beam Therapy”, edited by JSMP and NIRS. (This article is revised regularly. The newest edition is distributed by JSMP.)

［5］ H. Tsujii, *et al*., “Research on radiation protection in the application of new technologies for proton and heavy ion radiotherapy”, Igaku Butsuri 28, 2009, 172-206.

Hadrontherapy: ENLIGHT and EU funded projects

Manjit Dosanjh, Audrey Ballantine, Manuela Cirilli, Helen Dixon-Altaber, Virginia Greco

CERN (European Organization for Nuclear Research)
e-mail address: manjit.dosanjh@cern.ch

Abstract

State-of-the-art techniques borrowed from particle accelerators and detectors are a key element in hadron therapy, and several European projects are actively fostering the collaboration amongst the various disciplines and countries. The ENLIGHT network was established in 2002 to coordinate these European efforts in hadron therapy, and today it includes more than 300 participants from twenty European countries. A major achievement of ENLIGHT has been the blending of traditionally separate communities, so that clinicians, physicists, biologists and engineers with experience and interest in particle therapy can effectively work together. ENLIGHT demonstrates the advantages of regular and organized exchanges of data, information and best practices. It also determines strategies to be followed and actions to be implemented for future needs in research and technological development in the field, and to achieve a cost-effective high-precision cancer treatment. In 2006, the ENLIGHT community agreed that the goals of the collaboration could be best met by two complementary approaches: research in areas needed for highly effective hadron therapy, and networking, to establish and implement common standards and protocols for treating patients. The primary mandate of ENLIGHT is therefore to develop strategies for securing the funding necessary to continue the initiative in these two fundamental aspects.

ENLIGHT

State-of-the-art techniques borrowed from particle accelerators and detectors are a key element in hadron therapy, and several European projects are actively fostering the collaboration amongst the various disciplines and countries. The ENLIGHT network was established in 2002 to coordinate these European efforts in hadron therapy, and today includes more than 300 participants from twenty European countries. A major achievement of ENLIGHT has been the blending of traditionally separate communities so that clinicians, physicists, biologists and engineers with experience and interest in particle therapy can effectively work together. ENLIGHT demonstrates the advantages of regular and organised exchanges of data, information and best practices. It also determines strategies to be followed and actions to be implemented for future needs in research and technological development in the field, and to achieve a cost-effective high-precision cancer treatment. In 2006, the ENLIGHT community agreed that the goals of the collaboration could be best met by two complementary approaches: research in areas needed for highly effective hadron therapy, and networking, to establish and implement common standards and protocols for treating patients. The primary mandate of ENLIGHT is therefore to develop strategies for securing the funding necessary to continue the initiative in these two fundamental aspects.

Detailed information on ENLIGHT, including how to join, is available on the website http://cern.ch/ENLIGHT

PARTNER

Hadron therapy uses particle beams to treat tumours located near critical organs and tumours that respond poorly to conventional radiation therapy. It has become evident that there is an emerging need for reinforcing research in hadron therapy, and that it is essential to train professionals in this rapidly developing field.

PARTNER is a 4-year Marie Curie Training project funded by the European Commission with 5.6 million Euros aimed at the creation of the next generation of experts. Ten academic institutes and research centres and two leading companies are participating in PARTNER, that is coordinated by CERN, forming a unique multidisciplinary and multinational European network. The project offers research and training opportunities to 25 young biologists, engineers, physicians and physicists and is allowing them to actively develop modern techniques for treating cancer in close collaboration with leading European Institutions. For this purpose PARTNER relies on cutting edge research and technology development, effective networking, and open access to national facilities as well as providing training by specialists in this field.

Ongoing PARTNER activities aim to:
• Create new knowledge through multidisciplinary studies
• Enhance clinical research
• Implement the most recent developments from e-Health
• Develop the next generation of monitors and detectors
• Advance the European common demonstration platform
• Train and educate through workshops and courses the European clinicians and medical physicists.

Further information is available on the PARTNER website http://cern.ch/PARTNER

ULICE

Hadrontherapy is increasingly used to treat cancer with beams of protons or ions instead of conventional X-rays: at the end of 2009, the number of proton-treated patients has surpassed the 60,000 milestone, and there are encouraging results from Germany and Japan using carbon-ion therapy. Initially, therapeutic irradiations were performed in particle physics laboratories, and it is only in the past 20 years that hospital based centers were established – the first one being in Loma Linda, USA in 1990. In the past few years, Europe has made important steps in the development and construction of hospital-based 'dual' centers for carbon ions and protons. In particular, in November 2009 the Heidelberg Ion Radiation Therapy Centre (HIT) in Germany treated its first patient, and CNAO (the Italian Centro Nazionale di Adroterapia Oncologica in Pavia) should start treating patients at the end of 2011. However, the challenges posed by the size and cost of hadrontherapy centers are numerous, and the design of optimal and standardized facilities must necessarily come from a global, interdisciplinary and transnational research effort.

The ULICE project was launched in 2009 to address two different complementary issues:
• The development of the appropriate instruments for high-performance hadrontherapy, with particular emphasis on carbon ion therapy
• The need for intensive collaboration among the existing and planned centers, as well as with the European hadron therapy community at large

ULICE is funded for four years by the European Commission with 8.4 million Euros and involves 20 European institutions coordinated by CNAO. All the existing and planned European ion therapy facilities are involved in the project, together with two research centres (CERN and GSI) and two industrial companies (Siemens and IBA). The experience being built up in Heidelberg and Pavia will help the development of hadron therapy in Europe (and globally) and will provide patients throughout Europe access to these centres with treatment according to standardized protocols. In addition, other centres planned in Europe which are due to start, will benefit from this experience.

The project consists of 3 pillars:

• Joint Research Activities – focused on the development of instruments and protocols
• Networking – to increase cooperation between facilities and research communities
• Transnational access – to allow access to hadrontherapy facilities to researchers wanting to perform radiobiological and physics experiments as well as clinical studies.

As of summer 2011, researchers from eligible countries can apply to take part in research activi- ties or submit experimental proposals in the clinical, radiobio- logical and physical field at the University Hospital of Heidelberg and at CNAO. In the words of Jürgen Debus, medical director of the Department of Radiation Oncology and Radiation Therapy of Heidelberg University Hospital and co-ordinator of the ULICE transnational access: "A technology has worth in the medical field only if it is spread and if everyone can participate to its evolution with their experience and feedback." Applications for participa- tion in the transnational access programme will be reviewed by a multicentre scientific committee and successful applicants will be granted free access thanks to the European Union Transnational Access funding. For more information or to apply for access to these facilities, go to the ULICE website http://cern.ch/ULICE or contact ULICE-access@cern.ch

The outcome of the recent Mid Term Review of the project is described in the article published on the autumn issue of the ESTRO Newsletter.

ENVISION

Hadron therapy is a highly advanced technique of cancer radiotherapy that uses beams of charged particles (ions) to destroy tumour cells. While conventional X-rays traverse the human body depositing radiation as they pass through, ions deliver most of their energy at one point. Hadron therapy is most advantageous once the position of the tumour is accurately known, so that healthy tissues can be protected. Accurate positioning is a crucial challenge for targeting moving organs, as in lung cancer, and for adapting the irradiation as the tumour shrinks with treatment. Therefore, quality assurance becomes one of the most relevant issues for an effective outcome of the cancer treatment. In order to improve the quality assurance tools for hadron therapy, the European Commission is funding ENVISION, a 4-year project that aims at developing solutions for:

• real-time non invasive monitoring
• quantitative imaging
• precise determination of delivered dose
• fast feedback for optimal treatment planning
• real-time response to moving organs
• simulation studies

Launched in February 2010, ENVISION is a collaboration of sixteen leading European research centres and industrial partners, coordinated by CERN. More information is available on the project website at http://cern.ch/ENVISION

ENTERVISION

The European training network in digital medical imaging for radiotherapy (ENTERVISION) was established in February 2011 in response to the critical need for reinforcing research in online 3D digital imaging and the training of professionals in order to deliver some of the key elements and building blocks for realizing the vision for early detection and more precise treatment of tumours. This is an interdisciplinary (physics, medicine, electronics, informatics, radiobiology, engineering) multinational initiative, which has the primary goal of training researchers who will help technical developments at a pan-European level, for the benefit of all of Europe. ENTERVISION brings together ten academic institutes and research centres of excellence and the two leading European companies in particle therapy, IBA and Siemens. All partners are known worldwide in the diverse but complementary fields

associated with technological development for improving health. Thus the network covers a unique set of competencies, expertise, infrastructures and training possibilities. The network will train 12 ESR and 4 ER during a 48 month period. The context of a new technique and a dynamic research program in an area of great societal demand offers outstanding training opportunities for future careers of the young researchers.

Information on the project is available on the ENTERVISION website http://cern.ch/ENTERVISION.

Acknowledgements

PARTNER is funded by the European Commission within the FP7 People Programme, under Grant Agreement no. 215840.

ULICE is co-funded by the European Commission within the FP7 7 Capacities Specific Programme, under Grant Agreement no. 228436.

ENVISION is co-funded by the European Commission within the FP7 Cooperation Programme, under Grant Agreement no. 241851.

ENTERVISION is funded by the European Commission within the FP7 People Programme, under Grant Agreement no. 264552.

NIRS Scanning System: Present Status and Future Prospects

Takuji Furukawa, Taku Inaniwa, Toshiyuki Shirai, Kota Mizushima, Eri Takeshita, Yoshiyuki Iwata, Shinichiro Mori, Shinji Sato, Ken Katagiri and Koji Noda

Research Center for Charged Particle Therapy, National Institute of Radiological Sciences, Chiba, Japan
Corresponding Author: Takuji Furukawa, e-mail address: t_furu@nirs.go.jp

Abstract

A new treatment facility as an extension of the existing HIMAC facility is constructed for the further development of carbon-ion therapy in NIRS. This new treatment facility is equipped with a 3D irradiation system with pencil beam scanning. The challenge of this project is to realize treatment of a moving target by scanning irradiation. Thus, to realize this, the development of the fast scanning system is one of the most important issues in this project. After the installation of the scanning system, the commissioning of NIRS fast scanning system was started in September 2010. After intense commissioning and quality assurance tests, the treatment with scanned ion beam was started in May 2011. This paper describes the present status and future prospects of the NIRS scanning system.

1. Introduction

At the HIMAC, more than 6000 patients have been successfully treated by carbon beams since 1994. To make optimal use of these characteristics and to achieve accurate treatment, three-dimensional (3D) pencil beam scanning [1-3] is one of the sophisticated techniques in use. For implementation of this irradiation technique, at HIMAC [4], a new treatment facility [5] was constructed. The challenge of this project is to realize treatment of a moving target by scanning irradiation, because pencil beam scanning is more sensitive to organ motions compared with conventional broad-beam irradiation [6]. Our approach [7] is a combination of the rescanning technique and the gated irradiation method. One of the most important features of the system is fast scanning to realize moving target irradiation with a relatively large number of rescans within an acceptable irradiation time. The system was designed so as to provide a modulated dose delivery with beam-scanning velocities of 100 and 50 mm/ms at the isocenter. These scanning velocities enable us to achieve the fastest irradiation time of around 40 ms for an example uniform 2D field having a 102×102 mm^2 size with spot spacing of 3 mm. In the performance test of 3D delivery [8], the average of the spot-staying time was considerably reduced to 154 μs, while the minimum staying time was 30 μs. The commissioning of NIRS fast scanning system was performed from September 2010 to April 2011. After intense commissioning and quality assurance tests, the treatment with scanned ion beam was started in May 2011. On the other hand, the development toward the multiple energy operation [9] and the moving target irradiation [10] are in progress. The status and future prospects of the NIRS scanning system are described.

2. Specification of the scanning system

2.1. Layout of the system

Figure 1 shows a layout of the scanning irradiation system which has a 9 m length to the isocenter. To achieve the fast magnetic scanning, the distances from the scanning magnets, SCMX and SCMY, to the isocenter are set to 8.4 and 7.6 m, respectively. The vacuum window is made of 0.1mm-thick kapton and located 1.3 m upstream from the isocenter. Two screen monitor (SCN) is included in the beam line and it is used for the beam checking and tuning just before each treatment irradiation. The primary beam shutter and the neutron shutter are placed

downstream of the scanning magnets. The main and sub flux monitors (DSN_M and DSN_S), position monitor (DSN_P), mini-ridge filter (RGF) and range shifter (RSF) are placed after the vacuum window.

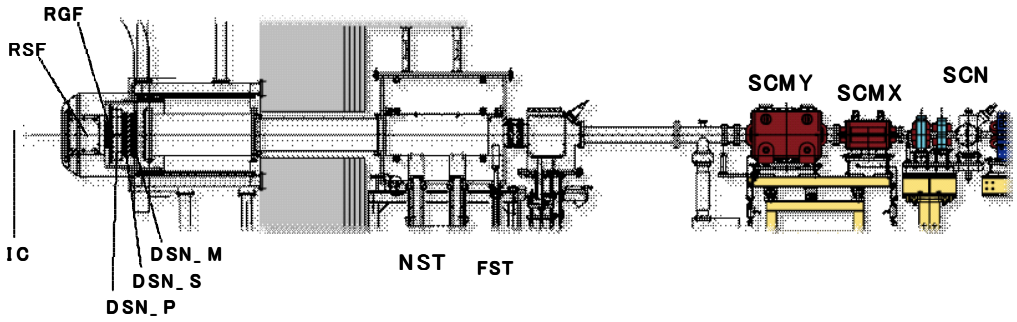

Fig. 1. Layout of the scanning system.

2.2. Control system

A schematic drawing of the scanning control system is shown in Fig. 2. The scanning beam delivery is realized by specific controllers which consist of the high-speed control part (order of a few hundred nanoseconds) and the low-speed control part (order of a few milliseconds). The high-speed part consists of field programmable gate arrays (FPGAs) and memory modules on the VME crate. Since the memory modules need to memorize the steering/log data including the rescans, each memory module has a memory area for 22 million spots. On the other hand, the low-speed part, including the system monitoring unit and the RSF controller, consists of the programmable logic controllers (PLCs) and their I/O modules. This part controls and monitors the components having slow response, such as the RSF, the HV for monitors, and the monitor gas. The control system of the high-speed part has two VME crates controller 1 and 2. The main task of controller 1 is to perform the scanning irradiation process excluding the monitoring, and that of controller 2 is to monitor the scanning process. Controller 1 counts the digitized beam signals from the main flux monitor, and realizes the scanning process, i.e. controls the currents of the scanning magnets, the beam ON/OFF, the beam intensity (beam current level) and the RSF setting in accordance with the steering file. Further, the setting values returned from these devices or controllers are stored in the memory modules on controller 1. On the other hand, controller 2 monitors the scanning process by using the beam position monitor and sub flux monitor. The beam position is compared with the predicted one just before each spot transition. The tolerance of this comparison is typically set to 2 mm. The signal from the sub flux monitor is used to ensure the correct operation of the main flux monitor. Furthermore, the beam current level is checked every 8 ms while ±20% is allowed fluctuation of the beam level. The beam position and counts of sub flux monitor for each spot are stored in the memory modules on controller 2. The KO controller [11] is used to control the RF-knockout (RF-KO) electrode in the synchrotron ring and to deliver the beam with required current level while keeping its uniform time structure.

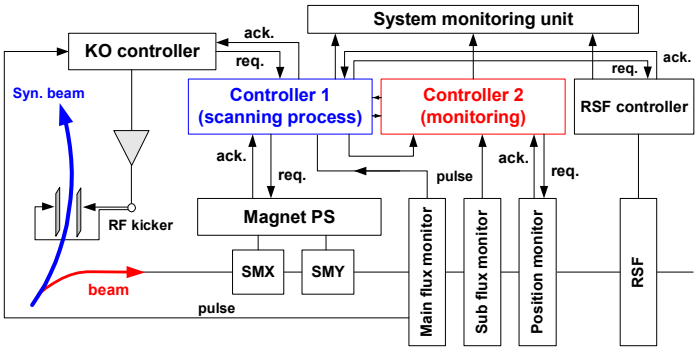

Fig. 2. Schematic of the scanning control system.

2.3. Fast scanning magnets and their power supply

The scanning magnets are designed to achieve the beam-scanning velocities of 100 and 50 mm/ms even in the maximum rigidity of 6.62 Tm. The maximum magnetic field of both magnets is designed to be less than 0.3 T to decrease the eddy current and the iron losses. In addition, the silicon-steel lamination thickness of 0.35 mm is employed. Consequently, a fast scanning magnet velocity faster than 100 mm/ms is realized. To avoid eddy current losses due to fast ramping of the field, the vacuum duct at the magnet region is made of FRP. For the power supply, 4 IGBT units and 18 FET units are employed, and separated functionally. The IGBT units are used to change the current quickly, and the FET units are used to keep the current constant by PID feedback control. The fast control of the IGBT is the most important part of this power supply to suppress over/undershoot of the current just after the spot transition. The switching timing precision of around 300 ns is necessary to suppress over/undershoot. The current overshoot just after the spot transition was successfully suppressed within 0.5 A corresponding to the beam-position shift of 0.2 mm with the 290 MeV/u beam. Consequently, FET units can control such over/undershoot within 100 μs. In addition, no delay of the field was observed by pickup coil measurements. The current ripple and drift less than ±0.2 A was also verified. In order to check the eddy current effect especially for the magnet edge, measurement of the temperature rise was carried out after continuous operation for 2 h. The temperature rise was not severe, even when operating at the maximum field and repetition rate.

2.4. Beam monitors

The flux monitors, which are parallel-plate ionization chambers, are set just after the exit of the vacuum window, and they are operated in air at atmospheric pressure. Each flux monitor consists of a signal foil (anode), two cathodes and two grounded shielding foils. For the cathodes, a wire mesh is employed to suppress the position dependence of the output signal. The wire used in the mesh is gold-coated tungsten (diameter: 50 μm) and it is set with the spacing of 1 mm. The signal foil is made of 25 μm-thick polyimide coated with Cu and Au. The gap between the anode and each cathode is 5 mm. The output current from the flux monitor is digitized by the current-frequency converter (maximum output frequency: 2 MHz). Frequency response of the amplifier is set to around 100kHz. To cover the dynamic range from $1\cdot 10^{7}$ to $1\cdot 10^{9}$ particles/s, this converter has three switchable ranges of 2MHz/100nA, 300nA and 1000nA.

The beam position and profile are measured with a multi wire proportional chamber (MWPC), which is set just after the main and sub flux monitors. While the anode wire spacing is 2 mm, this MWPC has 120 anode wires for x and y planes, respectively. Anode-cathode distance is set at 3 mm to avoid any gain drops due to the space charge effect. The electronics consists of I/V amplifiers and a digital control unit. The I/V amplifiers, which have the amplification rate of $2\cdot 10^{6}$ V/A, are directly connected to the monitor head. The output signals of the I/V amplifiers are fed into the 12 bit analog-digital converters (ADCs), which operate with the frequency of 200 kHz. By using these digital data, this digital unit handles two different tasks: 1) calculation of beam center and 2) production of the 2D fluence map for each slice.

2.5. Ridge filter and range shifter

It is necessary to slightly broaden the Bragg peak of the pristine beam to produce a “mini peak” by using a mini ridge filter (RGF) [12]. The RGF are designed to make Gaussian shaped mini peaks of 3 mm width at 1-sigma. Since the effective area of the RGF is required to be 240×240 mm^2, the RGF consists of 160 bar ridges made of aluminum with 1.5 mm spacing. The distance between the RGF and the isocenter is set to be 1 m. The range shifter (RSF) is used to precisely change the range slice-by-slice in the target. The entrance and exit of the RSF are 0.9 and 0.6 m upstream from the isocenter, respectively. The RSF consists of ten PMMA plates. Each plate has a thickness of 0.2 to 102.4 mm with an effective area of 240×240 mm^2. Thus, this binary type RSF can shift the range up to 237 mm in water equivalent length.

3. Commissioning of the scanning system

3.1. Stability check of non-scanned beam

In the 3D pencil beam scanning irradiation, the stability of the pencil beam, i.e. non-scanned beam, is very important issue to assure the scanned field quality. The slowly extracted beam from the synchrotron, needs to be stable in position, size and spill. Therefore, the measurement of the beam profile during 50s extraction with the extended flattop operation was carried out to test the stability of both beam size and position. The measurement was carried out by using the fluorescent screen with CCD camera system [13] set at the isocenter. As a result, it was verified that both the position and size during the extended flattop operation are well stabilized within ±0.5 mm. On the other hand, the spill stability was also tested by using the ionization chamber measurement, in which the commissioning of the RF-knockout control was performed [11]. Further, the beam ON/OFF response and its repeatability were verified. Typical results are shown in Fig. 3.

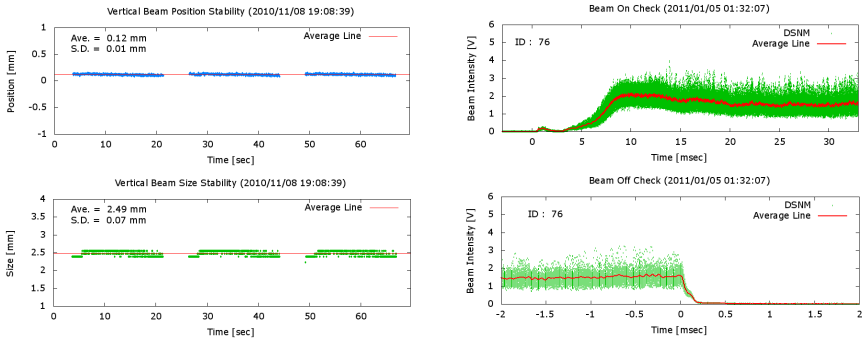

Fig. 3. Typical result of beam position and size stability measurement (left), and stability of beam on/off (right).

3.2. Accuracy of scanned beam position

Since the scanned beam position is directly affects the delivered dose distribution, the verification and the calibration of the conversion between the position and the scanning magnet current setting should be carefully performed. Thus, this verification was carried out by two different measurements: 1) film and 2) fluorescent screen with CCD camera system [14]. In order to check the effect of hysteresis and its correction, three different scanning amplitudes, ±120, ±80, and ±40 mm, were tested. Typical results are shown in Figure 4. In both measurements, the result show the accuracy of ±0.3mm at 2-sigma.

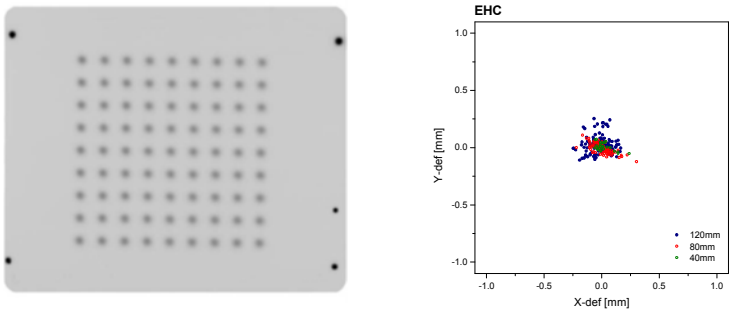

Fig. 4. Result of beam position measurement, left: film measurement, right: scatter plot of the deviation between preset position and measured one.

3.3. Commissioning of beam monitors

The position dependence of the main flux monitor and the scanning control was tested by using 2D uniform field irradiation. By applying the same count for regular grid spots, 2D uniform irradiation was carried out. The uniformity of the delivered field was measured by using the 2D ionization-chamber array (2D-ARRAY xdr, PTW Freiburg) and the film. Figure 5 shows results of 2D uniformity measurement by the film. We see a uniform field

distribution, indicating the main flux monitor has rather small position dependence. In both measurements, the standard deviation of the measured dose was around 1%. From these results, we concluded the position dependent calibration of the flux monitor is not necessary. Output linearity of the flux monitor was also checked by changing applied count in 2D uniform field delivery. The delivered dose was measured by reference ionization chamber of PTW30013 having sensitive volume of 0.6 cc. As shown in Fig. 5, the deviation from the linear relationship was less than 1%. The measurement of the recombination was also carried out. Although the typical beam intensity was 1-2· 10^8 particles/s, the severe recombination was not observed up to 6· 10^8 particles/s. The verification of the beam position monitor output was carried out by comparing the film dosimetry. In this test, the film was attached onto the beam position monitor and irradiated with the irradiation pattern similar with Fig. 4. The measured position differences between the monitor output and the film were less than 0.5 mm. Thus, the position monitor output can be used for position monitoring with the tolerance of 2 mm. On the other hand, the position output is used for online display of the beam scanning process. Figure 6 shows the typical view of position monitor console.

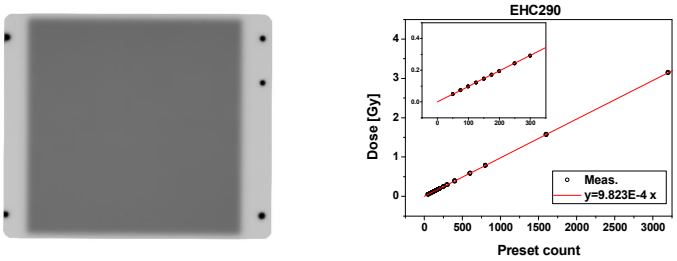

Fig. 5. Typical result of flux monitor commissioning, left: position dependence measurement by film, right: output linearity measurement.

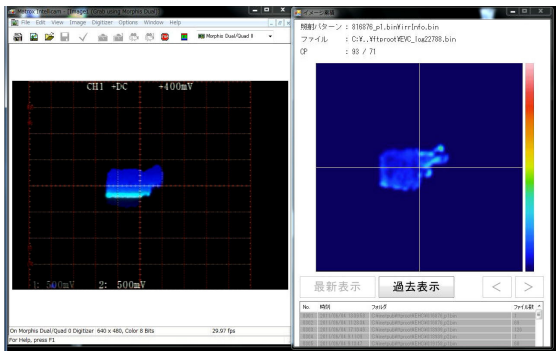

Fig. 6. Online display of position monitor measurement, left: online display of beam position, right: measured fluence map for each iso-energy slice.

3.4. Check of intensity modulation in 2D delivery

Overall verification of the scanned beam can be realized by checking the 2D delivery with intensity modulation. The checking irradiation pattern introduced by Flanz [15] was employed and measured by using the fluorescent screen with CCD camera system [14]. As shown in Fig. 7, we can see the 2D irradiation with the intensity modulation was successfully performed. Since the measured distribution was good agreement with the expected one, we can conclude that the beam control is correctly operating.

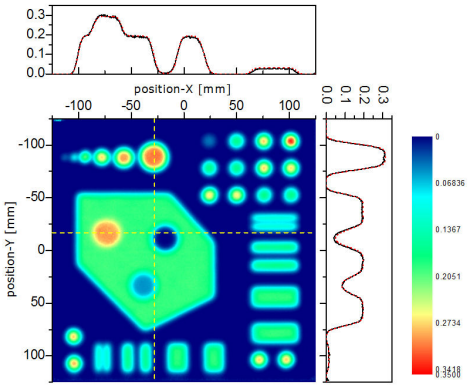

Fig. 7. Measured distribution in 2D intensity modulation. Red dotted line shows the prediction.

3.5. Three dimensional scanning beam delivery

As the basic performance of the system was verified, we moved to the next step which was the 3D irradiation test and its verification. Prior to the 3D irradiation test, it is necessary to prepare the data for a planning calculation [16-18], because the measured beam property is employed in the calculation. To acquire the data for the planning calculation, the following measurements were carried out for these energies: 1) integral depth dose distribution of pencil beam, 2) lateral dose distribution of pencil beam, and 3) measurement for characterization of large-angle scattered particles [17]. The measurements of 1) and 2) were carried out by using a cylinder-type water column with ionization chambers, which are a large area parallel-plate ionization chamber and a 94 channel cross-shaped monitor (pixel ionization chamber) with a spatial resolution of 2 mm. The measurement of 3) was carried out to obtain the parameters describing the multi-Gaussian form of the pencil beam in the planning calculation, in which the central-axis dose for the various sizes of frame-like field was measured [17]. By introducing this model to the planning calculation, the field-size effect due to large-scattered particles can be successfully corrected [17]. With the results of the measurements on 1), 2) and 3), we performed the 3D irradiation test cooperating with our planning software.

For verification of the 3D delivery and the planning software, various plans were tested. The MU calibration procedure, introduced by Jäkel et al [19], was employed. Typical results of the 3D dose conformation test are described as follows. Box-shaped targets with different SOBP thickness were planned to generate a uniform physical-dose field of 1 Gy. Figure 7 shows the dose distributions measured by an ionization chamber set in the water tank. These results were in good agreement with the planned values at various penetration depths. The uniformity was less than ±3%. Further, the reproducibility of the delivered dose within ±0.5% was also verified in these 3D delivery tests.

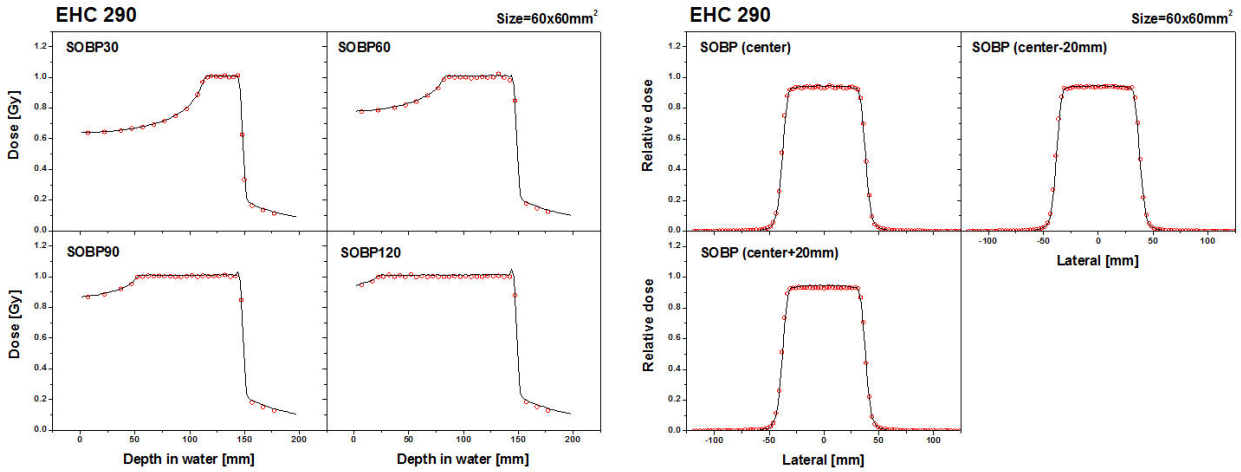

Fig. 8. Comparison between measured and planned dose distribution.

4. Future prospects

4.1. Multiple energy operation

In this stage, the range shifter plates are used for the depth scanning, with 4 steps of the initial energy. To enable the energy variation during the irradiation, and to decrease the range shifter usage, the preparation of multiple-energy operation [9] is in progress. As a first step of the multiple-energy operation, 11 steps of energy variation is under tested as shown in Fig. 9. Even with 11 steps of energy variation, the lateral penumbra will be significantly improved [20], because the maximum thickness of range shifter plates will be suppressed less than 30 mm. The 11 steps energy variation will be routinely used from 2012. After that, we will start the commissioning of more than 150 energy steps.

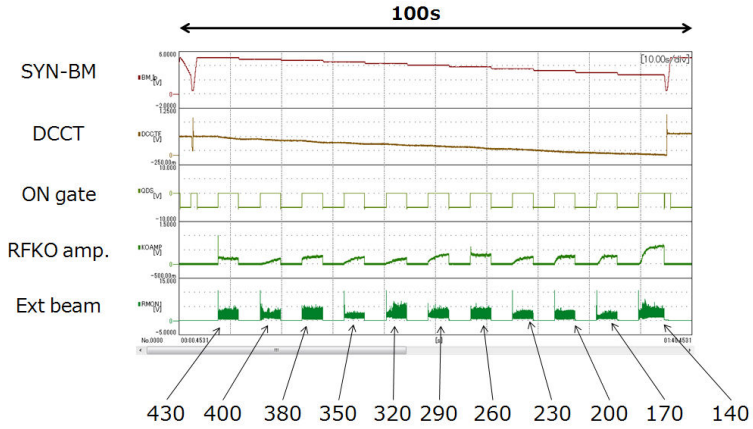

Fig. 9. Oscilloscope display in the beam test of multiple-energy operation.

4.2. Moving target irradiation with fast rescanning

A simulation and experimental study of moving target irradiation with fast rescanning and gating were performed [10]. By adjusting the beam current level to realize matching between the irradiation time and the motion cycle, as a result of 2D simulated and experimental irradiations, it was found that the rescanning method made it possible to realize the blurred distribution similar to the passive delivery. The experimental result for 3D delivery demonstrated a difference of less than 2% compared with the static case based on the pinpoint chamber measurements. Further tests and commissioning will be performed during 2012. After such preclinical tests, the treatment of the moving organ will be started.

5. Summary

The NIRS scanning system was installed into the new facility for further development of the carbon therapy in NIRS. To realize the rescanning for the moving target, we made strong efforts regarding: 1) the fast scanning magnet and its power supply; 2) the high-speed control system; and 3) the beam monitoring. After intense commissioning and quality assurance tests, the treatment with scanned ion beam was started in May 2011. On the other hand, few developments are continued to improve the performance of the system.

References

［1］ Kanai T, Kawachi K, Matsuzawa H, et al. Three-dimensional beam scanning for proton therapy. Nucl Instrum Methods Phys Res. 1983;214:491-496.

［2］ Haberer Th, Becher W, Schardt D, et al. Magnetic scanning system for heavy ion therapy. Nucl Instrum Methods Phys Res A. 1993;330:296-305.
［3］ Pedroni E, Bacher R, Blattmann H, et al. The 200 MeV proton therapy project at PSI: Conceptual design and practical realization. Med Phys. 1995;22:37-53.
［4］ Hirao Y, Ogawa H, Yamada S, et al. Heavy ion synchrotron for medical use–HIMAC project at NIRS-Japan. Nucl Phys A. 1992;538, 541c–550c.
［5］ Shirai T, Furukawa T, Inaniwa T, et al. Recent progress of new cancer therapy facility at HIMAC. Proc of International Particle Accelerator Conference. 2011:3604-3606.
［6］ Rietzel E, Bert C. Respiratory motion management in particle therapy. Med Phys. 2010;37:449–460.
［7］ Furukawa T, Inaniwa T, Sato S, et al. Design study of a raster scanning system for moving target irradiation in heavy-ion therapy. Med Phys. 2007;34:1085-1097.
［8］ Furukawa T, Inaniwa T, Sato S, et al. Performance of NIRS scanning system for heavy-ion radiotherapy. Med Phys. 2010;37:5672-5682.
［9］ Iwata Y, Kadowaki T, Uchiyama H, et al. Multiple-energy operation with extended flattops at HIMAC. Nucl Instrum Methods Phys Res A. 2010;624:33-38.
［10］ Furukawa T, Inaniwa T, Sato S, et al. Moving target irradiation with fast rescanning and gating in particle therapy. Med Phys. 2010;37:4874-4879.
［11］ Mizushima K, Furukawa T, Shirai T, et al. The HIMAC beam intensity control system for heavy ion scanning. Proc of International Particle Accelerator Conference. 2011:3592-3594.
［12］ Weber U, Kraft G. Design and construction of a ripple filter for a smooth depth dose distribution in conformal particle therapy. Phys Med Biol. 1999;44:2765-2775.
［13］ Takeshita E, Furukawa T, Iwata Y, et al. Semi-nondestructive monitoring system for high-energy beam transport line at HIMAC. Proc of International Particle Accelerator Conference. 2010:3218-3220.
［14］ Takeshita E, Furukawa T, Inaniwa T, et al. A fluorescent screen + CCD system for quality assurance of therapeutic scanned ion beams. Nucl Instrum Mehods Phys Res B. in press.
［15］ Flanz J. Quality assurance accelerator and beam delivery. Educational workshop of PTCOG49.
［16］ Inaniwa T, Furukawa T, Tomitani T, et al. Optimization for fast-scanning irradiation in particle therapy. Med Phys. 2007;34:3302-3311.
［17］ Inaniwa T, Furukawa T, Nagano A, et al. Field-size effect of physical dose in carbon-ion scanning using range shifter plates. Med Phys. 2009;36:2889–2897.
［18］ Inaniwa T, Furukawa T, Tomitani T, et al. Development of treatment planning for scanning irradiation at HIMAC. Nucl Instrum Methods Phys Res B. 2008;266:2194-2198
［19］ Jäkel O, Hartmann GH, Karger CP, et al. A calibration procedure for beam monitors in a scanned beam of heavy charged particles. Med Phys. 2004;31:1009–1013.
［20］ Inaniwa T, Furukawa T, Kanematsu N. Evaluation of hybrid depth scanning for carbon-ion radiotherapy. Med Phys. submitted.

TPS for NIRS Scanning: Present Status and Future Prospects

Taku Inaniwa, Takuji Furukawa, Shinji Sato, Nobuyuki Kanematsu, Naruhiro Matsufuji, Shinichiro Mori, Eri Takeshita, Takeshi Himukai and Koji Noda

Research Center for Charged Particle Therapy, National Institute of Radiological Sciences, Chiba, Japan
Corresponding Author: Taku Inaniwa, e-mail address:taku@nirs.go.jp

Abstract

In order to use an intensity-controlled raster scan method at the new particle-therapy research facility in HIMAC, we have developed a software program dedicated to the planning of radiotherapy with a scanned ^{12}C beam. Inverse planning techniques are implemented in the software in order to obtain uniform biological dose distribution within the target as well as to reduce the dose delivered to the organs at risk. The scan trajectory is determined so that the path length will be minimized by applying a fast simulated annealing algorithm for scan trajectory optimisation. The dose delivered along the scan trajectory during the beam transition time from one spot to the next spot is integrated into the inverse planning to shorten the treatment time. The lateral dose distribution of the scanned carbon beam is expressed by a sum of three Gaussians in order to account for the dose reduction observed in the irradiation of a small target volume. The code also copes with the planning for intensity modulated ion therapy. The reliability of the software has been confirmed through irradiation experiments at HIMAC.

1. Introduction

A project to construct a new particle-therapy research facility as an extension of the existing Heavy-Ion Medical Accelerator in Chiba (HIMAC) has been initiated for further development of carbon-ion therapy at the National Institute of Radiological Sciences (NIRS). The facility will be equipped with three treatment rooms, two of which will provide the horizontal and vertical fixed beam ports, and another one a rotating gantry [1]. In all rooms, three-dimensional (3D) irradiation with pencil beam scanning will be used in order to make full use of the advantages of heavy-ion therapy such as the high dose concentration and high relative biological effectiveness (RBE) around the Bragg peak. This method has already been implemented for clinical use at the Paul Scherrer Institute (PSI) with protons [2] and the Gesellschaft für Schwerionenforschung mbH (GSI) with carbon ions [3]. Recently, it has also been used at the Heidelberg Ion Therapy Center (HIT) with carbon ions [4]. In these facilities, only patients with static tumors, e.g., tumors in the head and neck or in the spinal cord, have been treated. In the new particle-therapy research facility, we intend to treat not only static tumors, but also movable tumors by using gated irradiation and re-scanning methods [5]. Faster scanning methods will be key to completing the treatment irradiation within a few minutes. The range shifter plates will be used in the new facility because of their capability to change the beam range within a few hundred milliseconds. The effect of the additional beam spread and the increase of the projectile fragments due to the insertion of the range shifter plates have to be included in the dose response function of the scanned beam in the treatment planning. To address the problems pertaining to the developmental flexibly and to allow for the irradiation of movable tumors, we developed a treatment planning software program for carbon-ion scanning which is suitable for the unique scanning system designed at NIRS. This paper describes the basic principles of this software program.

2. Materials and Methods

2.1 Beam Model

In 3D irradiation with pencil beam scanning, the prescribed dose distribution is realized by superimposing the dose of the individual pencil beams *d* according to their optimized weights *w*. The Bragg peak of the pristine beam is slightly broadened to produce a "mini peak" by the ridge filter, and is used as a pencil beam. In the new facility, pristine beams with 11 different energies will be prepared between 140 MeV/u and 430 MeV/u. The dose distribution at (x_i, y_i, z_i) delivered by the pencil beam stopped at (x_0, y_0, z_0) can be represented as follows:

$$d(x_i, y_i, z_i; x_0, y_0, z_0) = D_1(x_i; x_0, y_i; y_0, \sigma_1(z_i; z_0))d_z(z_i; z_0). \quad (1)$$

Here, $d_z(z_i; z_0)$ is the planner-integrated dose at a depth of z_i, while $D_1(x_i; x_0, y_i; y_0, \sigma_1(z_i; z_0))$ is the two dimensional normalized Gaussian functions with standard deviations $\sigma_1(z_i; z_0)$ representing the beam spread at a depth z_i. The planner-integrated dose $d_z(z_i; z_0)$ and the lateral beam spread, i.e., $\sigma_1(z_i; z_0)$, were determined from the measured dose distribution with a large area parallel plate ionization chamber and a profile monitor, respectively. Then these measured data are fitted to simple formulae and incorporated into the planning software as shown in Figure 1. With this algorithm, the effect of the beam spread due to multiple scattering in the range shifter can be incorporated, at least for the primary particles. However, our recent research revealed that the dose delivered to the target is reduced according to the field-size in carbon ion scanning with range shifter plates [6]. The observed dose reduction is referred to as the 'field-size effect of dose' in this paper. In order to account for this effect, we adopted three-Gaussian forms of lateral dose distributions for the pencil beam model used in the treatment planning software. In this case, equation (1) can be rewritten as follows:

$$d(x_i, y_i, z_i; x_0, y_0, z_0) = d_z(z_i; t) \times$$
$$\left\{\left(1 - \sum_{j=2}^{3} f_j(z_i; t)\right) D_1(x_i; x_0, y_i; y_0, \sigma_1(z_i; t)) + \sum_{j=2}^{3}\left(f_j(z_i; t) D_j(x_i; x_0, y_i; y_0, \sigma_j(z_i; t))\right)\right\}, \quad (2)$$

where $f_j(z_i; t)$ is the fraction of integrated dose assigned to the *j*-th Gaussian component at a depth z_i delivered by the pencil beam with the range shifter plate of thickness *t*, and $D_j(x_i; x_0, y_i; y_0, \sigma_j(z_i; t))$ is a two dimensional Gaussian function describing the lateral spread of the *j*-th component at a depth of z_i with the standard deviation $\sigma_j(z_i; t)$. The parameters $\sigma_j(z_i; t)$ and $f_j(z_i; t)$ are experimentally determined and registered as the pencil beam parameters in the software. The lateral dose profile expressed with the three-Gaussian beam model is schematically shown in Figure 2, along with that of the single-Gaussian beam model. This allows for the option of using the three-Gaussian beam model in the dose optimization. The observed field-size effect of doses can be accounted for with this beam model. However, it is time-consuming to implement the three-Gaussian beam model in the iterative dose optimization. The 'predicted-dose scaling factor' is usually used as an alternative approach to account for the field-size effect of the doses [6].

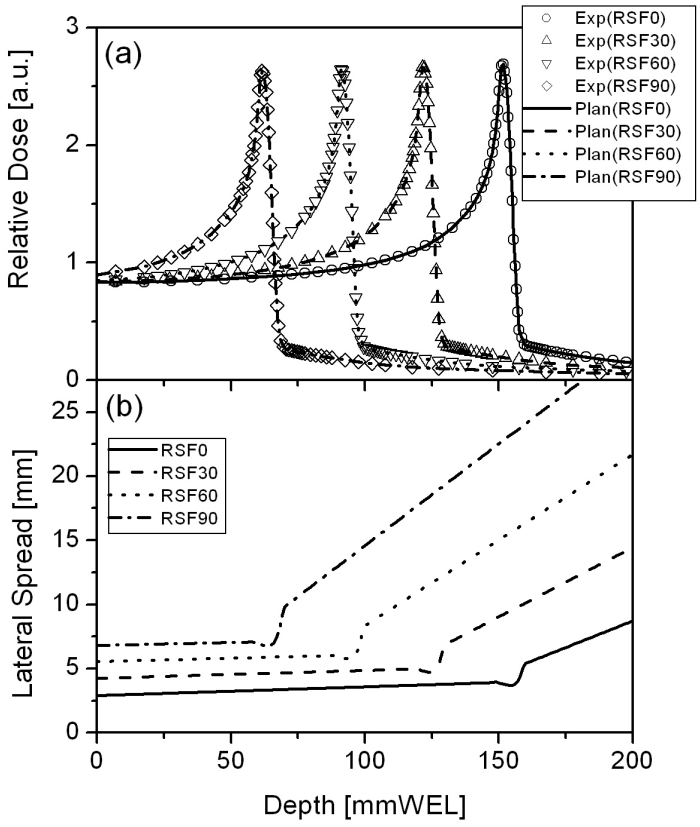

Figure 1. Pencil beam data for a 290-MeV/u carbon beam used by the treatment planning software. (a) Planner-integrated dose distribution d_z and (b) lateral beam spread σ_1 as a function of depth z_i for a range shifter of 0 (solid line), 30 (dashed line), 60 (dotted line) and 90 (dash-dotted line) mm water equivalent thicknesses.

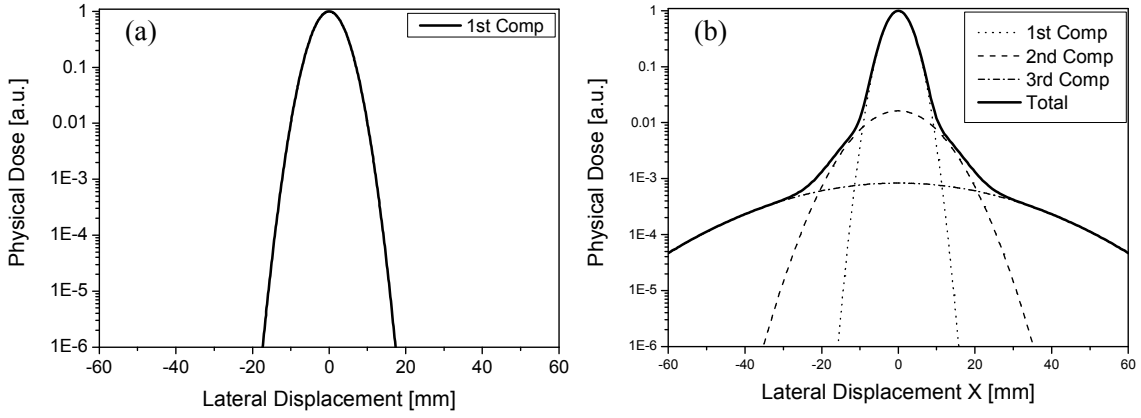

Figure 2. Schematics of the lateral dose distribution expressed by (a) a single-Gaussian beam model and (b) a three-Gaussian beam model.

2.2 Dose Optimization

The goal of dose optimisation in the treatment planning is to find the best particle numbers (weight) for each pencil beam, i.e. the best weighting matrix, so that the resulting dose distribution is as close as possible to the prescribed dose distribution within the target volume and does not exceed the dose restrictions within the organs at risk. When determining the weighting matrix, the dose-based objective function $f(w)$ is minimized through an iterative optimisation process. The objective function can be described as;

$$f(w)=\sum_{i\in \mathrm{T}}\left(Q_{\mathrm{P}}^{\mathrm{o}}\left[D_{biol,i}(w)+U_i-D_{\mathrm{P}}^{\max}\right]_+^2+Q_{\mathrm{P}}^{\mathrm{u}}\left[D_{\mathrm{P}}^{\min}+U_i-D_{biol,i}(w)\right]_+^2\right)+\sum_{i\in \mathrm{O}}Q_{\mathrm{O}}\left[D_{biol,i}(w)+U_i-D_{\mathrm{O}}^{\max}\right]_+^2 \quad (3)$$

where $D_{biol,i}(w)$, $D_{\mathrm{P}}^{\max}$, $D_{\mathrm{P}}^{\min}$, $Q_{\mathrm{P}}^{\mathrm{o}}$, $Q_{\mathrm{P}}^{\mathrm{u}}$, $D_{\mathrm{O}}^{\max}$, Q_{O} is the biological dose at a point i obtained with matrix w, the maximum and minimum doses applied to the target T, the penalties for over- and underdosage specified for the target, the maximum dose allowed for the OAR and the penalty for overdosage in OAR, respectively. In raster scanning irradiation, the beam delivery is not switched off during the transition time from one spot to the next. Therefore, in this scheme, the extra dose is inevitably delivered to the sites between two successive spots during the beam spot transition, along the scan trajectory. The contribution of the extra dose is included in the dose optimization by adding the term U_i to the objective function representing the amount of the extra dose delivered to a voxel i [7]. For the dose optimization, we used a gradient-based algorithm with the quasi-Newton method.

2.3 Flow of treatment planning

By using the developed software, the treatment plans are produced according to the flowchart shown in Figure 3. Each task in the flowchart is briefly explained below.

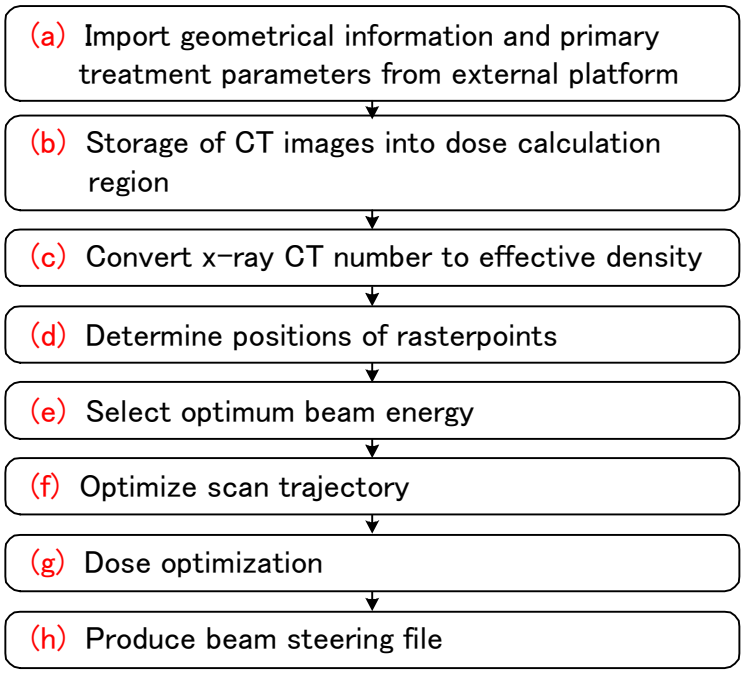

Figure 3: Flowchart of the treatment planning.

(a) Radio-oncologists delineate the PTV and OARs on the clinical CT images using an external platform, and determine the primary treatment parameters, e.g. isocenter, desired dose level, irradiation method (single field or IMIT), number of ports, and beam directions, based on the information about the position and type of tumor as

well as critical structures. The isocenter in the CT coordinates coincides with the origin of the raster scanner system. The scanner step size in the lateral and orthogonal directions, Δx and Δy, and step size of range shifter plate, Δz, are also determined at this stage. The CT images, geometrical information determined by the radio-oncologists and the primary treatment parameters are imported from the platform to the software program.

(b) The CT images are stored in the segmented region for dose calculation by using the tri-linear interpolation. The voxel size is determined taking both the precision and time required for the dose optimization into account. The voxels within the PTV and OARs are identified with different flags.

(c) The x-ray CT number stored in each voxel is converted to the stopping powers relative to the stopping power of water using a conversion table created based on the polybinary tissue model [8].

(d) The Bragg peaks are placed automatically by the software to account for the cold doses in the peripheral region of the PTV due to the finite size of the mini peak and beam width. In this step, the maximum range of the pencil beam is determined among all pencil beams placed within the PTV.

(e) From the maximum range determined in (d), the optimum beam energy is selected from 11 individual energies available from the HIMAC synchrotron.

(f) In the raster-scan method, the region of the raster-point was divided into slices of equal ion ranges. The beam scanning begins at the distal slice (highest energy) and laterally covers each slice on a discrete *x*-*y* grid, until the most proximal slice (lowest energy) is reached. In order to minimize the extra dose in raster scanning [7] and shorten the treatment time, we determined the scan trajectory on each slice so that the path-length would be minimized by applying a fast simulated annealing algorithm to scan trajectory optimization [9].

(g) The particle numbers (weight) for each raster-point are determined by the dose optimization method described in 2.2.

(h) Finally, the beam steering file is produced in which the position of the raster-point x_0, y_0, z_0, corresponding thickness of the range shifter plates *t*, and the particle numbers (weights) of all pencil beams are written in following the order of the optimized scan trajectory.

3. Results and Discussions

3.1 Correction of the field-size effect with the predicted-dose scaling factor

In order to account for the field-size effect of the doses, we tested the 'predicted-dose scaling factor'. Here, the physical dose distribution of 1 Gy was planned for the cylindrical target volume of 100 mm in diameter and 60 mm in spread-out Bragg-peak (SOBP) using the single-Gaussian beam model for the dose optimization. The dose distribution was recalculated with the three-Gaussian beam model only at the end of the optimization, and the 'predicted-dose scaling factor' was derived as a ratio of the averaged dose within the target volume for optimized dose distribution to that for the recalculated dose. The derived factor of 1.013 in the present case was multiplied with the spot-weights tabulated in the beam steering file. The irradiation experiments were carried out according to the derived beam steering file using the carbon-ion scanning system developed at HIMAC [10]. In Figure 4, the measured physical dose distribution along the beam axis is shown with the calculated distribution using the three-Gaussian beam model. Our calculation could reproduce the measured distribution within an inherent accuracy from point to point of less than 2%, including the errors pertaining to the irradiation and measurements. This result shows that the field-size effect of the physical doses can be corrected with a single 'predicted-dose scaling factor' derived by the three-Gaussian beam model.

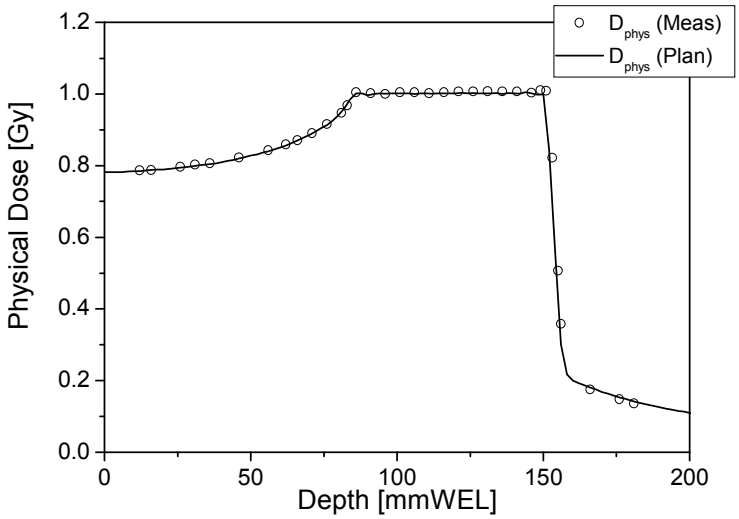

Figure 4. The measured physical dose distribution along the beam axis for the cylindrical target volumes of 100 mm in diameter and 60 mm in SOBP (open circles) are compared with the calculated distribution using the three-Gaussian form of the pencil beam model.

3.2 Treatment planning for patient data

In order to investigate the clinical applicability of the developed software program, treatment plans were produced based on data of a patient treated at HIMAC. As an example, a patient having a rectal tumor was selected (Figure 5(a)). The clinical dose of 4.6 GyE would be delivered from a single port in the anterior to posterior direction. In this plan, only the target volume is specified on the CT images and implemented for dose optimization. The size of the dose calculation voxel was set to $2 \times 2 \times 2$ mm^3, while the scanner step sizes and step size of range shifter plate were all set to 3.0 mm. The beam energy was determined to be 290 MeV/u, and the total number of pencil beams was 15659. In Figure 5(a), the planned biological dose distribution is shown with color-wash display on axial, sagittal and frontal CT images. To verify the treatment plan, we recalculated the physical dose distribution on a water phantom according to the produced beam steering file (Figure 5(b)). Then, the irradiation experiment was performed according to the same beam steering file. In the experiment, we use the verification system that consisted of a water phantom and 24 small thimble ionization chambers (PTW31015) connected to two 12 channels electrometers (Multidos, PTW) [11]. The positions of the ionization chambers within the water phantom are identified with open circles in Figure 5(b). The measured physical doses with the ionization chambers were compared with the recalculated ones in Figure 6. The error bars indicate the possible maximum and minimum doses caused by the setup errors of the mounting of the 24 ionization chambers. Here, we assumed the setup errors of ±0.5 mm, ±1.0 mm and ±1.5 mm in the lateral, orthogonal and beam directions as extreme cases, respectively. The deviations between the measured and the planned doses were less than 6% for all ionization chambers. These experimental results show the reliability of our treatment planning software, as well as the beam delivery system, for carbon-ion scanning developed at HIMAC [10].

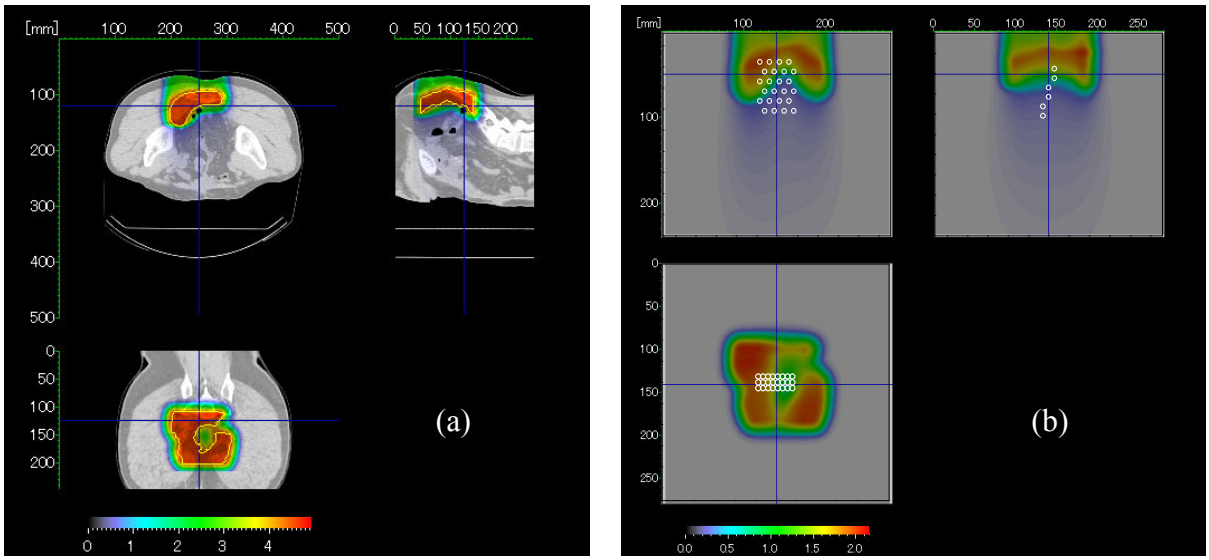

Figure 5. (a) Color wash display of clinical dose distribution for a patient with a rectal tumor. The yellow line encompassed the target volume. (b) The physical dose distribution recalculated on a water phantom. Positions of the 24 ionization chambers are indicated with open white circles.

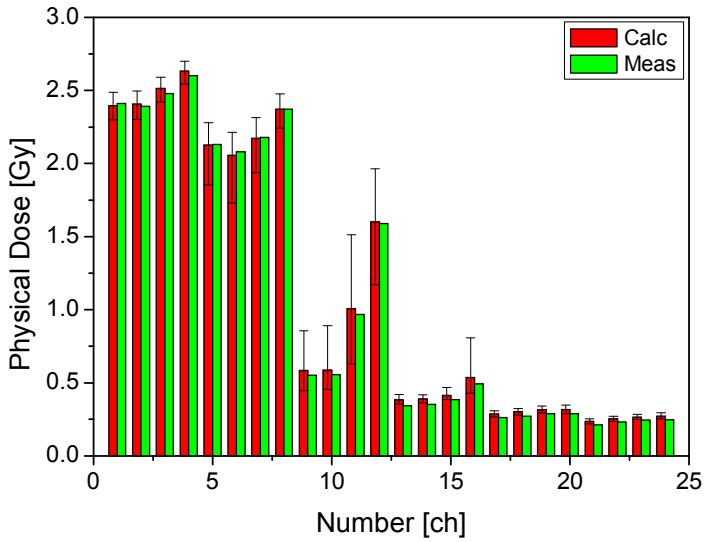

Figure 6. The comparison of dose values recalculated by the treatment planning software (red bars) and the dose values measured with the 24 ionization chambers (green bars) at the positions indicated with open circles in Figure 5(b).

4. Conclusions

We have developed a treatment planning software program dedicated to carbon-ion scanning. In the software, the lateral dose distribution of the scanned carbon beam is expressed by a single Gaussian or a sum of three Gaussians. By using the predicted-dose scaling factor derived with these two beam models, the field size effect of the physical doses could be corrected effectively. The maximum deviation between the measured and planned physical doses was less than 2% in the whole target region. The clinical applicability of the new

software program was tested based on the patient with a rectal tumor treated at HIMAC. The verification measurements were performed with the produced beam steering file. The good agreement between the measured and calculated doses shows the reliability of the treatment planning software program, in addition to that of the beam delivery system, for carbon-ion scanning developed at HIMAC.

References

［1］ Noda K, Furukawa T, Fujisawa T, et al. New accelerator facility for carbon-ion cancer-therapy. J Radiat Res. 2007; 48: Suppl. A43-A54.

［2］ Pedroni E, Bacher R, Blattmann H, et al. The 200 MeV proton therapy project at PSI: Conceptual design and practical realization. Med Phys. 1995;22:37-53.

［3］ Kraft G. Tumortherapy with ion beams. Nucl Instrum Methods Phys Res A. 2000;454:1-10.

［4］ Combs S E, Jäkel O, Haberer T and Debus J. Particle therapy at the Heidelberg Ion Therapy Center (HIT) – Integrated research-driven university-hospital-based radiation oncology service in Heidelberg, Germany. Radiat. Oncol. 2010; 95: 41-44.

［5］ Furukawa T, Inaniwa T, Sato S, et al. Design study of a raster scanning system with phase-controled rescanning toward conformal irradiation of moving target in heavy-ion radiotherapy. Med Phys. 2007;34:1085-1097.

［6］ Inaniwa T, Furukawa T, Nagano A, et al. Field-size effect of physical doses in carbon-ion scanning using range shifter plates. Med. Phys. 2009; 36: 2889-2897.

［7］ Inaniwa T, Furukawa T, Tomitani T, Sato S, Noda K, Kanai T, Optimization for fast-scanning irradiation in particle therapy. Med Phys. 2007;34:3302-3311.

［8］ Kanematsu N, Matsufuji N, Kohno R, Minohara S, Kanai T. A CT calibration method based on the polybinary tissue model for radiotherapy treatment planning. Phys Med Biol. 2003;48:1053-1064.

［9］ Kang J H, Wilkens J J, Oelfke U, Demonstration of scan path optimization in proton therapy. Med Phys. 2007;34:3457-3464.

［10］ Furukawa T, Inaniwa T, Sato S, et al. Performance of NIRS fast scanning system for heavy-ion radiotherapy Med. Phys. Submitted

［11］ Karger C P, Jäkel O and Hartmann G H. A system for three-dimensional dosimetric verification of treatment plans in intensity-modulated radiotherapy with heavy ions. Med. Phys. 1999; 26: 2125-2132

Multi-dimensional Image Guided Particle Therapy

Shinichiro Mori, PhD , Motoki Kumagai, PhD, Yuka, Matsuzaki, PhD, Taku Inaniwa, PhD,
Takuji Furukawa, PhD, Yuka Takei, Toshiyuki Shirai, PhD, Takeshi Murakami, PhD, Koji Noda, PhD.

Research Center for Charged Particle Therapy, National Institute of Radiological Sciences, Chiba, Japan
Corresponding Author: Shinichiro Mori, e-mail address: shinshin@nirs.go.jp

Abstract

Purpose: Organ movement due to respiration may change the run of a charged particle beam that can result in degradation of dose conformation to the target. We introduced our approaches to quantitatively assessing potential problems in treatment planning due to organ movement by using four-dimensional images.

Methods and Materials: Several tens of inpatients with lung, pancreas or liver cancer underwent 4DCT acquisition under free breathing conditions. For lung cancer cases, fluoroscopic images were acquired after 4DCT images. The patient respiratory signal was obtained by an external respiratory sensing monitor. For the 4DCT study, gross tumor volume (GTV) and normal tissues were contoured on the CT data set and the intrafractional motion was calculated. For the DFPD study, target motion was calculated by marker-less template matching and compared with the external respiratory signal.

Results: 4DCT images obtained improved the evaluation of tumor displacement without 4DCT artifacts that were observed using the conventional MSCT. The images were of sufficient quality to calculate particle dose distribution for scanning irradiation for target movement. The correlation between the external and internal intrafractional motions were slightly degraded.

Conclusions: It is necessary to capture intrafractional motion in both treatment planning and irradiation stages. By doing this, we can provide increased treatment accuracy.

Introduction

Worldwide, more than 28 particle treatment centers were operating in 2008, including three carbon ion beam centers, and the construction of new centers is set to continue. Compared with photon beams, charged particle beams provide superior dose conformation, and minimization of excessive dosing to normal tissues. These strengths are due to the characteristic increase in energy deposition of particle beams with penetration depth (proton and carbon ion beams) up to a sharp maximum at the end of the range (Bragg peak).

Organ motion due to respiration has been investigated using a variety of methods, including fluoroscopy, ultrasound (US), MRI, CT and PET, in the lung, liver, pancreas, kidney, and prostate sites. An understanding of motion characteristics in radiotherapy planning is useful for determining internal margins and optimizing beam parameters (beam angle, etc.), because the degradation of image quality due to respiratory motion affects radiotherapy planning and delivery of the treatment beam. We used fast rotating cone-beam CT, which employs approximately 13-cm wide cylindrical 2D detector system built into the frame of a conventional 16 multi-slice CT (Aquilion, Toshiba Medical Systems)(1), to evaluate organ motion. Within this scan range, the 4DCT obtains volumetric cine CT data without resorting to the respiratory phase. Motion artifacts due to breathing were frozen by a temporal resolution of 250 ms, allowing the tumor shape to be evaluated accurately. Moreover, thinner slice thickness and a shorter total acquisition time helped determine target margins without 4DCT artifacts. Organ movement due to respiration may change the run of a charged particle beam that can result in degradation of

dose conformation to the target. Moreover, treatment planning accounts for organ motion to avoid dose variation. Therefore, although the treatment beam sometimes misses due to movement of the target, better imaging will allow for better treatment accuracy. We herein introduce our approaches to capture images of a moving target and quantitatively assessing the potential problems in treatment planning due to organ movement.

Organ/target motion

We quantified organ and target motion due to respiration in the pancreas, liver and lung sites as a function of time using the 4DCT and DFPD. In the NIRS, patients receiving thoracic and abdominal treatments undergo carbon ion beam treatment with a custom-made immobilization device to improve patient positional reproducibility throughout the treatment course. To more accurately simulate typical clinical conditions, the same immobilization techniques were used during this study.

Geometrical variation was greater around the pancreas tail than the pancreas body and head regions. The average pancreas head, body and tail displacement in the inferior direction for the ungated phase was 8.3 mm, 9.6 mm and 13.4 mm, respectively, which was minimized in the gated phase to 2.8 mm, 2.8 mm and 3.6 mm, respectively. For all six patients with pancreatic cancer, the average pancreas COM displacement relative to that at peak exhalation was mainly in the inferior direction, at 9.6 mm for the ungated phase and 2.3 mm for the gated phase (2).

With regard to the liver site (irradiation administered with patients in the prone position), after the 1st 4DCT were done, the patient couch was moved to the adjacent position to cover the entire liver. As a result, an approximately 25cm longitudinal scan range could be acquired. Geometrical changes due to respiration were quantified by a deformable registration between the reference and respective respiratory phases. The magnitude of the intrafractional displacement was increased close to the inhalation phase, with both AP and SI movement around the diaphragm. However, around the middle abdominal region, the movement was almost SI. Another visualization technique is the intrafractional motion curve shown in Figure 1. These visualizations were useful to understand the rich information provided in the 4DCT, and were useful for optimizing treatment planning. The GTV-COM displacement average in 10 patients was 0.3mm (max: 1.8mm) in the left side, 2.2mm (max: 5.3mm) in the right side, 4.6mm (max: 10.8mm) in the anterior side, 0.1mm (max: 0.3 mm) in the posterior side, and 11.6 mm (max: 17.4mm) in the inferior side. No displacement was observed on the superior side.

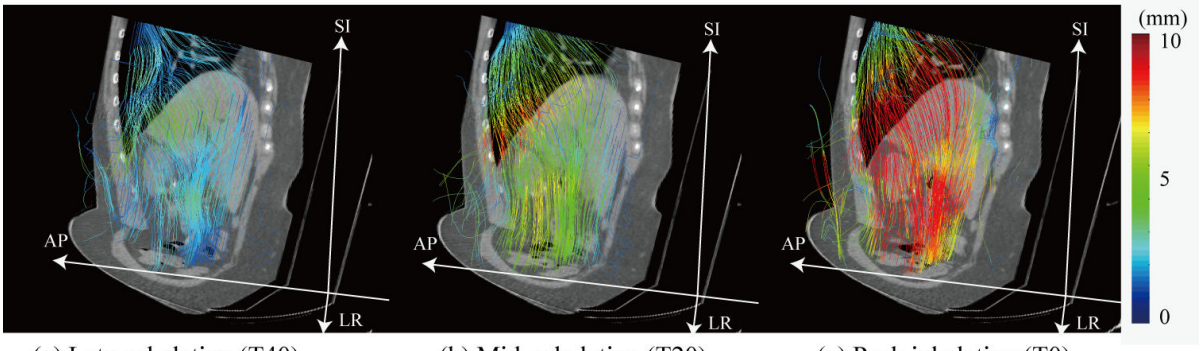

(a) Late exhalation (T40) (b) Mid-exhalation (T20) (c) Peak inhalation (T0)

Figure 1. Intrafractional motion curves overlaid on the CT images in oblique view. These curves represent the magnitude of displacement and motion direction from peak exhalation (T50) to respective phases (Tn).

A total of 14 lung cancer patients participated in the 4DCT immobilization study (supine position only). Volumetric cine imaging of the lungs showed continuous movement of the tumor in the axial and sagittal sections. The average GTV-COM displacement relative to that at peak exhalation was 1.4 mm (range 0.5-2.3

mm) in the left-right, 2.2 mm (range 0.8-4.7 mm) in the anterior-posterior, and 6.6 mm (range 1.6-21.8 mm) in the superior-inferior direction.

Some limitations to irradiating a moving target warrant further discussion. While tumor movement as a result of respiratory motion is now well understood, little attention has been paid to movement due to bowel gas movement. Gas bubble movement is due to two physiological processes, respiration and peristalsis. Since the charged particle beam stopping position is strongly dependent on the radiological pathlength from the patient surface, replacing dense tissue with a low-density material such as bowel gas changes the radiological pathlength significantly, resulting in a perturbation in the beam stopping position from that originally planned. Quantitative analysis of dose variation due to bowel gas movement in the treatment course is a more challenging task in charged particle therapy than photon therapy.

Although the human respiratory cycle is not strictly regular, and generally varies in amplitude and period from one cycle to the next, for this study we assumed that the patient respiratory cycle, pattern and tumor position were reproducible throughout the course of treatment. Current treatment planning uses a single respiratory cycle only because the inclusion of respiratory patterns during irradiation cannot be accounted for. Respiratory pattern variations can be considered in treatment planning via the acquisition of 4DCT data for multiple respiratory cycles before treatment, although consideration needs to be given to the very high patient dose this entails. Several approaches to this problem are available. The first is to include respiratory pattern variations in treatment planning via the use of margins, etc. The second is real-time monitoring of target position using either an external marker or internal monitoring system. Owing to the imperfect reproducibility of the respiratory cycle, this relatively extended treatment period may result in inconsistencies between respiratory phase as determined using an external marker on the diaphragm and the movement of the internal anatomy. Thanks to its high temporal resolution and reproducibility of setup position, fluoroscopy is currently the better choice.

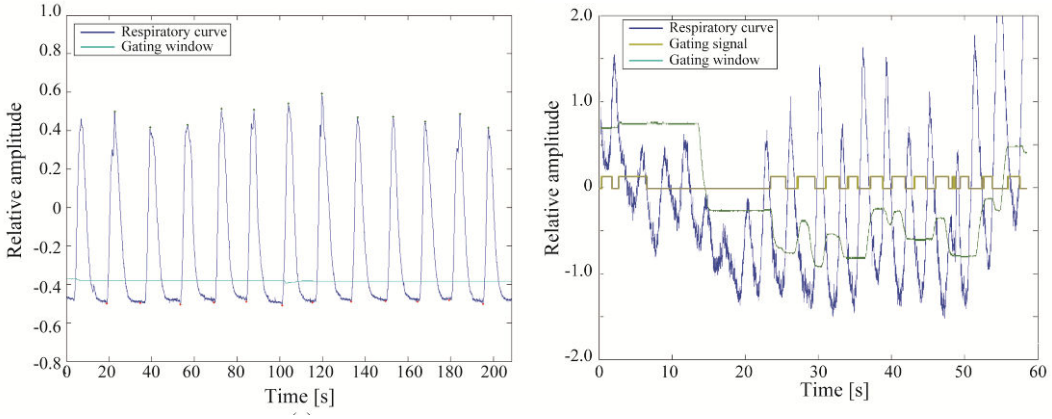

(a) (b)

Figure 2. Respiratory signal obtained using an external respiratory sensing monitor (blue line) and gating threshold (light green). (a) Regular breathing pattern. (b) Irregular breathing pattern.

Real time tracking

However, although external systems facilitate the measurement of patient surface position as a function of time, and are in fact in routine use at several treatment centers, they do not provide internal target position. Rather, this can be obtained using 4DCT data and the respiratory signal during 4DCT acquisition. Owing to the imperfect reproducibility of the respiratory cycle, this relatively extended treatment period may result in inconsistencies between respiratory phase as determined using an external marker on the diaphragm and the movement of the internal anatomy. The problem, however, is that neither provides insights into how variable patients' breathing is during the few minutes of treatment. Current 4DCT scans acquire only a single respiratory

cycle, so that, as a result, the patient's respiratory cycle and tumor position are not reproducible for all respiratory activity during treatment. Fluoroscopic images using DFPD were acquired for lung cancer patients from a 45 degree oblique view. To minimize the skin dose, 6 s fluoroscopy with 15fps was repeated 8 times with an acquisition interval time of 12s, thus resulting in a total image acquisition time and study time of 48 s and 180s, respectively (Figure 3). Respiratory signals were obtained by an external respiratory sensing system. The target position was captured by using a multi-template matching method as follows: First, ten template images were binned using the first respiratory cycle images (= 90 images). A bonding box sufficient to cover the target region was set on the template images. The target positions in the respective phase were calculated by using template images. The gating threshold was defined as 20% of the amplitude of the reference cycle (fist respiratory cycle) and the external respiratory signal is shown in Figure 3.

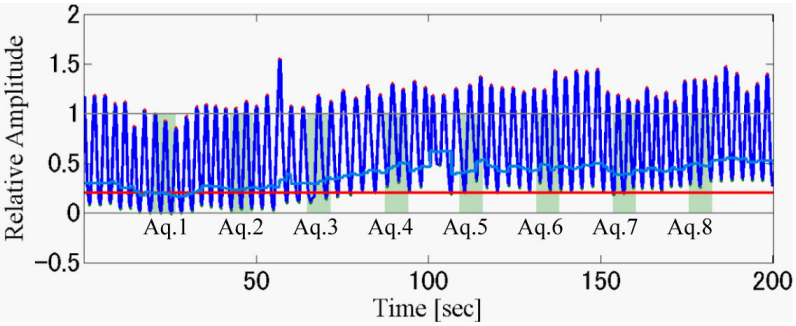

Figure 3. Respiratory signal obtained by the external respiratory sensing monitor (blue line). Red and light blue lines show the 20% gating threshold of the reference respiratory cycle and that of respective cycles. The green square region shows the DFPD image acquisition time. Red and light blue lines were gating threshold of 20% amplitude defined in a referenced cycle and for each cycle, respectively.

DFPD images with the calculated bonding box are shown in Figure 4. The tumor was small, and not clearly observed on the images. Tumor displacement was almost entirely in the SI direction. Quantitative results in SI and AP displacement are summarized in Figure . With regard to SI motion, the external respiratory signal and internal target position were well correlated in the 1st DFPD acquisition. These correlations, however, were degraded after 3rd acquisition. For AP motion, the external and internal correlation was not good for any of thel DFPD acquisition series, and the internal tumor position fluctuated because the tumor was close to the left atrium. As a result, the tumor position was also affected by the patient's heartbeat. In this patient, the SI motion determined by 4DCT was approximately 7 mm in a single respiratory cycle, however, that obtained by fluoroscopy was 17.5mm during a 180 s study time.

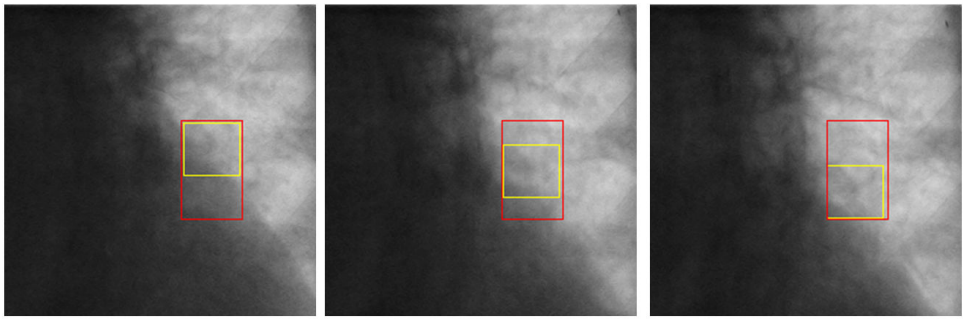

Figure 4. DFPD lung image as a function of respiratory phase. The yellow and red squares show the calculation region and the bounding box of calculation regions.

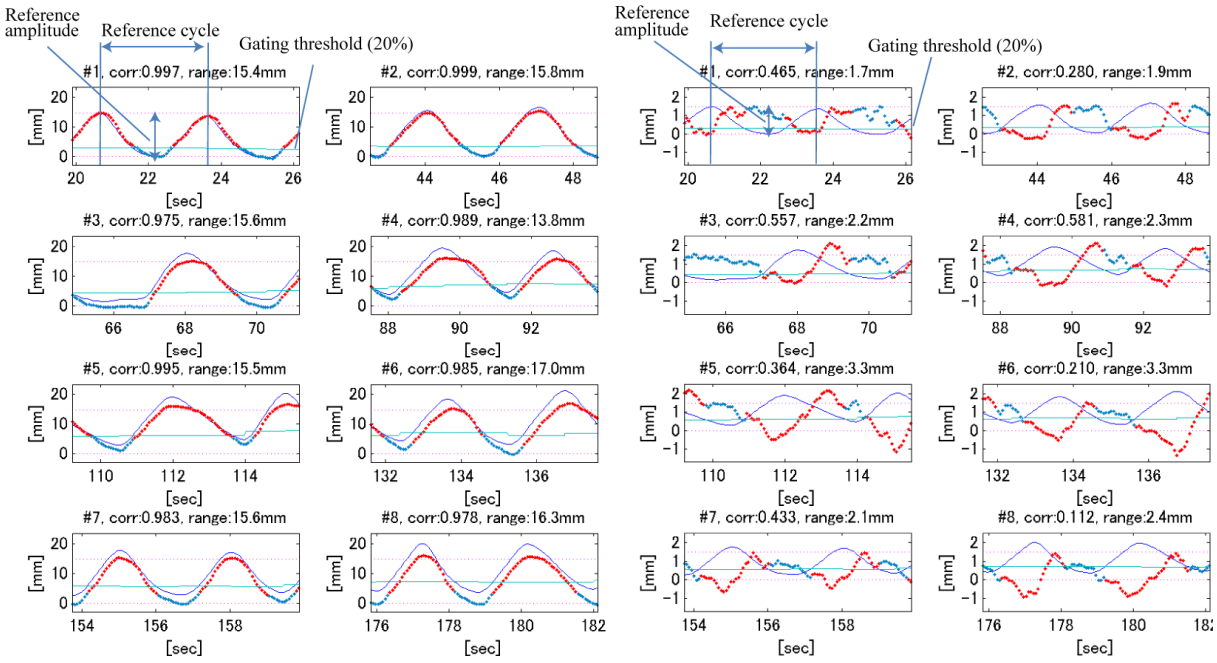

(a) SI motion (b) AP motion

Figure 5. The relationship between external respiratory signal (solid blue line) and tumor displacement obtained by DFPD images (dotted red/blue lines). (a) SI motion. (b) AP motion. The light blue solid line shows the gating threshold (20% of the external respiratory signal in each cycle). The tumor position during the gating window is shown by a dotted blue line.

Patient positional verification

Conventional patient positioning (patient setup) is commonly performed by use of a tattoo on the patient's skin for correct setup of the patient. Recently, several treatment centers have started using a laser marker on the treatment room wall or on the x-ray imaging system. However, patient positioning takes several minutes to complete, and adjustment of the rotational component of the coordinate transformation (yaw, pitch, roll) is more difficult than that for coordinate transformation (left-right, anterior-posterior, and superior-inferior). A more recently introduced patient positional system uses the 2D-3D image registration technique with a combination of 2D imaging, such as portal images, and volumetric CT data used for treatment planning, and it calculates patient positioning errors between the treatment and planning stages. Current CPUs have four or fewer cores in a single integrated circuit, limiting the performance of multithreading computation. An alternative approach, however, is to use a GPU (graphic processing unit) as a parallel computational architecture in place of the CPU. We were able to improve the patient positioning system by including a GPU-based auto-registration function programmed in C++ and CUDA (NVIDIA Corporation, CA, USA). The GPU-based version (NVIDIA TESLA C2050 board (NVIDIA Corporation, CA, USA) gives a 50-fold faster calculation time than the CPU-based software program (2.0 GHz single quad-core CPU Intel Xeon processor, 4 GB physical memory)(3). As a result, auto registration could be finished in less than 30s, with 0.3 mm and 0.2deg geometrical accuracy (Figure 6). This shorter calculation time can help decrease patient positional changes during the setup procedure. Moreover, the high geometrical accuracy could improve dose conformation to the target.

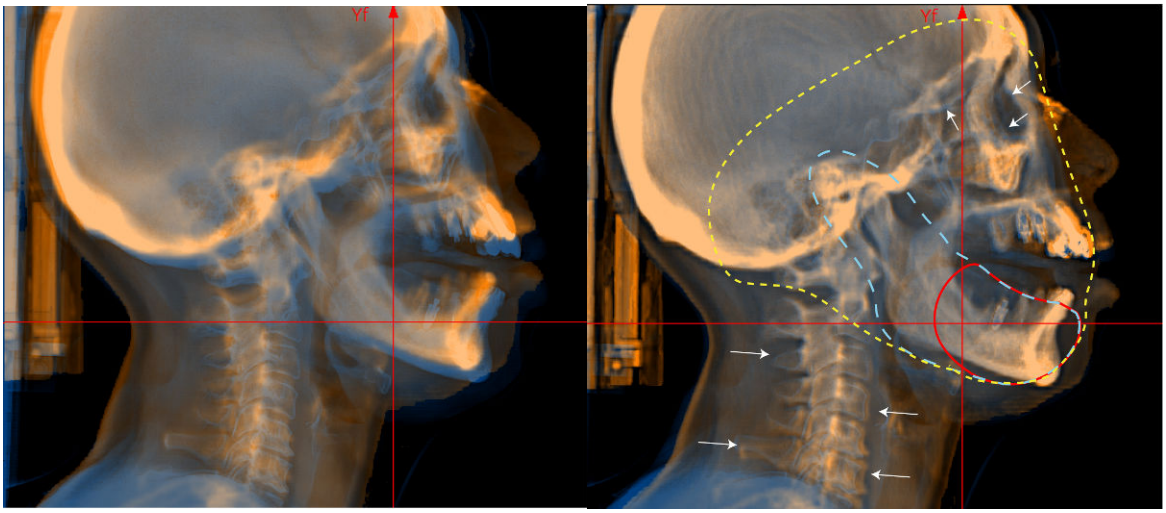

(a) (b)

Figure 6. FPD images (blue layer) overlaid on DRR images (orange layer) (a) before registration and (b) after registration. White arrows marked in lower panels are positional errors which differ from the referenced DRR images. Yellow and blue dotted lines and the reference solid line show large, middle and small ROI regions. Registration parameters were a computation gird of 2 mm, CT slice thickness of 2 mm, middle ROI, and image processing on.

Treatment workflow

Our center recently constructed a new treatment facility for carbon-ion beam scanning treatment as an extension of the existing treatment building (HIMAC: Heavy Ion Medical Accelerator in Chiba), which provides passive beam irradiation. The new treatment facility is designed to facilitate the integration of several devices with the overall goal of increasing treatment accuracy and improving treatment workflow in terms of their physical, technical and clinical aspects (Figure 7). Construction was started in February 2009 and completed in March 2010. Installation of treatment equipment was started in June 2010 and commissioning was completed in March 2011. The Tohoku earthquake (magnitude 9.0 M_w), one of the five most powerful earthquakes recorded since 1900, hit Japan on 11th March 2011, delaying the start of treatment until May 2011. The new facility is organized into three main systems, a Scanning Irradiation System (S-IR), a Treatment Planning System (TPS), and a Patient Handling System (PTH). The PTH covers a wide range of functions, including imaging, geometrical/position accuracy including motion management, layout of the treatment room, and treatment workflow. Because currently available software does not always handle workflow events flexibly, we focused on designing the treatment workflow to be suitable for use with any treatment situation, such as cancelation during irradiation or actual simulation etc., and the restarting of treatment processes.

(a) (b)

Figure 7 (a) Simulation room. (b) Treatment room

Conclusions

We introduced the NIRS approaches to a image guided particle study. It is necessary to capture intrafractional motion in both treatment planning and irradiation stages in order to provide better treatment accuracy. We are presently constructing a new treatment facility which will allow the provision of raster-scanning irradiation, including thoracic and abdominal regions (4). We are convinced, however, that our approach to moving targets in charged particle therapy will be a decisive factor in overcoming problems with treatment accuracy, and will be useful for improving treatment using the scanning irradiation method.

References

[1] Mori S, Endo M, Tsunoo T, *et al.* Physical performance evaluation of a 256-slice CT-scanner for four-dimensional imaging. *Med Phys* 2004;31:1348-1356.

[2] Mori S, Hara R, Yanagi T, *et al.* Four-dimensional measurement of intrafractional respiratory motion of pancreatic tumors using a 256 multi-slice CT scanner. *Radiother Oncol* 2009;92:231-237.

[3] Mori S, Kobayashi M, Kumagai M, *et al.* Development of a GPU-based multithreaded software application to calculate digitally reconstructed radiographs for radiotherapy. *Radiol Phys Technol* 2009;2:40-45.

[4] Noda K, Furukawa T, Fujisawa T, *et al.* New accelerator facility for carbon-ion cancer-therapy. *Journal of Radiation Research* 2007;48:A43-A54.

Modeling the Clinical and Biological Effect of Therapeutic Carbon Ion Beam

Naruhiro Matsufuji, Mami Wada, Yuki Kase*, Akiko Uzawa, Koichi Ando**

Research Center for Charged Particle Therapy, National Institute of Radiological Sciences, Chiba, Japan

* Proton Therapy Research Center, Shizuoka Cancer Center, Mishima, Japan

** Gunma University Heavy Ion Medical Center, Maebashi, Japan

Corresponding Author: Naruhiro Matsufuji, e-mail address: matufuji@nirs.go.jp

Abstract

A thorough understanding of the dose response is one of the keys for success in radiation therapy. Due to the relatively short history and increased fraction size resulting from hypofractionation by superior dose localization, verification of the appropriateness of the available dose response models for carbon ion radiotherapy is needed. In this study, the applicability of three dose response models, including the LQ, MT and RCR models was investigated for the endpoints of *in-vivo* mouse skin reaction and the clinical local control rate of non-small cell lung cancer with the carbon beam. We found that the RCR model is the most appropriate for determining the *in-vivo* skin reaction among the three models; however, the classical LQ model still gives the best reproducibility of the clinical results. The understanding of the difference between *in-vivo* and clinical data, as well as the uniqueness of single irradiation, is indispensable for establishing the optimum dose and technique for administering carbon ion radiotherapy in the future.

Introduction

The ability to administer hypofractionated irradiation is one of the advantages of carbon ions for cancer therapy realized by superior dose localization as a result of the fact that energy loss toward the range end can be elevated, and associated with increased biological effectiveness. At HIMAC (Heavy Ion Medical Accelerator in Chiba), the efficacy of hypofractionation has been investigated in most tumor sites, and ultimately, one-day irradiation has been tried against NSCLC (non-small cell lung cancer) [1].

Due to its simplicity and sufficient precision in conventional radiotherapy modality, the LQ (linear-quadratic) model has been preferred for estimating the biological or clinical response to radiation. In hypofractionated radiotherapy; however, the absorbed dose given to the tumor is far beyond the range where the LQ model has been experimentally verified. The RCR (Repairable-Conditionally Repairable) model recently proposed by Lind et al. of the Karolinska Institutet is expected to be applicable for a wider dose range [2]. In addition, the MT (multi-target two components) model [3] developed from hit-target theory is regarded as yet another approach for estimating the dose response. In this study, these models were applied to estimate the *in-vivo* findings, as well as the clinical, response to carbon ions.

Methods and Materials

1. Materials

From a single dose up to 6 fractionated irradiation experiments have been conducted at the HIMAC BIO cave with carbon ions of various LETs (13.6, 28.4, 43.0, 58.0 keV/μm) and X-rays to mice [4]. The main endpoint of the current study was the incidence of grade 2 skin reactions, *i.e.*, a complete epilation with or without slight edema. To assess the clinical response, the local control rate of NSCLC derived through a dose escalation study with carbon ions at HIMAC [5] was used.

2. LQ model

The LQ model gives the probability of cell killing by two components, one dependent on the dose and the other on the square of the dose. The linear term with regard to the absorbed dose is explained as the probability of a DNA double strand break (DSB) by a single track, while the quadratic term, related to the dose, shows the probability of two independent tracks. The cell survival S_{LQ} after exposure to the fractional dose d is calculated as:

$$S_{LQ} = \exp(-\alpha d - \beta d^2) \tag{1}$$

When the LQ model is valid, a linear relationship is expected between the dose per fraction and the reciprocal total dose on the same biological endpoint by different fractionations as shown below.

$$E = n(\alpha d + \beta d^2) \tag{2}$$

$$1/nd = \alpha/E + (\beta/E)d \tag{3}$$

When plotting the isoeffective reciprocal total dose (1/nd) as a function of dose per fraction (d) as known as the Fe-plot [6], the ratio of the intercept (α/E) to the gradient (β/E) corresponds to the α/β value.

3. MT model

The cell survival is expressed using the equation below in the MT model.

$$S_{MT} = \exp(-Ad)[1 - \{\exp(-d/d_0)\}^m] \tag{4}$$

The first exponential term corresponds to the "ion kill", *i.e.*, irrepairable cell killing by a single hit to a single target expected in the core of the ion track, while the rest of the equation shows the probability of the "gamma kill", *i.e.*, repairable cell killing by a shingle hit to multiple targets.

4. RCR model

The RCR model also uses the exponential expression, but in a different form.

$$S_{RCR} = \exp(-ad) + bd\exp(-cd) \tag{5}$$

The first term indicates the probability of "unhit" and the second term corresponds to the probability of cell survival after repairing the resulting damage.

5. Tumor control probability (TCP)

The LQ, MT and RCR models are, in their basic form, used for the estimation of cell survival probability. By taking the number of clonogens in a tumor into this estimation of cell survival, the TCP (tumor control probability) can be estimated. The TCP of a tumor containing N clonogens in n fractionated irradiation is given as:

$$TCP = exp(-NS^n) \tag{6}$$

Here, it is stated that the distributions of the parameter values are needed for realistic TCP modeling [7]. In this study, Gaussian distribution was introduced to one of the parameters in each model for the sake of simplicity.

$$\mathrm{TCP}_{LQ} = \frac{1}{\sqrt{2\pi}\sigma}\int\left[exp\left(-\frac{(\alpha-\alpha_0)^2}{2\sigma_\alpha^2}\right)\times exp\left(-\mathrm{N}\{\exp(-\alpha d-\beta d^2)\}^n + 0.693\frac{T-T_k}{T_d}\right)\right]d\alpha \tag{7}$$

$$\mathrm{TCP}_{MT} = \frac{1}{\sqrt{2\pi}\sigma}\int\left[exp\left(-\frac{(A-A_0)^2}{2\sigma_A^2}\right)\times exp(-\mathrm{N}\{\exp(-\mathrm{Ad})[1-\{\exp(-d/d_0)\}^m]\}^n)\right]dA \tag{8}$$

$$\mathrm{TCP}_{\mathrm{RCR}} = \frac{1}{\sqrt{2\pi}\sigma}\int\left[\exp\left(-\frac{(c-c_0)^2}{2\sigma_c^2}\right)\times\exp(-\mathrm{N}\{\exp(-\mathrm{ad})+bd\exp(-cd)\}^n)\right]\mathrm{dc} \tag{9}$$

In the case of the LQ model, the distribution is convoluted into the parameter α as the α is dominant in a typical fractionation size. The effect of cell repopulation is also taken into account in the equation by the tumor doubling time T_d and the kickoff time of the proliferation T_k. This formalism of TCP was proposed by Webb and Nahum [8]. The distribution is attributed to the parameter *A* in the MT model as the "ion kill", to extent of which is expressed with this *A*, and is considered to be the leading term for the carbon ion irradiation. In the RCR model, the parameter *c* is assigned for the distribution by assuming that the repair capacity represented has patient-dependent variation.

6. Data analysis

As for the *in-vivo* case, at first, the α/β value of the mouse skin for 58 keV/μm was determined to be 13.0 by giving a linear fit to the data on the Fe-plot while omitting the data point of the single irradiation. Then, by assuming the β as 0.05, the isoeffect *E* is calculated with the eq. (2). Then, the parameters in each model (eqs. (1), (4) and (5)) was determined for each different LET irradiation result by least square fit in order to obtain the same isoeffect E. Finally, the isoeffective dose estimated by the models was plotted on the Fe-plot together with the experimental data.

In the case of clinical data analysis, the parameters in each model (eqs. (7), (8) and (9)) were determined by least-square fit to the observed local control rate of NSCLC with carbon ions in 18 fractions at HIMAC. Then, using the parameters, the TCP in hypofractionation from 9 fractions down to a single fraction was estimated and compared with the clinical observations. The calculation in this study was powered by the *Wolfram Mathematica* © version 7 software program.

Results and Discussion

1. Applicability of the models for *in-vivo* mouse skin reactions

Figure 1 shows the Fe-plot of the *in-vivo* mouse skin reactions together with the estimates provided by the models. The experimental results of the mouse skin reaction tests show a drop in the Fe-plot following a single dose of radiation. This drop is unique to carbon ion irradiation, and is not observed during X-ray irradiation. This

means that the LQ model shows a dissociation in the response between single and multiple irradiations with carbon ions.

On the other hand, MT and RCR models both succeeded in reproducing the drop following the single irradiation. The RCR model shows more favorable reproducibility than the MT model for high LET data. The LET dependency of the parameters in the RCR and MT models are shown in Fig. 2. The LET dependency of parameters used in the RCR model suggests that cluster-like, less repairable lesions are produced significantly by high LET irradiation. The LET dependency of the parameters in the MT model suggests that there is an increase in the "ion-kill" and the decrease in "gamma-kill" with the elevation of LET, as would be expected.

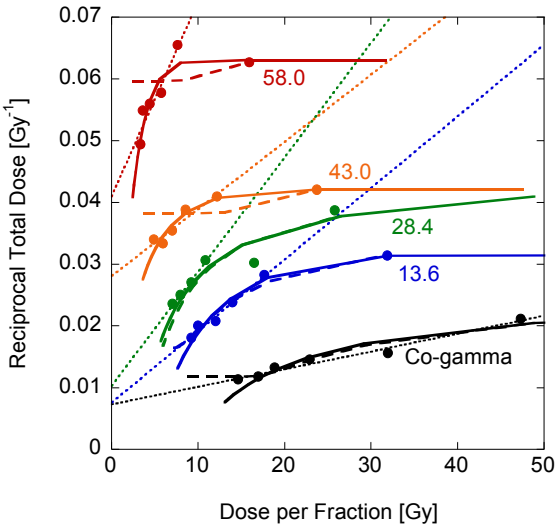

Fig.1. Fe-plot of the *in-vivo* mouse skin reaction. The numbers in the figure correspond to the LET value of the carbon beam. The estimation of LQ, MT and RCR models are shown with narrow dashed, thick dashed and thick solid lines, respectively.

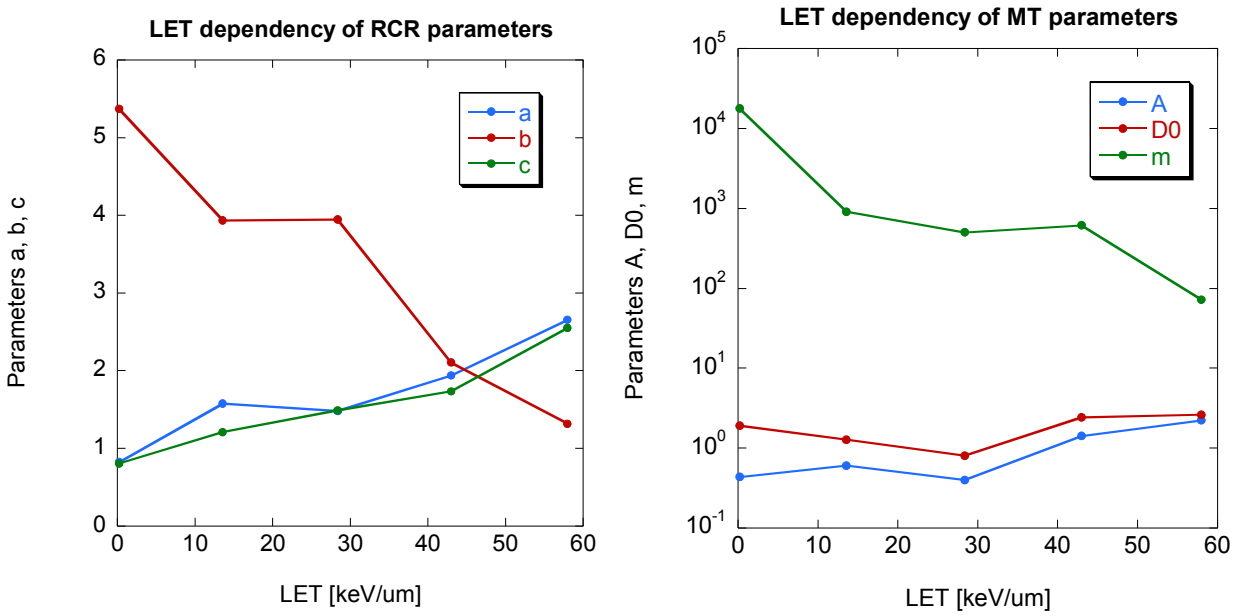

Fig.2. LET dependency of the parameters in the RCR model (left) and the MT model (right).

2. Applicability of the models for clinical data

Regarding their clinical application, all the three models succeeded in giving satisfactory fit to the local control rate for 18 fractionations, as shown in Fig. 3. The calculated parameters are summarized in Table 1. Interestingly, about 30% variation in sensitivity was found to give the best fit to the data.

The estimation of the hypofractionated clinical data is, however, not perfect (as shown in Fig. 4). The RCR model tends to underestimate the dose response in hypofractionation, while the MT model overestimates the response. The LQ model is, among the three models, the best, but is still not perfect. The disagreement between the models is found only on single irradiation. However, even in the case of a single irradiation, the 50% TCP level agrees to the clinical result. The dissociation at high TCP levels can be explained from the viewpoint of the TCP model, as there in an increase in the variation of radiosensitivity. It is necessary to investigate the reason for this unique increase in the variation in the case of single irradiation with the more detailed analysis of the clinical results.

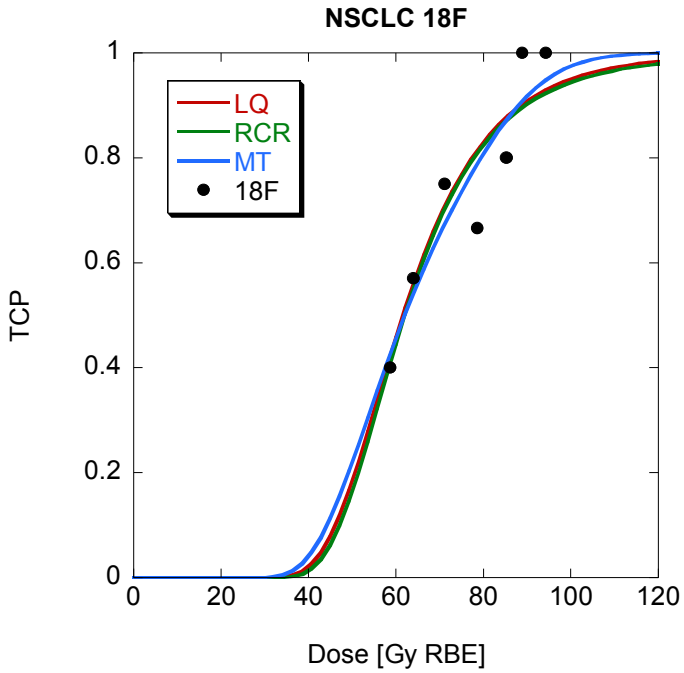

Fig. 3. TCP fitting by the LQ, RCR and MT models for the local control of NSCLC by 18 fractions

When considering the reason(s) for the contradiction in the applicability between the LQ and the MT or the RCR models between *in-vivo* and clinical data, the robustness of the parameters can play a role. The calculated parameters in the MT and the RCR models were highly sensitive to the initial value. This suggests that the obtained values are not in global, but in a local minimum. The applicability might be improved by finding the global minimum values; however, such oversensitivity makes the practical application of the MT and RCR models more difficult. The other possibility is that there are differences in the biological damage obtained during *in-vivo* and clinical data. While the clinical data is directly connected to the tumor cell killing, the damage from the *in-vivo* data is considered to be repairable. Further study is necessary in order to understand the mechanism behind the observed tendency toward differences in the *in-vivo* versus clinical data.

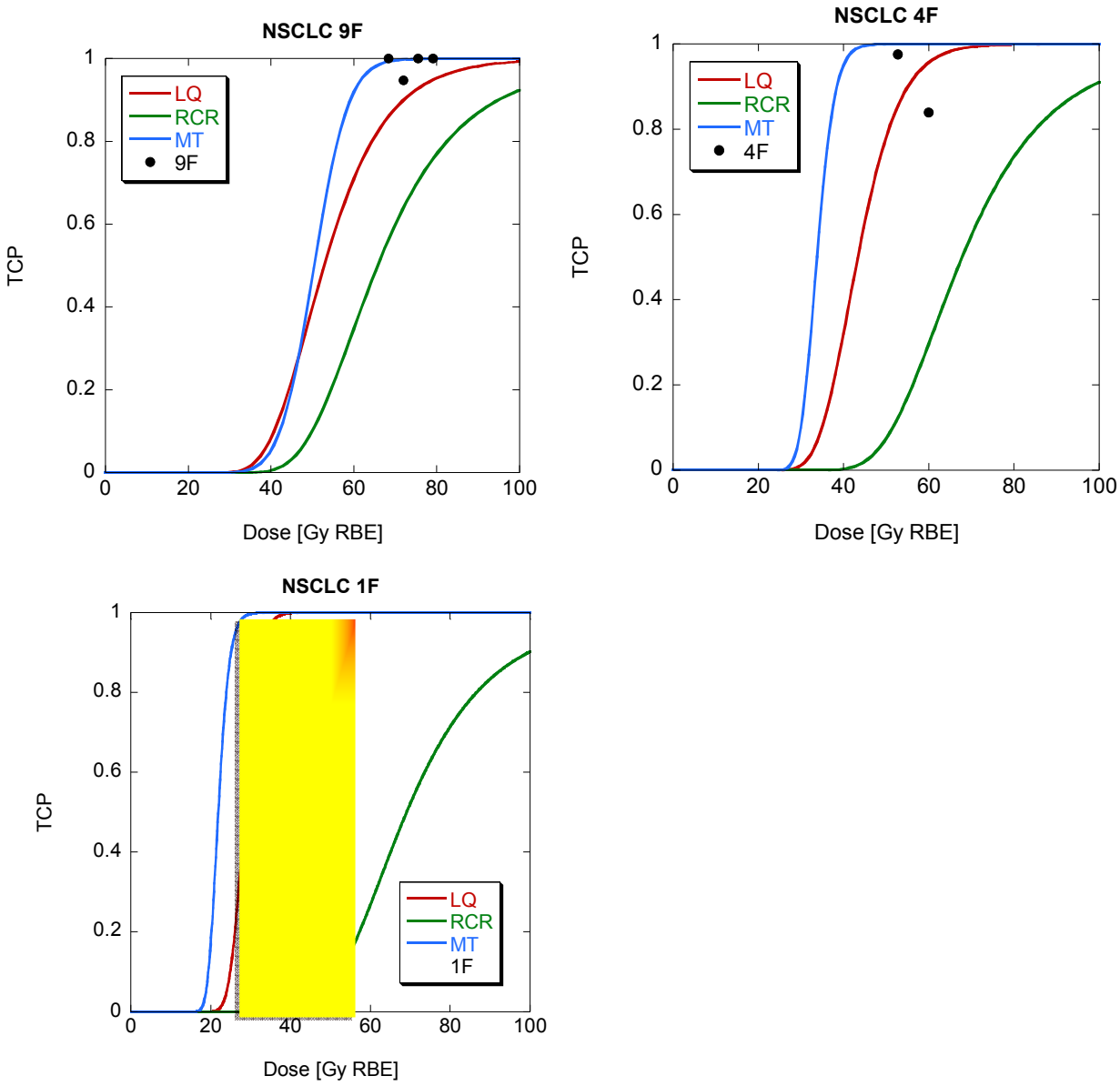

Fig. 4. TCP estimation of 9, 4 and single irradiations by the LQ, RCR and MT models with the parameters for the 18 fractions as summarized in Table 1. Due to the insufficient follow-up period, only the dose range is shown in the case of single irradiation.

Conclusions

The verification of the LQ, MT and RCR models has previously been tried using the cell survival response as an endpoint, and due to the experimental difficulties in the cell survival experiments, the dose range was limited to less than 10 Gy or 10^{-3} survival level. This aim of the present study was to verify the appropriateness of the models for the application of the dose prescribed in the practice of carbon ion radiotherapy. Regarding the fractionated *in-vivo* mouse skin reaction, while the LQ model failed to reproduce the experimental results of single irradiation by the carbon beam, the RCR model was found to be useful in the dose and fraction range used for the experiment. In contrast, for the clinical response, the LQ model was preferable to the other models. In both the *in-vivo* and clinical cases, further study is necessary, especially on the dose response following a single irradiation.

Table 1. Parameters in LQ, RCR and MT models for the fit to the local control of NSCLC in 18 fractions

Model	Variable		σ	Fitting parameters				Fixed parameters
LQ	α	0.865	0.268 (31.0%)					β=0.076, T_d=7, N=10^9
MT	A	0.816	0.248 (30.4%)	D_0	0.498	m	115.3	N=10^9
RCR	c	0.729	0.171 (23.5%)	A	6.317	b	0.880	N=10^9

References

［1］ Tsujii H, Kamada T, Baba M et al. Clinical advantages of carbon-ion radiotherapy. *New J. of Phys.* 2008;10:075009.

［2］ Lind B K, Persson L M, Edgren M R, Hedlöf I and Brahme A. Repairable-conditionally repairable damage model based on dual Poisson processes. *Rad. Res.* 2003;160:366-375.

［3］ Butts J J and Katz R. Theory of RBE for heavy ion bombardment of dry enzymes and viruses. *Rad. Res.* 1967; 30:855-871.

［4］ Uzawa R, Ando K, Koike S et al. Research on the tumor control effect and complications of therapeutic charged beam. *2008 Annual Report of the Research Project with Heavy Ions at NIRS-HIMAC*. 2009; 47-49.

［5］ Miyamoto T, Yamamoto N, Nishimura H, et al. Carbon ion radiotherapy for stage I non small cell lung cancer. *Radiother. Oncol.* 2003;66:127-140.

［6］ Douglas B G and Fowler J F. The Effect of Multiple Small Doses of X Rays on Skin Reactions in the Mouse and a Basic Interpretation. *Radiat. Res.* 1976;66:401-426.

［7］ Dasu A, Toma-Dasu I and Fowler J F. Should single or distributed parameters be used to explain the steepness of tumour control probability curves? *Phys. Med. Biol.* 2003;48:387-397.

［8］ Webb S and Nahum A E. A model for calculating tumour control probability n radiotherapy including the effect of inhomogeneous distributions of dose and clonogenic cell density. *Phys. Med. Biol.* 1993;38:653-666.

Imaging system for QI: Present status and future prospects

E. Testa[1*], D. Dauvergne[1], G. Dedes[1], N. Freud[2], J. Krimmer[1], J.M. Létang[2], V. Maxim[2], G. Montarou[3], C. Ray[1], M.-H. Richard[1], F.Roellinghoff[2]

[1]IPNL, Université de Lyon, F-69003 Lyon; Université Lyon 1 and IN2P3/CNRS, UMR 5822, F-69622 Villeurbanne, France ; [2]CREATIS, Université De Lyon, INSA-LYON, Villeurbanne, [3]LPC Clermont-Ferrand, IN2P3, Université Blaise Pascal, Clermont-Ferrand, France

[*] e-mail address:e.testa@ipnl.in2p3.fr

We present the ongoing studies aiming at providing a real-time control of the dose distribution during ion therapy. These studies are undertaken in the frame of the National and Rhône-Alpes Regional Research Programs for Hadontherapy. We aim at implementing combined modalities for real-time quality control of the deposited dose for future therapy centers. Several modalities are under development within this research program. Improvements on Positron Emission Tomography (PET) can be obtained by means of Time of Flight, using fast scintillators or resistive plate chambers, with dedicated readout and electronics. In-beam prompt gamma imaging systems are under developments. Recent measurements show that Time of Flight is necessary to properly discriminate gamma from neutrons and scattered particles. Prompt emission of light charged particles like protons is also discussed, and looks very promising according to feasibility simulations.

Introduction

The main distinctive characteristic of ion-therapy, as compared to conventional radiotherapy, is the highly non-uniform profile of dose deposition inside the irradiated body. The dose increases gradually along the ion path to reach a steep maximum at the Bragg peak. Beyond this point, the longitudinal dose drops down quite abruptly, since only a small flux of secondary particles contributes to it. The lateral dose distribution is also quite narrow. Indeed, the transverse dispersion comes mostly from multiple scattering of the charged projectiles before stopping.

Therefore, *in vivo* 3D-imaging of the dose is of utmost importance for quality control during patient treatment, and drives a diversified R&D program which includes a variety of techniques. The uncertainty on the location of the Bragg peak in the patient may be large, as much as 1 cm in some cases, due to the stoichiometric calibration of the CT images used in treatment planning, as well as to possible morphologic changes occurring between CT and treatment and during the treatment itself, such as patient mispositioning, tumour shrinkage, weight change and organ motion. Since no primary radiation emerges from the patient, *in vivo* imaging must be performed exploiting secondary radiations. To be useful, such radiation must emerge from the patient, *i.e.* to have a weak interaction probability, and be correlated to the primary beam dose distribution. This information on the electromagnetic energy deposition (the LET) can be extracted from hadronic interactions [1–3].

A significant effort has been already deployed to address these issues and several techniques have been proposed and tested. The present paper reviews the various developments underway on on-line beam dose deposition imaging that are performed within the Rhône-Alpes Regional Program for Research in Hadrontherapy, with the motivation of providing new methods for quality control in future therapy centers like ETOILE in Lyon. These developments include improvement of in-beam Positron Emission Tomography

(IBPET) by means of time of flight, in-beam imaging by prompt gamma-rays and secondary charged particles.

Positron Emission Tomography

So far the only operating control system available during ion therapy is PET, which is based on the observation of the radiation from radioisotopes formed in the nuclei fragmentation process, namely the annihilation of β^+ particles into two photons [4–7]. The main β^+ radioactive isotopes formed during proton or carbon irradiation are ^{11}C, ^{15}O and ^{10}C, with respective half-lives of 20 min, 2 min and 20 s. The suitability of various light ion beams for PET imaging has been studied at GSI and HIMAC [8–10]. Although only the target nuclei undergo fragmentation during proton therapy, the absolute rate of β^+ emission induced during a treatment is higher by a factor of 3-5 for proton than for carbon irradiation, where also projectile fragmentation occurs, due to the larger fluence of protons required to provide the same effective dose.

The relatively short radioisotope lifetimes cited above make IBPET very attractive. This is the solution that was proven by Enghardt *et al.* [11] with the dual-head PET BASTEI (Beta Activity Measurements at the Therapy with Energetic Ions) that has been installed at the GSI pilot project and has demonstrated its ability to provide a control of neck and head irradiations with carbon ions. The IBPET was used at GSI until 2008, whereas most of PET devices used in ion-therapy centers are offline, which necessitates the transport of the patient immediately after the treatment. However, the relatively low induced activities [12] require the acquisition of PET data for about 10 minutes or more, which limits considerably the patient flow in routine clinical environment in the case of IBPET. In addition, the integration of an IBPET device into a treatment site has to be arranged as a limited angle scanner, in order to avoid interference with the patient positioning. This causes artefacts in the reconstructed β^+ activity distributions which partly destroys the relationship between dose and activity. Moreover, over such a period of acquisition time, the metabolism causes a wash-out of the radioactive nuclei, which blurs the image of the implanted radioactive isotopes [13]. The low statistics problem could be circumvented by using radioactive ^{11}C ion beams instead of stable ions which, in addition, provide additional therapeutic dose after implantation due to the projectile radioactivity [14]. Tomitani *et al* have studied the biologic lifetime, *i.e.* the metabolic wash-out, of the implanted radio-elements in clinical conditions with rabbits. They reported that more than 50% of the β+ activity is lost within 4 minutes or less, depending on the tissue irradiated [15].

Improvements of IBPET involve mainly the use of TOF between the two detected gammas. Indeed, during heavy ion treatments, a considerable amount of activity is coming from outside the field of view of the IBPET camera. An accuracy below 200 ps FWHM would reduce considerably the region of interest to a size of the same order as the tumor volume, and therefore decrease the number of background events registered. An important issue of PET imaging is the computer procedure needed to reconstruct an image and extract information about the deposited dose [16-17]. A significant gain on the reconstruction time could be obtained by increasing the coincidence accuracy by means of TOF between the two detected photons. This increase in image processing speed arises from the possibility to calculate at once the point of positron annihilation as soon as the coordinates of the hit detectors and the TOF information are known. Such an algorithm needs to process one single iteration through the collected data, unlike standard iterative reconstruction algorithms. Thus this would also reduce limited solid angle artifacts and open the way to quantitative imaging.

Lanthanum halide ($LaBr_3$) scintillating crystals can in principle reach such 10^{-10} s time resolution. For the readout of the scintillating material, several alternatives could be explored: fast, position-sensitive photomultipliers having sub-ns rise times, multi-anode microchannel plate photomultipliers (MCP-PMTs), and the recently developed solid state Silicon PhotoMultiplier (SiPM). The SiPMs operate in the Geiger mode due to the avalanche nature of their signal, and they have a fast response time with nominal resolution of 50 ps or better. Unlike photomultipliers, SiPMs are not sensitive to magnetic fields, which makes them candidates for

use in a multimodal TOF-PET – MRI. But they have not been used in large systems to date.

Prompt gamma imaging

Since the probability for prompt gamma emission is expected to be of the same order of magnitude as that for fragmentation, gamma imaging may be regarded as a competitive technique to provide real-time information about the local dose [18–20] both for proton and carbon ion therapy.

Prompt gamma-rays are emitted by excited fragments with sufficiently small decay times so that the largest part of the photons are emitted in flight, keeping somewhat the information on the nuclear fragmentation location.

However, measuring prompt gamma during a therapy treatment is not straightforward, since a major source of background arises from the emission of other secondary species like neutrons and light fragments, and also from Compton scattering of photons emitted in all directions. In particular, neutrons have a high multiplicity and high scattering probability in surrounding materials, and they may not be correlated to the ion path. Therefore, various alternatives are offered to provide selective information about the prompt gamma emission profile.

1. Collimated gamma-camera

The first one consists in a selective collimation and shielding. This method was followed by Min *et al* [18] during proton irradiation of a water phantom target. Using a scanning system based on a thick lead and paraffin collimator, the authors could demonstrate that the gamma emission profile keeps correlated with the proton range in water up to projectile incident energy of 200 MeV. However, the limited solid angle imposed by the heavy and oversized collimation setup may prevent this method from being operated in a clinical environment.

2. Time Of Flight-gamma camera with beam tagging

In order to improve the background rejection, our group proposed a prompt gamma detection method [21, 22] which uses time-of-flight information to discriminate between photons and massive particles. Indeed, massive particles and scattered radiations in the surrounding materials are delayed before reaching the photon detector, as compared to direct photons. The concept was tested on a carbon ion beam at GANIL, taking advantage of the pulsed structure of the incident beam, 1 ns pulse each 80 ns. A collimated scintillator was located at 90° from the beam axis at a distance of 60 cm from a PMMA cubic target of 5 cm irradiated with a ^{13}C ion beam energy of 74 MeV/u impinging a thick PMMA target. The gamma profile was measured for the first time for a carbon ion beam and the interest of time of flight was demonstrated. Further studies performed at 95 MeV/u with ^{12}C ions at GANIL, and at higher beam energies at GSI confirm that the correlation between prompt gamma yields and ion range is preserved for carbon ions with longer ranges (in the latter case, the TOF was triggered by a thin scintillator intercepting the low intensity beam) [21]. This makes the proposed method feasible for the typical energies of carbon ion therapy.

The absolute photon yields measured are encouraging in view of designing a real-time control device during therapy. Although the solid angle of the collimated detector was small in this experiment, one can extrapolate the observed yields in view of a more efficient detection device. By increasing the solid angle by two orders of magnitude or more, enough contrast between the irradiated and non-irradiated zones should be observed within a few seconds exposure, thus allowing a real-time control during patient treatments.

A 2D-transverse position information on the incoming ions is required to complete the longitudinal profile. The incident beam tagging, in both time and transverse position, requires the development of a fast position-sensitive detector, with a count rate capability of 10^8 ions/s and 1 ns time resolution. A prototype,

consisting in a scintillating fibers hodoscope read out by flat-panel PMs, is under development at IPN Lyon. Although 3D-data are recorded by this method, the limited statistics imposed by the collimation may restrict the quantitative imaging to 1D or 2D projections. Nevertheless, this represents a considerable breakthrough in the quality control for ion-therapy, since this information is not yet available.

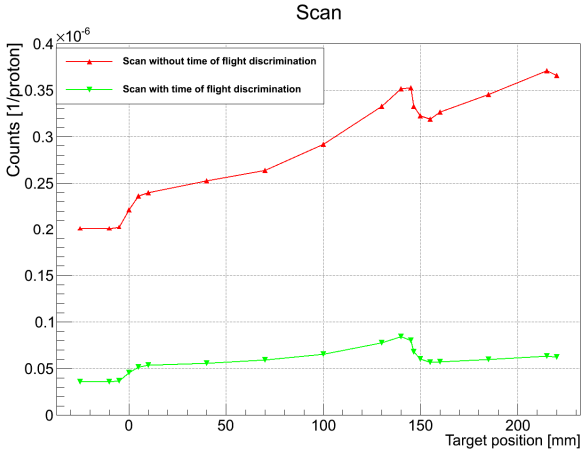

Figure 1. Yields of prompt gamma detected in a collimated LYSO crystal as a function of the target depth. The target is a cylindrical PMMA target of 25 cm in length and 15 cm in diameter irradiated with 160 MeV protons. The tungsten alloy collimator is 10 cm thick and has a 2 mm single slit. These yields correspond to energy deposition larger than 1 MeV with a time-of-flight selection of prompt-gamma rays (green line) and without time-of-flight selection (red line).

Gamma yield profiles have been recently measured in the protontherapy center of Essen with a proton beam of 160 MeV. Figure 1 presents the measurements obtained with a LYSO scintillator (40 mm×3 mm entrance surface and 50 mm thickness) placed behind a tungsten alloy collimator with a thickness of 10 cm and a single slit of 2 mm. Yields correspond to energy deposition larger than 1 MeV with a time-of-flight selection of prompt-gamma rays (green line) and without time-of-flight selection (red line). It shows in particular that, even with proton beam, the neutron background is much larger than the prompt-gamma signal: the signal to noise ratio at the Bragg peak location is about 0.1 for a threshold energy selection of 1 MeV. The increase of this ratio by a factor 5 with time-of-flight selection may be crucial for real-time ion-range monitoring that will involve gamma-yield profiles with low statistics.

These feasibility studies are combined with Geant4 simulations which, in a first step, provide direct comparison with theoretical models, and, in a second step, will help for designing an optimized detection setup. First studies with Geant4 9.1 have shown that this Geant4 version overestimated the overall prompt-gamma depth profile yields by more than an order of magnitude [23]. Interactions with Geant4 developers have led to improvements in the last version of Geant4: the factor of disagreement with state of the art hadronic model in Geant4 is close to 6 for the carbon ion beam case, and to a lesser extent close to the Bragg peak for the proton beam case. As further step, we investigate improvements to the aforementioned Geant4 theoretical models, in order to achieve the desired prediction accuracy required in the context of development and optimization of a prompt gamma beam monitoring device.

3. Compton camera

A considerable improvement in the detection of prompt photons can be achieved with a Compton Camera. The system can be considered to function like a standard γ-camera where the performance-limiting absorbing collimator is replaced by an electronically-operating collimator. A gamma ray emitted undergoes a Compton scattering in a first (scatter) detector, and the scattered photon which interacts in a secondary (absorption) detector conveys information on the direction of the incoming gamma ray. Information on energy deposition and interaction position in these detectors confines the possible incoming path of the initial gamma ray to lie on the surface of a cone, whose apex is the interaction position in the scatter detector. Compton cameras are currently under development worldwide, for application in gamma astronomy, medical imaging or homeland security [24, 25]. For the case of prompt gamma imaging, where the source is extended and the energy spectrum is broad, the position and energy resolutions of the scatter detector are the key issues. As many photons do not deposit all their energy in the camera detectors, a first design of the Compton camera consisted of two Si(Li) scatterers (1 cm thick) and one LYSO absorber (2.5 cm thick). The originality of the method proposed relies on the use of a beam hodoscope together with the Compton camera. The use of the hodoscope greatly simplifies the reconstruction problem. Indeed, it makes possible to reduce the reconstruction problem to the intersection between a straight line and a cone whereas with a classical Compton camera the reconstruction problem consists of cone intersections. For a photon source which spectrum is that of the prompt emitted during the irradiation of a water phantom by a ^{12}C ion beam at 310 MeV/ u [26, 27], the FWHM resolution is 5.6 mm and the detection efficiency is 1.08×10^{-5}. The relatively low detection efficiency made it difficult to apply this device. That is why another design with a stack of Si(Li) detectors (2 mm thick) was envisaged with the same LYSO absorber (Figure 2a) . The detection efficiency was increased by a factor 25 as compared to the efficiency of the first design at the cost of a slightly degraded spatial resolution of 8.3 mm FWHM. Note that the control of the dose fall-off is an edge finding problem that may lead to precision much better than the intrinsic resolution of the camera, depending on the γ and background statistics.

In parallel, a specific reconstruction strategy, based on a precise iterative and fast analytic reconstruction algorithm, is under development [28, 29]. A filtered backprojection algorithm, exact for an ideal, infinite extent Compton camera and capable to take advantage from the redundancy of the model was proposed in [30]. A new calculation method for the system matrix, proposed in [31] aims to faithfully discretize the continuous surface model. Further developpments are required to account for the finite resolution and the finite extent of the camera.

The Compton camera solution, with an efficiency increase of nearly two orders of magnitude compared to a collimated gamma-camera, is a much more ambitious and promising technology allowing online real 3D-imaging of the dose. Beyond the R&D challenges, a successful development of such a device would represent a major breakthrough in ion therapy imaging [32].

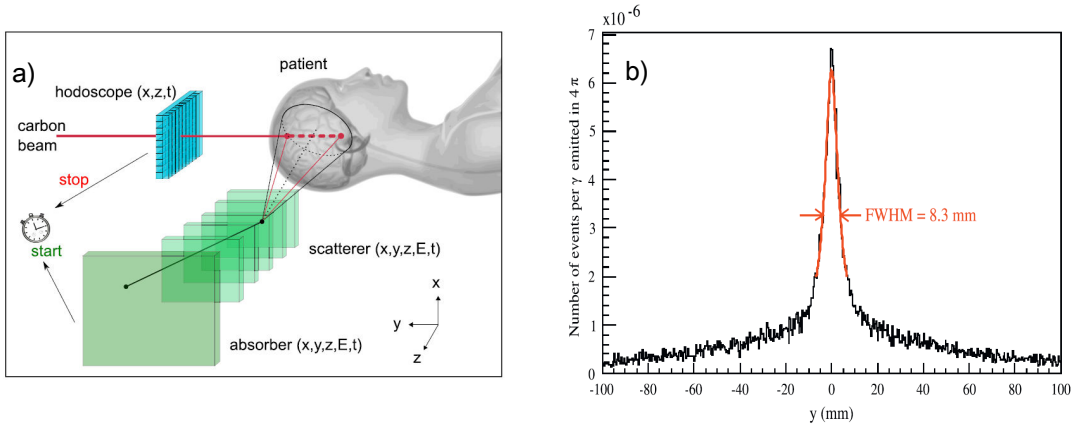

Figure 2. a) a schematic representation of the detection system combining a Compton camera and a beam hodoscope. b) Reconstructed source position for a source at the center of the camera field of view.

Interaction Vertex Imaging

The analysis of charged particles, created in the ion interaction and fragmentation processes, which emerge from the patient offer a potential complementary opportunity to determine the points of interaction of the primary beam. The principle, which resembles that of vertex identification in fixed target particle physics experiments, is to reconstruct the trajectories of the particles emerging form the interactions by a precise charged particle tracker and extrapolate them back to their production point [33]. A feasibility study have been carried out with Geant4 simulations to evaluate two detection techniques: a first one with double-proton detection by means of two forward-located trackers, and a second one with single-proton detection, in coincidence with the incoming carbon ion detected by means of a beam hodoscope. The first conclusion of this feasibility study is that the single-proton detection appears the most promising with a detection efficiency ten times larger than the one of double-proton detection. Then parameter influences have been considered with head-like phantom (Figure 3a). Figure 3b shows reconstructed-vertex distributions in this phantom for various ion beam energies (300, 250, 200 and 150 MeV/u). The smooth lines correspond to fits with complementary error function which provides the position of the inflection point. As expected, the shorter the ion range, the lower the reconstructed-vertex yields due to proton attenuation in the target. There is a clear correlation between the ion range and the inflection-point position of the vertex-distribution edge determined with fits of complementary error function [34] (Figure 3c). This correlation is not strictly linear so that a calibration procedure is required to set the function between the ion range and the inflection point position. Nevertheless the distance between the four points of Figure 3b and a linear fit does not exceed 10 mm which tends to show that this calibration is not a critical issue to achieve millemetric precision.

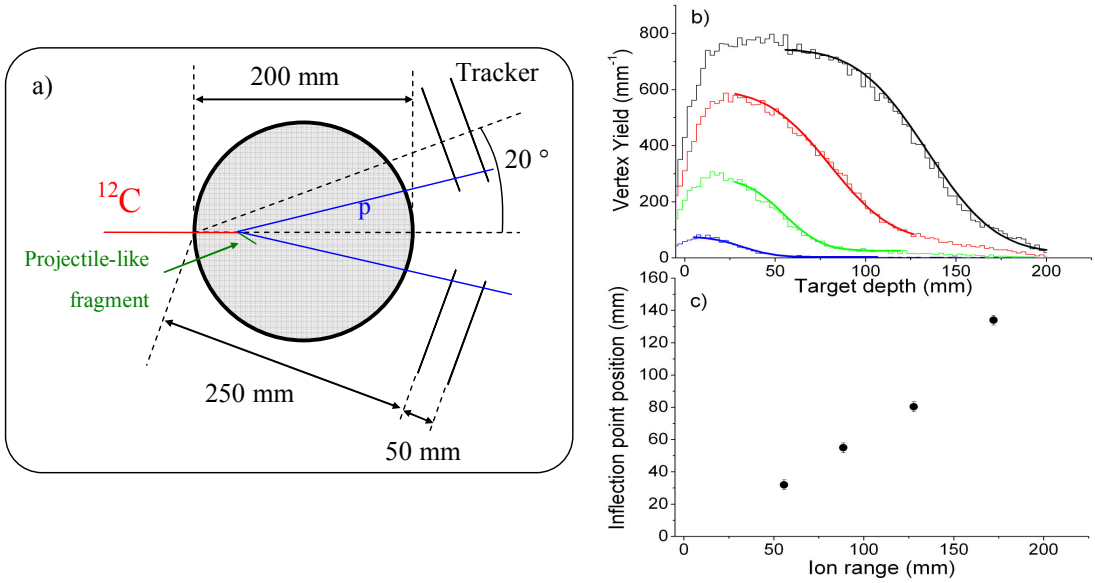

Figure 3. a) Scheme of the spherical head phantom simulation: a hollow bone-equivalent sphere in which cortical tissue-equivalent material is located. The sphere diameter and thickness are 200 and 3 mm, respectively. b) IVI reconstructed vertex distributions in the head phantom (diameter of 20 cm) for various ion beam energies (300, 250, 200 and 150 MeV/u). The smooth lines correspond to fits with complementary error function. c) Inflection point position (determined from fits) as a function of ion range. Number of incident ions per simulation: 10^6.

Moreover the precision on the inflection point position determined by a complementary function fit has been evaluated as a function of the incident ion amount: with the detection setup of Figure 3a, this precision is 5 mm (FWHM) with a number of incident ions close to 10^5 which corresponds to the mean number of incident ions per raster position during a regular treatment of head-tumor [35].

Conclusion

A diversified research program on online dose monitoring during ion therapy is currently ongoing, supported by the Rhône Alpes Regional Program for Research in Hadrontherapy. The program is carried out in the perspective of providing advanced solutions for the treatment quality insurance to the ETOILE ion therapy, which is expected to treat the first patients by late 2012. These studies are also supported by CNRS-GDR MI2B. They are part of the European project ENVISION proposed by the ENLIGHT++ research network in the frame of the FP7 (grant agreement n°241851).

References

[1] D. Schardt, I. Schall, H. Geissel, et al. Nuclear fragmentation of high-energy heavy-ion beams in water. Advances in Space Research 1996;17:87-94.

[2] T. Inaniwa, T. Kohno, T. Tomitani, et al. Experimental determination of particle range and dose distribution in thick targets through fragmentation reactions of stable heavy ions. Physics in Medicine and Biology 2006;51:4129-4146.

[3] N. Matsufuji, A. Fukumura, M. Komori, et al. Influence of fragment reaction of relativistic heavy charged particles on heavy-ion radiotherapy. Physics in Medicine and Biology 2003;48:1605-1623.

[4] W. Enghardt, P. Crespo, F. Fiedler, et al. Charged hadron tumour therapy monitoring by means of PET. Nuclear Instruments and Methods in Physics Research Section A: Accelerators, Spectrometers, Detectors and Associated Equipment 2004;525:284-288.
[5] K. Parodi, T. Bortfeld, W. Enghardt, et al. PET imaging for treatment verification of ion therapy: Implementation and experience at GSI Darmstadt and MGH Boston. Nuclear Instruments and Methods in Physics Research Section A: Accelerators, Spectrometers, Detectors and Associated Equipment 2008;591:282-286.
[6] P. Henriquet Etude de l'émission de particules chargées secondaires dans l'optique d'un monitorage faisceau et de la dosimétrie en ligne en hadronthérapie, Université de Lyon, 2011.
[7] T. Nishio, A. Miyatake, K. Inoue, et al. Experimental verification of proton beam monitoring in a human body by use of activity image of positron-emitting nuclei generated by nuclear fragmentation reaction. Radiological Physics and Technology 2008;1:44-54.
[8] Y. Iseki, H. Mizuno, Y. Futami, et al. Positron camera for range verification of heavy-ion radiotherapy. Nuclear Instruments and Methods in Physics Research Section A: Accelerators, Spectrometers, Detectors and Associated Equipment 2003;515:840-849.
[9] J. Pawelke, W. Enghardt, T. Haberer, et al. In-beam PET imaging for the control of heavy-ion tumour therapy. IEEE Transactions on Nuclear Science 1997;44:1492-1498.
[10] T. Inaniwa, T. Tomitani, T. Kohno, et al. Quantitative comparison of suitability of various beams for range monitoring with induced β+ activity in hadron therapy. Physics in Medicine and Biology 2005;50:1131-1145.
[11] W. Enghardt, J. Debus, T. Haberer, et al. The application of PET to quality assurance of heavy-ion tumor therapy. Strahlentherapie und Onkologie 1999;175:33-36.
[12] W. Enghardt, K. Parodi, P. Crespo, et al. Dose quantification from in-beam positron emission tomography. Radiotherapy and Oncology 2004;73:S96-S98.
[13] F. Fiedler, M. Priegnitz, R. Jülich, et al. In-beam PET measurements of biological half-lives of 12C irradiation induced beta+-activity. Acta Oncologica (Stockholm, Sweden) 2008;47:1077-1086.
[14] A. Kitagawa, Y. Furusawa, T. Kanai, et al. Medical application of radioactive nuclear beams at HIMAC. Review of Scientific Instruments 2006;77:03C105.
[15] T. Tomitani, J. Pawelke, M. Kanazawa, et al. Washout studies of 11C in rabbit thigh muscle implanted by secondary beams of HIMAC. Physics in Medicine and Biology 2003;48:875-889.
[16] T. Inaniwa, T. Kohno, F. Yamagata, et al. Maximum likelihood estimation of proton irradiated field and deposited dose distribution. Medical Physics 2007;34:1684-1692.
[17] G. Shakirin, P. Crespo, et W. Enghardt A Method for System Matrix Construction and Processing for Reconstruction of In-Beam PET Data. IEEE Transactions on Nuclear Science 2007;54:1710-1716.
[18] C.-H. Min, C. H. Kim, M.-Y. Youn, et al. Prompt gamma measurements for locating the dose falloff region in the proton therapy. Applied Physics Letters 2006;89:183517-183517-3.
[19] E. Testa, M. Bajard, M. Chevallier, et al. Monitoring the Bragg peak location of 73 MeV/u carbon ions by means of prompt γ-ray measurements. Applied Physics Letters 2008;93:093506.
[20] J. C. Polf, S. Peterson, G. Ciangaru, et al. Prompt gamma-ray emission from biological tissues during proton irradiation: a preliminary study. Phys. Med. Biol 2009;54:731-743.
[21] M. Testa, M. Bajard, M. Chevallier, et al. Real-time monitoring of the Bragg-peak position in ion therapy by means of single photon detection. Radiation and Environmental Biophysics 2010;49:337-343.
[22] E. Testa, M. Bajard, M. Chevallier, et al. Dose profile monitoring with carbon ions by means of prompt-gamma measurements. Nuclear Instruments and Methods in Physics Research Section B 2009;267:993-996.
[23] F. Le Foulher, M. Bajard, M. Chevallier, et al. Monte Carlo Simulations of Prompt-Gamma Emission During Carbon Ion Irradiation. IEEE Transactions on Nuclear Science 2010;57:2768-2772.
[24] T. Tanimori, K. Hattori, S. Kabuki, et al. Advanced Compton Camera with the ability in electron tracking based on Micro Pixel Gas Detector for Medical Imaging IEEE 2006; 3870-3874.
[25] D. Protic, E. L. Hull, T. Krings, et al. Large-volume Si(Li) orthogonal-strip detectors for Compton-effect-based instruments. IEEE Transactions on Nuclear Science 2005;52:3181-3185.
[26] M.-H. Richard, M. Chevallier, D. Dauvergne, et al. Design Guidelines for a Double Scattering Compton Camera for Prompt- Imaging During Ion Beam Therapy: A Monte Carlo Simulation Study. IEEE Transactions on Nuclear Science 2011;58:87-94.
[27] F. Roellinghoff, M.-H. Richard, M. Chevallier, et al. Design of a Compton camera for 3D prompt-[gamma] imaging during ion beam therapy. Nuclear Instruments and Methods in Physics Research Section A: Accelerators, Spectrometers, Detectors and Associated Equipment 2011;648:S20-S23.

[28] M. Frandes, A. Zoglauer, V. Maxim, et al. A Tracking Compton-Scattering Imaging System for Hadron Therapy Monitoring. IEEE Transactions on Nuclear Science 2010;57:144-150.
[29] V. Maxim, M. Frandeş, et R. Prost Analytical inversion of the Compton transform using the full set of available projections. Inverse Problems 2009;25:095001.
[30] X. Lojacono, V. Maxim, A. Zoglauer, et al. A filtered backprojection reconstruction algorithm for Compton camera. Fully 3D Potsdam: 2011; 96-99.
[31] X. Lojacono, V. Maxim, et R. Prost Calcul de la matrice des probabilités de transfert en imagerie Compton 3D. XXIIIe Colloque GRETSI Bordeaux: 2011; ID432.
[32] Y. Feng, J. Baciak, et A. Haghighat TU-D-352-03: A Design of Compton Cameras for Imaging Gamma Emission in Proton Therapy. Medical Physics 2008;35:2898.
[33] U. Amaldi, W. Hajdas, S. Iliescu, et al. Advanced Quality Assurance for CNAO. Nuclear Instruments and Methods in Physics Research Section A: Accelerators, Spectrometers, Detectors and Associated Equipment 2010;617:248-249.
[34] P. Henriquet Etude de l'émission de particules chargées secondaires dans l'optique d'un monitorage faisceau et de la dosimétrie en ligne en hadronthérapie, Thesis, Université de Lyon, 2011.
[35] M. Krämer, O. Jäkel, T. Haberer, et al. Treatment planning for heavy-ion radiotherapy: physical beam model and dose optimization. Physics in Medicine and Biology 2000;45:3299-3317.

Carbon Ion Therapy at Gunma University

Tatsuaki Kanai, Tatsuya Ohno and Takashi Nakano

Heavy Ion Medical Center, Gunma University, Gunma, Japan
Corresponding Author: Tatsuaki Kanai, e-mail address: kanai@showa.gunma-u.ac.jp

Abstract

C-ion RT facility is installed at Gunma University Heavy Ion Medical Center (GHMC) and the clinical treatment was initiated in March of 2010. The major specifications of the facility were determined based on the experience of clinical treatments at the National Institute of Radiological Sciences (NIRS). Treatments under protocols of C-ion therapy, lung, prostate, head and neck, liver, rectum, bone and soft tissue, are now running at GHMC. Until July 2011, a total of 177 patients were treated at GHMC.

1. Introduction

Cancers of various sites in more than 6,000 patients have been treated at the National Institute of Radiological Sciences (NIRS) using carbon ions. Many promising clinical outcomes have been obtained from NIRS clinical trials. In order to spread the C-ion therapy in Japan, a compact facility for the carbon ion radiotherapy has been designed and installed at Gunma University based on the design and R&D studies carried out by NIRS. By using the compact prototype of the accelerator system, C-ion RT for the first patient at Gunma University Heavy Ion Medical Center (GHMC) took place on schedule in March 2010. In the present symposium, we introduce the facility of GHMC and clinical experiences at Gunma University [1].

2. Gunma Facility

The layout of the facility at GHMC is shown in Figure 1. The facility has 3 treatment rooms with 4 irradiation ports (horizontal, horizontal + vertical, and vertical). In addition, dedicated CT simulators, PET/CT, and MRI were installed in the facility to support efficient and accurate treatment procedures. We adopted a beam wobbling method for broadening the accelerated beams. The beam delivery system comprises of dose monitors, wobbler magnets, a scatterer, a ridge filter, a range shifter, a multi-leaf collimator (MLC), a compensator and a patient positioning system. The basic specifications of the beam delivery system are summarized in Table 1. The requirements have been determined from the experiences of carbon ion therapy at NIRS.

For moving targets during the irradiation, a respiration-gated irradiation method is adopted to reduce a planning target volume. And a layer stacking conformal irradiation method is also adopted to reduce unwanted extra-dose volume in normal tissues [2,3].

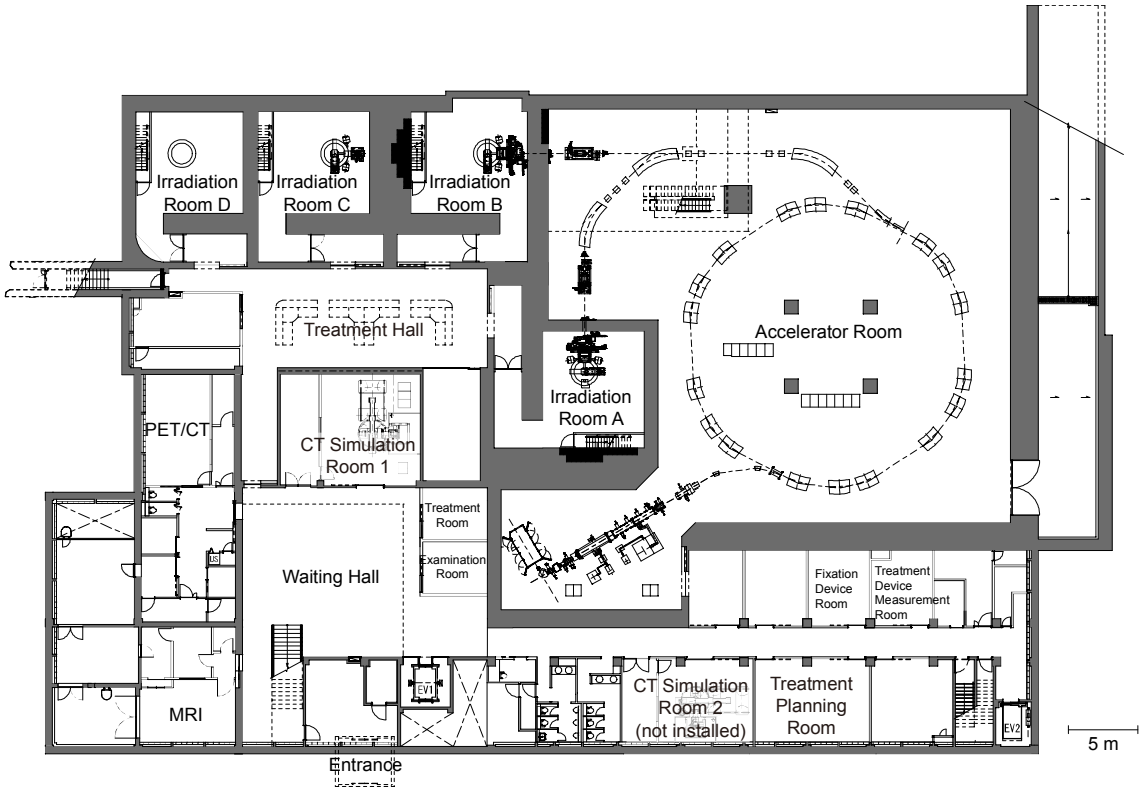

Figure 1. Layout of the carbon ion facility at GHMC (Copy from ref. [1])

Table 1. The basic specifications of the beam delivery system (Copy from ref[1])

Treatment Rooms/Courses	3 Rooms and 4 Courses Room A: Horizontal Room B: Vertical + Horizontal Room C: Vertical
Residual Range	over 25 cm in water (400 MeV/n)
Irradiation Field Size	15 cm × 15 cm at maximum
Beam Broadening Method	Beam Wobbling + Ridge Filter Single Circle Wobbling Pattern Spiral Wobbling Pattern
SOBP Variations	2–14 cm in Water
Dose Rate	5 GyE/min (typical)
Irradiation Methods	Respiration-Gated Irradiation Layer Stacking Conformal Irradiation

3. Clinical preparations

The staffs for C-ion RT consists of 5 radiation oncologists, 6 physicists, 2 treatment planning assistants, 8 operation members, 3 oncology nurses, and 6 radiology technologists at the first year of the clinical treatment.

The members at department of radiation oncology of Gunma University Hospital are also treating patients at GHMC using carbon ion beams. Further staff employments are planned at GHMC according to the increase in patients.

Phase I/II and phase II studies for various tumor sites have been carried out at NIRS since 1994 [4]. At GHMC, the efficacy and safety of carbon ion radiotherapy were reviewed for each tumor type, and the best available dose and fractionation schedules determined at NIRS were adopted for our clinical protocols. All clinical protocols have been prepared by the disease-specific committees consisting of radiation oncologist, surgical oncologist, medical oncologist, and pathological oncologist. Until July 2011, a total of 177 patients were treated at GHMC. The most common site of cancer was prostate (n=139), followed by lung (n=14), liver (n=9), bone and soft tissue sarcoma (n=8), and head and neck tumor (n=7). Table 2 shows clinical protocols at GHMC.

Table 2 Clinical protocols at GHMC

Sites	Total Dose (GyE)	Fractionation (Fr.)	Duration (weeks)	No. patients
Head & Neck	64	16	4	7
Lung (stage I)	52.8 or 60	4	1	14
Liver	52.8	4	1	9
Prostate	57.6	16	4	139
Sarcoma	64 or 70.4	16	4	8
Rectum (pelvic rec.)	73.6	16	4	-

4. Clinical flow of treatments at GHMC

Since only fixed beam ports are available at GHMC, the patient couch should be rotated if necessary. The most common treatment position is the supine position, but a fixation device for the prone position is also available when the posterior beam is used. CT scan is carried out with the fixation devices. CT images are used for treatment planning. After the treatment plan was approved at a staff conference, bolus range compensators made of polyethylene are ordered to be fabricated, and they are designed to adjust the beam ranges to the shapes of distal edges of the target for all beam ports.

The plan data were sent to the beam delivering system. Because the treatment planning system of the carbon ion therapy is still in a developing stage, a dose monitor of the beam delivery system should be calibrated against measured dose at the center of SOBP of the planned data for each patient. Furthermore, the planned physical dose distributions are verified by comparing them with measured dose profiles.

Patients are fixed on the treatment coach with fixation devices using the positioning system, which compares digital reconstructed radiograph (DRR) images derived from the planning CT data and X-ray fluoroscopic images from the X-TV system on site. Figure 2 shows the typical clinical flow at GHMC.

For moving targets, Lung, Liver for example, moving CT data (4 dimensional CT) are usually taken to measure the moving length of the target. The obtained length of the movement is used for estimating margin from CTV to PTV with other uncertainties of the geometrical determination of the irradiation volume.

Figure 2. Typical clinical flow. (copy from ref. [1])

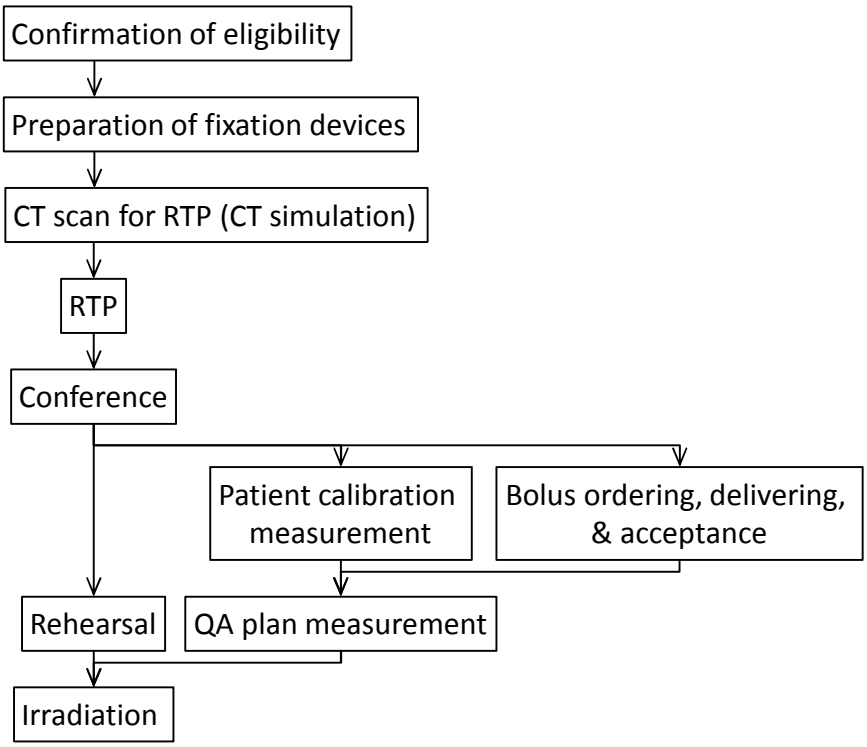

5. Conclusions

With the above procedures using compact accelerator, we successfully treat patients at GHMC.

References

[1] Ohno T, Kanai T, *et al.*, Carbon Ion Radiotherapy at the Gunma University Heavy Ion Medical Center: New Facility Set-up Cancers 2011, 3(4), 4046-4060;

[2] Kanai, T; Kanematsu, N; Minohara, S; Komori, M; Torikoshi, M; Asakura, H; Ikeda, H; Uno, T; Takei, Y; Commissioning of a conformal irradiation system for heavy-ion radiotherapy using a layer-stacking method. *Medical Physics* **2006**, *33,* 2989-2997.

[3] Kanematsu, N; Endo, M; Futami, Y; Kanai, T; Treatment planning for the layer-stacking irradiation system for three-dimensional conformal heavy-ion radiotherapy. *Medical Physics* **2002**, *29,* 2823-2829.

[4] Tsujii H, Kamada T, Baba M, *et al.* Clinical advantages of carbon-ion radiotherapy. New Journal of Physics 2008; 10: online at http://www.njp.org/

CNAO the Italian Particle Therapy Facility

Piero Fossati[1,2],Maria Rosaria Fiore[1], Viviana Vitolo[1], Barbara Vischioni[1], Alberto Iannalfi[1], Roberto Orecchia[1,2,3]

(1)CNAO National Centre for Oncological Hadrontherapy, Pavia, Italy

(2)Department of Biomedical Sciences and Technologies, University of Milano , Milano, Italy

(3)European Institute of Oncology, Milano, Italy

e-mail address: fossati@cnao.it

Abstract

CNAO is a dual centre capable of providing therapeutic beams of protons and carbon ions with maximum energy of 400 MeV/u. At present, it is equipped with three treatment rooms with fixed horizontal and vertical beam lines. In a subsequent phase, two more rooms with a rotating gantry are foreseen. An active spot scanning dose delivery system is employed. Patient treatment with protontherapy (PT) has started in September 2011; treatments with carbon ions radiotherapy (CIRT) are foreseen to start in spring 2012. At present all treatments are performed within clinical protocols specifically authorized by the Italian Ministry of Health and aiming at a certification for routine clinical use. Five protocols have been approved for PT: skull base chordoma and chondrosarcoma, spinal chordoma and chondrosarcoma, meningioma, re-irradiation of head and neck cancer and boost after photons RT in locally advance head and neck cancer. In the next future there is the plan to activate other protocols with PT for high grade glioma (primary treatment and re-irradiation of recurrence), and other central nervous system tumours. The first indications for CIRT (always to be treated within protocols that are part of a certification process) will be salivary gland cancers, other non-squamous cellular head and neck cancers, head and neck bone and soft tissue sarcoma, trunk bone and soft tissue sarcoma and selected limbs bone and soft tissue sarcoma.

The CNAO Facility

CNAO is a hospital for outpatients treatments with both PT and CIRT. The synchrotron is the heart of the facility and can accelerate proton and carbon ion to a maximum energy of 400 MeV/u (corresponding to 27 cm penetration depth in water). Three rooms equipped with fixed beam line (two rooms with horizontal beam and one room with vertical and horizontal beam) can be used for patients treatment. The facility has been designed to allow a foreseen upgrading with two more rooms equipped with rotating gantries with minimal impact on its daily clinical activities. In every room it is possible to perform PT and CIRT and all the devices are designed for both the beams. CNAO employs an active spot scanning system. Two orthogonal magnetic fields are used to scan the beam in planes parallel to its direction. Magnets are designed to allow scanning of square slices of 20 x 20 cm. Depth is varied directly by adjusting the beam energy. The smallest step of penetration range achievable is 0.2 mm. The synchrotron allows varying the energy at each spill, so that every second it is possible to irradiate a layer of different depth. Scanning magnets, sensors to measure position and intensity of the beam and control systems are integrated in the nozzle. Different spot size are available (with a radial size adjustable from 4 mm to 10 mm in steps of 1 mm). The active scanning system and the dose rate have been designed to be able to deliver 2 Gy to a volume of 1 liter in 1 – 1.5 minutes.

Planning is performed with the same LEM based TPS (syngo® PT) employed at HIT in Heidelberg. This TPS allows inverse planning and simultaneous beams optimization. Treatments are performed with patients immobilized on specially designed couches or chairs docked to a state-of the art, 6 degree of freedom, mobilization robot. Set-up verification is performed with orthogonal KV images of diagnostic quality and 2D✍ 3D registration. Additionally optoelectronic system with markers detection and surface detection capability are used. Treatment simulation is performed with the help of a dedicated imaging department with a big bore Ct scanner, a PET-CT scanner and a 3 Tesla MR.

Approved PT protocols

Details of already approved protocols are reported here.

1. Protocol 01/2011 : phase II study of protontherapy for skull base chordoma and chondrosarcoma

Sample size : 30 patients.

Inclusion criteria:

- histological/cytological diagnosis of chordoma/ grade I – II chondrosarcoma confirmed by pathology review
- age between 15 and 85
- Karnofsky 70 or more
- prognosis of at least 6 months
- no severe co-morbidities with worse prognosis as compared to the disease under investigation
- N0 M0
- patient (or his legal tutor) can give consent.

Exclusion criteria:
- previous RT in the same area
- psychiatric or medical condition counter indicating RT
- concomitant chemotherapy
- high grade tumor (for chondrosarcoma only)
- local extension that forbids respecting normal organ dose constraints
- metallic implants that forbid adequate planning
- pregnancy.

Prescription dose:
Chordoma: 74Gy [RBE]; 2Gy[RBE]/fraction;
Chondrosarcoma: 70 Gy [RBE]; 2Gy[RBE]/ fraction.

Endpoints:
primary endpoints are local response and acute (90 days toxicity);
secondary endpoints are local control , disease free survival, cause specific survival, overall survival, mid-term (6 months) and long term toxicity.

2. Protocol 02/2011 : phase II study of protontherapy for spinal chordoma and chondrosarcoma

Sample size : 20 patients.

Inclusion criteria:
- histological/cytological diagnosis of chordoma/ grade I – II chondrosarcoma confirmed by pathology review
- measurable cancer
- age between 15 and 85
- Karnofsky 70 or more
- prognosis of at least 6 months
- no severe co-morbidities with worse prognosis as compared to the disease under investigation
- inoperable or recurrent or residual disease
- N0 M0
- patient (or his legal tutor) can give consent.

Exclusion criteria:
- previous RT in the same area
- psychiatric or medical condition counter indicating RT
- concomitant chemotherapy
- high grade tumor (for chondrosarcoma only)
- local extension that forbids respecting normal organ dose constraints
- metallic implants that forbid adequate planning
- pregnancy.

Prescription dose:
Chordoma: 74Gy [RBE]; 2Gy[RBE]/fraction;
Chondrosarcoma: 70 Gy [RBE]; 2Gy[RBE]/ fraction.

Endpoints:
primary endpoints are local response and acute (90 days toxicity);
secondary endpoints are local control , disease free survival, cause specific survival, overall survival, mid-term (6 months) and long term toxicity.

3. Protocol 03/2011 : phase II study of protontherapy for meningioma

Sample size : 30 patients.

Inclusion criteria:
- histological/cytological diagnosis of intracranial meningioma confirmed by pathology review
- age between 15 and 85
- Karnofsky 70 or more
- prognosis of at least 6 months
- no severe co-morbidities with worse prognosis as compared to the disease under investigation

- malignant or atypical histology (WHO grade II-III); benign (WHO grade I) tumor is accepted only in case of inoperable/residual disease in dimensional progression
- patient (or his legal tutor) can give consent.

Exclusion criteria:
- previous RT in the same area
- distant metastasis
- multifocal disease
- spinal primary tumor
- psychiatric or medical condition counter indicating RT
- concomitant chemotherapy
- local extension that forbids respecting normal organ dose constraints
- metallic implants that forbid adequate planning
- pregnancy.

Prescription dose:
benign meningioma: 60Gy [RBE]; 2Gy[RBE]/fraction;
malignant/atypical meningioma: 66 Gy [RBE]; 2Gy[RBE]/ fraction.

Endpoints:
primary endpoints are local response and acute (90 days toxicity);
secondary endpoints are local control , disease free survival, cause specific survival, overall survival, mid-term (6 months) and long term toxicity.

4. Protocol 05/2011 : phase II study of protontherapy for re-irradiation of head and neck cancer.

Sample size : 40 patients.

Inclusion criteria:
- visible and measurable recurrent cancer in the head and neck area after previous RT, radical or post-operative
- histological confirmation of recurrence(except cases in which biopsy is not feasible)
- age between 15 and 75
- Karnofsky 70 or more
- prognosis of at least 6 months
- at least 6 months interval form previous RT
-no other therapeutic option with radical intent
- no severe co-morbidities with worse prognosis as compared to the disease under investigation
- malignant or atypical histology (WHO grade II-III); benign (WHO grade I) tumor is accepted only in case of inoperable/residual disease in dimensional progression
- patient (or his legal tutor) can give consent.

Exclusion criteria:
- more than one previous RT in the same area
- unavailability of previous RT details
- distant metastasis
- local conditions (e.g. radio-induced brain or bone necrosis, active infections) counter indicating RT
-histology for which high LET RT is indicated
- psychiatric or medical condition counter indicating RT
- concomitant chemotherapy
- local extension that forbids respecting normal organ dose constraints
- metallic implants that forbid adequate planning
- pregnancy.

Prescription dose:
ranging from 50 to 76 Gy [RBE]; 2Gy[RBE]/fraction, depending on site histology and previous treatment.

Endpoints:
primary endpoints are local response and acute (90 days toxicity);
secondary endpoints are local control , disease free survival, cause specific survival, overall survival, mid-term (6 months) and long term toxicity.

5. Protocol 06/2011 : phase II study of protontherapy boost for locally advanced head and neck cancer.

Sample size : 160 patients.

Inclusion criteria:
- histological/cytological diagnosis of primitive malignant epithelial or neuro-endocrine cancer
- locally advanced, inoperable disease

- tumor site in the head and neck area: hypopharynx oropharynx and epipharynx, nasal and paranasal sinuses and larynx
- measurable disease
- age between 15 and 75
- Karnofsky 70 or more
- prognosis of at least 6 months
- at least 6 months interval form previous RT
- adequate liver function (bilirubin < 1.5 mg/dL, SGOT, SGPT <3 x ULN, GGT<5 x ULN)
- adequate bone marrow function (neutrophils > 1.5 x 10^9/l, platelets > 100 x 10^9ll, hemoglobin >10.0 g/dl)
- start of treatment within 7 days of first phase of photons RT (50-60 Gy) to wider CTV at lower risk of tumor infiltration
- pregnancy excluded with negative Beta-HCG test
- patient (or his legal tutor) can give consent.

Exclusion criteria:

- M1
- previous surgery on the main tumor (except biopsy)
- previous RT in the area (except the first phase of photons RT foreseen by this protocol)
- other malignant tumor in the previous 5 years (except in situ cancers and non melanoma skin tumors)
- G3-G4 toxicity due to the first phase photons RT that forbid prosecution with PT boost
- peripheral symptomatic neuropathy > G2
- Ototoxicity > G2 (except if due to tumor compression)
- psychiatric or medical condition counter indicating RT
- concomitant chemotherapy
- local extension that forbids respecting normal organ dose constraints
- metallic implants that forbid adequate planning
- pregnancy.

Prescription dose:

Boost to a total dose of at least Gy [RBE]; 2-3Gy[RBE]/fraction, depending on site histology and previous treatment.

Endpoints:

primary endpoints are local response and acute (90 days toxicity);
secondary endpoints are local control , disease free survival, cause specific survival, overall survival, mid-term (6 months) and long term toxicity.

Future protocols

Other PT protocols are under development for central nervous system tumors. CIRT protocol will take advantage of existing Japanese and German experience. In the first phase NIRS fractionation scheme of 4 fraction per week will be employed. Bone and soft tissue sarcoma and head and neck cancer (non squamous cellular histology) will be treated. Prescription dose will be derived from NIRS experience. Simulation studies are ongoing to convert NIRS based equivalent dose into LEM equivalent dose. The rather relevant differences in the two system of RBE calculation make this conversion critical. Limited dose escalation studies may be mandatory to check the clinical validity of this dose conversion. Treatment of thoracic and abdominal target will be postponed to a subsequent phase after successful testing of organ motion coping procedures.

Conclusions

CNAO has started its clinical activity with protons.. Patient treatment is taking place within a clinical research framework specifically agreed with the Italian Ministry of Health and aiming at obtaining certification for routine clinical use. Present protocols are tailored according to this specific need. This is a necessary preliminary step that will be followed by a phase in which the focus will be shifted on expanding the indications of PT and CIRT and contributing to the creation of sound evidence to better establish the role of hadrontherapy in the multidisciplinary treatment of cancer.

The Current Status of the Saga HIMAT

Sho Kudo, Masahiro Endo, Hirohiko Tsujii, Tadahide Totoki
Saga HIMAT Foundation, Tosu, Saga, Japan

Corresponding Author: Sho Kudo, e-mail address: kudo-sho@saga-himat.jp

Abstract

The Saga HIMAT (Heavy Ion Medical Accelerator in Tosu) will open in the Spring of 2013 in Tosu, Saga Prefecture, and will become the fourth carbon ion beam cancer treatment center in Japan.

Introduction

The Saga HIMAT stands for the Heavy Ion Medical Accelerator in Tosu. Saga is one of 7 prefectures located on Kyushu Island. Tosu is a city of about 70,000 people, and is located on the cross-point of railroad and highway networks on Kyushu Island. It is also close to Fukuoka Airport. Fukuoka is the largest city in Kyushu. The Saga HIMAT is in front of the Shin-Tosu Station of Kyushu-Shinkansen Railway. The facility is now under construction and the pictures shown below were taken in September 2011. In Japan, there are currently 9 particle beam cancer treatment centers in operation, three of which utilize carbon ion beams. The Saga HIMAT will become the fourth carbon ion beam cancer treatment center in Japan.

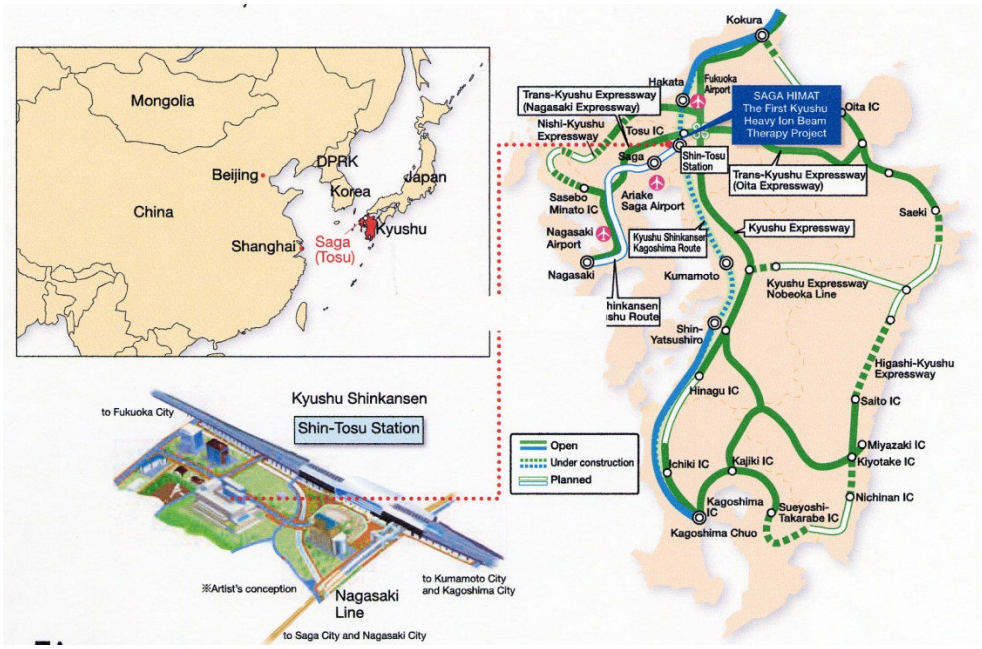

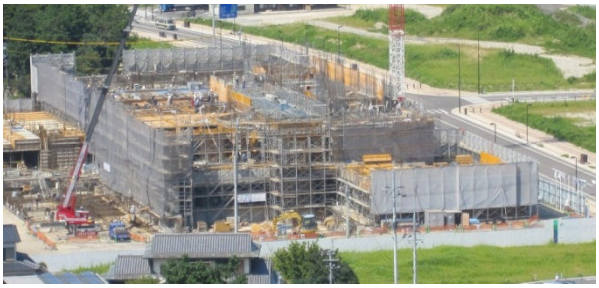

The Saga HIMAT Project

The Saga HIMAT project is a collaborative effect among the Saga prefectural government, regional industries and universities in Kyushu. The project started in 2008, and the buildings will be completed in October 2012. Then, test treatments for patients will be performed to obtain governmental approval for the use of the facility. We plan to have a grand opening sometime in the Spring in 2013. The initial cost of the project is about 15 billion yen. There will be no beds in the facility. All of the patients will be treated as out-patients. The therapy is not covered by the public health insurance in Japan, and it costs about 3 million yen for each patient. However, many companies sell medical insurance products that cover the heavy ion beam therapy fee in Japan.

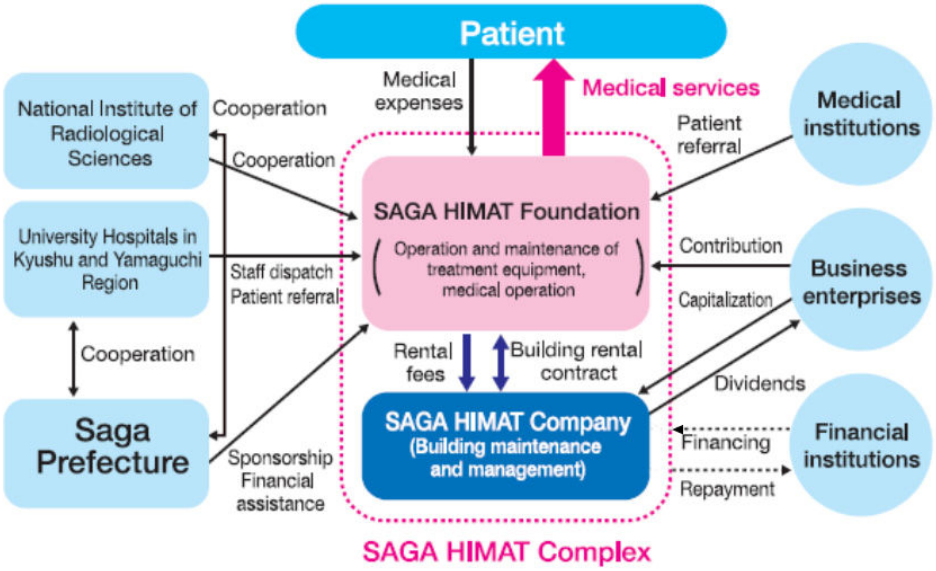

Outline of the Saga HIMAT

At the Saga HIMAT, we are going to use three different types of beams; horizontal, vertical, and 45 degree oblique. The diameter of the synchrotron is about 20 meters. The maximum energy is 400 MeV/u. Three treatment rooms will be prepared, but we will start treating patients with two rooms. We plan to start with about 200 patients in the first year and hope to increase that number to 800 patients/year in the near future. We will collaborate with the National Institute of Radiological Sciences, Gunma University, and the universities and medical centers on Kyushu Island. We will also be receiving support from the Saga prefectural government, regional business enterprises, and financial institutions. The Saga HIMAT Foundation will perform the medical treatments and maintenance of the equipment. The Saga HIMAT Company, a special purpose company, will own and maintain the buildings.

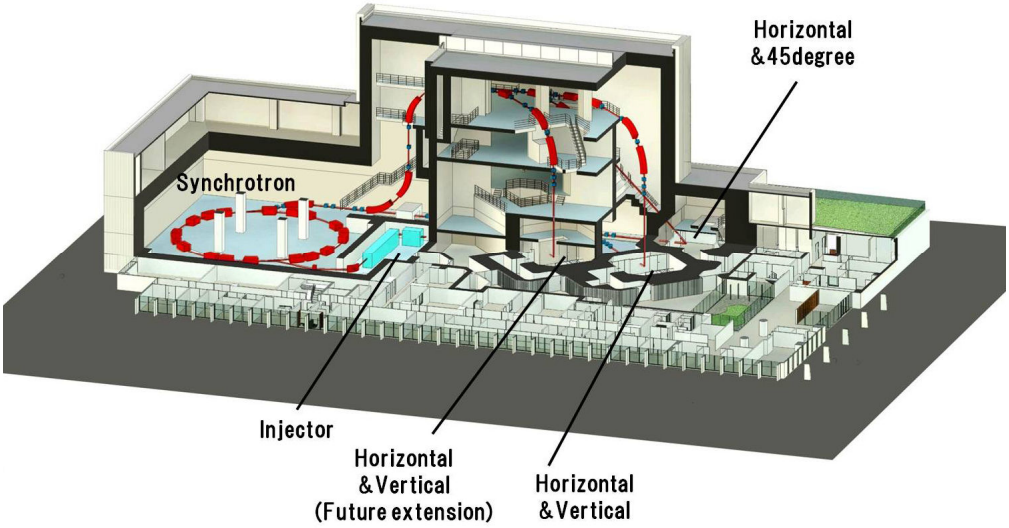

Conclusion

The Saga HIMAT will open in the Spring in 2013 in Tosu, Saga Prefecture, and will become the fourth carbon ion beam cancer treatment center in Japan.

MedAustron in Wiener Neustadt

Ramona Mayer on behalf of the MedAustron Team

EBG Med Austron Ltd, Wiener Neustadt, Austria
e-mail address:ramona.mayer@medaustron.at

Abstract

MedAustron is a dual beam ion therapy and research centre which is presently under construction in Wiener Neustadt, Austria. The facility is based on a synchrotron which will deliver proton beams with kinetic energies up to 250 MeV and carbon ion beams up to 400 MeV/nucleon for clinical applications. In addition to the clinical applications, the accelerator will provide beams for nonclinical research in the fields of medical radiation physics, radiation biology and experimental physics with a proton energy range extended beyond medical requirements to 800 MeV.

Introduction

Parameters affecting the outcome after radiotherapy of malignant tumours

The so called "outcome" after radiotherapy, which means local control and survival of patients undergoing (radiation) treatment for cancer, depends mainly on two factors - treatment independent (see 1.) and treatment dependent factors (see 2.).

1. Treatment independent factors

- Stage of disease

– *Localized disease*: At time of cancer diagnosis about 55% of the patients do not show metastases on radiological and/or histopathological examinations. Indications for proton or carbon ion therapy are described later on in detail (see Section 3.5 for the patient group with localized disease.

– *Micrometastatic disease*: Out of those 55% of patients who are diagnosed to have no distant metastases, a not negligible number show so called "micrometastases". These are small numbers of cancer cells that have spread from the primary tumour to other parts of the body and are too few to be picked up in any diagnostic test currently available. Unfortunately, at present those patients who are staged as "non-metastatic" and are treated with solely local treatment options like surgery and/or radiotherapy, show metastatic disease on radiological studies shortly after the "local" treatment. Most important, a local procedure like radiotherapy is considered to be "ineffective" in the opinion of the patients and referring physicians. More sensitive methods for detecting such cells should increase knowledge about the biologic mechanisms of metastasis and improve the diagnosis and treatment of micrometastatic disease. In contrast to solid metastatic tumours, micrometastatic tumour cells are appropriate targets for intravenously applied agents because macromolecules and immune-competent effectors cells should have access to the tumour cells. Because the majority of micrometastatic tumour cells may be non-proliferative (G0 phase), standard cytotoxic chemotherapies aimed at proliferating cells may be less effective, which might explain, in part, the failure of chemotherapy. Thus, adjuvant therapies that are aimed at dividing and quiescent cells, such as antibody-based therapies, seem to be of considerable interest.

- *Metastatic disease*: About 45% of the patients show loco-regional or distant metastases on radiological and/or histopathological examinations at time of first cancer diagnosis. These patients will receive palliative treatment, which helps a patient feel more comfortable and improves the quality of life, but does not cure the disease. Most of those patients would not be candidates for ion therapy. An exception could be made, if the patient is a) in a good/excellent performance status, b) shows only one metastatic site and c) the primary tumour is under control. In such a case an ion irradiation of the metastatic site could be discussed, if the lesion is located near a critical organ like the spinal cord.
- Age (prognostic factor in some, but not all cases)
- Performance status

2. Treatment dependent factors

- Correct treatment volume identification
- Fractionation and total dose
- Temporal dose distribution e.g. organ motion etc.
- Spatial dose distribution
- Normal tissue restraints
- Intrinsic tumour radio-curability

The last three factors seem to be – in many cases – controllable by using highly sophisticated treatment techniques like ion beam therapy

Physics background

1. Radiation with low Linear Energy Transfer (LET) -protons and helium ions

Protons are low LET particles, which exhibit a LET of less than 30 keV/µm over their entire range. This LET is similar to the conventional beam qualities applied in radiation oncology, i.e. high energy photon and electron beams. Consequently protons exhibit only a slightly increased biological effectiveness as compared to conventional beam qualities. Due to the characteristic depth dose profile with a Bragg-Peak that spares healthy tissue distal to the tumour, they give in general a smaller dose to healthy tissue surrounding the tumour. Thus the fundamental rationale for their use is the *improved physical selectivity*, i.e. better dose conformation properties which enable better sparing of organs at risk and hence the potential of reducing side effects.

From the physics point of view h*elium ions* are superior to protons, as their lateral and range scattering is much less pronounced. A well known particular disadvantage of protons is their lateral scattering characteristics which reduces the sharpness of the lateral dose fall-off at larger depths. However, at present the large clinical experience gathered with proton therapy over a long time period makes them the state-of-the-art particle for ion therapy for many different tumour types. Other ion species have to be "benchmarked" against protons in order to evaluate their clinical potential. So far, the clinical experience made with helium ions is very much restricted to ocular tumours.

2. Radiation with high LET

Ions from lithium to flour offer an ideal combination of enhanced biological efficiency in the target region and a very high degree of dose conformation to the target. These ions can be characterised by an (intermediate) LET between 30 and 100 keV/µm. The highest LET values are restricted to the Bragg-Peak, while the entrance or plateau region of these ion species exhibits mainly low LET. In other words, the high radiobiological

efficiency resulting from the high LET can be in principal restricted to the tumour volume, while the surrounding normal tissue is irradiated predominantly with a lower LET. In addition to the radiobiological efficiency the physical selectivity of these ions is excellent due to their advantageous lateral scattering and range straggling properties. It is important to note that the radiobiological feature of high LET radiation cannot be emulated by dose escalation with low LET radiation such as photons or protons.

Nevertheless, the tail of the depth dose curve beyond the Bragg peak is impaired due to nuclear fragmentation of the ions, which is increasing with atomic number. If modeled properly, nuclear fragmentation is still acceptable for clinical applications. Furthermore, these ion species produce a number of positron emitting nuclei when interacting with tissue that allow an online therapy monitoring using an in-situ Positron Emitter Tomography (PET) system. The complexity of the spectrum of positron emitters is increasing from lower to higher atomic numbers: while carbon exhibits only 4 relevant isotopes, neon already exhibits 12. In that respect, it is important to note that during the last years in-situ PET monitoring has been also investigated for proton beam therapy.

The ideal combination of high LET particle, low fragmentation contribution and simple positron emitter spectrum are probably *carbon ions* and therefore are they the preferred high LET ion species for MedAustron.

3. Type of ions used at MedAustron

Protons and carbon ions have their specific but partly different merits, and represent the ion beams with which treatments are planned *in the first place*. However, when setting up an ion beam centre, it is important to consider possible future aspects of ion beam therapy. If several ions can be accelerated to clinically useful energies in the same treatment centre, e.g. helium, nitrogen, or oxygen ions, they are likewise interesting for research purposes and offer flexibility for future medical ion beam applications.

When starting the facility, initially proton beams will be used for patient treatment. In the first years of operation about 60-70% of the patients will be treated with proton beams, preferably with two or more fields and 30-40% of patients will be irradiated with carbon ions. Intensive clinical studies will be performed at MedAustron to increase knowledge about the treatment with carbon ions. In the following years the percentage of protons and carbon ions will be changed to 50% vs. 50% and maybe even to 30% vs. 70% in the long run.

Description of the MedAustron facility

1. Technical equipment

The MedAustron accelerator complex consists of an injector, a synchrotron as main accelerator and the extraction line, that brings the beam towards the treatment rooms. The accelerator complex is designed to allow fully active beam delivery which is presently the most advanced technique in the field of hadron therapy. The complex will cycle with a typical repetition rate of 0.5 Hz and beam energy, size and intensity can be changed on a cycle-to-cycle basis. A change of the ion type, i. e. protons or carbon ions will also be possible on the sub-minute level. The design of the accelerator complex is based on machines that already exist or which are in the process of being built and also takes into account experience from running facilities. Collaborations for the realization of the MedAustron accelerator complex have been established with the European Organisation for Nuclear Research (CERN) and the Italian CNAO hadron therapy centre.

The injector will comprise three ion sources with the possibility of adding a fourth source. Two sources (protons and carbon ions) are the standard configuration for medical treatment, the third source serves as spare

and the alternative fourth source can be used for research with a different ion type. The sources are connected by the low-energy beam transport that brings the beam from the active source to the radio-frequency quadrupole that serves as pre-injector for the drift tube linac. The drift tube linac (IH structure) will accelerate the beam to 7MeV per nucleon which is the injection energy of the synchrotron.

The synchrotron is based on the CERN Proton Ion Medical Machine Study (PIMMS) and was further developed into a technical design by the Italian CNAO group. The synchrotron will use the so-called "slow resonant extraction" method to provide the beams for treatment. The energy range is 60MeV to 250MeV for protons and 120MeV per nucleon to 400MeV per nucleon for carbon ions.

The extraction lines are based on a modular concept that was developed within the PIMMS study at CERN. The beam size is controlled in the common part of the line and the beam is then passed onto the different treatment rooms by similar beam line modules with special optical transport properties. This concept is expected to ease operation because of similar beam optics settings.

2. Overall building concept

The project will be realised within the industrial zone "Civitas Nova" located in the northern periphery of Wiener Neustadt. This is a small city with 40.000 inhabitants, located about 60 kilometres away from Vienna.

The building will be characterised by a clear zoning of the various functional parts of the project: the medical area (treatment rooms, medical infrastructure), the technical and research area (offices, labs, technical infrastructure) and the accelerator area.

The thickness of the shielding walls has been chosen to allow unlimited access to the areas outside the accelerator bunker and the treatment rooms. The shielding walls and the related floors and ceilings are out of a sandwich construction. Between lateral concrete walls of 30 cm thickness the excavation material will be inserted and compressed. This sustainable approach limits the track traffic on site during construction, since about 25'000 m^3 of excavation material can be re-used and correspondingly the same amount of concrete can be spared which is also an important economic saving. Floors and ceilings are made of a honeycomb structure of concrete filled with excavation material.

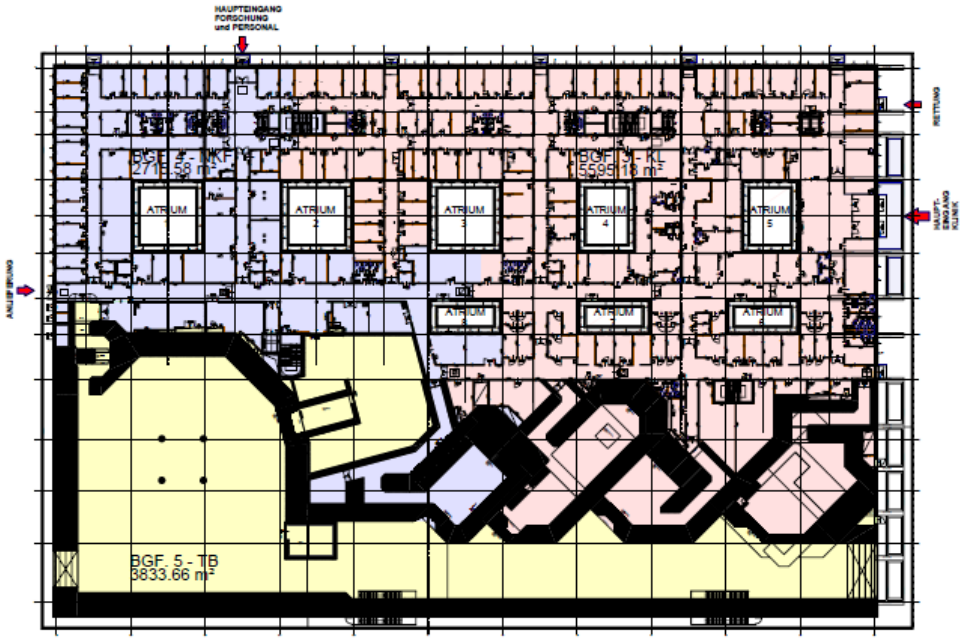

Fig. 1: Sandwich construction: Filling process and subsequent compression of the material.

3. Medical facility

The number patients to be treated and the envisaged *modus operandi* defined the layout of the medical part of the facility. In the full operational phase, up to 1400 patients per year will be treated at MedAustron; for the medical operation of the facility two shifts on normal working days will be foreseen. Consequently three treatment rooms are needed in this scenario to efficiently use the accelerator and to achieve the desired patient numbers. The choice was made for two fixed beam rooms for proton and carbon ion treatments and one gantry room for proton treatment only. One of the fixed-beam rooms is equipped with a horizontal beam line and the other with a horizontal and a vertical beam line with a common isocentre.

While patient treatment will be performed on week days from 6:00 to 22:00 the remaining night time and the weekends can be used for non-clinical research which corresponds roughly to 50% of the total available beam time.

Dynamical treatment is foreseen for all treatment rooms, by so-called active pencil-beam scanning. The tumor volume is subdivided in layers of typically 2-5 mm thickness each at a constant penetration depth, corresponding to a specific particle energy. Every voxel of an iso-energy layer is then irradiated by a particle beam with a 4 - 10 mm cross-section. When the required dose for the voxel is reached, the beam is moved (without being switched off) to the next voxel.

The MedAustron facility will be equipped with adequate imaging tools to meet the future requirements for precise radiotherapy planning and delivery:

- computed tomography (CT)
- 3 T magnetic resonance imaging (MRI);
- 3D ultrasound;
- positron emission tomography (PET)-CT for offline verification;
- patient alignment system (patient positioning systems and patient position verification systems with X-ray devices in all medical treatment rooms with an additional sliding gantry-CT in the proton gantry room)

4. Outlook

The key milestones from 2011 onward are as follows:

- start of construction: February 2011;
- building weatherproof: January 2012;
- civil engineering works finished: September 2012;
- start of installation and integration of particle accelerator: October 2012;
- start of technical commissioning of particle accelerator: mid of 2013;
- start of medical commissioning and certification of the project: mid of 2014;
- first treatment of patient: fall of 2015.

Currently, all engineering, procurement and construction processes are within the time schedule.

Fig.2. Construction site, October 2011

The Belgian Hadron Therapy Centre project: rationale and current status.

Wilfried De Neve*, Philippe Coucke, Dirk Van den Berge, Paul Van Houtte, Karin Haustermans, Pierre Scalliet, Danielle Van den Weyngaert, Didier Vander Steichel, Eric Lartigau, Roger De Croock and Frank Deconinck

**UZGent, Radiotherapie P7, De Pintelaan 185, BE-9000 Gent, Belgium.*

Email address: Wilfried.DeNeve@uzgent.be

Abstract

The Belgian Hadron Therapy Centre project (BHTC) has been granted governmental funding for the first part of a feasibility study for a Hadron Therapy Center in Belgium: "Definition of the medical concept in terms of patient population and of clinical research". The conclusions will be submitted in the Spring of 2012. This paper shortly outlines the rationale behind the project.

Introduction

The radiotherapy specialists of all 7 University Hospitals in Belgium (Gent, Liège, Brussel, Bruxelles, Leuven, Louvain, Antwerpen), the Centre Oscar Lambret in Lille, France, the Fondation against Cancer and the Belgian Nuclear Research Centre (SCK•CEN) –each of them member of the Belgian Hadron Therapy Centre Foundation (BHTC)- are convinced that there is sufficient scientific evidence to demonstrate the need of at least one Belgian Hadron Therapy Centre for a population of 10 million people.

In the frame of BHTC, they will gather evidence for this need by performing a study on the eligible patients as a first part of a comprehensive feasibility study for such a HT centre.

What would be the purpose of a HT centre in Belgium?

The Belgian University Hospitals propose that the objective of a HT centre would be restricted to perform clinical and translational research at the start of its exploitations and, as evidence is gathered and exploitation allows the treatment of larger patient numbers, it would increasingly progress to a treatment centre that assures cost break-even with the treatment reimbursement income.

This centre should be designed for both proton and carbon ion beam delivery, a position to re-assess with the outcome of this first study.

On the necessity and suitability of Randomised Clinical Trials (RCT)

Because of practical and ethical constraints there are very few RCT reports available from the existing hadron therapy centres worldwide, to demonstrate the medical evidence of their superior treatment.

The international society of radiotherapists is convinced that RCT cannot and should not remain the only methodology to clinically assess the need of HT. There are other more appropriate, and at the same time scientifically and statistically robust methods, of estimating the potential of the eligible indications for HT.

What are the eligible indications to be studied for a HT centre?

There exists a group of generally accepted historical indications. In Belgium, this group was estimated by the Belgian Health Care Knowledge Centre (KCE) at some 50 to 100 patients per year. The Belgian National Institute for Health and Disability Insurance (RIZIV / INAMI) decided 2 years ago to pay their treatment in HT centres abroad. Practice however is that these possibilities are more theoretical than feasible. Less than a handful of patients could be treated during the past 2 years, sometimes at extremely high costs. One paediatric patient was treated in the USA at a cost of well over 350.000 €, the costs at the accompanying Belgian university hospital not taken into account.

Since this shortage of treatment possibilities is not going to improve in the next future, we have the moral duty to raise the question whether we want to continue to deprive patients from the appropriate therapy. Today we are in the best case financing research abroad, or in the worst case spending public money for commercial goals.

A far larger group of patients, estimated at 1500 to 5000 per year for a population of 10 million people, would greatly benefit from HT. This group is growing steadily as new results emerge from the operational HT centres worldwide.

Today it consists of:

- patients for whom the decreased dose of radiation of healthy tissue using HT should drastically improve their life quality by avoiding side effects in these tissues.
- a subgroup of tumours for which the present best treatments do not allow to administer the required radiation dose, because of sensitive tissues in the vicinity.
- very radio-resistant tumours. In their case the required radiation dose on the tumour is much too large and would inadmissibly endanger all tissue in the radiation path.
- paediatric patients because of the very high sensitivity to side effects, impaired growth and development, and secondary induced tumours in the healthy tissue of younger people.

On methods for assessing HT treatment

Since the 2007 KCE study, very interesting publications have been published or others are expected to appear shortly, bringing new information on the benefits and the needs of HT.

Most important however is the facts that, when one does not restrict oneself to the most obvious and direct clinical data, the potentials of HT do dramatically expand. This means that all data (in clinical jargon also the data of “phase I and phase II clinical studies”, “case-based studies” as well as “in-silico studies”) should be used to their full extent whenever they permit to study the comparative effects of HT and standard best practice radiotherapy.

These effects can be expressed in terms of dose distribution in both cancerous and healthy tissues, of biological effects in these tissues, in patient response to them and in epidemiological feedback. A large toolbox for modelling physical, biological and clinical trials is available for the purpose of consolidating this data and should now be fully deployed for the purpose this study!

HT costs unacceptably high?

It is often argued that HT is simply too expensive because of the impressive investment costs as well as the extensive and highly schooled personnel requirements to run such a HT centre. One of the goals of the BHTC study is exactly to compare the cost of HT over the life of a HT eligible cancer patient with other state of the art radiotherapies. Reputed universities and research centres have reported on their experience and almost invariably come to the conclusion that the costs for a QALY (quality adjusted life year) for HT treatments is well below today’s accepted standards for new anti-cancer targeted treatments. This study should cast a clearer light on this matter.

Final remarks

The negative perception of cancer as a fatal, non-treatable disease has greatly been eradicated in the last 4 decades. Radiotherapy has been cornerstone in this evolution by successfully implementing novel diagnostic and treatment technology as well as by optimizing comprehensive treatment modalities. Classical radiotherapy however approaches the end of this long and successful road. Further potential for marginal improvements rapidly becomes alarmingly expensive. Society in its due right however, requires further improvement and expects cancer survivors to restore their quality of life to the pre-treatment level and to maintain it for long.

All arguments for and against HT are no less valid in France, the Netherlands, Germany, Italy and the UK or in Sweden than is the case for Belgium. These countries have decided - very often only after large scale feasibility studies - to invest in HT centres in one or another form.

Biological specificity of Carbon Ion Beam : Present Status and Future Prospects

Claire Rodriguez-Lafrasse

Radiobiologie Cellulaire et Moléculaire, EMR3738, Faculté de Médecine Lyon-Sud, Université Lyon1, Oullins, France
e-mail address : Claire.Rodriguez@sante.univ-lyon1.fr

Abstract

The carbon ions, thanks to their relative biological effectiveness (RBE) much higher than photons' and protons' one and their ballistic characteristics similar to those of protons, can effectively treat radioresistant tumors. The reasons for this increased efficiency are found in the microdosimetric and radiobiological features of ions. The energy deposit or linear energy transfer (LET) is increasing along the range and reaches a very high level at the end producing the Bragg peak where the LET is about 100 times higher than that of photons. These massive energy deposits create complex DNA lesions that are difficult to repair. DNA repair is slow and associated with longer blockage of the cell cycle and more frequent chromosomal aberrations that are lethal to cells. The mechanisms of cell death are largely unchanged, but triggered more efficiently by ions. Radiobiological differences between ions and photons have been studied for some years and many aspects remain to be explored. In general these phenomena tend to reduce the differences of radiosensitivity among different tissues. It is therefore in the situations of relative tumors' radioresistance compared to healthy tissue that carbon ions must be used and not in the reverse situations where the fractionation of low LET radiation is sufficient to provide the necessary differential effect to cure the tumor.

Introduction

Despite very significant improvements, two disadvantages of external beam radiotherapy with photons cannot be completely erased: i) low biological effectiveness of photons causing cell damage repairable in most cases, ii) the dose to healthy tissue surrounding the tumor which inevitably increases regardless of the technical sophistication (or stereotactic IMRT) when the dose should be increased because of the level of radioresistance of the tumor and / or tumor volume exceeding one hundred milliliters. Thus photon radiation is defeated as soon as a certain volume of a tumor, particularly if radioresistant, is surrounded by tissue sensitive enough. Exceeding these limits requires having a type of radiation irradiating a very little amount of healthy tissue, with the ability to deliver the energy it carries only to the tumor and not to the entire crossing of the body and if possible, a radiation producing cell damages not repaired by the tumors. The beams of charged particles of sufficient mass (at least the mass of the proton, which is a hadron) to be free of scattering in the body, provide the ballistic characteristics and dose distribution required, and moreover, if we choose high mass particles (eg carbon ions) the density of energy deposition (high LET) will cause damage that will be very complex and not repairable then lethal for the cells. These two features: the strong anatomic restriction of dose deposition and the increased biological effectiveness are inseparable for the effective implementation of such a radiation, because this increased biological efficiency is indiscriminately true for healthy tissue and tumor and only the accuracy of the dose deposition allows discrimination and therapeutic success. Soon after the discovery of the specific physical characteristics of charged particles in the 1940s, especially by Robert Wilson, their use for treating cancer has been proposed. It took many years for the hadrontherapy to become reality for economic, technical, medical and biological reasons. However, the sustained interest which comes mainly from the biological aspects that constitute the most original feature of ions compared to X-ray photons which is due above all to the extraordinary density of energy deposit in their tracks.

Relative biological effectiveness of carbon ions

Physical qualities of carbon ion beams result in the biological benefits of their use in radiotherapy. Their high LET relative to photons is able to induce more complex radiation damages in the DNA of tumor cells. These damages, more difficult to repair, thus lead to a very significant increase in cell killing. This increase effect is quantified by the concept of relative biological effectiveness (RBE). The RBE is defined as the ratio of doses of the reference radiation (X rays) and radiation studied (carbon ions) that produce an identical biological effect [1]. It depends on many parameters such as dose and LET of the radiation but also the biological effect considered

and the cell or tissue type studied. For carbon ions, the RBE determined from survival curves of different tumor cell lines using as criterion the ratio of dose to 10% survival is depending on the TEL from 1.1 (beginning of the plateau at 13 keV / µm) and 3 (Bragg peak at 180 keV / µm) [2-5]. RBE has been calculated less frequently from the rate of apoptosis (same order of magnitude) [1] or that of chromosomal aberrations (10 to 40) [6]. Finally, comparison of the clinical beam of GSI (Darmstadt) and NIRS (Chiba) [7] showed similar RBE's for various TEL, either after irradiation in single or fractionated dose.

Radiobiological specificities of carbon ions

1. Direct / indirect effect

While low LET radiation such as photons act mainly by indirect effect involving the radiolysis of water (60-70%), the respective proportion of direct and indirect effects in response to carbon ions remains controversial. The predominance of direct effects (80%) was initially described [8] and could be explained by the high density of ionization and excitation compared to the more diffuse distribution of these events for low LET radiation, which therefore have a greater probability of ionization of water molecules. More recent works, however, favor the hypothesis of an indirect effect mainly through the study, in plasmid or cellular systems, of oxidized bases [9] or the protective effect of DMSO [10,11].

About free radicals, formed along the trajectories of carbon ions representing areas of high ionization density, they tend to recombine with each other and therefore not spreading away. This results in a clear decrease in the yield of radiolytic free radical $OH^{\cdot}$, aqueous e- and $H^{\cdot}$ compared to radiation of low-TEL, while the yield of the molecular species H2 and H2O2 increases. In addition, superoxide radicals ($O2^{-\cdot}$) and their protonated form ($HO2^{\cdot}$) are formed in large quantities in the heart of traces, even in the absence of oxygen [12]. These are, among others, the source of secondary production of peroxynitrite ONOO- toxic for the cells, and H2O2, able to release oxygen, which is a potent radiosensitizer. These phenomena would partly explain the decrease in the oxygen effect observed in response to carbon ions. Indeed, the OER (Oxygen enhancement ratio), defined as the ratio of doses required to achieve a particular biological effect depending on whether the system is in condition of hypoxia or normoxia is approximately 3 for X-ray and near 1 for carbon ions at high LET.

2. DNA complex lesions

At the beginning of the track of an ionizing particle such as carbon ions, discrete lesions (isolated) of DNA are produced, such as bases or sugars oxidations, abasic sites, single strand breaks (SSB) and double strand (DSB). While the kinetic energy of particles decreases, their LET increases and simultaneously the diameter of the track is reducing, resulting in much denser ionizations. This densification then generates complex damage to the DNA molecule, called Locally Multiple Site Damaged (LMDS) whose spatial distribution is located. Since the work of Ward in 1988 [13], LMDS are considered a signature of high LET radiations. Currently, these complex lesions are defined by the existence of at least two localized damage on twenty pairs of adjacent bases [14]. Characterization came from multiple parameters such as the types of damage (changes in sugars and bases or strand breaks), number (related to the nature of radiation) and their relative distribution along DNA strands [15]. Three configurations of LMDS are defined: tandem lesions (SSB, oxidized base or abasic site on the same strand of DNA); lesions on the two complementary DNA strands « non-DSB oxydated clustered DNA lesions = OCDL » without initial DSB or with complex DSB (cDSB) associated with base oxidations and / or abasic sites [16]. The complexity of LMDS increases with the increase of the LET [17]. The hypothesis proposed by Shikazono et al. [14] is that, depending on the TEL, OCDL damages decrease while increasing the complexity of the lesions, thus promoting the appearance of cDSB in increasing numbers with the LET.

3. DNA repair

Repair of LMDS does not set specific repair system but involves all the processes described classically. This is the BER system (base excision repair) for the repair of oxidized bases, abasic sites, and CSB; the NHEJ (non homologous end-joining) system to repair DSB working throughout the cell cycle, whereas the homologous recombination is occurring in late phase S and G2 / M. The hierarchy of response of these systems is extremely difficult to establish, due to the variety of possible combinations of lesions in the LMDS and the large number of proteins involved. Activation of BER creates intermediates repair patterns modifying the initial conformation of the lesions, and even the local structure of DNA. For example on OCDL, the presence of abasic sites on opposite

strands but separated by at least 5 base pairs resulted in 85% of the cases to the formation of a DSB [14]. The complexity of LMDS, related to the increase of LET, will influence the rate of repair by open competition of the different systems [14,15]. The kinetics of disappearance γ H2AX foci (DSB repair) following irradiation with carbon ions of 70 keV / µm is much slower than the response to an irradiation of 13 keV / µm [18]. The complexity of LMDS also influences repair capabilities. For example, 40% of tandem lesions involving 8-oxo-purine cannot be repaired by the BER [19]. Replication of DNA before complete repair of the lesions may further increase the complexity of the lesions and produce a double-strand break difficult to repair [20] or leads to the integration of mutations due to base repair default. Complex lesions are therefore specific genotoxic damage that can impede the DNA repair systems.

4. Cell cycle arrest

High LET radiations induce blockages in the cell cycle much longer than those of low LET's [21-23]. The duration of the blocking correlates with the number and complexity of damages in the resistant tumor cell lines, which should facilitate their repair [24]. Preferential arrest in the G1 phase of the cycle has been described for a glioma cell line with a functional p53 irradiated with carbon ions, LET between 20 and 40 keV / µm [21], but not beyond 80 keV / µm. However, stopping in G2 / M phase is usually observed in response to irradiation with carbon ions, whether in colon tumor cell lines [22], glioblastoma [23,25,26], or head and neck cancer [27]. Few studies have examined the cell cycle regulatory proteins, they showed that the blockage in G2 / M was associated with the phosphorylation of proteins Wee1 and Cdc2 [28] and protein Chk1 [27]. Finally, the majority of the work agreed to conclude the absence of p53 status role in the induction of stopping in G2 / M phase after irradiation with carbon ions [25].

5. Chromosomal aberrations - Genetic instability

Chromosomal abnormalities are a direct consequence of the persistence of DNA damage, breakage or chromosome deletions resulting from unrepaired DSB while chromosomal rearrangements derived from DSB generally poorly repaired due to default of NHEJ system [29]. Chronologically, the events identified as early in tumor cells in response to irradiation by carbon ions are deletions associated with chromosome breaks, often leading to cell death. Then simple rearrangements (dicentrics and translocations) are observed and finally complex rearrangements (involving at least three unrepaired breaks events involving two different chromosomes) [30, 6]. They are observed in response to carbon ions regardless of the dose and unlike photons. The number and severity of complex rearrangements increase, compared to simple rearrangements, with the dose and LET of carbon ions. The effectiveness of carbon ions to kill cells is due to complex chromosomal exchanges that prevent cell to pass mitosis [31]. Some intrinsic factors may influence the occurrence of chromosomal aberrations. Thus, cells resistant to carbon irradiation are repairing damage faster, show less deletions and complex rearrangements than radiosensitive cells. A dose of 1 Gy is necessary to induce at least one complex rearrangement in 50% of MCF7 cells radiosensitive type, whereas for the resistant line WiDr, 4Gy are needed [30]. Other intrinsic factors such as cellular protection systems against oxygen free radicals, particularly glutathione, can limit the number of radiation-induced deletions [32]. Finally, the geometry of the tracks of particles passing through the cell nuclei or the distribution of chromosomal territories also appear to alter the number of complex rearrangements [6]. The long-term consequences of the aberrations observed in the progeny of tumor cells surviving to carbon irradiation are to be determined.

6. Cell death

The establishment of cell survival curves in different tumor models demonstrated the superior efficacy of carbon ions compared to photons to induce clonogenic death. Understanding the increased RBE needs to compare the types of cell death involved in response to both types of radiation. All types of cell death have been described in response to carbon ions. The works of our group [27] have shown that the death process involved did not depend on LET, but on the cell type and therefore is part of the intrinsic radiosensitivity.

Apoptosis

It is now well established that carbon ions induce a greater level of apoptosis than X-rays in different types of human tumor cell lines and that it increases with the LET [25.33] [27]. In addition, Takahashi et al. [34] have demonstrated the effectiveness of carbon ions to induce apoptosis in vivo on sections of human brain tumors

introduced in mice as xenograft. Since over 50% of human cancers have non-functional p53 protein, many studies have focused on the relationship between p53, the apoptotic death and tumor radiosensitivity. Most of them show that there is no difference in survival or the induction of apoptotic death of tumor cells with different p53 status after irradiation with carbon ions, in contrast to the response to X-rays However, two studies show that glioblastoma cell lines lacking functional p53 are more resistant to irradiation even with carbon ions [35.21]. The signaling pathway of the apoptotic mechanisms involves a p53-independence, the mitochondria [36] and the caspase cascade [37] [38]. This p53-independent pathway was recently identified as involving ceramide [39], a second messenger derived from membrane lipids. The production of ceramide is present regardless of p53 status, and acts upstream of mitochondrial damage and the caspases and correlates with the level of apoptosis [40].

Mitotic death

Mitotic catastrophe, abrupt loss of the ability to successfully complete mitosis, is the predominant mechanism of cell death induced by ionizing radiation. It occurs as a result of the accumulation of chromosomal aberrations and is characterized by the formation of multinucleated giant cells and of micronuclei. This type of cell death is still very little studied in response to high LET radiations. Holgersson et al, [37] demonstrated the presence of multinucleated cells in response to irradiation by nitrogen ions of glioblastoma cell lines. In response to carbon ions, this process has been clearly identified in a line of radioresistant head and neck squamous cell carcinoma [27]. Although mitotic catastrophe is a clearly oriented towards cell death (linked to necrosis or late apoptosis), a mechanism of depolyploïdization back in the cell cycle may also help the survival of some tumor cells [41] . The cell population subject to this mechanism is composed in part of cancer stem cells which could be the cause of local recurrence [42].

Necrosis

Very few articles are about cell death by necrosis, its induction appears to depend on carbon ions LET but is independent of p53 status [43,44]. In addition, it is not an alternative mechanism of death to apoptosis in the presence of a mutation in p53.

Senescence

Replicative or premature senescence is defined as a process leading to a slowdown and an irreversible cessation of cell division. This process, found in response to photon irradiation, involves the p53 pathways and / or p16-pRb [45]. Premature senescence has been described [46] in response to irradiation by carbon ions in glioblastoma cell lines with a functional p53 protein or not.

Autophagy

Autophagic death, characterized by a set of catabolic processes leading to the degradation of cellular components by the lysosome, was found after exposure to carbon ions in cells of liver tumors [47] or glioblastomas with p53 status, wild or mutated [48] [46].

Conclusion

The use of high LET ion to cure cancer made biologists aware once again of the extreme complexity of events leading from an energy deposition in cell to cell death. The ability to bypass the phenomena of radioresistance by this radiation represents a new tool for understanding the molecular mechanisms involved, but also to anticipate and manage them more efficiently. The fact remains that all these phenomena are quite similar from a cell line to another, and especially since it uses higher LET radiation, which is the major advantage of radiation therapy. Indeed, it is much less limited in its effectiveness by tumor heterogeneity, which is the major obstacle of anti-neoplastic targeted therapies continuously renewed and diversified but which allowed up to now only a modest decline of the limits of the cancer disease.

References

[1] Ando K, Kase Y. Biological characteristics of carbon-ion therapy. Int. J. Radiat. Biol. 2009;85:715-728.

[2] Weyrather WK, Ritter S, Scholz M, Kraft G. RBE for carbon track-segment irradiation in cell lines of differing repair capacity. Int. J. Radiat. Biol. 1999;75:1357-1364.

[3] Iwadate Y, Mizoe J, Osaka Y, Yamaura A, Tsujii H. High linear energy transfer carbon radiation effectively kills cultured glioma cells with either mutant or wild-type p53. Int. J. Radiat. Oncol. Biol. Phys. 2001;50:803-808.

[4] Suzuki M, Kase Y, Yamaguchi H, Kanai T, Ando K. Relative biological effectiveness for cell-killing effect on various human cell lines irradiated with heavy-ion medical accelerator in Chiba (HIMAC) carbon-ion beams. Int. J. Radiat. Oncol. Biol. Phys. 2000;48:241-250.

[5] Beuve M, Alphonse G, Maalouf M, Colliaux A, Battiston-Montagne P, Jalade P, et al. Radiobiologic parameters and local effect model predictions for head-and-neck squamous cell carcinomas exposed to high linear energy transfer ions. Int. J. Radiat. Oncol. Biol. Phys. 2008;71:635-642.

[6] Ritter S, Durante M. Heavy-ion induced chromosomal aberrations: A review. Mutat Res. 2010;701:38-46.

[7] Uzawa A, Ando K, Koike S, Furusawa Y, Matsumoto Y, Takai N, et al. Comparison of biological effectiveness of carbon-ion beams in Japan and Germany. Int. J. Radiat. Oncol. Biol. Phys. 2009;73:1545-1551.

[8] Roots R, Chatterjee A, Chang P, Lommel L, Blakely EA. Characterization of hydroxyl radical-induced damage after sparsely and densely ionizing irradiation. Int. J. Radiat. Biol. Relat. Stud. Phys. Chem. Med. 1985;47:157-166.

[9] Douki T, Ravanat J, Pouget J, Testard I, Cadet J. Minor contribution of direct ionization to DNA base damage inducedby heavy ions. Int. J. Radiat. Biol. 2006;82:119-127.

[10] Usami N, Furusawa Y, Kobayashi K, Lacombe S, Reynaud-Angelin A, Sage E, et al. Mammalian cells loaded with platinum-containing molecules are sensitized to fast atomic ions. Int. J. Radiat. Biol. 2008;84:603-611.

[11] Hirayama R, Ito A, Tomita M, Tsukada T, Yatagai F, Noguchi M, et al. Contributions of direct and indirect actions in cell killing by high-LET radiations. Radiat. Res. 2009;171:212-218.

[12] Meesungnoen J, Jay-Gerin J. High-LET ion radiolysis of water: oxygen production in tracks. Radiat. Res. 2009;171:379-386.

[13] Ward JF. DNA damage produced by ionizing radiation in mammalian cells: identities, mechanisms of formation, and reparability. Prog. Nucleic Acid Res. Mol. Biol. 1988;35:95-125.

[14] Shikazono N, Noguchi M, Fujii K, Urushibara A, Yokoya A. The yield, processing, and biological consequences of clustered DNA damage induced by ionizing radiation. J. Radiat. Res. 2009;50:27-36.

[15] Sage E, Harrison L. Clustered DNA lesion repair in eukaryotes: Relevance to mutagenesis and cell survival. Mutat Res [Internet]. 2010 Déc 24 [cité 2011 Fév 18];Available from: http://www.ncbi.nlm.nih.gov.gate2.inist.fr/pubmed/21185841

[16] Hada M, Georgakilas AG. Formation of clustered DNA damage after high-LET irradiation: a review. J. Radiat. Res. 2008;49:203-210.

[17] Nikjoo H, O'Neill P, Wilson WE, Goodhead DT. Computational approach for determining the spectrum of DNA damage induced by ionizing radiation. Radiat. Res. 2001;156:577-583.

[18] Rothkamm K, Löbrich M. Evidence for a lack of DNA double-strand break repair in human cells exposed to very low x-ray doses. Proc. Natl. Acad. Sci. U.S.A. 2003;100:5057-5062.

[19] Bergeron F, Auvré F, Radicella JP, Ravanat J. HO* radicals induce an unexpected high proportion of tandem base lesions refractory to repair by DNA glycosylases. Proc. Natl. Acad. Sci. U.S.A. 2010;107:5528-5533.

[20] Harper JV, Anderson JA, O'Neill P. Radiation induced DNA DSBs: Contribution from stalled replication forks? DNA Repair (Amst.). 2010;9:907-913.

[21] Tsuboi K, Moritake T, Tsuchida Y, Tokuuye K, Matsumura A, Ando K. Cell cycle checkpoint and apoptosis induction in glioblastoma cells and fibroblasts irradiated with carbon beam. J. Radiat. Res. 2007;48:317-325.

[22] Topsch J, Scholz M, Mueller-Klieser W. Radiobiological characterization of human tumor cell multilayers after conventional and particle irradiation. Radiat. Res. 2007;167:645-654.

[23] Holgersson A, Heiden T, Castro J, Edgren MR, Lewensohn R, Meijer AE. Different G2/M accumulation in M059J and M059K cells after exposure to DNA double-strand break-inducing agents. Int. J. Radiat. Oncol. Biol. Phys. 2005;61:915-921.

[24] Ljungman M. The DNA damage response--repair or despair? Environ. Mol. Mutagen. 2010;51:879-889.

[25] Tsuboi K, Moritake T, Tsuchida Y, Tokuuye K, Matsumura A, Ando K. Cell cycle checkpoint and apoptosis induction in glioblastoma cells and fibroblasts irradiated with carbon beam. J. Radiat. Res. 2007;48:317-325.

[26] Tsuboi K, Tsuchida Y, Nose T, Ando K. Cytotoxic effect of accelerated carbon beams on glioblastoma cell

lines with p53 mutation: clonogenic survival and cell-cycle analysis. Int. J. Radiat. Biol. 1998;74:71-79.
[27] Maalouf M, Alphonse G, Colliaux A, Beuve M, Trajkovic-Bodennec S, Battiston-Montagne P, et al. Different Mechanisms of Cell Death in Radiosensitive and Radioresistant P53 Mutated Head and Neck Squamous Cell Carcinoma Cell Lines Exposed to Carbon Ions and X-Rays. International Journal of Radiation Oncology*Biology*Physics. 2009;74:200-209.
[28] Matsumura S, Matsumura T, Ozeki S, Fukushima S, Yamazaki H, Inoue T, et al. Comparative analysis of G2 arrest after irradiation with 75 keV carbon-ion beams and 137Cs gamma-rays in a human lymphoblastoid cell line. Cancer Detect. Prev. 2003;27:222-228.
[29] Geard CR, Ponnaiya B. Chromosomal changes and cell cycle checkpoints in Mammalian cells. Methods Mol. Biol. 2004;241:315-328.
[30] Virsik-Köpp P, Hofman-Huether H. Chromosome aberrations induced by high-LET carbon ions in radiosensitive and radioresistant tumour cells. Cytogenet. Genome Res. 2004;104:221-226.
[31] Lee R, Sommer S, Hartel C, Nasonova E, Durante M, Ritter S. Complex exchanges are responsible for the increased effectiveness of C-ions compared to X-rays at the first post-irradiation mitosis. Mutat Res. 2010;701:52-59.
[32] Hanot M, Boivin A, Malesys C, Foray N, Douki T, Ardail D, et al. Glutathione Depletion Potentiates DNA Damage and Prevents Transmissible Chromosomal Aberrations Induced by Carbon Ions in Oral Cancers. Submitted.
[33] Meijer AE, Jernberg AR, Heiden T, Stenerlöw B, Persson LM, Tilly N, et al. Dose and time dependent apoptotic response in a human melanoma cell line exposed to accelerated boron ions at four different LET. Int. J. Radiat. Biol. 2005;81:261-272.
[34] Takahashi A, Matsumoto H, Furusawa Y, Ohnishi K, Ishioka N, Ohnishi T. Apoptosis induced by high-LET radiations is not affected by cellular p53 gene status. Int. J. Radiat. Biol. 2005 ;81:581-586.
[35] Coelho D, Fischer B, Holl V, Dufour P, Denis JM, Guoulette J, et al. Induction of apoptosis by high linear energy transfer radiation: role of p531. Can. J. Physiol. Pharmacol. 2002;80:644-649.
[36] Mori E, Takahashi A, Yamakawa N, Kirita T, Ohnishi T. High LET heavy ion radiation induces p53-independent apoptosis. J. Radiat. Res. 2009;50:37-42.
[37] Holgersson A, Jernberg AR, Persson LM, Edgren MR, Lewensohn R, Nilsson A, et al. Low and high LET radiation-induced apoptosis in M059J and M059K cells. Int. J. Radiat. Biol. 2003;79:611-621.
[38] Yamakawa N, Takahashi A, Mori E, Imai Y, Furusawa Y, Ohnishi K, et al. High LET radiation enhances apoptosis in mutated p53 cancer cells through Caspase-9 activation. Cancer Sci. 2008;99:1455-1460.
[39] Alphonse G, Aloy MT, Broquet P, Gerard JP, Louisot P, Rousson R, Rodriguez-Lafrasse C. Ceramide induces activation of the mitochondrial/caspases pathway in Jurkat and SCC61 cells sensitive to gamma-radiation but activation of this sequence is defective in radioresistant SQ20B cells. Int J Radiat Biol. 2002;78:821-35.
[40] Kolesnick R, Fuks Z. Radiation and ceramide-induced apoptosis. Oncogene. 2003;22:5897-5906.
[41] Vakifahmetoglu H, Olsson M, Zhivotovsky B. Death through a tragedy: mitotic catastrophe. Cell Death Differ. 2008;15:1153-1162.
[42] Boivin A, Hanot M, Malesys C, Maalouf M, Rousson R, Rodriguez-Lafrasse C, Ardail D. Transient alteration of cellular redox buffering before irradiation triggers apoptosis in head and neck carcinoma stem and non-stem cells. PLoS One. 2011;6:e14558.
[43] Takahashi A, Matsumoto H, Yuki K, Yasumoto J, Kajiwara A, Aoki M, et al. High-LET radiation enhanced apoptosis but not necrosis regardless of p53 status. Int. J. Radiat. Oncol. Biol. Phys. 2004;60:591-597.
[44] Hamada N, Imaoka T, Masunaga S, Ogata T, Okayasu R, Takahashi A, et al. Recent advances in the biology of heavy-ion cancer therapy. J. Radiat. Res. 2010;51:365-383.
[45] Jones KR, Elmore LW, Jackson-Cook C, Demasters G, Povirk LF, Holt SE, et al. p53-Dependent accelerated senescence induced by ionizing radiation in breast tumour cells. Int. J. Radiat. Biol. 2005;81:445-458.
[46] Jinno-Oue A, Shimizu N, Hamada N, Wada S, Tanaka A, Shinagawa M, et al. Irradiation with carbon ion beams induces apoptosis, autophagy, and cellular senescence in a human glioma-derived cell line. Int. J. Radiat. Oncol. Biol. Phys. 2010;76:229-241.
[47] Altmeyer A, Jung AC, Ignat M, Benzina S, Denis J, Gueulette J, et al. Pharmacological enhancement of autophagy induced in a hepatocellular carcinoma cell line by high-LET radiation. Anticancer Res. 2010;30:303-310.
[48] Benzina S, Altmeyer A, Malek F, Dufour P, Denis J, Gueulette J, et al. High-LET radiation combined with oxaliplatin induce autophagy in U-87 glioblastoma cells. Cancer Lett. 2008;264:63-70.

RBE of therapeutic Hadron Beams at Clinical Facilities and the Intercomparison

Yoshiya Furusawa[1], Koichi Ando[2], Mizuho Aoki-Nakano[1], Akiko Uzawa[1], Yoshitaka Matsumoto[1], Ryoichi Hirayama[1], Nobuhiko Takai[1], Ryonfa Lee[3], Silvia Ritter[3], and Michael Scholz[3],

[1]*Research Center for Charged Particle Therapy, National Institute of Radiological Sciences, Chiba, Japan,*
[2]*Heavy-ion Medical Center, Gunma University, Gunma, Japan,*
[2]*GSI, Biophysik, Darmstadt, Germany*
Corresponding Author: Yoshiya Furusawa, e-mail address: furusawa@nirs.go.jp

ABSTRACT

To compare the biological effectiveness of 6 cm SOBP carbon ion therapy beams between the GSI and NIRS. We tested the survival of human salivary gland tumor HSG cells and the crypt survival of C3H mice exposed to HIMAC and GSI carbon therapeutic beams with a 6 cm SOBP. The relative biological effectiveness of the SOBP beams was uniform, and no significant differences were noted when the depth-dose distribution was similar. However the depth-dose distribution between the HIMAC passive beam and the 4Gy RBE GIS spot scanning beam with LEM-I showed were different.

INTRODUCTION

The HIMAC (Heavy-ion Medical Accelerator in Chiba) was constructed in 1993, and clinical trials with carbon ions started in 1994, together with academic research activities, including studies related to physics, engineering, and biology. Pre-clinical radiobiological studies were performed to estimate the clinical RBE for carbon beams before the start of clinical trials. At the same time, another clinical trial, also using carbon ions, was started at GSI, in Germany. The treatment systems were developed individually at each facility and the procedures to obtain the SOBP field were different. The HIMAC employs a passive system, while the GSI uses a spot scanning method. We hypothesized that the biological effectiveness may be different for these facilities, and performed a biological experiment to determine the differences between the HIMAC and GSI. Following the development of the HIMAC, several additional hadron therapy facilities (HARIMAC; Hyogo, NCCHE; Kashiwa, WERC; Tsuruga, PMRC; Tsukuba, SCC; Shizuoka, GHMC; Gunma, WERC/FPH-PTC; Fukui) started or will soon be starting treatments in Japan. We have evaluated the RBE of each of the hadron beams for the HIMAC and all of these facilities with the same biological system and technical staff. We expose cells and mice at the facility using methods that were established during pre-clinical radiobiological studies at the HIMAC.

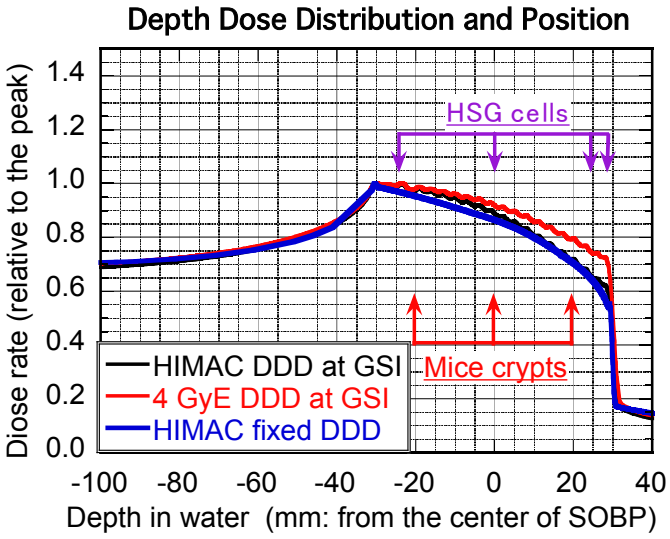

Fig. 1. Irradiation positions in the 6 cm SOBP for HSG cells and mouse crypts at the HIMAC and GSI.

MATERIALS AND METHODS

Irradiation system

The details of each irradiation system and the treatment planning system are provided elsewhere (REFS). We used the same system used for patient treatment at each facility for the biological experiments. We also set biological samples on the patient couch except for at the HIMAC. Each 6-cm SOBP carbon beam was used, and samples were set at the middle of the SOBP (+/-0), and at the +20 and -20 mmH_2O positions for the mouse crypt experiment and at the 0, -25, +25, and +28 mmH_2O positions for the cell experiment.

The depth-dose distribution (DDD) at the HIMAC and the 4 GyE (RBE) DDD at GSI are shown in Figure 1, together with the GSI DDD that fits to the HIMAC DDD.

Fig. 2. A cell-stack irradiation chamber.

Cell experiment

HSG (Human salivary gland tumor original) cells were cultured in E-MEM medium supplemented with 10% Fetal Bovine Serum and antibiotics in humidified air containing 5% CO_2 at 37ºC. The cells were seeded at a concentration of $5x10^5$ cells per T25 flask, or at a concentration of $1.5x10^5$ cells per 25 mm culture cover slip in a 35 mm Petri dish 1.5 days before irradiation. The cells on cover slips were transferred at defined depth positions in the SOBP of special made chambers of the so called "cell-stack" device (Fig. 2), and filled with medium before irradiation.

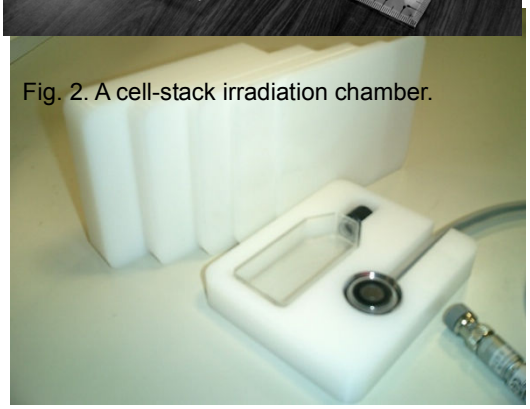

Fig. 3. Irradiation materials for culture bottles and the ionization chamber

Cell exposure was performed at the Medical Cave in GSI and the Biology Experiment Port at HIMAC in the NIRS. The dose distribution at GSI was adjusted to be the same as that at the HIMAC for the primary intercomparison experiments, or conformed to the 4GyE dose distribution at GSI treatment planning for the second series of experiments. For the second series of experiments, culture bottles were set with polypropylene blocks having different thicknesses to adjust the irradiation depth to be the same as the cell-stack irradiation position (Fig. 3).

Irradiated cells were harvested in medium by trypsinization, the cell concentration was determined, and cells were diluted then seeded at an adequate number in each of three 60 mm Petri dishes to obtain approximately 100 colonies. Colonies consisting of more than 50 cells were counted as survivors after 13 days of incubation post-irradiation.

The Mouse experiment

Female C3H/He mice aged 10-14 weeks were transported from the NIRS to GSI. They were fed with standard pellets and provided drinking water *ad libitum*. Shortly before irradiation, the mice received an intraperitoneal injection of 0.2 ml anesthesia (13.79 mg/ml ketamine and 0.69 mg/ml xylazine in a NaCl solution). Two (2) mice were placed in a jig specially designed for the gut irradiation experiment, and received carbon ion radiation. Carbon ions with various mono-energies scanned mouse whole body so that mouse gut was irradiated in the desired positions within a 6-cm SOBP. We selected 3 positions within the

SOBP; the proximal, middle and distal positions were respectively located at -20 mm from the center, in the center and + 20 mm from the center. Three and a half days after irradiation, the mouse jejunums were removed and fixed in formalin. Cross sections of the jejunum were prepared for histology, and used to count crypts under light microscopy.

For the NIRS experiments, materials and methods identical to GSI experiments were used, except that a fixed energy of 290 MeV/u carbon ions was spread by a ridge filter to make a 6-cm SOBP.

RESULTS AND DISCUSSION

Survival of HSG Cells

The survival curves for HSG cells exposed at GSI using the HIMAC DDD at different positions or at the entrance are shown in Figure 3. The curve showed the highest efficiency at the high dose region and the largest shoulder at the proximal position. That for the distal or distal end showed smaller shoulders, indicating the contribution of higher LET beams.

These data were analyzed together with the cell-stack data that were obtained after GSI-style dose distribution performed at GSI and experiments performed at the HIMAC. The depth-dose distribution was designed to show an uniform effectiveness at 4 GyE by the therapeutic treatment planning system at GSI. The D_{10} values to the depth position in the SOBP are shown in Figure 4 compared with that at the entrance at the HIMAC. The results showed a good agreement with the HIMAC SOBP beam, and the biological DDD in the SOBP was within +/- 6.5% for all depth positions (proximal, middle, distal and distal end) at the 10% survival level when the exposures were defined with the peak dose.

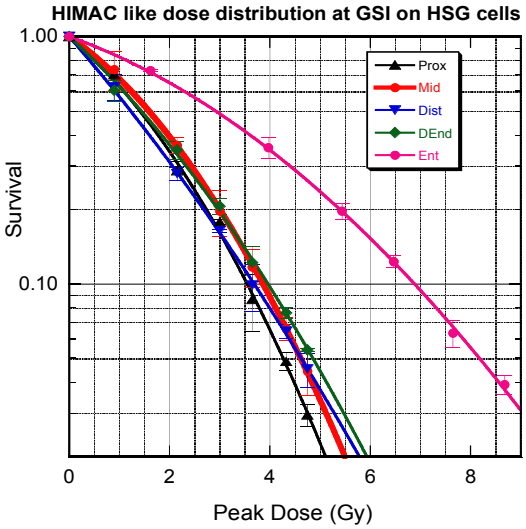

Fig.4. Survival curves of HSG cells exposed to a SOBP beam having the HIMAC SOBP DDD in T25 culture flasks at GSI at different positions.

Crypt Survival of Mice

The three irradiation positions within the 6-cm SOBP are shown in Figure 1. Crypt survival curves obtained for both the NIRS and GSI carbon ions showed 3 separate curves, meaning that the biological effectiveness of the 3 positions depends on the position, as expected. Figure 6 shows a comparison between the curves from the GSI and the NIRS beams. The survival curves were well matched between the GSI and NIRS experiments, indicating that the biological effectiveness of therapeutic carbon ions is almost identical between the GSI and the NIRS facilities.

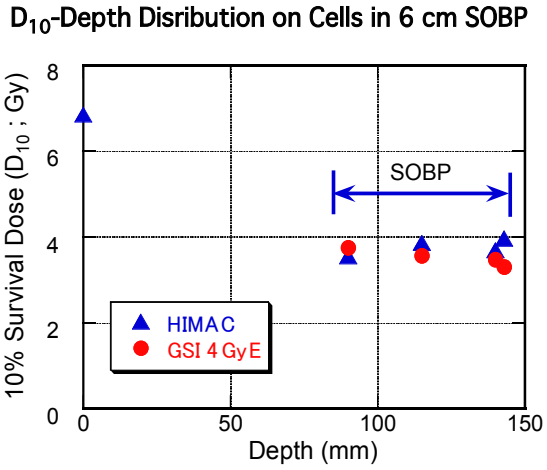

Fig. 5. The D_{10} dose for HSG cells survival in a 6 cm SOBP at the HIMAC and GSI

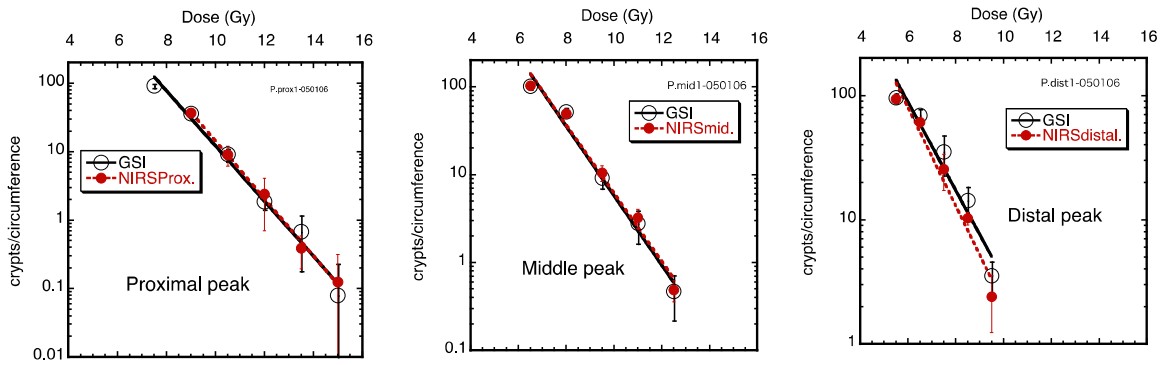

Fig. 6. Comparison of crypt survivals between GSI and NIRS. Left: proximal, Middle: middle, Right: distal positions in the 6 cm SOBP carbon beam.

References

[1] Furusawa Y, Fukutsu K, Aoki M, *et al.* Inactivation of aerobic and hypoxic cells from three different cell lines by accelerated 3He-, 12C- and 20Ne-ion beams. *Radiat Res* **154**; 485-496. (2000).

[2] Ando K, Furusawa Y, Suzuki M, *et al.* Relative biological effectiveness of the 235 MeV proton beams at the National Cancer Center Hospital East. *J Radiat Res* **42**; 79-89. (2001).

[3] Kagawa K, Furusawa Y, Ando K, et al. Preclinical biological assessment of proton and carbon ion beams at Hyogo Ion Beam Medical Center. *Int J Radiat Oncol Biol Phys* **54**; 928-938. (2002)

[4] Demizu Y, Kagawa K, Furusawa Y, et al. Cell biological basis for combination radiotherapy using heavy-ion beams and high-energy X-rays. *Radiother Oncol* **71**; 207-211. (2004)

[5] Ando K, Koike S, Uzawa A, *et al.* Biological gain of carbon-ion radiotherapy for the early response of tumor growth delay and against early response of skin reaction in mice. *J Radiat Res* **46**; 51-57. (2005)

[6] Ando K, Koike S, Uzawa A, *et al.* Tumor induction in mice locally irradiated with carbon ions: a retrospective analysis. *J Radiat Res* **46**; 185-190. (2005)

[7] Ando K, Koike S, Uzawa A, *et al.* Repair of skin damage during fractionated irradiation with gamma rays and low-LET carbon ions. *J Radiat Res* **47**; 167-174. (2006)

[8] Uzawa A, Ando K, Furusawa Y, *et al.* Biological intercomparison using gut crypt survivals for proton and carbon-on beams. *J Radiat Res* **48s**; A75-A80. (2007)

[9] Baek HJ, Kim TH, Shin D, *et al.* Radiobiological Characterization of Proton Beam at the National Cancer Center in Korea. *J Radiat Res* **49**; 509-515. (2008)

[10] Uzawa A, Ando K, Koike S, *et al.* Comparison of Biological effectiveness of Carbon-Ion Beams in Japan and Germany. *Int J Radiat Oncol Biol Phys* **73**; 1545-1551. (2009)

[11] Ando K, Aoki M, and Furusawa Y. Measurement of RBE of Carbon Ions for Cells, Tumor Response and Tissue Reactions in Experimental Systems. *In "Technical Reports Series* **461"**, Annex III, pp. 120-134, Int'l Atomic Energy Agency. (2008)

RBE modelization: Present Status and Future Prospects

D. Dabli [1], G.Montarou [1], M.Beuve[2] and C. Rodriguez-Lafrasse [3]

[1] Clermont Université, Université Blaise Pascal, CNRS/IN2P3, Laboratoire de Physique Corpusculaire, BP 10448, F-63000 Clermont-Ferrand, France

[2] IPNL, LIRIS, IN2P3/CNRS, Université Lyon1, Villeurbanne, France.

[3] Laboratoire de Radiobiologie Cellulaire et Moléculaire, EA3738, Faculté de Médecine Lyon-Sud, Université Lyon 1, Université de Lyon, Oullins, France

.e-mail address: dabli@clermont.in2p3.fr

Abstract

The main objective of this presentation is to review the RBE simulation models considered for application in hadrontherapy planning treatment. We focus on the two most advanced models for clinical application which are the Microdosimetric Kinetic Model and the Local effect Model. We present the formalism of the both models and a comparison of their basic concepts. Then we apply the MKM using the published data for HSG cell lines in order to compare our results with other published MKM results for the same cell line. Finally we apply the MKM for head and neck squamous cell carcinomas (SCC61 and SQ20B Cells) exposed to high LET ions. The results obtained with the Microdosimetric Kinetic model are analyzed and the model parameters of the SCC61 and SQ20B cell lines are compared in term of radiosensitivity to high-LET ions. We have seen that the parameters obtained in this study for both cell lines reflect the difference in their radiosensitivity. All these results are discussed in terms of parameter analysis and comparison between cell lines, benefits and limits of the MK model and leads to some prospects.

Introduction

Cell survival to ionizing radiations is a relevant biological endpoint to plan radiotherapy and hadrontherapy treatments since it can be linked to the probability of tumor control. Generally, cell survival is estimated by *in-vitro* measurements of cell-survival curves. To be integrated into a treatment planning system, experimental data have to be accurately reproduced by a model, which can predict survival values at any dose. In the field of radiotherapy with light ions (hadrontherapy), cell survival depends not only on dose, but also on ion species and ion energy. Consequently, a complex model is needed in order to take into account for the biological dependence of the radiation. Then, several models have been proposed to describe the biological efficiency of radiation on cells. The assumptions and formalisms of these models evolve with the development of knowledge in radiobiology. However the complexity of the radiochemical and radiobiological mechanisms involved in the formation of biological damages complicates the elaboration of such models. Consequently, some models, based on assumptions and approximations extrapolated from experimental results allow useful predictions. Most of the recent models are based on micrometric and nanometric scale calculation. Among others, two models have been the subject of study and development in the context of applications to hadrontherapy treatment planning. These models are the Local Effect Model (LEM) [1][2] and the Microdosimetric Kinetic Model (MKM) [3][4]. The LEM is already used in clinical routine in Germany [5] and the MKM is seriously considered by NIRS group, which has published several studies testing this model in order to adapt it to their treatment planning system [6][7]. Therefore, we focus in this paper on both these models and applied the MKM model to three cell lines.

Material and method

1. The LEM formalism

To predict cell survival, the Local Effect Model (LEM), considers that cell killing arises from the induction of lethal events by the ionizing radiation. Assuming that the distribution of lethal events obeys a Poisson distribution, the probability for the cell to survive reads:

$$S(D) = e^{-N_{lethal}(D)} \quad (1)$$

Where $N_{lethal}(D)$ is the mean number of lethal events induced in the cell after a dose *D*. The first key assumption of the LEM is to consider lethal events as point-like events generated by the local dose deposited by the radiation. Thus, the number of lethal events in the cell is the summation of the local lethal events over the cell sensitive volume:

$$N_{lethal}(D) = \iiint_{\text{Sensitive Volume}} \rho_{lethal}(\mathbf{r})d\mathbf{r} \quad (2)$$

Where the local density of lethal events is assumed to be a simple function of the local dose ***d(r)***:

$$\rho_{lethal}(\mathbf{r}) = \rho_{lethal}(d(\mathbf{r})) \quad (3)$$

In the LEM, the local dose is calculated by cumulative effects, superimposing the local dose deposited by each ion, which is represented by the radial dose d_R :

$$d(\mathbf{r}) = \sum_i d_R(r_i) \quad (4)$$

Where r_i is the radial distance of the point r to the trajectory of the i^{th} ion in the transversal plane to the beam axis.

The second key assumption of the LEM consists in extracting the relation between the density of lethal events and the local dose from survival measurements performed with *X-ray* radiation. Indeed, the local dose deposited by *X-ray* radiation is considered as uniform within the cell. Neglecting stochastic effects, it is therefore equal to the macroscopic dose D , which is delivered to the sample by the *X-ray* source:

$$d(\mathbf{r}) = D \quad (5)$$

Therefore for *X-ray* irradiation, Eq. (2) becomes simply:

$$N_{lethal}(D) \approx \rho_{lethal}(D).V_{sensitive} \quad (6)$$

According to equation (2), $N_{lethal}(D)$, and therefore $\rho_{lethal}(D)$ can be deduced from the measurement of cell survival to *X-ray* irradiation (described by the α and β parameters) and from an estimation of the cell sensitive volume $V_{sensitive}$. This latter is assumed to be uniformly distributed over the cell nucleus. The diameter of the sensitive volume depends on the cell and ranges from 5-20 µm. An explicit expression for the average number of lethal events can thus be obtained as:

$$N_{lethal} = \iiint_{\text{Sensitive Volume}} \frac{-\ln S_X(d(r))}{V_{sensitive}} d\mathbf{r} \quad (7)$$

The photon dose-effect relation is parameterized using an additional parameter, the threshold dose D_t, allowing extrapolating the radiation effect to very high dose. This special parameterization is presented in equation (8) :

$$-\ln S(D(r)) = \begin{cases} \alpha_X D(r) + \beta_X D^2(r) & \text{si} \quad D(r) \le D_{seuil} \\ (\alpha_X + 2\beta_X D_{seuil}) D(r) - \beta_X D_{seuil}^2 & \text{si} \quad D(r) > D_{seuil} \end{cases} \qquad (8)$$

Practically, the threshold dose cannot be measures and is fitted using experimental data measured for high-LET ions [8].

The LEM authors have changed their model by incorporating the effect of ionization clusters [9] and by modifying the parameterization of the radial dose in integrating an expression of the minimum radial distance r_{min} dependent on ion energy. However, the basic formalism of the LEM is still the same. The basic concepts of this model was extensively analyzed by *Beuve et al* [10][11].

2. The MKM formalism

The MK model is based on the statistical theory and the microdosimetric formalisms and quantities. In the MK model, the lesions are produced in sub-volumes of the cell nucleus called ”domains”. The dose deposited in these domains is quantified by the so-called “specific energy” stochastic variable z. The lesions are classified into two different types [12], Type I are lethal and non-repairable, type II are initially not lethal but may become lethal if they undergo some specific transformations. The probability of forming a type I lesion in a domain is proportional to the dose absorbed by the domain z. The non-lethal type II lesions may be repaired or transformed to lethal lesions. The processes that the type II lesions may undergo are 1°) a monomolecular-like process with first-order rate constant *a*. 2°) a pairwise combination with another type II lesion located in the same domain to form a lethal unrepairable lesion with second-order rate constant *b*. 3°) a repair process by a monomolecular-like process with first-order rate constant *c*.4°) a persistence for a period of time *tr*, after which it becomes lethal and not repairable. These possibilities are resumed in figure 1.

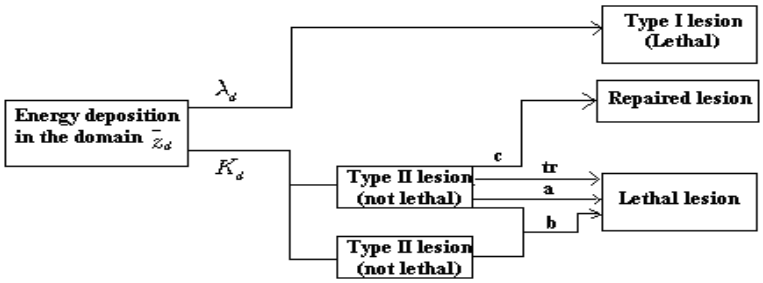

Figure 1: Schematic representation of the MKM formalism

For a short time irradiation and assuming a Poisson distribution of lethal lesions, the mean number of lesions in nucleus is expressed by:

$$\varepsilon(D) = \alpha_p D + \beta D^2 \qquad (9)$$

Where the index p indicates the Poisson distribution; $\alpha_p = (\alpha_0 + \beta \bar{z}_{1D})$ and α_0 and β are cell-dependent but LET independent parameters; $\bar{z}_{1D}$ is the single event dose mean specific energy in the domain. Therefore the expression of RBE_{1P} in the limit of the zero dose is given by:

$$RBE_{1p} = \frac{\alpha_0}{\alpha_R} + \frac{\beta}{\alpha_R} \bar{z}_{1D} \qquad (10)$$

Replacing $\bar{z}_{1D}$ by its expression versus the mean dose lineal energy $\bar{y}_D$ assuming spherical domain, equation (10) reads:

$$RBE_{1p} = \frac{\alpha_0}{\alpha_R} + \frac{\beta}{\alpha_R}\frac{0.2}{d^2}\bar{y}_D \qquad (11)$$

This expression allows deducing the two parameters α_0 and the domain diameter d by fitting experimental data for LET below the saturation effect. The value of β is deduced from the X rays radiation and assumed to be unchanged with changing LET or particle type.

However, for the very high-LET ions, the distribution of lethal lesions in the nucleus cannot be described by a Poisson distribution and the RBE value decreases with increasing LET. Then, Equation (10) requires a correction in order to take into account for this saturation effect in RBE. This correction was proposed by *R.B Hawkins* [12]:

$$RBE_1 = \frac{\alpha}{\alpha_R} = \frac{(1-\exp(-\alpha_p \bar{z}_{1Dn}))}{\alpha_p \bar{z}_{1Dn}} RBE_{1P} \qquad (12)$$

Where $\bar{z}_{1Dn}$ is the dose mean specific energy in the nucleus. It is expressed as a function of $\bar{y}_D$ by:

$$\bar{z}_{1Dn} = 0.16\frac{\bar{y}_D}{\sigma} \text{ Gy} \qquad (13)$$

Where σ is the cross sectional area of the sensitive nuclear volume expressed in µm²

If one replaces $\bar{z}_{1Dn}$, α_p and RBE_{1P} given respectively by equations (13), (9) and (11), in the equation (12), one can express the corrected linear coefficient of dose by equation (13).

$$\alpha^* = \sigma\frac{\left(1-\exp\left(\frac{-0.16(\alpha_0+\beta\frac{0.2}{d^2}\bar{y}_D)\bar{y}_D}{\sigma}\right)\right)}{0.16\bar{y}_D} \qquad (14)$$

Finally the equation (14) is fitted with experimental data for large LET range in order to deduce the value of σ.

3. The LEM vs MKM comparison

An interesting conceptual comparison was published by *Y. Kase et al 2008* [13]. In their work, *Kase et al* have adapted the MKM to amorphous track calculation in order to compare it to the LEM. We present here some conclusions of this comparison.

In the LEM, the biological effect is related to an energy deposition in infinitesimal small nuclear sub-volume assimilated to point-like target *(Scholz et al 1996* [1]*)*. Regarding the MKM, the biological effect is related to an energy deposition in nuclear sub-volumes with micrometric dimensions named "Domains". The domain is a small homogeneous reaction vessel with boundary that is impermeable to lesions. *(Hawkins 2003* [12]*)*. Both models need the photon dose-effect relation as an input parameter. In addition, the LEM needs the radial dose distribution of the incident ions. The LEM parameterization of this dose effect relation is presented in the equation (8). In the case of LEM the β parameter is considered as dependent of the LET and the particle type. For the MKM the photon dose-effect relation is parameterized by the linear quadratic model whatever the dose range and the β parameter is considered independent of the particle LET and type. In the case of the MKM the

additional input parameters are the lineal energy distribution in the domain and the experimental RBE-LET relation for at least two different LET values.

In the LEM the critical parameter is the threshold dose D_t , used in the parameterization of the experimental photon dose-effect relation for high dose. It is practically difficult to precisely determine the photon dose effect at very high dose. Then, D_t is kept as an adjustable parameter in order to allow the best representation of the experimental data [8]. In the case of the MKM, *Kase et al* [13] have reported that the model predictions are sensitive to relative variations of the domain size. Finally, both models provide a good description for different sets of experimental data. However, for some LET–energy combinations, the agreement with the experimental results is better with the MKM. Finally, *Kase et al* reported in their paper that there is a tendency for overestimation of RBE by the LEM model for high energetic ions at comparably low LET *(Kase et al* [13]*)* .

Results

Application of the MKM with experimental data of Furusawa et al[14]

The user needs to establish two experimental relations to calculate the necessary parameters of the MK model. These parameters are used later to characterize the cell radiosenstivity and predict the response of this cell to ion irradiation. These two experimental relations are 1°) the photon dose-effect relation of the cell. This relation is used to extract the domain diameter d. 2°) The RBE-LET relation which allow to calculate α_0 and σ . Then, we followed these steps to apply the MKM on experimental data published by *Furusawa et al* [14] for HSG cell line irradiated with carbon ion in aerobic conditions. The fitting of the photon dose-effect relation by the linear quadratic model resulted in the determination of the parameters: α_X =0,313Gy^{-1} and β =0,062 Gy^{-2}. The index x indicates that the alpha parameter is calculated for the X rays irradiation.

The second step of the MKM-parameter calculation is the determination of the domain diameter d and the effective area of the sensitive volume σ . These two parameters are extracted from the RBE-LET or RBE-lineal energy relation. Then we determine the domain diameter according to the equation (11) and the effective area of the HSG cells according to the equation (14). The result of these adjustments are shown in figure 2 .

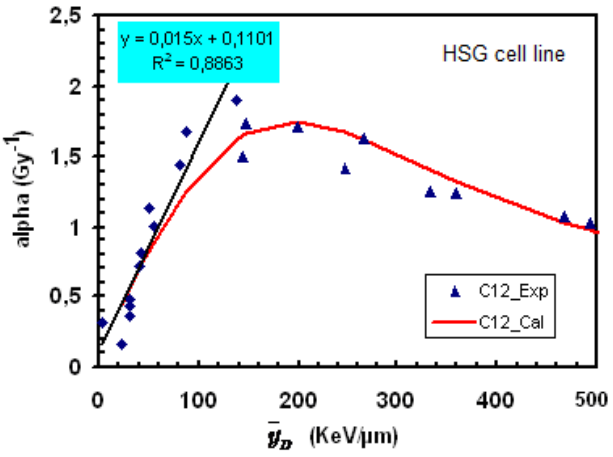

Figure 2: results of our MKM parameter calculation for HSG cell line irradiated with carbon ions of different energies. The experimental data are extracted from *Furusawa et al.* [14].

Therefore, the domain radius of the HSG cells is $r_d = 0,45\mu m$ and their effective nucleus area is $\sigma = 75\mu m^2$. If we assume that the nucleus sensitive volume has a cylindrical shape with radius R_n and

area σ . Therefore σ , can be expressed by: $\sigma = \pi R_n^2$. By replacing σ and π we obtain $R_n = 4,88\mu m$ for HSG cell line.

The MKM was also applied for HSG cell by *Kase et al (2006)* [15]. In their work *Kase et al.* have used the dose-effect of 200 KV X rays and of 290 MeV/n carbon ions to extract the domain diameter and α_0 parameter. However, they used another formula to correct the saturation effect and extract the nucleus effective area using the lineal energy saturation (details are presented in reference [15]). The table 1 resumes the MKM parameters obtained by our application of the original MKM and those obtained by *Kase et al* [15].

Table 1. *Comparison of our application of the MKM with those of Kase et al*[15] *on the HSG cell line*

MKM Parameters for HSG cell line	**Our application of the MKM**	***Y. Kase et al* results**
β (Gy^{-2})	0,0615	0,05
α_0 (Gy^{-1})	0,11 ± 0,02	0,13 ± 0,03
r_d (µm)	0,45 ± 0.05	0,42 ± 0,04
R_n (µm)	4,88 ± 0,4	4,1

The modified formulation used by *Kase and al* [15] can explain the difference between our calculation of R_n and that of *Kase et al* . Concerning r_d and α_0 , these parameters are extracted using the original formulation of the MKM in both cases. We note that *Kase et al* [15] used as input, the dose-effect relation based on two experimental relations determined by an irradiation with 200 kV photons and with 290 MeV /n carbon ions, in order to fit the linear equation expressed in equation (10). Instead we used a larger set of experimental data. Despite this, the differences between the both calculation results are acceptable taking into account the uncertainties associated to each calculation.

Application of the MKM to characterize two cell lines with different radio-sensitivities

The MK model is applied here to reproduce the experimental data of the irradiation of two cell lines. The cell lines used in this study are extracted from the same histological type of head and neck carcinoma. The first one is the radiosensitive SCC61 cells, extracted from a pharynx carcinoma. The second line is the radioresistant SQ20B cells, extracted from a neck carcinoma. These cells are prepared and cultured as described in reference [16]. The irradiation procedures and the results of theses irradiations was reported by *Beuve et al (2008)* [8]. The cells were irradiated with carbon ions of 72 MeV/n and with 85 MeV/n argon ions at GANIL facility in France. The energies mentioned above are the ion energies at the entrance of the cells. X-ray irradiations of both cell lines were performed using the same experimental protocols as used for ion irradiations. This is very important in order to compare the high-LET radiation results with the X rays ones. The approach used previously to calculate the MKM parameters for the HSG cell line is followed here in order to calculate the MKM parameters for SQ20B and SSC61 cell lines. The figure 3 below presents the data adjustment of the alpha parameter versus the dose mean lineal energy in the domain according to the equation (14). The calculated parameters, with this fit, are summarized in the Table 2. We note that in this case, we do an MKM application similar to that made by *Y Kase et al* [15]. This application is based on the use of two experimental dose-response relations obtained with photon irradiation and with low LET ion (72 MeV/n carbon ions), in order to estimate the domain size. However,

for the estimation of the effective nucleus area, we used the original formulation of the MKM with an additional experimental relation obtained using a very high LET (85 MeV/n argon ions).

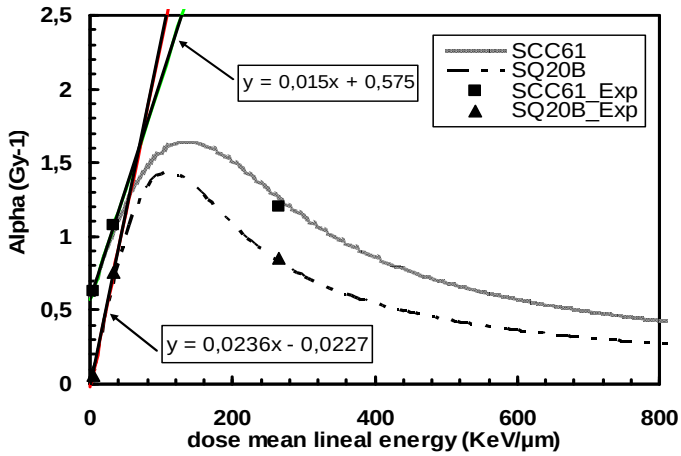

Table 2 : MKM parameters calculated for SCC61 and SQ20B cell lines

MK parameters	SCC61 cells	SQ20B cells
β (Gy^{-2})	0.02	0.0615
α_0 (Gy)	0.57	0.02
d (µm)	0.88	0.67
σ (µm²)	55	35

Figure 3: Results of MKM parameter calculation for SQ20B and SCC61 cell lines irradiated with carbon ions of 72 MeV/n and argon ions of 85MeV/n. The experimental data are extracted from *Beuve et al.* [8].

Discussion

The radiobiological significance of the MK model parameters allows an analysis of the biological response of the cells and comparison between different cell lines. In the case of SCC61 and SQ20B cell lines, the parameters obtained in this study reflect the difference in their radiosensitivity. The first difference consists in α_0. A mathematical description of this parameter is given by *Hawkins* [12]. It depend on the formation rate of non-reparable type I lesions, the formation rate of the lethal lesions by the monomolecular transformation of type II lesions and the transformation of the type II lesions to lethal lesion after a period t_r (see section 2 in method and result). Therefore, the cell lines which have low or zero value of α_0 are dominated by the formation of type I lesions or the monomolecular transformation of the type II lesions. In our case, the α_0 value for SCC61 cells is higher than for SQ20B. This implies that the lethal lesions produced in SCC61 cells are the result of the type I lesions or the monomolecular transformation of the type II lesions. The β parameter of the SQ20B cells is higher than those of SCC61, this means that the transformation rate of the type II lesions into lethal lesion by the bimolecular processes (interaction of two sublesions) is higher in the SQ20B cells. However, the MK model assumes that the production rate of type II lesions is constant regardless of the LET. While, the author of the MKM relay the type II lesions to the DSB lesions [12], consequently any change in the LET may affect the production rate of type II lesions and probably the β. Concerning the parameter σ, which reflects the nuclear sensitive volume, is more important in the SCC61 than in SQ20B cell.

Finally, this behavior of the MKM parameters can be exploited clinically to adapt the radiation depending on the degree of radiosensitivity tumor cells based on the model parameters. In this optic, it will be interesting to determine a common experimental protocol in order to calculate the MKM parameters and construct a parameter tables for each cell line considered in hadrontherapy treatement.

Conclusion

We have seen that the application of the MKM in its original version gives comparable results with the MKM version used by *Kase et al* [15] except for the determination of the effective nucleus area where *Kase et al* [15] included a new formula to correct the saturation effect using the lineal energy saturation. We have also seen that the MKM parameters allow characterizing the response mechanisms and the radiosensitivity of a cell lines. The MKM parameters calculated for the SCC61 and SQ20B cell lines reflect well their different radiosensitivity.

Then, this characteristic of the MKM parameters can be beneficial in clinical application of the MKM in order to improve treatments by adapting the radiation depending on radiosensitivity of tumor cells. The MK model still has some weaknesses especially regarding the change of beta parameter with LET since the MKM assumes that the β is independent of particle type and energy used. The α and β parameters are expressed in the MKM as a function of several other parameters related to production rates of type II and type I lesions and to their kinetic evolution in the cell. It assumes also that the production rate of type II lesions is constant regardless of the LET and is equal to 30 lesions / Gy. However, the MKM relay the type II lesions to the DSB lesions [12], consequently any change in the LET may affect the production rate of type II lesions and probably the β.

For the prospects of RBE modeling for hadrontherapy treatments, we adopted two approaches. The first approach is to continue the investigations of MKM in order to better understand the behavior of its parameters in different biological conditions. We are working on changing the expression given the production rate of type II lesions in order to include the influence of the LET. For this, we rely on the experimental data we are producing by irradiation with x-rays and carbon ions (at GANIL) of several types of cell lines following a well-defined protocol.

The second approach is to develop a new model, which in particular will include concept or element inspired from the models presently available in the literature and we considered as key points.

References

[1] M. Scholz and G. Kraft. Track structure and the calculation of biological effects of heavy charged particles. *Adv. Space. Res.*, 1996 ,18(1/2):5–14.
[2] M. Scholz, A.M. Kellerer, W. Kraft-Weyrather, and G. Kraft. Computation of cell survival in heavy ion beams for therapy the model and its approximation. *Radiat. Environ. Biophys*, 1997, 36:59–66.
[3] R. B. Hawkins, "A Statistical Theory of Cell Killing by Radiation of Varying Linear Energy Transfer"; *Radiat Res.* 1994; 140, 366-374.
[4] R. B. Hawkins ; "A Microdosimetric Kinetic Model of cell death from exposure to ionizing radiation of any LET, with experimental and clinical applications". 1996; *Int Journal Radiation Biology* ;Vol 69; No 6; 739-755.
[5] M Krämer and M Scholz Treatment planning for heavy-ion radiotherapy: calculation and optimization of biologically effective dose. 2000 *Phys. Med. Biol.* **45** 3319
[6] Yuki Kase, Nobuyuki Kanematsu, Tatsuaki Kanai and Naruhiro Matsufuji:" Biological dose calculation with Monte Carlo physics simulation for heavy-ion radiotherapy"; *Phys. Med. Biol*. 2006; 51**,** N467–N475.
[7] Sato T, Kase Y, Watanabe R, Niita K, Sihver L." Biological dose estimation for charged-particle therapy using an improved PHITS code coupled with a microdosimetric kinetic model." *Radiat Res.* 2009; Jan;171(1):107-
[8] M.Beuve et al."Parameters and Local Effect Model predictions for head and neck squamous cell carcinomas exposed to High Linear Energy Transfer ions"; *International Journal Radiation* Oncology *Biology Physics*. 2008; 71(2):635-642,.
[9] T. Elsasser and M. Scholz. Cluster effects within the local effect model. *Radiat. Res.*, 2007; 167(3):319–29.
[10] M. Beuve , A. Colliaux , D. Dabli et al "Statistical effects of dose deposition in track-structure modelling of radiobiology efficiency"; *Nuclear Instruments and Methods in Physics Research Section B: Beam Interactions with Materials and Atoms* . 2009; **267**; 983-988.
[11] M. Beuve " Formalization and theoretical analysis of the local effect model"; *Radiat. Research.* 2009; 172(3): 394-402.
[12] Roland B. Hawkins ; "A Microdosimetric Kinetic Model for Effect of Non Poisson Distribution of Lethal Lesions on the Variation of RBE with LET."; *Rad Research*, 2003; 160, 61-69.
[13] Yuki Kase, Tatsuaki Kanai, Naruhiro Matsufuji et al; "Biophysical calculation of cell survival probabilities using amorphous track structure models for heavy-ion irradiation"; *Phys. Med. Biol*; 2008; 53; 37-59.
[14] Furusawa, Y., Fukutsu, K., Aoki et al . " Inactivation of aerobic and hypoxic cells from three different cell lines by accelerated 3He–,12C– and 20Ne–ion beams" . *Radiat. Res.* 2000; 154, 485–496.
[15] Kase Y, Kanai T,Matsumoto Y, Furusawa Y et al; "Microdosimetric measurements and estimation of human cell survival for heavy-ion beams"; *Radiat. Res.* 2006; 166 629–38.
[16] Alphonse G *et al*. Ceramide induces activation of the mitochondrial/caspases pathway in Jurkat and SCC61 cells sensitive to gamma-radiation but activation of this sequence is defective in radioresistant SQ20B cells. Int J Radiat Biol ; 2002, 78:821-835.

Proceedings of NIRS-ETOILE Joint Symposium on Carbon Ion Radiotherapy

・Date of Publishing: November 2011

・Editing and Publication: International Affairs Section

Dept. of Planning and Management

National Institute of Radiological Sciences

Anagawa 4-9-1, Inage-ku, Chiba, Japan 263-8555

tel : +81-43-206-9999 fax : +81-43-206-9999

e-mail : kokusai@nirs.go.jp Homepage : http://www.nirs.go.jp

NIRS-M-243 Printed in Japan

NIRS

National Institute of Radiological Sciences
International Affairs Section
4-9-1 Anagawa, Inage-ku, Chiba 263-8555, Japan
E-mail:kokusai@nirs.go.jp
Tel:+81-43-206-3025
Fax:+81-43-206-4061
Homepage: http://www.nirs.go.jp/ENG/index.html

GSC ETOILE

Groupement de Coopération Sanitaire ETOILE
60, avenue Rockefeller,69008-Lyon, France
E-mail:info@centre-etoile.org
Tel:33(0)4 72 78 89 20
Fax:33(0)4 78 76 06 43
Homepage: http://www.centre-etoile.org/

Scientific Secretariat